FUNCTIONALIZED SELENOPHENE OLIGOMERS AND CO-OLIGOMERS AND THEIR APPLICATION IN ORGANIC SOLAR CELLS

Dissertation

zur Erlangung des akademischen Grades

Dr. rer. nat.

der Fakultät für Naturwissenschaften

Universität Ulm

vorgelegt von

Stefan Haid

aus Biberach an der Riß

2012

Amtierender Dekan:	Prof. Dr. Joachim Ankerhold
Erstgutachter:	Prof. Dr. Peter Bäuerle
Zweitgutachter:	Prof. Dr. Tanja Weil
Drittgutachter:	Prof. Dr. Marcel Mayor
Tag der Promotionsprüfung:	30. Oktober 2012

Fakultät für Naturwissenschaften, Universität Ulm

„Zwei Dinge sind zu unserer Arbeit nötig: Unermüdliche Ausdauer und die Bereitschaft, etwas, in das man viel Zeit und Arbeit gesteckt hat, wieder wegzuwerfen.“
Albert Einstein

Danksagung

Zu allererst möchte ich mich bei meinem Doktorvater Prof. Dr. Peter Bäuerle dafür bedanken, dass er mir sehr große Freiheiten bei der Wahl und Gestaltung meines Promotionsthemas eingeräumt hat und mir die Möglichkeit gegeben hat, mit dem doch recht kostspieligen Baustein Selenophen zu arbeiten. Ich bedanke mich auch für die großzügige Finanzierung von Konferenzteilnahmen und Auslandsaufenthalten.

Ein großer Dank geht auch an Prof. Dr. Tanja Weil und Prof. Dr. Marcel Mayor für die Übernahme der weiteren Gutachten.

Meinen „Lektoren“ danke ich ganz herzlich für das aufmerksame Korrekturlesen dieser Arbeit. Ohne sie wäre bestimmt so mancher Fehler unentdeckt geblieben.

Ein sehr großer Dank geht an meine Kooperationspartner Magdalena Marszałek, Mateusz Wielopolski, Joël Teuscher, Jacques-E. Moser, Robin Humphry-Baker, Shaik M. Zakeeruddin und Michael Grätzel an der EPFL in Lausanne sowie Christian Uhrich und Martin Pfeiffer bei Heliatek in Dresden, die immer versucht haben, die bestmöglichen Effizienzen aus meinen Molekülen herauszuholen. Außerdem möchte ich mich bei Prof. Andrew B. Holmes, Dr. Wallace Wong und Dr. Helga Seyler bedanken für die große Unterstützung und angenehme Atmosphäre während meines Forschungsaufenthalts am Bio21 Institute in Melbourne.

Natürlich möchte ich mich auch bei allen Institutsmitgliedern bedanken für die freundliche Arbeitsatmosphäre und so manche „fruitful discussion“. Ein ganz besonderer Dank geht an meine aktuellen und ehemaligen Laborkollegen und –kolleginnen Angela Digennaro, Sascha Erhardt, Arne Guta, Mirjam Löbert, Eva Schillinger, Martin Schikora und Martin Weidelener. Außerdem möchte ich auch Astrid Vogt, Melanie Bader und Dr. Gisela Schulz danken. Ganz herzlichen Dank auch an meinen Gruppenleiter Dr. Amaresh Mishra für die große Unterstützung vor allem bei der Publikation meiner Forschung.

Frau Dr. Sylvia Schmid möchte ich dafür danken, dass sie mir so manchen Gang zum NMR erspart hat. Herrn Ulrich Ziegler danke ich für die Aufnahme diverser Hochtemperatur-NMRs, Herrn Dr. Markus Wunderlin für die Messung der Massenspektren und Frau Margit Lang für die Durchführung der Elementaranalysen. Ein weiterer Dank geht an Prof. Dr. Matthias Weil für die Messung und Auswertung der Röntgenstruktur des Quaterselenophens.

Ich möchte auch Katharina Stahl, Jonas Higl und Eduard Brier danken, die mich während ihrer Forschungspraktika bzw. Bachelorarbeit tatkräftig unterstützten und mir so manche lästige Routine-arbeit abnahmen.

Mein größter und herzlichster Dank geht schließlich an meine Familie, ganz besonders meine Eltern, die mich all die Jahre sowohl moralisch als auch finanziell unterstützt haben.

CONTENTS

CONTENTS I

Preface V

Abbreviations VI

Compounds Synthesized and Described in this Thesis X

1 SELENOPHENE AND ITS APPLICATION IN ORGANIC SEMICONDUCTING MATERIALS 1

1.1 Selenophene – Synthesis and Reactivity 2

1.2 Preparation of Selenophene 3

1.3 Polyselenophene and Selenophene-containing Copolymers 6

1.3.1 Polyselenophenes 6

1.3.2 Selenophene-containing Copolymers 9

1.4 Oligoselenophenes 12

1.5 Summary 14

1.6 References 15

2 ORGANIC SOLAR CELLS 19

2.1 Introduction 20

2.2 Organic Thin Film Solar Cells 21

2.2.1 Fundamental Principles 21

2.2.2 Characterization of Solar Cells 24

2.2.3 Planar Heterojunction Solar Cells 27

2.2.4 Bulk-Heterojunction Solar Cells 28

2.3 Dye-sensitized Solar Cells 31

2.4 Summary 34

2.5 References 35

3 DICYANOVINYL-SUBSTITUTED (CO-)OLIGOMERS BASED ON SELENOPHENE 39

3.1 General Introduction 40

3.2 Dicyanovinyl-substituted Mixed Selenophene-Thiophene Co-oligomers 44

3.2.1 Introduction 44

3.2.2 Synthesis of Co-oligomers 1-4 45

3.2.3 Attempts Towards the Synthesis of 3,4-Dialkylselenophene 50

3.2.4 Thermal Properties of Co-oligomers 1-4 54

3.2.5 Optical Properties of Co-oligomers 1-4 55

3.2.6 Electrochemical Properties of Co-oligomers 1-4 59

3.2.7 Photovoltaic Performance of Co-oligomers 1-4 62

3.3 Dicyanovinyl-substituted Oligoselenophenes 66

3.3.1 Introduction 66

3.3.2 Synthesis of Oligoselenophenes 67

3.3.3 Thermal Properties of Oligoselenophenes 69

3.3.4 Optical Properties of Oligoselenophenes 70

3.3.5 Electrochemical Properties of Oligoselenophenes 72

3.3.6 Single Crystal Structure Analysis of Quaterselenophene 6 75

3.3.7 Photovoltaic Performance of Oligomers 6-8 78

3.4 Summary 82

3.5 Experimental Section 83

3.6 References 102

4 DICYANOVINYL-SUBSTITUTED DICHALCOGENOPHENOPYRROLE-BASED CO-OLIGOMERS 107

4.1 General Introduction 108

4.2 Vacuum-processable Co-Oligomers with a Dichalcogenophenopyrrole Core 112

4.2.1 Introduction 112

4.2.2 Synthesis of Vacuum-processable Co-oligomers 113

4.2.2.1 Synthesis of Dithienopyrrole Co-oligomers 114

4.2.2.2 Synthesis of Diselenophenopyrrole Co-oligomers 115

4.2.3 Thermal Properties of Co-oligomers 9-14 123

4.2.4 Optical Properties of Co-oligomers 9-14 124

4.2.5 Electrochemical Properties of Co-oligomers 9-14 126

4.2.6 Photovoltaic Performance of Co-oligomers 9-14 127

4.3 Solution-processable Co-oligomer 128

4.3.1 Introduction 128

4.3.2 Synthesis of Co-oligomer 15 129

4.3.3 Optical and Electrochemical Properties of Co-oligomer 15 131

4.3.4 Photovoltaic Performance of Co-oligomer 15 133

4.4 Summary 135

4.5 Experimental Section 136

4.6 References 159

5 BENZOTHIADIAZOLE-BASED ORGANIC SENSITIZERS 163

5.1 Introduction 164

5.2 Synthesis of Dyes 16-19 166

5.3 Optical and Electrochemical Properties of Dyes 16-19 169

5.4 Quantumchemical Calculations for Dyes 17 and 19 171

5.5 Photovoltaic Performance of Dyes 16-19 in DSSCs 174

5.6 Photophysical Investigation of Dyes 17 and 19 177

5.7 Summary and Conclusion 182

5.8 Experimental Section 182

5.9 References 201

Summary 204

Zusammenfassung 208

Curriculum Vitae 212

Publications and Presentations 213

Preface

The goal of this thesis was the synthesis of functionalized oligomers and co-oligomers based on selenophene. The optoelectronic properties of these compounds should be investigated and compared to corresponding thiophene analogs. Furthermore, they should be implemented in organic solar cells. In contrast to thiophene, one of the most frequently used building blocks in oligomeric and polymeric organic semiconductors, selenophene has only scarcely been incorporated in organic semiconducting materials. Especially in the field of oligomers for organic solar cells, only a very limited number of publications using selenophene as building block have appeared so far.

Chapter 1 gives a short overview of the chemistry of selenophene and its application in organic electronics, in particular organic solar cells. In **Chapter 2**, fundamental construction principles and characterization parameters for organic solar cells are presented. Furthermore, a summary of state-of-the-art donor materials for organic solar cells is given. **Chapter 3** deals with the synthesis and characterization of acceptor-functionalized selenophene-thiophene co-oligomers and oligoselenophenes as well as their use as donor materials in vacuum-processed organic solar cells. Similarities and differences with corresponding thiophene compounds are discussed in detail. In **Chapter 4** acceptor-functionalized co-oligomers with dithienopyrrole or diselenophenopyrrole core units are described and characterized by optical and electrochemical methods. These compounds were implemented in vacuum-processed and solution-processed organic solar cells and their device performance is discussed in detail. The first part of **Chapter 5** deals with the synthesis of benzothiadiazole-based organic sensitizers, their optoelectronic characterization and application in dye-sensitized solar cells. The second part of this chapter is focused on theoretical and photophysical investigations carried out to elucidate the astounding difference in the power conversion efficiencies of two of these sensitizers which only differ in one additional phenyl unit. The photophysical measurements and theoretical calculations were carried out by the group of Prof. Grätzel at EPFL in Lausanne.

Abbreviations

A	acceptor
Ac	acetyl
AM 1.5G	air mass 1.5 global
aq.	aqueous
BHJ	bulk-heterojunction
BHJSC	bulk-heterojunction solar cell
BPAPF	9,9-bis[4-(*N*,*N*-bis-biphenyl-4-yl-amino)phenyl]-9*H*-fluorene
Bu	butyl
calc.	calculated
CB	chlorobenzene
CI	chemical ionization
CV	cyclic voltammetry
D	donor
d	doublet
dba	dibenzylideneacetone
DCE	1,2-dichloroethane
DCM	dichloromethane
DCV	dicyanovinyl
DFT	density functional theory
DMF	*N*,*N*‘-dimethylformamide
DMII	1,3-dimethylimidazolium iodide
DMSO	dimethyl sulfoxide
dppp	1,3-bis(diphenylphosphino)propane
DPV	differential pulse voltammetry
DSC	differential scanning calorimetry
DSP	4*H*-diselenopheno[3,2-*b*:2',3'-*d*]pyrrole
DSSC	dye-sensitized solar cell
DTP	4*H*-dithieno[3,2-*b*:2',3'-*d*]pyrrole
EDOS	3,4-ethylenedioxyselenophene
EDOT	3,4-ethylenedioxythiophene
E_g^{CV}	electrochemical band gap
E_g^{opt}	optical band gap
EI	electron impact

EIS	electrochemical impedance spectroscopy
eq.	equivalent
EQE	external quantum efficiency
Et	ethyl
Fc	ferrocene
FF	fill factor
FTO	fluorine-doped tin oxide
GC	gas chromatography
GuNCS	guanidinium thiocyanate
Hex	hexyl
HOMO	highest occupied molecular orbital
HTL	hole transport material
I	current
IPCE	incident photon to current conversion efficiency
I_{SC}	short-circuit current
ITDB	2-isopropoxy-4,4,5,5-tetramethyl-1,3,2-dioxaborolane
ITO	indium-doped tin oxide
J	coupling constant
J_{SC}	short-circuit current density
k_B	Boltzmann constant
L_D	exciton diffusion length
LUMO	lowest unoccupied molecular orbital
M	molar
m	multiplet
m.p.	melting point
m-CPBA	*meta*-perchlorobenzoic acid
Me	methyl
MS	mass spectrometry
NBS	*N*-bromosuccinimide
n-BuLi	*n*-butyllithium
NMR	nuclear magnetic resonance
OFET	organic field effect transistor
OLED	organic light emitting diode
OSC	organic solar cell
OTFT	organic thin film transistor

Ox	oxidation
P	power
P3HS	poly(3-hexylselenophene)
P3HT	poly(3-hexylthiophene)
PCBM	phenyl-fullerene-butyric acid methyl ester
PCE	power conversion efficiency
PEDOS	poly(3,4-ethylenedioxyselenophene)
PEDOT	poly(3,4-ethylenedioxythiophene)
Ph	phenyl
PHJ	planar heterojunction
PHJSC	planar heterojunction solar cell
ppm	parts per million
q	elemental charge
q	quartet
r.t.	room temperature
Red	reduction
R_s	series resistance
R_{sh}	shunt resistance
s	singlet
Sel	selenophene
SMOSC	small molecule organic solar cell
t	triplet
TBAF	tetra-*n*-butylammonium fluoride
$TBAPF_6$	tetra-*n*-butylammonium hexafluorophosphate
TBP	*tert*-butylpyridine
^{t}Bu	*tert*-butyl
TCE	1,1,2,2-tetrachloroethane
TCSPC	time-correlated single photon counting
T_d	decomposition temperature
TGA	thermogravimetric analysis
Th	thiophene
THF	tetrahydrofurane
T_m	melting temperature
TMEDA	*N*,*N*,*N*',*N*'-tetramethylethylenediamine
TMS	trimethylsilyl

TOF	time of flight
UV	ultra-violet
V	voltage
v/v	volume-to-volume
Vis	visible
V_{OC}	open-circuit voltage
w/w	weight-to-weight
XRD	X-ray diffraction
δ	chemical shift
ε	molar extinction coefficient
λ	wavelength

Compounds Synthesized and Described in this Thesis

Target Compounds

Chapter 3

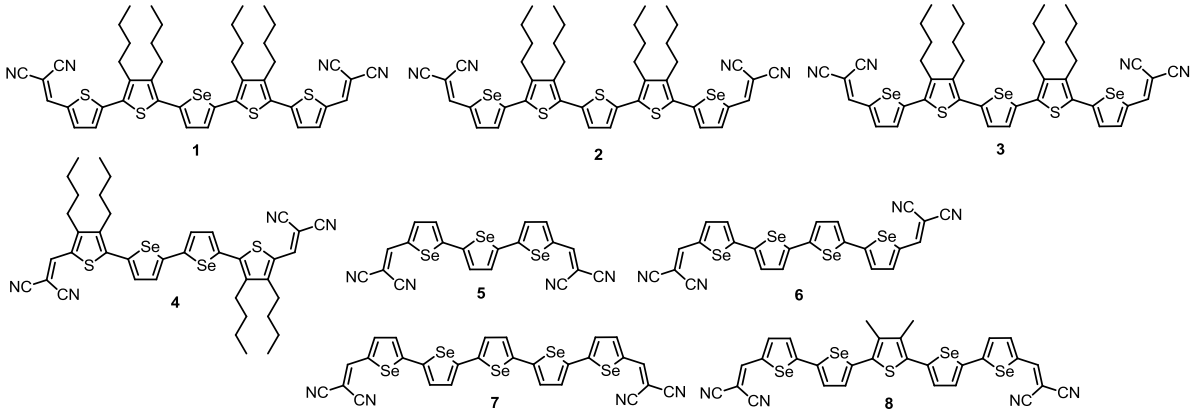

Chapter 4

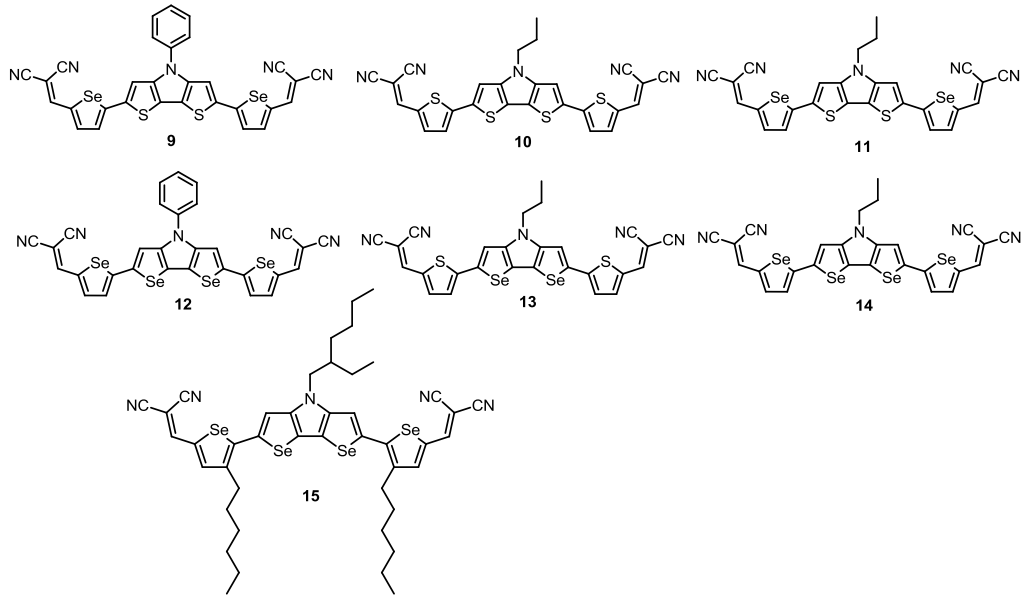

Chapter 5

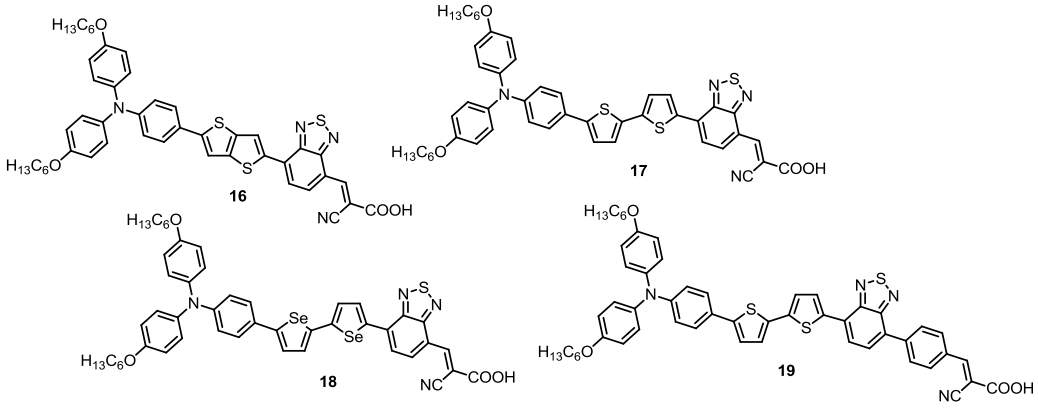

Building blocks

Chapter 3

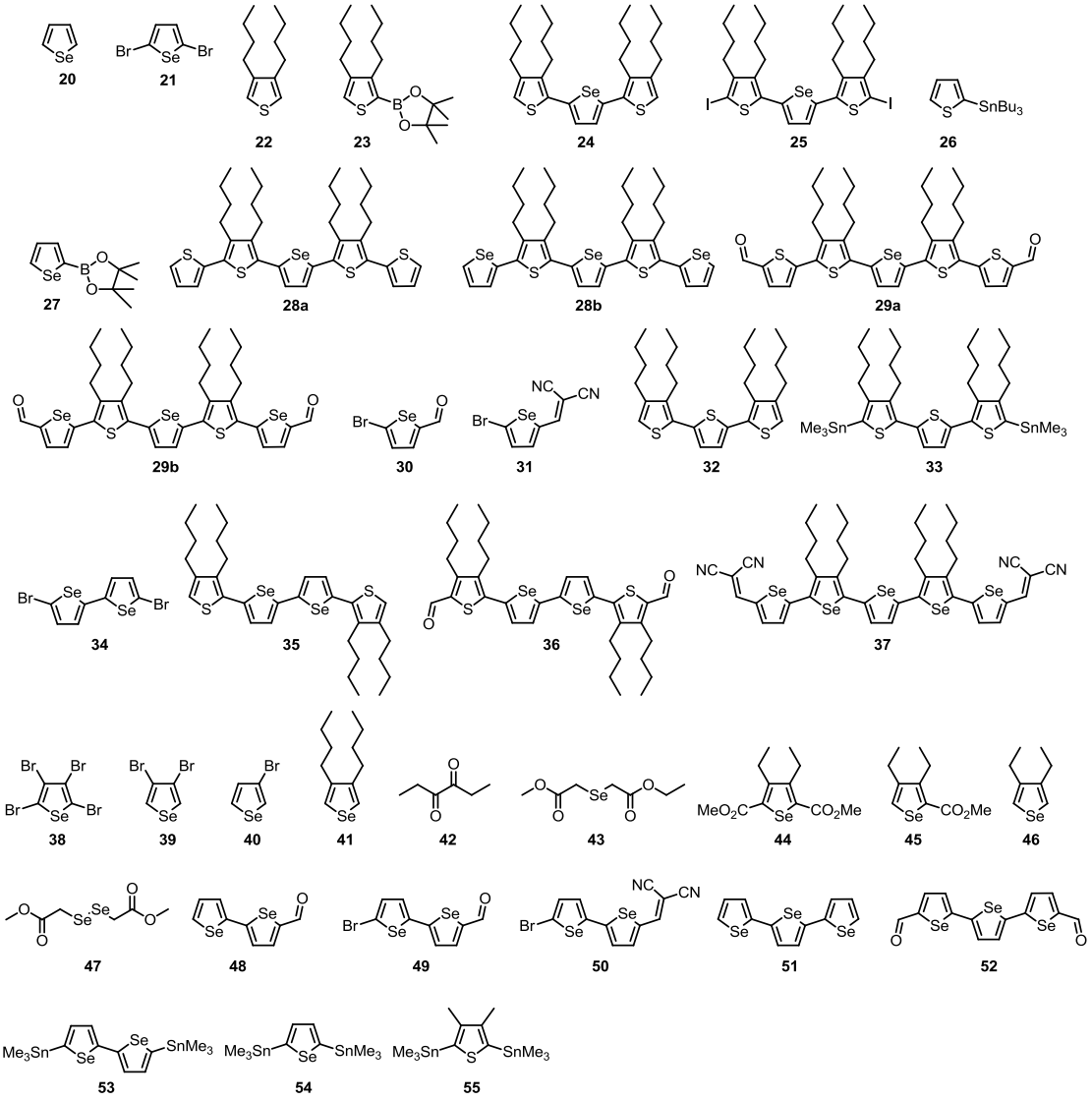

Chapter 4

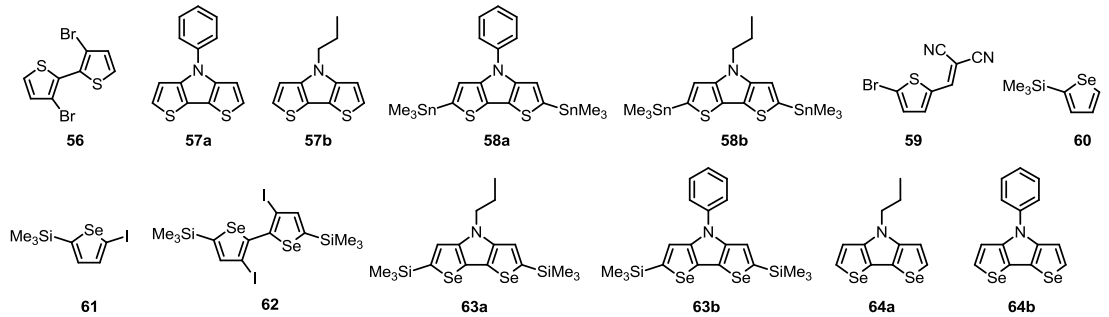

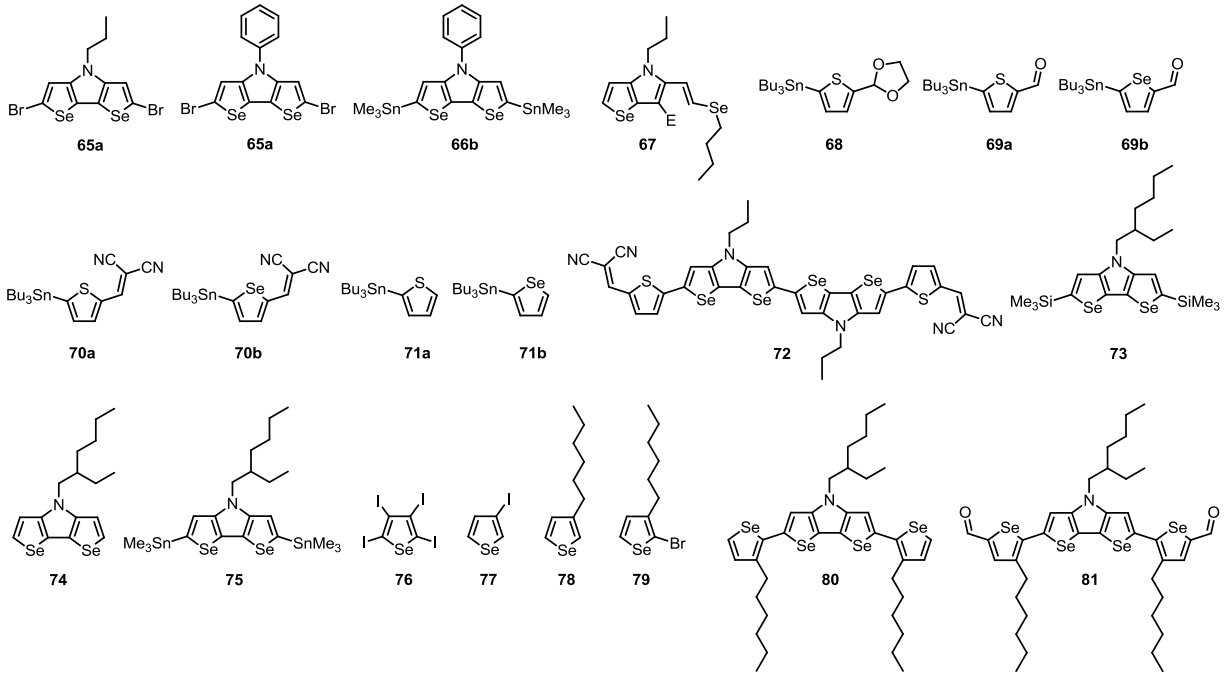
65a
65a
66b
67
68
69a
69b
70a
70b
71a
71b
72
73
74
75
76
77
78
79
80
81

Chapter 5

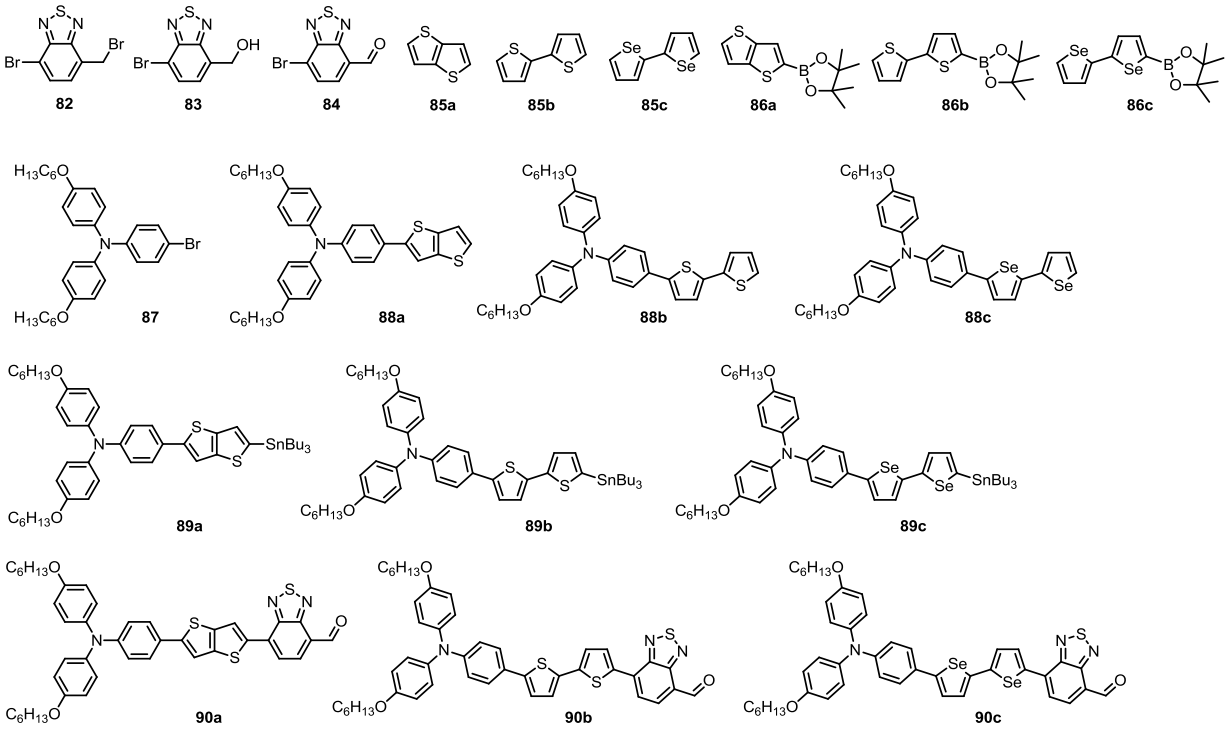
82
83
84
85a
85b
85c
86a
86b
86c
87
88a
88b
88c
89a
89b
89c
90a
90b
90c

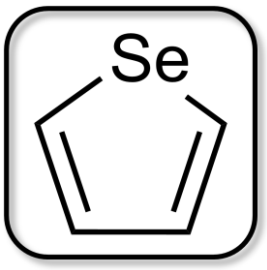

CHAPTER 1

SELENOPHENE AND ITS APPLICATION IN ORGANIC SEMICONDUCTING MATERIALS

1.1 Selenophene – Synthesis and Reactivity

Selenophene is the "bigger brother" of thiophene, which is one of the most frequently used building blocks in organic semiconducting materials.[1] In contrast, selenophene has not been studied as intensively due to its higher price, the limited number of commercially available derivatives and the less developed chemistry.

Selenophene is a pale yellow liquid with a characteristic stench, a boiling point of 110 °C and a melting point of −38 °C. Its density (d = 1.6003 g mL^{-1} at 25 °C) is significantly higher than that of thiophene (d = 1.0649 g mL^{-1}), while its dipole moment (μ = 0.52 D) is similar to thiophene (μ = 0.54 D).[2] The bond lengths and angles of selenophene (**Figure 1.1**) are almost identical to those of thiophene, except for the carbon-heteroatom bonds and the C2-heteroatom-C5 angle. The carbon-selenium bond (186 ppm) is longer than the carbon-sulfur bond (171 ppm) due to the larger van der Waals radius of selenium (1.90 Å) compared to sulfur (1.80 Å).[3] As a consequence, the C2-Se-C5 angle (88°) is smaller than the C2-S-C5 angle (92°). The ^{13}C NMR chemical shifts of both compounds are relatively similar, but the ^{1}H NMR chemical shift of the α-proton is shifted downfield in the case of selenophene (8.10 ppm) compared to thiophene (7.40 ppm).[2] Among the six natural isotopes of selenium, only one is NMR-active (^{77}Se, 7.58% natural abundance), which can be used to perform ^{77}Se NMR spectroscopy or to gain further structural information from ^{1}H and ^{13}C NMR spectra by analyzing ^{77}Se satellite signals.[4]

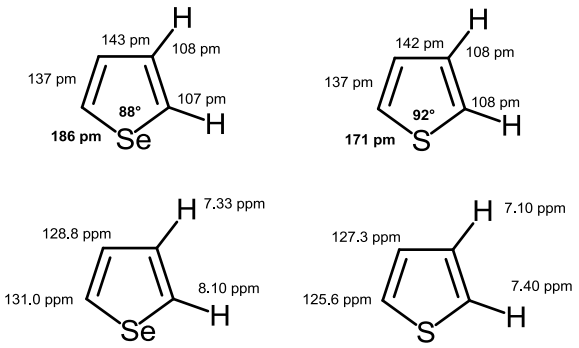

Figure 1.1: Bond lengths, angles and chemical shifts in selenophene and thiophene.

Selenophene is an electron rich five-membered heteroaromatic compound and slightly less aromatic than thiophene,[5-8] which results in a higher reactivity in both electrophilic and nucleophilic aromatic substitution reactions.[9-11] Compared to thiophene, the α-position is even more preferred to the β-position in electrophilic substitution reactions. This is due to the better stabilization of the positive charge in the σ-complex by the bigger and more easily polarizable selenium atom. Furthermore, the higher electrophilicity of the selenium atom also results in a greater tendency towards ring-opening

reactions. Strong nucleophiles can attack at the selenium atom, which leads to ring-opening if there is a suitable leaving group in the β-position.[12-13]

The chemistry of selenophene is similar to thiophene chemistry and has been described in detail in several reviews.[2, 13-18] The next section will be focused on preparation methods and reactions with some relevance for the syntheses described in the following chapters.

1.2 Preparation of Selenophene

The first synthesis of selenophene was reported by Paal in 1885, who reacted hexane-2,5-dione with phosphorous pentaselenide to obtain 2,5-dimethylselenophene (**Scheme 1.1**).[19]



Scheme 1.1: First selenophene synthesis by Paal.

Since then, numerous synthetic routes for substituted and unsubstituted selenophenes have been described. The most suitable method for a preparation on a larger scale was established by McMahon in 1933[20] and further improved by Gronowitz *et al.*[21] and Mohmand *et al.*[22] (**Scheme 1.2**).

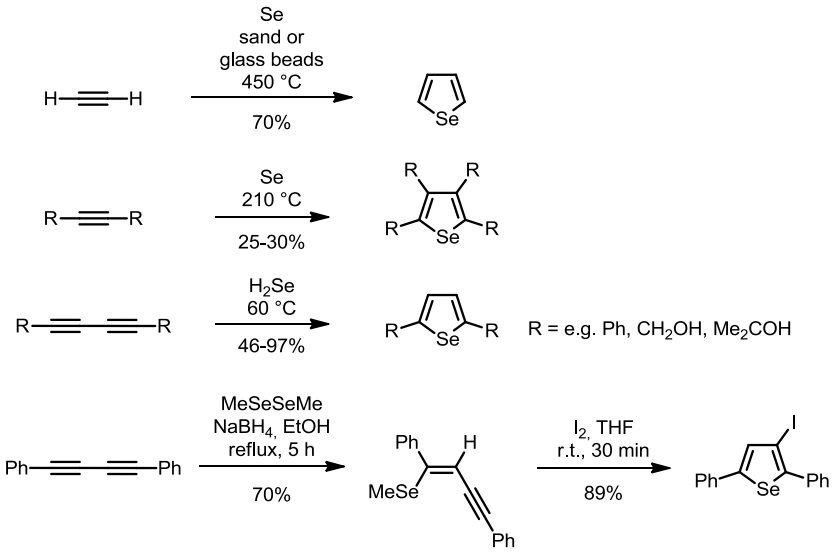

Scheme 1.2: Synthesis of selenophenes using acetylenes and diacetylenes.

In the synthetic protocol of Mohmand, selenophene was prepared by heating selenium powder together with glass or sand beads in an acetylene stream at 450 °C. The yield was about 70%. Fully substituted selenophenes have been synthesized from disubstituted acetylenes and elemental selenium at 210 °C. Regardless of the substituent, the yields were always low and did not exceed 30%

(**Scheme 1.2**).[23] 2,5-Disubstituted selenophenes can be prepared from diacetylenes and hydrogen selenide at 60 °C in yields of 46-97%.[24] 3-Iodo-2,5-diphenylselenophene was synthesized in high yields from 1,4-diphenylbuta-1,3-diyne by hydroselenation with methane selenolate, prepared *in situ* from dimethyl diselenide and sodium borohydride, and subsequent cyclization with iodine in THF at r.t. The product was used as starting material for the synthesis of various 3-alkynylselenophenes.[25]

Another method for the synthesis of substituted selenophenes is the Hinsberg synthesis (**Scheme 1.3**), which is well-established in thiophene chemistry.[26] In order to obtain 2,5-disubstituted selenophenes, di-β-ketoselenides were condensed with glyoxal under base catalysis. Depending on the substituents, yields between 13 and 73% were obtained. Aliphatic substituents like methyl or *tert*-butyl gave only very low yields while aromatic substituents gave moderate yields. The main side reaction, which reduced the yield, was the cleavage of the carbon-selenium bond.[27] When diketones are used instead of glyoxal, selenophenes with additional substituents at the 3- and 4-position can be synthesized. Thus, 2,5-dicarbomethoxy-3,4-dimethylselenophene was prepared from 2,3-butadione and dimethyl selenodiacetate under sodium hydroxide catalysis at room temperature.[28-29] Unfortunately, the selenophene carboxylic ester was not decarboxylated to the corresponding 3,4-disubstituted selenophene in these publications. By a similar method, Aqad *et al.* prepared 3,4-dihydroxy-2,5-carbethoxyselenophene from diethyl oxalate and diethyl selenodiacetate using sodium ethylate as base.[30]

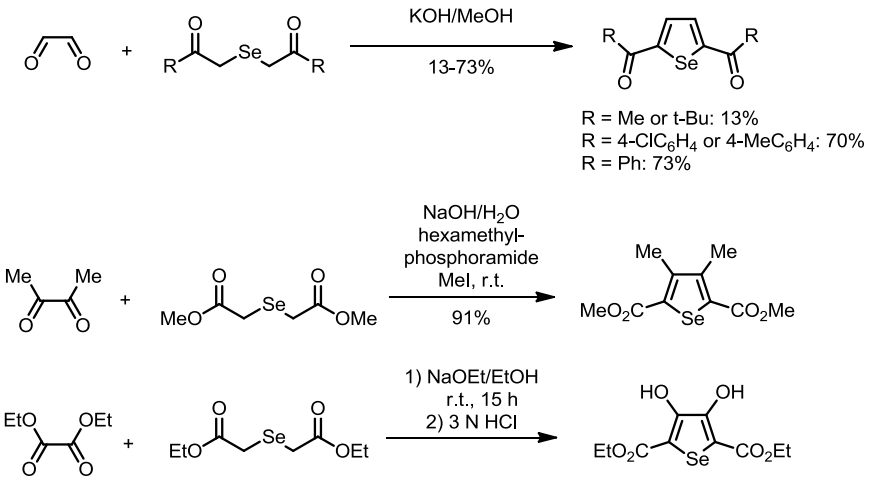

Scheme 1.3: Hinsberg synthesis of substituted selenophenes.

The synthesis of 3,4-dimethylselenophene can be achieved by reacting the corresponding butadiene with either selenium powder at 450 °C[31] or selenium dioxide at 500 °C using a zeolite catalyst.[32] 3,4-Dimethoxyselenophene, which was used by Patra *et al.* in their synthesis of 3,4-ethylenedioxy-selenophene (EDOS, **Scheme 1.4**), was prepared from 2,3-dimethoxybuta-1,3-diene and freshly prepared selenium(II) chloride in a moderate yield of 42%. The advantage of this reaction is the mild conditions. No elevated temperatures are needed, it occurs at room temperature.[33]

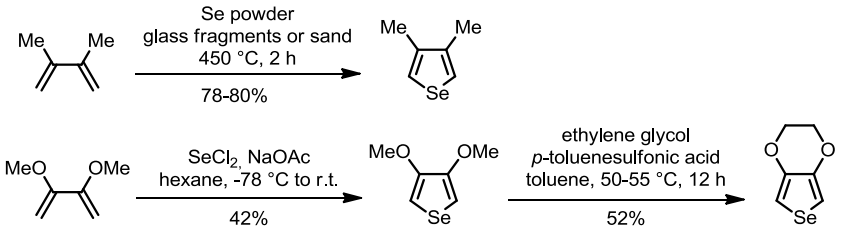

Scheme 1.4: Synthesis of 3,4-dimethylselenophene and 3,4-dimethoxyselenophene.

3,4-Disubstituted selenophenes can also be synthesized by replacing the sulfur in 3,4-disubstituted thiophenes by selenium.[34] This was achieved by oxidation of thiophene with *m*-chloroperbenzoic acid (*m*-CPBA) to the corresponding sulfone and subsequent reaction with elemental selenium at 210 °C in an autoclave. Unfortunately, the yield of the second step was relatively low (~20%).

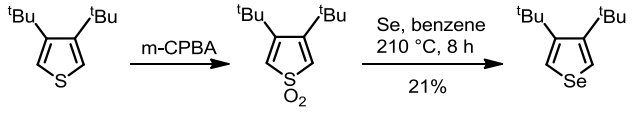

Scheme 1.5: Synthesis of 3,4-disubstituted selenophenes from the corresponding thiophenes.

Until 2010, the standard preparation method of 3-alkylselenophenes was the method published by Mahatsekake *et al.* (**Scheme 1.6**).[35] This method consists of four steps: reaction of α-chloroketones with ethynylmagnesium bromide, substitution of chlorine with sodium hydrogen selenide, ring closure with potassium hydroxide and aromatization with toluenesulfonic acid. The drawbacks of this method are the long reaction sequence and the modest overall yields of 26-52%.

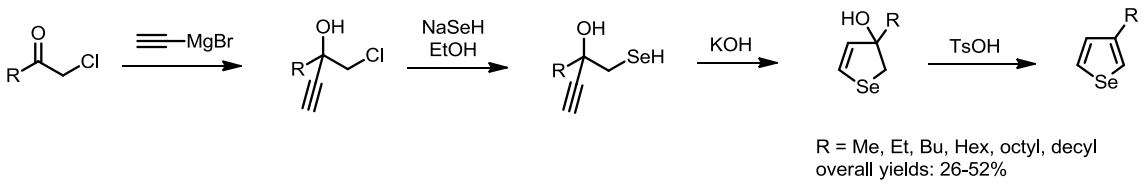

Scheme 1.6: Synthesis of 3-alkylselenophenes.

In 2010, Hollinger *et al.* published a more convenient method for the preparation of 3-hexylselenophene (**Scheme 1.7**).[36] They reacted 3-iodoselenophene, prepared from selenophene by tetraiodination and subsequent reduction of tetraiodoselenophene with zinc in acetic acid, with hexylmagnesium bromide in a Kumada cross-coupling reaction. While the Kumada reaction is a well-established method for the synthesis of 3-alkylthiophenes, this was the first example for the alkylation of selenophenes at the β-position via Kumada cross-coupling. Although the overall yield of this method is not better than that of Mahatsekake, it has one important advantage: starting from 3-iodoselenophene, different alkyl chains can be introduced without synthesizing the entire selenophene ring again.

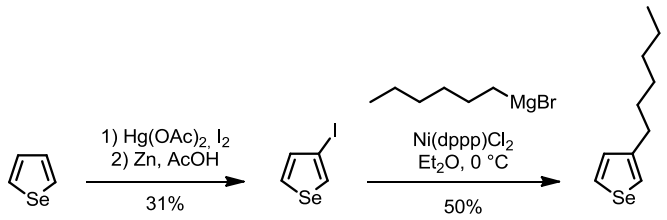

Scheme 1.7: Synthesis of 3-hexylselenophene.

Some years before, Alves *et al.* had shown that 3-alkynylselenophenes could be synthesized in good to excellent yields by a copper-free Sonogashira reaction of 3-iodoselenophenes with terminal alkynes (**Scheme 1.8**).[25, 37]

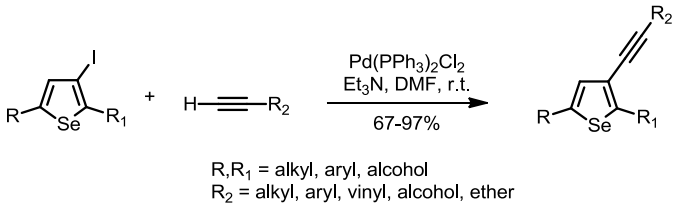

Scheme 1.8: Preparation of 3-alkynylselenophenes by Sonogashira reaction.

1.3 Polyselenophene and Selenophene-containing Copolymers

Polyselenophenes and selenophene-containing copolymers have recently been reviewed in detail by Patra/Bendikov[38] and Otsubo/Takimiya[39]. Only a short summary will be given here.

1.3.1 Polyselenophenes

Computational studies revealed that polyselenophenes should have a lower band gap, a more quinoid character and a more rigid backbone than polythiophenes. In the solid state, higher conductivities were predicted due to strong Se···Se interactions.[40]

The first preparation of polyselenophenes by electrochemical polymerization was reported in 1983.[41] In this publication, a band gap of 1.95 eV and conductivity in the doped state of 10^{-4} S cm^{-1} was determined. However, the authors described the quality of the polyselenophenes as “not too good”. Therefore, further attempts to prepare better films were made in the following ten years.[42-45] It was found that the film quality depended on the combination of solvent and electrolyte, and the conductivity was increased to $3.7 \cdot 10^{-2}$ S cm^{-1}, which was still far below typical values for polythiophenes (10-100 S cm^{-1}).[46] More recently, this value was further increased to $2.8 \cdot 10^{-1}$ S cm^{-1} by electropolymerization of selenophene in boron trifluoride diethyl etherate.[47-48] In 2008, an even higher conductivity of 2.3 S cm^{-1} was reported.[49] However, the UV-Vis spectrum of this polymer was not consistent with previously published spectra, which makes the reliability of these measurements

very doubtful. The conductivities of poly(oligoselenophenes), prepared by electrochemical polymerization of bi-, ter- and quaterselenophene, lay at about $1 \cdot 10^{-2}$ S cm^{-1}.[50] The lower conductivities of polyselenophenes compared to polythiophenes are usually ascribed to overoxidation during polymerization, resulting in poor film quality.

For the chemical polymerization of selenophene, two methods have been published: oxidative polymerization of selenophene or 2,2'-biselenophene using iron(III) chloride[51-52] or nickel-catalyzed cross-coupling of (5-bromoselenophen-2-yl)magnesium bromide.[53-54] The polyselenophene prepared from 2,2'-biselenophene showed a band gap of 1.9 eV and a conductivity of 0.1 S cm^{-1} in the doped state.[52] Very recently, the synthesis of polyselenophene by oxidative vapor deposition of selenophene was reported, and an optical band gap of 1.72 eV was determined.[55]

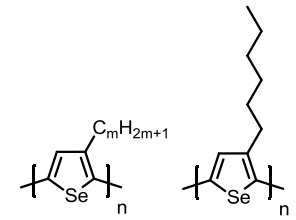

Figure 1.2: Various poly(3-alkylselenophene).

In order to obtain more soluble polyselenophenes, various 3-alkylselenophenes have been electropolymerized (**Figure 1.2**).[56-59] While the conductivities of these polymers lay in the range of 10^{-3} S cm^{-1}, they were later improved to > 1 S cm^{-1} by electropolymerization under more controlled conditions.[60-61] Especially regioregular poly(3-hexylselenophene) (**P3HS**), which was first synthesized by Grignard metathesis of 2,5-dibromo-3-hexylselenophene in 2007, has been studied intensively in the last few years.[62] The polymer showed an absorption maximum at 499 nm in chlorobenzene solution and at 630 nm in the solid state. Thus, the absorption of **P3HS** is bathochromically shifted by 40 nm in solution and 80 in the solid state compared to its thiophene analog poly(3-hexylthiophene) (**P3HT**). Consequently, the optical band gap of **P3HS** (1.6 eV) is lower than that of **P3HT** (1.9 eV). Later, this polymer was used as donor material in bulk-heterojunction solar cells (BHJSC) with phenyl-C_{61}-butyric acid methyl ester ($PC_{61}BM$) as acceptor, and a power conversion efficiency (PCE) of 2.7% was obtained. Under the same conditions, **P3HT** showed a slightly higher PCE of 3.0%.[63] A BHJSC of **P3HS** with zinc oxide as acceptor showed a low PCE of only 0.4%, whereas a corresponding device with **P3HT** reached a PCE of up to 2% due to a higher open circuit voltage (V_{OC}) and short circuit current density (J_{SC}) (for a detailed explanation of important solar cell parameters, see **Chapter 2.2.2**). It was found that only the amorphous **P3HS** part of the blend film contributed to the photocurrent, while the semicrystalline domains were not photoactive.[64] In 2011, Maurano *et al.* studied the loss processes in **P3HS**/$PC_{61}BM$ blend layers using transient optical and optoelectronic

measurements and developed a model that could reproduce the experimental *J-V* curves.[65] The crystallization behavior of **P3HS** was investigated by Li *et al.* using wide angle X-ray scattering and scanning transmission electron microscopy. They found significant differences in the self-assembly and crystallization behavior of **P3HS** and **P3HT**, e.g., the formation of large nanofibres in **P3HS** films.[66] In another report, this different self-assembly behavior was used to induce phase separation in a block-copolymer of 3-hexylthiophene and 3-hexylselenophene. Spin-cast films of this block-copolymer showed a clear phase separation into **P3HT**-like and **P3HS**-like domains.[36]

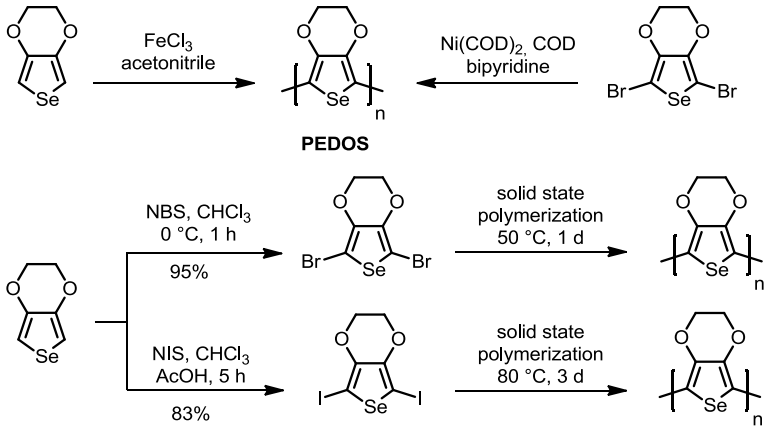

Scheme 1.9: Synthesis of poly(3,4-ethylenedioxyselenophene) (PEDOS).

Another well-studied polyselenophene is poly(3,4-ethylenedioxyselenophene) (**PEDOS**). It is the selenium analog of poly(3,4-ethylenedioxythiophene) (**PEDOT**), the most important commercially available conducting polymer, which has already found broad application in conductive and antistatic coatings for electronic devices.[67] Monomeric **EDOS** was first synthesized in 2001 via a five-step synthesis.[30] It was electropolymerized to **PEDOS** and the polymer was characterized by cyclovoltammetry. In 2008, the Bendikov group published an improved synthesis of **EDOS** in two steps starting from commercially available 2,3-dimethoxy-1,3-butadiene (**Scheme 1.4**).[33] Several methods for the chemical polymerization of **EDOS** were published (**Scheme 1.9**), e.g., oxidative polymerization with $FeCl_3$, Yamamoto-type nickel-catalyzed polymerization of dibromo-**EDOS** or solid state polymerization of dibromo- and diiodo-**EDOS**.[33] Thus, **PEDOS** with conductivities of 3-7 S cm^{-1} in the doped state was obtained, which is close to the value of similarly prepared **PEDOT**.

In the past few years, several **PEDOS**-analogous polymers (**Figure 1.3**) were synthesized by varying the heteroatom in the cyclohexane ring, introducing additional alkyl chains at the ethylene bridge or replacing the ethylene bridge by e.g. a propylene bridge.[68-71] The variation of the heteroatoms was used to tune the optical and electrochemical properties as well as the rigidity of the polymeric backbone. The introduction of alkyl side chains led to improved solubility of the polymers, resulting in better films with improved electrochromic properties and stabilities.

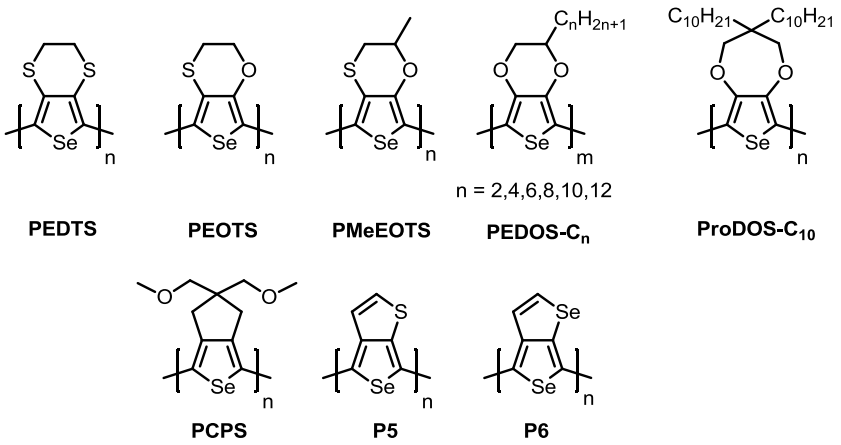

Figure 1.3: **PEDOS**-analogs and other fused ring polyselenophenes.

Poly(cyclopenta[*c*]selenophene) (**PCPS**) showed increased solubility due to the alkyl-substituted cyclopentane ring, while avoiding the sterical hindrance caused by 3,4-substitution with alkyl chains or bigger rings. Thus, the planarity of the polymer backbone was maintained.[72-73] The fused-ring polymers poly(selenolo[3,4-*b*]thiophene) (**P5**) and poly(selenolo[3,4-*b*]selenophene) (**P6**) are examples of conjugated polymers with very low band gaps (< 1 eV). The different aromaticity of thiophene and selenophene was used to control the band gap in this series of polymers.[74]

1.3.2 Selenophene-containing Copolymers

In the last 5-7 years, several selenophene-containing copolymers have been synthesized and applied in organic field effect transistors (OFET) and organic solar cells (OSC). The main reasons for the implementation of selenophenes into these polymers were the expected lower band gap due to a lowering of the LUMO and higher hole mobility due to the better polarizability of selenophene and resulting strong interchain Se···Se interactions.

The most important selenophene-copolymers applied in OFETs are shown in **Figure 1.4**. Some of them contain simple selenophene or biselenophene building blocks,[75-77] some more sophisticated building blocks such as selenolo[3,2-*b*]selenophene,[78] selenolo[3,2-*b*]thiophene,[79] or diketopyrrolo-pyrroles.[80-81] These copolymers showed good hole mobilities, sometimes exceeding those of their thiophene analogs. The *all*-selenophene copolymer **PSSS-C10**, e.g., exhibited hole and electron mobilities in the range of 0.03 $cm^2 V^{-1} s^{-1}$. These values are among the highest for solution-processed ambipolar organic semiconductors.[82] The diketopyrrolopyrrole-copolymer **PSeDPP** showed even higher hole and electron mobilities of up to 1.62 and 0.14 $cm^2 V^{-1} s^{-1}$.[80]

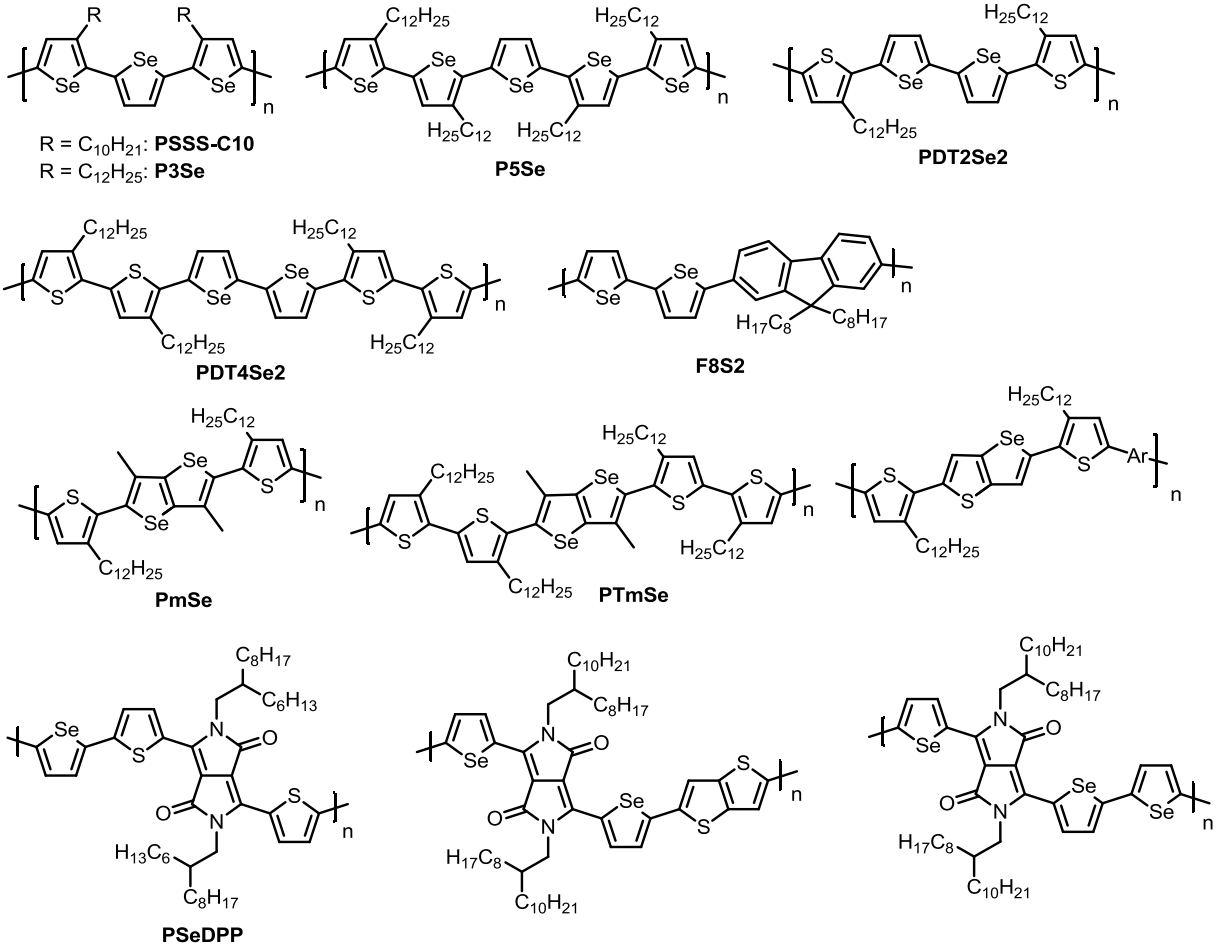

Figure 1.4: Selenophene-based copolymers applied in OFETs.

The number of selenophene-based copolymers applied in OSCs is very limited. Usually, these copolymers showed the expected lower band gaps and red-shifted absorption spectra compared to their thiophene analogs. However, when used as donor (D) materials in BHJSCs, the PCEs usually stayed below 2% and were inferior to the corresponding thiophene analogs (**Figure 1.5**).[83-87]

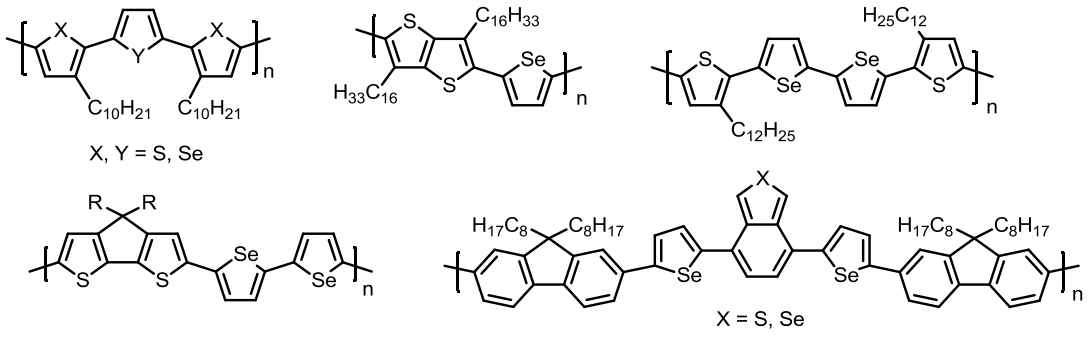

Figure 1.5: Selenophene-based copolymers applied in OSCs with PCEs lower than 2%.

Recently, efficiencies of 3% and higher were achieved, although usually with phenyl-C_{71}-butyric acid methyl ester ($PC_{71}BM$) as acceptor (A), which generally leads to higher efficiencies than $PC_{61}BM$ due

to its increased absorption in the visible region (**Figure 1.6**). In combination with $PC_{61}BM$, the two polymers **P3SDTQ** and **P3SDTDPP** showed PCEs of 0.72% (D:A ratio 1:3 w/w) and 1.85% (D:A ratio 1:1 w/w), which were similar to those of their thiophene analogs. With $PC_{71}BM$, the PCE of **P3SDTDPP** was increased to 2.81% due to a high J_{SC} of 12.33 mA cm^{-2}. Although this J_{SC} value was higher than for the corresponding thiophene polymer (J_{SC} = 10.65 mA cm^{-2}, PCE = 3.18%), the efficiency was lower because of a lower fill factor (45% vs. 56%).[88] The fluorene-selenophene-quinoxaline copolymer **PFSeQ** showed a PCE of 3.3% in a blend ratio of 1:4 w/w with $PC_{71}BM$. The corresponding device with $PC_{61}BM$ still attained a PCE of 2.4%.[89] The diketopyrrolopyrrole-selenophene-dithienothiophene co-polymer **PSeDPPDTT** showed a PCE of 4.05% in a blend with $PC_{71}BM$ (1:2 w/w), while its thiophene analog attained a higher PCE of 5.10%. Both polymers gave similar J_{SC} values (~11.5 mA cm^{-2}) but the V_{OC} of the selenophene co-polymer was by 0.1 eV lower than that of its thiophene analog due to a lower-lying LUMO energy level.[90]

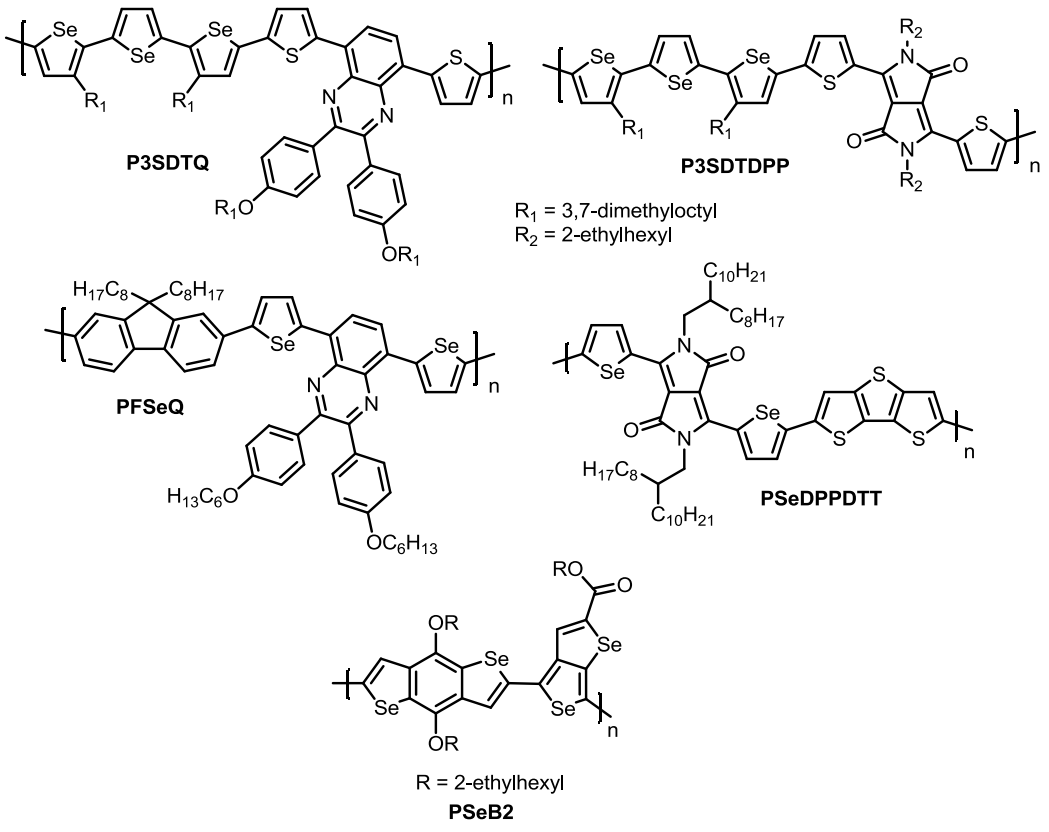

Figure 1.6: Selenophene-based copolymers applied in OSCs with PCEs higher than 2.5%.

Very recently, a PCE of 6.87% was published for the selenophene copolymer **PSeB2** as donor material in a BHJSC with $PC_{71}BM$ as acceptor (D:A ratio 1:1.2). The PCE for this copolymer was higher than for its thiophene analog (PCE = 5.66%), mainly due to a very high J_{SC} value (16.8 vs. 14.3 mA cm^{-2}).[91] To date, this efficiency is by far the highest reported value for a selenophene-based donor material in OSCs.

1.4 Oligoselenophenes

While oligothiophenes are a well-investigated class of organic semiconducting materials and have been widely applied in organic electronics,[92-93] oligoselenophenes have only rarely been studied. When searching for oligoselenophene in the literature database SciFinder, only 10 hits were displayed, whereas 2172 entries were found for the keyword "oligothiophene".[94]

The first series of oligoselenophenes were published and characterized in 1997 by Nakanishi *et al.*[50, 95] The authors synthesized a series of unsubstituted oligoselenophenes and two series of oligoselenophenes functionalized at the terminal α-positions (**Figure 1.7**). These oligomers were prepared in a linear way by Stille cross-coupling. Due to decreasing solubility with increasing chain length and resulting purification problems, the unsubstituted and α-hexyl-substituted oligoselenophenes could only be synthesized up to the pentamer. The α-1-dodecyloxytridecyl-substituted derivatives were slightly more soluble; therefore, allowing the synthesis of a hexamer in the series.

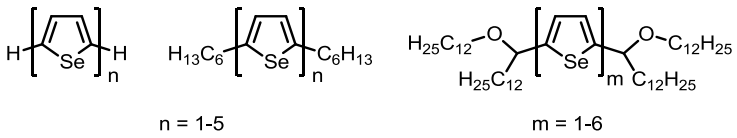

Figure 1.7: First published series of oligoselenophenes.

These oligoselenophenes exhibited higher melting points, bathochromically shifted absorption spectra ($\Delta\lambda_{max} \approx 30$ nm) and similar conductivities in the doped state compared to their thiophene analogs. Although they were characterized by UV-Vis absorption spectroscopy and cyclovoltammetry, no HOMO-LUMO energy levels or band gaps were calculated. Thus far, no further series of oligoselenophenes have been synthesized, and only some theoretical studies have been published.[40, 96-97] It was found in these studies that oligoselenophenes, similar to polyselenophenes, should have a more quinoid character, lower band gaps and a higher twisting barrier of the interring C-C bonds compared to oligothiophenes.

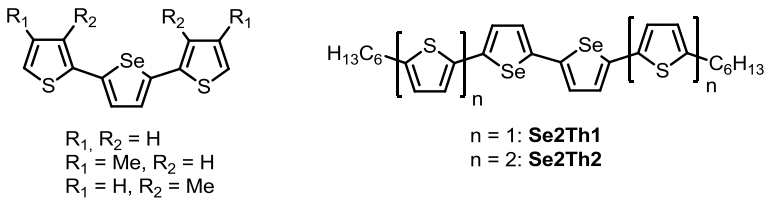

Figure 1.8: Mixed selenophene-thiophene oligomers.

Apart from pristine oligoselenophenes, some mixed thiophene-selenophene oligomers were published (**Figure 1.8**).[98-100] The biselenophene-based materials **Se2Th1** and **Se2Th2** were used in

organic thin film transistors (OTFT), and showed good hole mobilities (0.023 and 0.16 $cm^2 V^{-1} s^{-1}$) and on/off ratios of 10^5-10^6. These values are higher than for the corresponding *all*-thiophene compounds.[98]

The application of oligoselenophenes and selenophene-based small molecules in organic electronics has been limited to some rare examples. 2,2':5',2'':5'',2'''-Quaterselenophene and several other selenophene-based small molecules (**Figure 1.9**) were used as p-channel semiconducting materials for OFETs.[101-102] Quaterselenophene exhibited a hole mobility of $3.6 \cdot 10^{-3}$ $cm^2 V^{-1} s^{-1}$, which is similar to that of quaterthiophene.[103] The hole mobility of 2,6-diphenylbenzo[1,2-*b*:4,5-*b*']bis(selenophene) (**DPh-BDSe**) was even doubled compared to its thiophene counterpart (0.17 vs. 0.08 $cm^2 V^{-1} s^{-1}$), which was assigned to interactions between the heavy selenophene atoms.[104] On the other hand, the regioisomer 2,6-diphenylbenzo[1,2-*b*:5,4-*b*']bis(selenophene) (**iso-DPh-BDSe**) showed a lower mobility of 0.02 $cm^2 V^{-1} s^{-1}$ due to the less symmetrical structure, which led to the formation of less uniform films. The best hole mobilities of ~0.3 $cm^2 V^{-1} s^{-1}$ were achieved with the selenolo[3,2-*b*]-selenophene-based compounds **DNSS** and **DPh-BSBS**.[105-106]

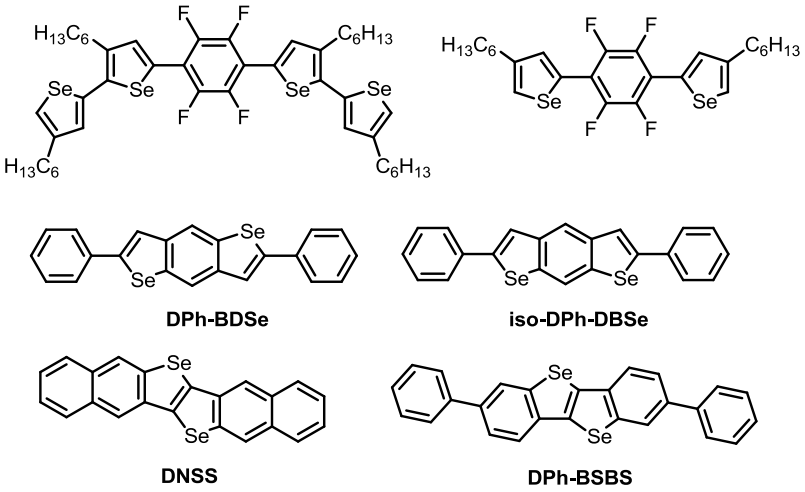

Figure 1.9: Selenophene-based small molecules for OFETs.

No oligoselenophenes longer than a biselenophene and only a handful of selenophene-based small molecules have been used in OSCs so far (**Figure 1.10**). The selenophene-substituted ruthenium complex **C105**, whose molar extinction coefficient (18,400 L mol^{-1} cm^{-1}) was slightly higher than that of its thiophene analog (17,500 L mol^{-1} cm^{-1}), was used in liquid electrolyte dye-sensitized solar cells (DSSC) and achieved high PCEs of up to 10.6%. The thiophene analog, however, exhibited a slightly higher PCE of 11.0% under the same conditions due to a higher V_{OC} and FF.[107] The selenophene-based organic sensitizers **C215** and **C216** achieved PCEs of 7.15 and 7.77% in an acetonitrile electrolyte and 6.42 and 6.60% in an ionic liquid electrolyte. Their efficiencies were marginally higher than those of their thiophene analogs ($\Delta\% < 0.2$).[108] The PCE of the organic dye **MK-49** (5.44%) was nearly

identical to the PCE of its thiophene analog (5.41%).[109] The only examples for selenophene-based materials used in heterojunction OSCs are the diketopyrrolopyrrole compounds **DPPS** and **DPPDS**. When blended with $PC_{61}BM$ in a ratio of 1:1 w/w (solvent chloroform), they exhibited PCEs of 1.53% (**DPPS)** and 0.84% (**DPPDS**). In this case, the use of $PC_{71}BM$ did not cause a significant improvement compared to $PC_{61}BM$. The lower PCE and external quantum efficiency (EQE) of **DPPDS** compared with **DPPS**, despite a much broader absorption in thin film and higher molar extinction coefficient, was ascribed to the lower hole mobility ($2 \cdot 10^{-5}$ vs. $4 \cdot 10^{-5}$ cm^2 V^{-1} s^{-1}).[110]

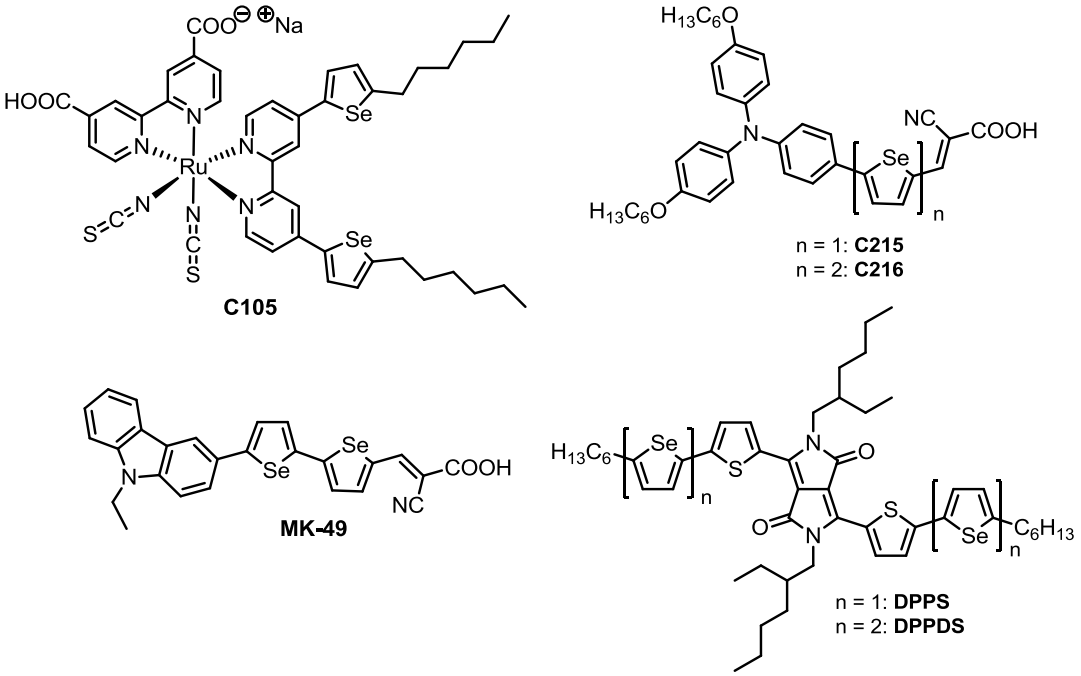

Figure 1.10: Selenophene-based compounds used in dye-sensitized and bulk-heterojunction solar cells.

1.5 Summary

In this chapter, a short overview of synthetic methods for the preparation of selenophene and its derivatives was given. Furthermore, polyselenophenes, selenophene copolymers, oligoselenophenes and their application in organic electronics was discussed. In comparison with their thiophene analogs, all these classes of selenophene-containing materials have been significantly less studied. In general, selenophene materials exhibit similar properties compared to thiophene materials, but there are examples where they outperform their thiophene counterparts. In the last two or three years, some encouraging results have been obtained, especially in the field of selenophene-based OSCs. Consequently, there is a good reason for further investigations in this field.

1.6 References

[1] *Handbook of Thiophene-Based Materials*, Eds. I. F. Perepichka, D. F. Perepichka, John Wiley & Sons Ltd, 1st edition, **2009**.

[2] J. Schatz, in *Science of Synthesis, Vol. 9*, **2000**, p. 423.

[3] A. Bondi, *J. Phys. Chem.* **1964**, *68*, 441.

[4] H. Duddeck, *Prog. Nucl. Magn. Reson. Spectrosc.* **1995**, *27*, 1.

[5] F. Fringuelli, G. Marino, A. Taticchi, G. Grandolini, *J. Chem. Soc., Perkin Trans. 2* **1974**, 332.

[6] C. W. Bird, *Tetrahedron* **1985**, *41*, 1409.

[7] C. W. Bird, *Tetrahedron* **1992**, *48*, 335.

[8] M. K. Cyranski, T. M. Krygowski, A. R. Katritzky, P. v. R. Schleyer, *J. Org. Chem.* **2002**, *67*, 1333.

[9] P. Linda, G. Marino, *J. Chem. Soc. B: Phys. Org.* **1970**, 43.

[10] S. Clementi, F. Fringuelli, P. Linda, G. Marino, G. Savelli, A. Taticchi, *J. Chem. Soc., Perkin Trans. 2* **1973**, 2097.

[11] L. I. Belen'kii, I. A. Suslov, N. D. Chuvylkin, *Chem. Heterocycl. Compd.* **2003**, *39*, 36.

[12] S. Gronowitz, A. Hallberg, T. Frejd, *Tetrahedron* **1979**, *35*, 2607.

[13] S. Gronowitz, *Phosphorus, Sulfur, Silicon Relat. Elem.* **1998**, *136*, 59.

[14] N. N. Magdesieva, A. R. Katritzky, A. J. Boulton, in *Adv. Heterocycl. Chem., Vol. Volume 12*, Academic Press, **1970**, pp. 1.

[15] A.-B. Hörnfeldt, *Adv. Heterocycl. Chem.* **1982**, *30*, 127.

[16] L. E. E. Christiaens, in *Comprehensive Heterocyclic Chemistry II, Vol. 2* (Eds.: A. R. Katritzky, C. W. Rees, E. F. V. Sriven), Elsevier, Oxford, **1996**, pp. 731.

[17] G. L. Sommen, *Mini-Rev. Org. Chem.* **2005**, *2*, 375.

[18] C. R. B. Rhoden, G. Zeni, *Org. Biomol. Chem.* **2011**, *9*, 1301.

[19] C. Paal, *Ber. Dtsch. Chem. Ges.* **1885**, *18*, 2255.

[20] F. A. McMahon, T. G. Pearson, P. L. Robinson, *J. Chem. Soc.* **1933**, 1644.

[21] S. Gronowitz, T. Frejd, A. Moberg-Ogard, L. Trege, *J. Heterocycl. Chem.* **1976**, *13*, 1319.

[22] S. Mohmand, J. Bargon, R. J. Waltman, *J. Org. Chem.* **1983**, *48*, 3544.

[23] J. Nakayama, R. Yomoda, M. Hoshino, *Heterocycles* **1987**, *26*, 2215.

[24] R. F. Curtis, S. N. Hasnain, J. A. Taylor, *Chem. Commun. (London)* **1968**, 365.

[25] D. Alves, C. Luchese, C. W. Nogueira, G. Zeni, *J. Org. Chem.* **2007**, *72*, 6726.

[26] in *Name Reactions in Heterocyclic Chemistry* (Eds.: J.-J. Li, E. J. Corey), John Wiley & Sons, Inc., **2005**, pp. 183.

[27] J. Nakayama, M. Shibuya, M. Hoshino, *Heterocycles* **1987**, *26*, 909.

[28] S. Gronowitz, A. Konar, *J. Chem. Soc., Chem. Commun.* **1977**, 163.

[29] A. Konar, S. Gronowitz, *Chem. Scripta* **1984**, *23*, 5.

[30] E. Aqad, M. V. Lakshmikantham, M. P. Cava, *Org. Lett.* **2001**, *3*, 4283.

[31] G. Barbey, G. Dian, N. Merlet, F. Outurquin, C. Paulmier, *Synthesis* **1989**, 181.

[32] E. S. Mamedov, S. B. Kurbanov, R. D. Mishiev, T. N. Shakhtakhtinskii, *Dokl. Akad. Nauk. USSR* **1978**, *34*, 41.

[33] A. Patra, Y. H. Wijsboom, S. S. Zade, M. Li, Y. Sheynin, G. Leitus, M. Bendikov, *J. Am. Chem. Soc.* **2008**, *130*, 6734.

[34] J. Nakayama, Y. Sugihara, K. Terada, E. L. Clennan, *Tetrahedron Lett.* **1990**, *31*, 4473.

[35] C. Mahatsekake, J. M. Catel, C. G. Andrieu, M. E. Et, Y. Mollier, G. Tourillon, *Phosphorus, Sulfur, Silicon Relat. Elem.* **1990**, *47*, 35.

[36] J. Hollinger, A. A. Jahnke, N. Coombs, D. S. Seferos, *J. Am. Chem. Soc.* **2010**, *132*, 8546.

[37] D. Alves, J. S. d. Reis, C. Luchese, C. W. Nogueira, G. Zeni, *Eur. J. Org. Chem.* **2008**, *2008*, 377.

[38] A. Patra, M. Bendikov, *J. Mater. Chem.* **2010**, *20*, 422.

[39] T. Otsubo, K. Takimiya, in *Handbook of Thiophene-Based Materials* (Eds.: I. F. Perepichka, D. F. Perepichka), Wiley-VCH, Chichester, UK, **2009**.

[40] S. S. Zade, N. Zamoshchik, M. Bendikov, *Chem. Eur. J.* **2009**, *15*, 8613.

[41] K. Yoshino, K. Kaneto, S. Inoue, K. Tsukagoshi, *Jpn. J. Appl. Phys.* **1983**, *22*, L701.

[42] K. Yoshino, Y. Kohno, T. Shiraishi, K. Kaneto, S. Inoue, K. Tsukagoshi, *Synth. Met.* **1985**, *10*, 319.

[43] G. Dian, G. Barbey, B. Decroix, *Synth. Met.* **1986**, *13*, 281.

[44] S. Glenis, D. S. Ginley, A. J. Frank, *J. Appl. Phys.* **1987**, *62*, 190.

[45] C. Chorro, B. Moukala, J.-P. Lere-porte, J. Petrissans, *Mol. Cryst. Liq. Cryst.* **1990**, *187*, 199.

[46] *Handbook of Conducting Polymers*, Eds. T. A. Skotheim, J. R. Reynolds, CRC Press: Taylor & Francis Group, Boca Raton, 3rd edition, **2007**.

[47] S. Pu, J. Hou, J. Xu, G. Nie, S. Zhang, L. Shen, Q. Xiao, *Mater. Lett.* **2005**, *59*, 1061.

[48] J. Xu, J. Hou, S. Zhang, G. Nie, S. Pu, L. Shen, Q. Xiao, *J. Electroanal. Chem.* **2005**, *578*, 345.

[49] B. Dong, Y. Xing, J. Xu, L. Zheng, J. Hou, F. Zhao, *Electrochim. Acta* **2008**, *53*, 5745.

[50] S. Inoue, H. Nakanishi, K. Takimiya, Y. Aso, T. Otsubo, *Synth. Met.* **1997**, *84*, 341.

[51] R.-i. Sugimoto, K. Yoshino, S. Inoue, K. Tsukagoshi, *Jpn. J. Appl. Phys.* **1985**, *24*, L425.

[52] T.-T. Ong, S.-C. Ng, H. S. O. Chan, *Polymer* **2003**, *44*, 5597.

[53] M. D. Bezoari, P. Kovacic, S. Gronowitz, A.-B. Hörnfeldt, *J. Polym. Sci., Polym. Lett. Ed.* **1981**, *19*, 347.

[54] J. P. Montheard, T. Pascal, G. Seytre, G. Steffan-Boiteux, A. Douillard, *Synth. Met.* **1984**, *9*, 389.

[55] D. Bhattacharyya, K. K. Gleason, *J. Mater. Chem.* **2012**, *22*, 405.

[56] A. Bourahla, J. M. Saiter, C. Vautier, *Mater. Chem. Phys.* **2001**, *69*, 163.

[57] N. Merlet, G. Dian, G. Barbey, F. Outurquin, C. Paulmier, *Synth. Met.* **1988**, *24*, 77.

[58] K. Yoshino, M. Onoda, Y. Manda, K. Sawada, R.-i. Sugimoto, S. Inoue, *Jpn. J. Appl. Phys.* **1989**, *28*, 138.

[59] G. Dian, N. Merlet, G. Barbey, F. Outurquin, C. Paulmier, *J. Electroanal. Chem. Interf. Electrochem.* **1987**, *238*, 225.

[60] C. Mahatsekake, J. M. Catel, C. G. Andrieu, M. E. Et, Y. Mollier, G. Tourillon, *Phosphorus, Sulfur, Silicon Rel. Elem.* **1990**, *47*, 35

[61] G. Tourillon, E. Dartyge, D. Guay, C. Mahatsekake, C. G. Andrieu, S. Bernstorff, W. Braun, *J. Electrochem. Soc.* **1990**, *137*, 1827.

[62] M. Heeney, W. Zhang, D. J. Crouch, M. L. Chabinyc, S. Gordeyev, R. Hamilton, S. J. Higgins, I. McCulloch, P. J. Skabara, D. Sparrowe, S. Tierney, *Chem. Commun.* **2007**, 5061.

[63] A. M. Ballantyne, L. Chen, J. Nelson, D. D. C. Bradley, Y. Astuti, A. Maurano, C. G. Shuttle, J. R. Durrant, M. Heeney, W. Duffy, I. McCulloch, *Adv. Mater.* **2007**, *19*, 4544.

[64] S. D. Oosterhout, M. M. Wienk, M. Al-Hashimi, M. Heeney, R. A. J. Janssen, *J. Phys. Chem. C* **2011**, *115*, 18901.

[65] A. Maurano, C. G. Shuttle, R. Hamilton, A. M. Ballantyne, J. Nelson, W. Zhang, M. Heeney, J. R. Durrant, *J. Phys. Chem. C* **2011**, *115*, 5947.

[66] L. Li, J. Hollinger, A. A. Jahnke, S. Petrov, D. S. Seferos, *Chem. Sci.* **2011**, *2*, 2306.

[67] K. Reuter, S. Kirchmeyer, A. Elschner, in *Handbook of Thiophene-Based Materials* (Eds.: I. F. Perepichka, D. F. Perepichka), John Wiley & Sons, Ltd, **2009**, pp. 549.

[68] M. I. Ozkut, S. Atak, A. M. Onal, A. Cihaner, *J. Mater. Chem.* **2011**, *21*, 5268.

[69] Y. H. Wijsboom, Y. Sheynin, A. Patra, N. Zamoshchik, R. Vardimon, G. Leitus, M. Bendikov, *J. Mater. Chem.* **2011**, *21*, 1368.

[70] Y. H. Wijsboom, A. Patra, S. S. Zade, Y. Sheynin, M. Li, L. J. W. Shimon, M. Bendikov, *Angew. Chem.* **2009**, *121*, 5551; *Angew. Chem. Int. Ed.* **2009**, *48*, 5443.

[71] M. Li, Y. Sheynin, A. Patra, M. Bendikov, *Chem. Mater.* **2009**, *21*, 2482.

[72] S. Das, A. Bedi, G. R. Krishna, C. M. Reddy, S. S. Zade, *Org. Biomol. Chem.* **2011**, *9*.

[73] S. Das, S. S. Zade, *Chem. Commun.* **2010**, *46*, 1168.

[74] A. Patra, Y. H. Wijsboom, G. Leitus, M. Bendikov, *Chem. Mater.* **2011**, *23*, 896.

[75] H. Kong, D. S. Chung, I.-N. Kang, J.-H. Park, M.-J. Park, I. H. Jung, C. E. Park, H.-K. Shim, *J. Mater. Chem.* **2009**, *19*, 3490.

[76] Y. M. Kim, E. Lim, I.-N. Kang, B.-J. Jung, J. Lee, B. W. Koo, L.-M. Do, H.-K. Shim, *Macromolecules* **2006**, *39*, 4081.

[77] D. Khim, W.-H. Lee, K.-J. Baeg, D.-Y. Kim, I.-N. Kang, Y.-Y. Noh, *J. Mater. Chem.* **2012**, DOI: 10.1039/c2jm16546e.

[78] H. Kong, Y. K. Jung, N. S. Cho, I.-N. Kang, J.-H. Park, S. Cho, H.-K. Shim, *Chem. Mater.* **2009**, *21*, 2650.

[79] S. P. Mishra, A. E. Javier, R. Zhang, J. Liu, J. A. Belot, I. Osaka, R. D. McCullough, *J. Mater. Chem.* **2011**, *21*, 1551.

[80] H.-W. Lin, W.-Y. Lee, W.-C. Chen, *J. Mater. Chem.* **2012**, *22*, 2120.

[81] M. Shahid, T. McCarthy-Ward, J. Labram, S. Rossbauer, E. B. Domingo, S. E. Watkins, N. Stingelin, T. D. Anthopoulos, M. Heeney, *Chem. Sci.* **2012**, *3*, 181.

[82] Z. Chen, H. Lemke, S. Albert-Seifried, M. Caironi, M. M. Nielsen, M. Heeney, W. Zhang, I. McCulloch, H. Sirringhaus, *Adv. Mater.* **2010**, *22*, 2371.

[83] D. S. Chung, H. Kong, W. M. Yun, H. Cha, H.-K. Shim, Y.-H. Kim, C. E. Park, *Org. Electron.* **2010**, *11*, 899.

[84] T. M. Clarke, A. M. Ballantyne, S. Tierney, M. Heeney, W. Duffy, I. McCulloch, J. Nelson, J. R. Durrant, *J. Phys. Chem. C* **2010**, *114*, 8068.

[85] S. K. Lee, N. S. Cho, S. Cho, S.-J. Moon, J. K. Lee, G. C. Bazan, *J. Polym. Sci. Part A: Polym. Chem.* **2009**, *47*, 6873.

[86] W.-H. Lee, S. K. Lee, S. K. Son, J.-E. Choi, W. S. Shin, K. Kim, S.-H. Lee, S.-J. Moon, I.-N. Kang, *J. Polym. Sci. Part A, Polym. Chem.* **2012**, *50*, 551.

[87] F. Qiao, X. Hou, Y. Lu, H. Chen, A. Liu, X. Hu, N. Siu Choon, *Sol. Energy Mater. Sol. Cells* **2010**, *94*, 442.

[88] W.-H. Lee, S. K. Son, K. Kim, S. K. Lee, W. S. Shin, S.-J. Moon, I.-N. Kang, *Macromolecules* **2012**, *45*, 1303.

[89] J.-Y. Lee, S.-H. Kim, I.-S. Song, D.-K. Moon, *J. Mater. Chem.* **2011**, *21*, 16480.

[90] M. Shahid, R. S. Ashraf, Z. Huang, A. J. Kronemeijer, T. McCarthy-Ward, I. McCulloch, J. R. Durrant, H. Sirringhaus, M. Heeney, *J. Mater. Chem.* **2012**, DOI: 10.1039/c2jm31189e.

[91] H. A. Saadeh, L. Lu, F. He, J. E. Bullock, W. Wang, B. Carsten, L. Yu, *ACS Macro Lett.* **2012**, 361.

[92] A. Mishra, C.-Q. Ma, P. Bäuerle, *Chem. Rev.* **2009**, *109*, 1141.

[93] A. Mishra, C.-Q. Ma, J. L. Segura, P. Bäuerle, in *Handbook of Thiophene-Based Materials* (Eds.: I. F. Perepichka, D. F. Perepichka), John Wiley & Sons, Ltd, **2009**, pp. 1.

[94] Search date: 16/04/2012.

[95] H. Nakanishi, S. Inoue, T. Otsubo, *Mol. Cryst. Liq. Cryst.* **1997**, *296*, 335.

[96] S. S. Zade, M. Bendikov, *Chem. Eur. J.* **2008**, *14*, 6734.

[97] S. S. Zade, N. Zamoshchik, M. Bendikov, *Acc. Chem. Res.* **2011**, *44*, 14.

[98] N. S. Cho, S. K. Lee, J. H. Seo, M. Elbing, J. D. Azoulay, J. Park, S. Cho, A. J. Heeger, G. C. Bazan, *J. Mater. Chem.* **2008**, *18*, 4909.

[99] R. Shabana, A. Galal, H. B. Mark, H. Zimmer, S. Gronowitz, A. B. Hörnfeldt, *Phosphorus, Sulfur, Silicon Relat. Elem.* **1990**, *48*, 239.

[100] H. Zimmer, R. Shabana, A. Galal, H. B. Mark, S. Gronowitz, A. B. Hörnfeldt, *Phosphorus, Sulfur, Silicon Relat. Elem.* **1989**, *42*, 171.

[101] K. Takimiya, Y. Kunugi, T. Otsubo, *Chem. Lett.* **2007**, *36*, 578.

[102] K. Takimiya, T. Otsubo, *Phosphorus, Sulfur, Silicon Relat. Elem.* **2005**, *180*, 873.

[103] Y. Kunugi, K. Takimiya, K. Yamane, K. Yamashita, Y. Aso, T. Otsubo, *Chem. Mater.* **2002**, *15*, 6.

[104] K. Takimiya, Y. Konda, H. Ebata, T. Otsubo, Y. Kunugi, *Mol. Cryst. Liq. Cryst.* **2006**, *455*, 361.

[105] K. Takimiya, Y. Kunugi, Y. Konda, H. Ebata, Y. Toyoshima, T. Otsubo, *J. Am. Chem. Soc.* **2006**, *128*, 3044.

[106] T. Yamamoto, K. Takimiya, *J. Am. Chem. Soc.* **2007**, *129*, 2224.

[107] F. Gao, Y. Cheng, Q. Yu, S. Liu, D. Shi, Y. Li, P. Wang, *Inorg. Chem.* **2009**, *48*, 2664.

[108] R. Li, X. Lv, D. Shi, D. Zhou, Y. Cheng, G. Zhang, P. Wang, *J. Phys. Chem. C* **2009**, *113*, 7469.

[109] S. Tamba, R. Fujii, A. Mori, K. Hara, N. Koumura, *Chem. Lett.* **2011**, *40*, 922.

[110] K. A. Mazzio, M. Yuan, K. Okamoto, C. K. Luscombe, *ACS Appl. Mater. Interf.* **2011**, *3*, 271.

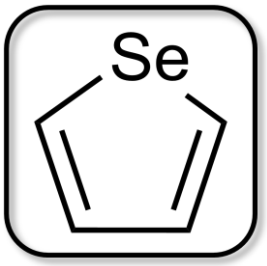

CHAPTER 2

ORGANIC SOLAR CELLS

2.1 Introduction

The world's energy consumption is constantly growing from year to year. To satisfy this hunger for energy without further accelerating global warming, it is inevitable to replace fossil energy sources by renewable energy sources such as wind, sun and biomass. At the moment, 18% of the total energy production in Germany is based on renewable energy sources. The biggest fraction of these 18% is produced by wind and biomass, only ~20% by solar energy. In total, about 4% of the electric energy in Germany is produced by solar technology.[1] However, solar energy is the fastest growing technology in this field and will play a more and more important role in the future.

To date, photovoltaic devices are usually based on inorganic semiconductors. In the last twenty years, the progress of this technology has been enormous and remarkable power conversion efficiencies (PCE) have been achieved. At the moment, the efficiencies of laboratory devices based on silicon are in the range of 20-25%, thin film GaAs devices reach PCEs of ~28%, and the PCEs of multijunction GaInP/GaInAs/Ge devices are higher than 34%. When the materials are used in commercially relevant modules, the efficiencies are lower but still in the range of 18-24%.[2]

The PCEs of solar cells based on organic semiconductors are generally lower due to the fundamentally different conduction mechanisms in organic semiconductors. According to their fundamental functional principles, organic solar cells (OSC) can be divided into two groups: dye-sensitized solar cells (DSSC) and organic thin film solar cells.[3] The second group can be further divided into planar heterojunction and bulk-heterojunction solar cells based on both, polymers and small molecules. The certified record efficiency for DSSCs is 12.3%.[4] For organic thin film solar cells, it has just passed the 10% threshold in the beginning of 2012, with a reported certified efficiency of 10.6% for a polymer tandem solar cell.[5] In April 2012, Heliatek released an even higher record value of 10.7% for a small molecule tandem solar cell.[6]

At the moment, organic photovoltaics is on the verge of commercialization. Some first products and modules based on polymer solar cells are available from, e.g., Konarka[7] and Solarmer,[8] while first DSSC-based products can be purchased from, e.g., Samsung[9] and G24 Innovations.[10] In March 2012, Heliatek inaugurated the first roll-to-roll production line for the fabrication of vacuum-processed small molecule tandem cells.[11]

2.2 Organic Thin Film Solar Cells

2.2.1 Fundamental Principles

The generally lower power conversion efficiencies of OSC compared to inorganic solar cells are a consequence of the different charge transport mechanisms. In an inorganic solar cell absorbed photons excite electrons from the valence band into the conduction band, leaving behind so-called "holes" in the conduction band. The charge carriers can move freely with relatively high mobilities. In an organic semiconductor molecule, the absorption of a photon leads to the excitation of an electron from the highest occupied molecular orbital (HOMO) into the lowest unoccupied molecular orbital (LUMO). Thus, an exciton, a closely bound electron-hole pair, is formed. In order to create free charge carriers, these excitons need to dissociate into electrons and holes. To overcome the typical exciton binding energies of 0.2 to 0.5 eV,[12-14] an electric field of > 10^6 V cm^{-1} would be necessary. Due to the low dielectric constants of organic semiconductors, this value is usually not reached in these materials.[15-17] Therefore, the exciton must diffuse to a heterointerface between two materials with different electron affinities. The simplest devices, so-called Schottky diodes, consist of an organic semiconductor sandwiched between two metals with different work functions. However, the PCEs of these devices are typically very low (< 0.1%)[18-20] because the excitons are not only dissociated into charge carriers at the electrodes, but the latter are also efficiently quenched there.[21] To overcome this problem, Tang used a bilayer of two different organic materials, one acting as electron donor (copper phthalocyanine), the other as electron acceptor (a perylene derivative).[22] In this seminal work from 1986, a PCE of 1% was obtained with this cell architecture. The schematic build-up of such a bilayer or planar heterojunction (PHJ) device is shown in **Figure 2.1**.

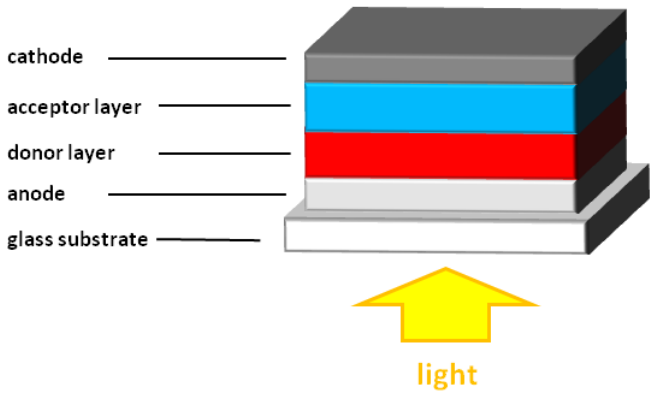

Figure 2.1: Device architecture of a PHJ solar cell.

On a glass substrate covered with a (semi)transparent anode, usually a conducting metal oxide like indium-doped tin oxide (ITO), first a donor (D) layer and then an acceptor (A) layer is deposited. The deposition can be carried out by successive vacuum sublimation of both components, solution-

processing of one component and sublimation of the second or solution-processing of both components using orthogonal solvents. Usually a thin metal layer, e.g., aluminum or gold, is used as top electrode. The working principle of such a bilayer device is depicted in **Figure 2.2**. The fundamental steps are as follows: (a) Excitation of an electron from the HOMO into the LUMO upon absorption of a photon and formation of an exciton. (b) Diffusion of the exciton to the donor/acceptor interface. (c) Charge separation into an electron and a hole and formation of a charge transfer state also called "geminate pair". (d) Charge transport of electrons to the cathode and holes to the anode and charge collection at the electrodes.[16, 23-24]

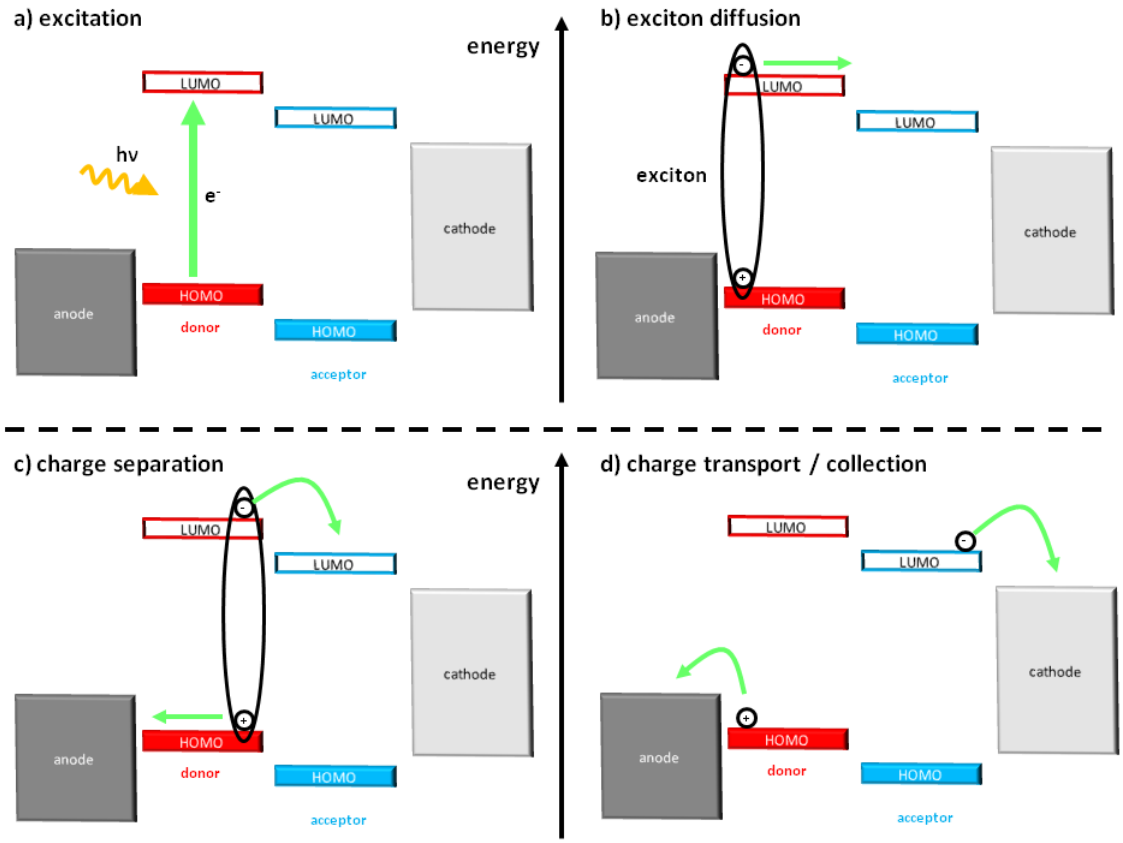

Figure 2.2: Fundamental processes occurring upon photoexcitation of an organic solar cell.

The number of generated charges that are collected at the electrodes determines the electric current that an OSC can produce. Thus, the overall current efficiency η_j depends on the photon absorption efficiency η_A, the exciton diffusion efficiency η_D, the charge transfer efficiency η_{CT} and the charge collection efficiency η_{CC} (equation 2.1).[17]

$$\eta_j = \eta_A \times \eta_D \times \eta_{CT} \times \eta_{CC} \quad (2.1)$$

η_A is determined by the absorption spectrum, the absorption coefficient and the layer thickness of the absorbing material. η_D is proportional to the exciton diffusion length, while η_{CT} depends on the energy offset between the LUMO energy levels of donor and acceptor. For efficient dissociation, this

energy offset should be about 0.3-0.4 eV.[13, 25] Finally, η_{CC} depends on how charge carriers are transported and collected at the electrodes.[16-17] Typical loss mechanisms in the last step are the recombination of not completely separated geminate pairs and bimolecular recombination of free charge carriers.[26]

In order to absorb more photons and to avoid shorts and recombinations, it would be beneficial to increase the layer thickness of the photoactive layer. However, the layer thickness is limited by the exciton diffusion length L_D because excitons must be able to reach the donor/acceptor interface to dissociate into free charges. Exciton diffusion lengths of organic semiconductors are usually in the range of 5-50 nm.[24, 27-28] If the donor or acceptor layer is thicker than this length, only excitons that are closer to the heterointerface than their diffusion length can dissociate into free charges and contribute to the photocurrent. The other excitons recombine before they reach the interface. To overcome this limitation, the bulk-heterojunction (BHJ) concept was developed.[29-30] In this solar cell architecture, the separate donor and acceptor layers are replaced by a blend layer of donor and acceptor (**Figure 2.3)**. This layer must form a bicontinuous interpenetrating network of donor and acceptor domains with percolation pathways allowing charge transport to the electrodes. Thus, the donor/acceptor interface is largely increased and the excitons only have to travel a small distance (usually smaller than L_D) before reaching the heterointerface. The ideal width of the phases is generally considered to be in the order of $2L_D$, so that excitons generated in the center of the respective domain can still reach the heterointerface and dissociate there.[17] As a consequence, control of the morphology and phase separation of the blend layer is of crucial importance for the overall performance of a BHJ solar cell. The morphology can be influenced by various factors such as solvent, additives, deposition method, temperatures etc.[31-34]

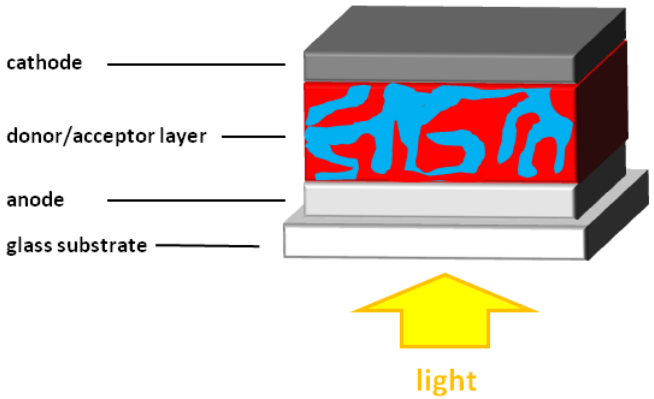

Figure 2.3: Device architecture of a BHJ solar cell.

State-of-the-art developments in the field of PHJ and BHJ solar cells will be presented in sections **2.2.3** and **2.2.4**, but firstly, a short overview of typical parameters for the characterization of solar cells will be given.

2.2.2 Characterization of Solar Cells

In the simplest model, a photovoltaic device can be considered as a diode connected in parallel with a current source simulating the photocurrent. In the dark, the device works as a diode; under illumination, the total current I is given as the difference of the photocurrent (I_{ph}) and the diode current (I_D) (equation 2.2).[35]

$$I = I_{ph} - I_D = I_{ph} - I_0\left(e^{\frac{qV}{nk_BT}} - 1\right) \quad (2.2)$$

I_0 is the saturation current of the diode, q is the elementary charge, V is the measured cell voltage, n is the ideality factor of the diode (typically between 1 and 2), k_B is the Boltzmann constant and T the cell temperature. This model completely neglects all occurring resistances in a real device. They can be modeled by an additional series resistor (R_s) and shunt resistor (R_{sh}). This leads to the equivalent circuit shown in **Figure 2.4**. The series resistance accounts for contact resistances at metal-material interfaces and ohmic losses due to bulk resistivity of the material, whereas the shunt resistance models leakage currents, e.g., due to recombination or pinholes.[35]

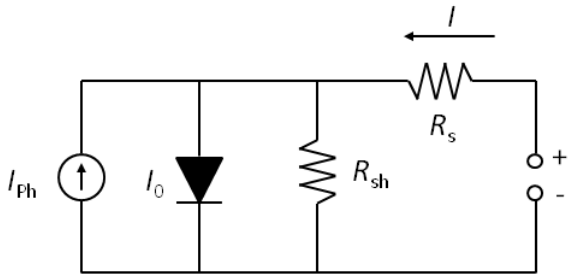

Figure 2.4: Equivalent circuit for a solar cell.

The total current I is now given by equation 2.3.

$$I = I_{ph} - I_D - I_{sh} = I_{ph} - I_0\left(e^{\frac{qV_j}{nkT}} - 1\right) - \frac{V_j}{R_{sh}} \quad (2.3)$$

V_j is the voltage across the junction, given by the difference between the cell voltage V and the voltage across the series resistance represented by R_sI. When replacing V_j by $V - R_sI$, equation 2.4 is obtained.

$$I = I_{ph} - I_0\left(e^{\frac{q(V-R_sI)}{nkT}} - 1\right) - \frac{V-R_sI}{R_{sh}} \quad (2.4)$$

In a first approximation, this equation describes the current-voltage (*I-V*) curves of photovoltaic devices quite well. Typical *I-V* curves for a solar cell in the dark (blue line) and under illumination (red line) are depicted in **Figure 2.5**. For better comparability, *I-V* curves are usually measured under

standard illumination conditions. The most common standard is called “air mass 1.5 global” (AM 1.5G), simulating the solar spectrum on the ground when the sun is at a zenith angle of 48.2° with a radiation intensity of 100 mW cm^{-2} at a temperature of 25 °C.[35]

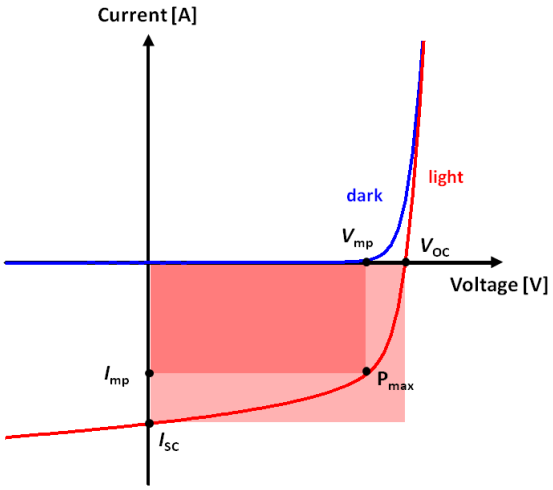

Figure 2.5: *I-V* curve for a solar cell with important characterization parameters.

From the *I-V* curve under illumination, important parameters for the characterization of solar cells can be derived. Those parameters are defined as follows:

The **short circuit current I_{SC}** is the current measured under short circuit conditions, i.e., when the voltage is 0. I_{SC} is the current value at the y-intercept of the *I-V* curve. For an ideal cell, I_{SC} is the maximum current produced by photoexcitation. It is dependent on the cell area, the light intensity, the device thickness, the absorption range and extinction coefficient of the absorber material as well as charge transport.[36]

The **short circuit current density** (J_{SC}) is defined as short circuit current I_{SC} divided by the cell area A.

The **open circuit voltage** (V_{OC}) is the voltage measured when $I = 0$, i.e., no current is passing through the cell. V_{OC} is the voltage value at the interception point of the *I-V* curve with the x-axis. It is the maximum voltage produced by the solar cell under ideal conditions. V_{OC} is mainly determined by the energy difference between the LUMO of the acceptor and the HOMO of the donor,[25, 37-38] but in certain device architectures it can also be dependent on the work function difference of the electrodes.[39-40]

The power which is produced by the solar cell is given by the product of current and voltage. It corresponds to the area under the *I-V* curve. At the interception points with the axes, which determine I_{SC} and V_{OC}, the power is zero. At a certain point on the curve in between, the product of current and voltage reaches a maximum called **maximum power** P_{max}. The current and voltage at this point are denoted as I_{mp} and V_{mp}.[16]

The **fill factor** (FF) is a criterion for the quality of a solar cell. It is defined as the ratio of the maximum power P_{max} to the theoretical power P_T, which is calculated by multiplying I_{SC} and V_{OC} (equation 2.5).[36]

$$FF = \frac{P_{max}}{P_T} = \frac{V_{mp}I_{mp}}{V_{OC}I_{SC}} \quad (2.5)$$

The FF can be interpreted graphically as the ratio of the dark red and light red rectangles in **Figure 2.5**. The more "rectangular" the *I-V* curve, the higher the fill factor and the better the power conversion efficiency. The shape of the *I-V* curve is strongly influenced by the series and shunt resistance. The series resistance corresponds to the reciprocal slope of the tangent at $I = 0$ (equation 2.6).

$$R_s = \left(\frac{dV}{dI}\right)_{I=0} \quad (2.6)$$

The shunt resistance is represented by the reciprocal slope of the tangent at $V = 0$ (equation 2.7).

$$R_{sh} = \left(\frac{dV}{dI}\right)_{V=0} \quad (2.7)$$

If R_s was zero (no contact losses at the layer interfaces) and R_{sh} was infinite (no losses due to charge recombination), the *I-V* curve would be perfectly rectangular.[41]

The **power conversion efficiency** (PCE or η) is the quotient of the electrical power output P_{out} and power input by incident light (P_{in}). In order to calculate the maximum power conversion efficiency, P_{max} can be used instead of P_{out} (equation 2.8).[16]

$$\mathrm{PCE} = \eta = \frac{P_{out}}{P_{in}} = \frac{P_{max}}{P_{in}} = \frac{V_{OC}I_{SC}FF}{P_{in}} \quad (2.8)$$

This equation shows that η is directly proportional to V_{OC}, I_{SC}, and FF. Consequently, all these factors should be maximized in order to obtain high efficiencies.

The **external quantum efficiency** (EQE) or **incident photon-to-current efficiency** (IPCE) is defined as ratio of the number of collected charges to the number of incident photons at a certain wavelength (equation 2.10).[42]

$$EQE(\lambda) = IPCE(\lambda) = \frac{number\ of\ collected\ charges}{number\ of\ incident\ photons} \quad (2.10)$$

If EQE = 1, every absorbed photon at a certain wavelength feeds one electron into the electric circuit.

2.2.3 Planar Heterojunction Solar Cells

Planar heterojunction organic solar cells are usually constructed by subsequent vacuum sublimation of the different components. Since polymers cannot be sublimed, small molecule or oligomeric donor and acceptor materials are generally used in this type of solar cells. The most commonly used acceptor is fullerene C_{60}. It can be reversibly reduced by up to six electrons, and the photoinduced electron transfer from the donor to C_{60} is by orders of magnitudes faster than the back electron transfer.[42] The best-studied and most frequently used donors are squaraines,[43-44] perylene derivatives,[45] phthalocyanines,[46] and functionalized oligothiophenes.[47]

At present, the highest achieved PCE with a PHJ device is 5.7%. This cell contained a donor layer of squaraine-based donor **1-NPSQ** (**Figure 2.6**), annealed at 90 °C, and C_{60} as acceptor.[48] At this optimized temperature, a V_{OC} of 0.90 V, a J_{SC} of 10.0 mA cm^{-2}, and a FF of 0.64 was obtained. The perylene derivative **DBP**, in combination with C_{60} as acceptor and an exciton blocking layer consisting of a triphenylamine derivative, gave an efficiency of 5.25% with a very high FF of 0.77 and a high V_{OC} of 0.94 V. J_{SC}, however, was relatively moderate (7.25 mA cm^{-2}), thus limiting the overall efficiency.[49] The best oligothiophene donor material used in PHJ solar cells is **DCV5T-Bu**. In combination with C_{60}, it showed a PCE of 4.0%, with high J_{SC} (11.4 mA cm^{-2}) and V_{OC} (1.00 V) values and a moderate FF of 0.50. For the calculation of the PCE, a spectral mismatch of ~0.7 was taken into account.[50]

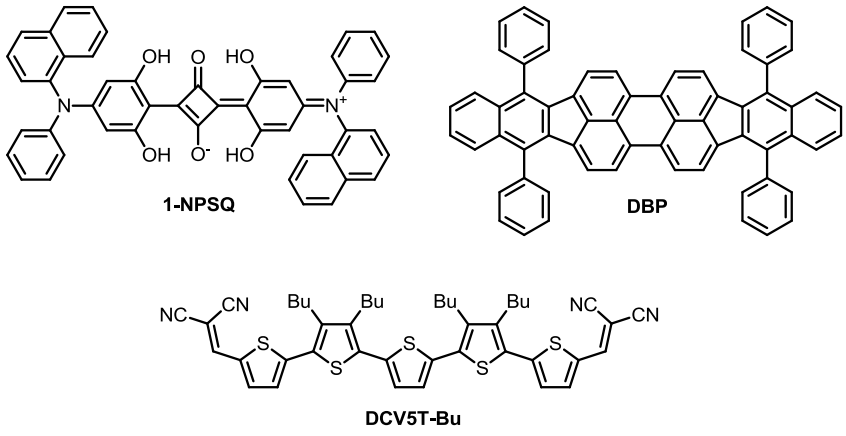

Figure 2.6: Donor materials for PHJ solar cells with efficiencies over 4%.

Due to the already mentioned limitations of the PHJ concept, especially concerning the exciton diffusion length, the research in the field of organic thin film solar cells has been focused more and more on BHJ devices in the last few years.

2.2.4 Bulk-Heterojunction Solar Cells

Bulk-heterojunction solar cells can be processed from solution and by vacuum sublimation. For solution-processing, donor and acceptor are dissolved together in one solvent and deposited by various techniques such as spin casting, doctor blading or inkjet printing.[51] In the beginning, solution-processing was mainly applied for polymer solar cells, but more recently, it has also been proven to be a suitable method for the preparation of efficient small molecule organic solar cells (SMOSC).[52] In the field of SMOSCs, BHJ devices are also fabricated by co-evaporation of donor and acceptor materials. A detailed overview of solution and vacuum-processed SMOSCs can be found in a recent review by Mishra and Bäuerle.[47] Several reviews on polymer BHJ devices have appeared, some giving a general overview,[23, 34, 53] others dealing with the rational design of novel polymers[54-55] and future perspectives for this technology.[56-57]

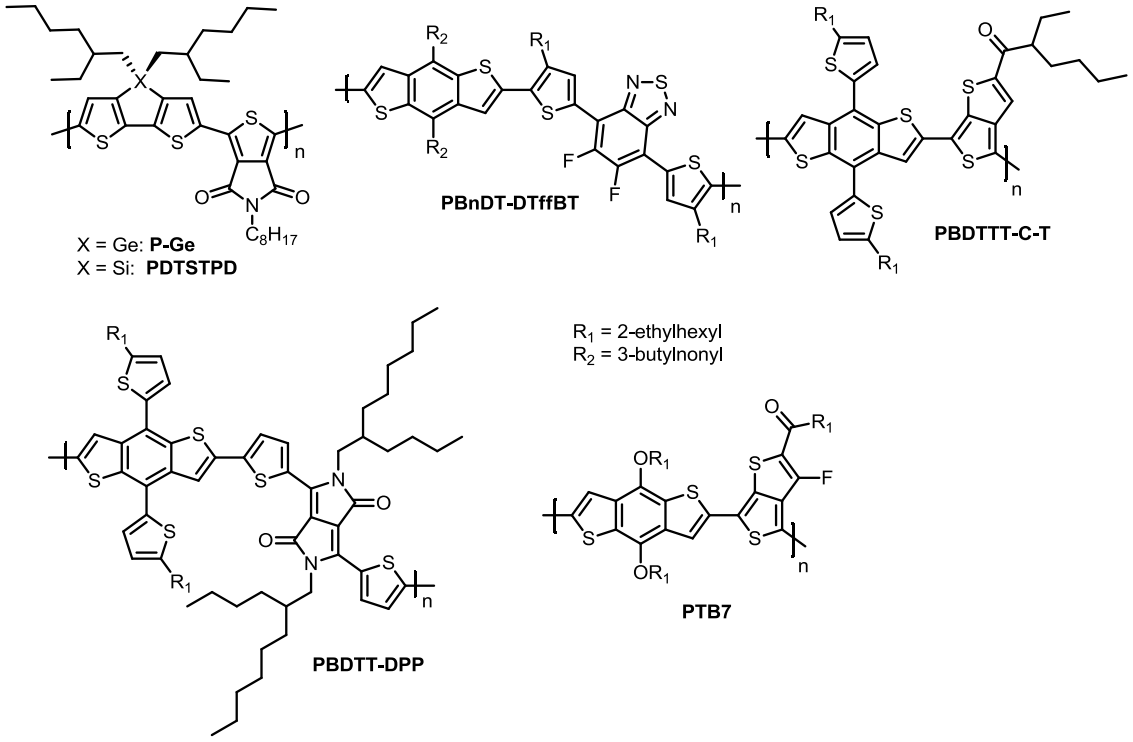

Figure 2.7: Donor-acceptor polymers with PCEs of > 7%.

Polymer BHJ solar cells are generally fabricated from solution. Since fullerenes are only poorly soluble in common organic solvents, more soluble derivatives have to be used as acceptor materials. Usually, those are [6,6]-phenyl-C_{61}-butyric acid methyl ester ($PC_{61}BM$) or [6,6]-phenyl-C_{71}-butyric acid methyl ester ($PC_{71}BM$). The latter often leads to higher efficiencies due to its increased absorption coefficient in the visible region.[58] The most investigated conjugated polymer used as the donor in BHJ devices is regioregular poly(3-hexylthiophene) (**P3HT**), and PCEs of up to 5 % have been achieved with the **P3HT**/$PC_{61}BM$ system.[12, 59-61] However, the band gap (1.9 eV) and high HOMO energy level (-5.1 eV vs. vacuum) limit the efficiency of **P3HT**. Therefore, recent research in the field of conjugated

polymers has focused on donor-acceptor polymers with lower band gaps caused by intramolecular charge transfer from the donor to the acceptor moieties.[62] By this approach, efficiencies of over 7% have been achieved. Some of the most efficient polymers are shown in **Figure 2.7**, the PCE being 7.2% for **PBnDT-DTffBT**,[63] 7.3% for **PDTSTPD**[64] and **P-Ge**,[65] 7.4% for **PTB7**[66] and 7.6% for **PBDTTT-C-T**.[67] Later, the PCE of **PTB7** was increased to a certified record value of 8.37%, with very high J_{SC} (15.75 mA cm^{-2}) and FF (0.70) values and a good V_{OC} of 0.76 V.[68]

Very recently, an efficiency of 8.6% was published for a tandem cell consisting of two subcells, one containing a blend of **PBDTT-DPP** and $PC_{71}BM$, the other containing a blend of **P3HT** and the indene-C_{60} bisadduct $IC_{60}BA$. Despite the moderate J_{SC} (8.27 mA cm^{-2}), a high PCE was obtained due to the high V_{OC} of 1.56 V and good FF of 0.67.[69] With the same device structure, a certified record efficiency of 10.6 % was achieved according to a recent press release.[70] Unfortunately, the polymers used in this record device were not disclosed.

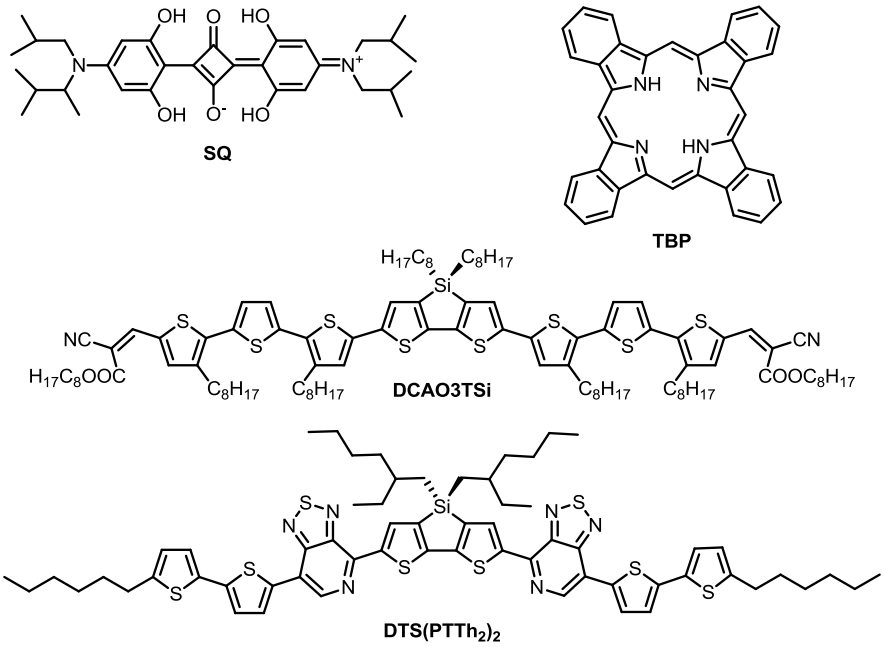

Figure 2.8: Donor materials for solution-processed small molecule BHJ devices with efficiencies > 5%.

The efficiencies of solution-processed and vacuum-processed small molecule BHJ solar cells have recently been improved to over 6%. Some examples for donor materials with more than 5% efficiency are given in **Figure 2.8**. The best PCE of 6.7% was achieved with a blend of compound **DTS(PTTh$_2$)$_2$** and $PC_{71}BM$ (D:A ratio 7:3 w/w) processed from chlorobenzene with 0.25% 1,8-diiodooctane, showing a very high J_{SC} of 14.4 mA cm^{-2} and good V_{OC} (0.78 V) and FF (0.59) values. In this investigation, a large variation for the PCE was observed (0.43-6.7%), depending on the donor/acceptor ratio and the amount of additive.[71] This example nicely shows the influence of the processing conditions on the morphology and, consequently, on the efficiency of BHJ solar cells. The

dithienosilole-based compound **DCAO$_3$TSi** also gave a good PCE of 5.8% (J_{SC} = 11.5 mA cm^{-2}, V_{OC} = 0.80 V and FF = 0.64) in a blend with $PC_{61}BM$ (D:A ratio 1:0.8 w/w).[72] The squaraine compound **SQ** and tetrabenzoporphyrin (**TBP**) showed both a PCE of 5.2%. **TBP**, however, was used in a blend with a soluble C_{60} derivative, while **SQ** was blended with $PC_{71}BM$. The porphyrin device was a combined planar heterojunction / bulk heterojunction device, fabricated by subsequent spin-casting of a pristine donor solution, a mixed donor/acceptor solution and a pristine acceptor solution. This device exhibited a J_{SC} of 10.5 mA cm^{-2}, a V_{OC} of 0.75, and a FF of 0.65.[73] The squaraine device was fabricated by spin-casting of a **SQ**/$PC_{71}BM$ (1:6 w/w) mixture and subsequent annealing in solvent vapor to induce further phase separation. The best efficiency of 5.2% was achieved when the **SQ** crystallite size matched the exciton diffusion length.[74]

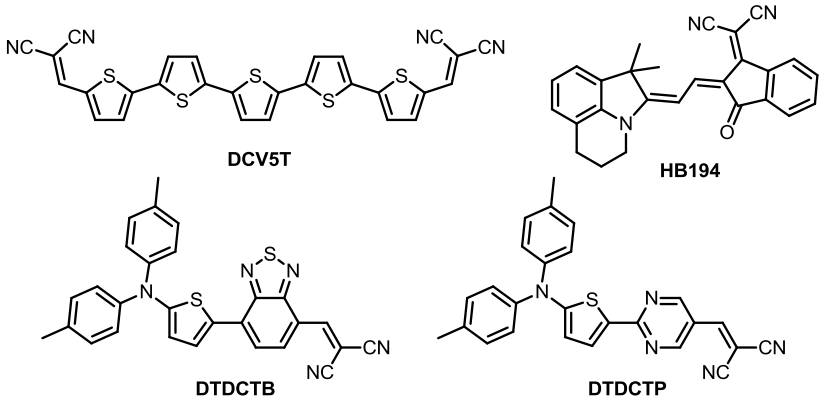

Figure 2.9: Donor materials for vacuum-processed small molecule BHJ solar cells with efficiencies > 5%.

The best efficiencies in vacuum-processed BHJ single cells were obtained with the donor-acceptor-acceptor dyes **DTDCTB** and **DTDCTP**, both containing a diphenylamine donor moiety and a dicyanovinyl (DCV) acceptor group. In **DTDCTB**, these moieties are connected by a benzothiadiazole bridging unit, while **DTDCTP** contains a pyrazine unit (**Figure 2.9**). Due to their high polarity, these molecules crystallize in antiparallelly arranged coplanar pairs. When blended with C_{60} (1:1 v/v), **DTDCTB** showed an efficiency of 4.4%. In a blend with C_{70}, the PCE was improved to 5.8% due to an improvement of J_{SC} from 11.4 to 14.7 mA cm^{-2}.[75] **DTDCTP** even reached a PCE of 6.4% in a blend with $PC_{71}BM$ (1:1 v/v). This increase compared to **DTDCTB** was caused by a higher V_{OC} (0.95 V vs. 0.79 V) due to the lower HOMO energy level of **DTDCTP**. On the other hand, J_{SC} was lower for **DTDCTP** (12.1 mA cm^{-2}) than for **DTDCTB**.[76] With the merocyanine dye **HB194**, a PCE of 5.8% was obtained in combination with C_{60} as acceptor (D:A 45:55 v/v), with high J_{SC} (12.6 mA cm^{-2}) and V_{OC} (0.96 V) values and a moderate FF of 0.47. The PCE dropped drastically (1.4%) when C_{70} was used instead of C_{60}, the reason remaining unclear.[77] The best oligothiophene donor material in vacuum-processed single junction cells is the DCV-substituted quinquethiophene **DCV5T**. In a BHJ device with C_{60} (D:A 2:1 v/v), it showed a PCE of 5.2% with a J_{SC} of 11.1 mA cm^{-2}, a V_{OC} of 0.97 V, and a FF of 0.49. The efficiency

increased with the thickness of the active layer due to a large increase in J_{SC}. The best PCE was obtained with a 40 nm active layer. While J_{SC} increased, FF dropped significantly with increasing thickness.[78]

The best small molecule tandem cell that has been published so far is also based on a DCV-functionalized oligothiophene. This cell consists of two subcells separated by a spacer layer, one cell based on an active layer with a blend of sexithiophene **DCV6T-Bu(1,2,5,6)** and C_{60}, the other based on a blend of fluorinated zinc phthalocyanine (**F4-ZnPc**) and C_{60} (**Figure 2.10**). The device showed a certified PCE of 6.07% with a J_{SC} of 6.18 mA cm^{-2}, a V_{OC} of 1.59 V, and a FF of 0.62. J_{SC} was largely depending on the thickness of the spacer layer with a maximum at 165 nm, whereas V_{OC} and FF remained unaffected hereof.[79] In April 2012, Heliatek published a press release with a PCE of 10.7% for a small molecule tandem cell, but the device architecture and materials were not disclosed.[80]

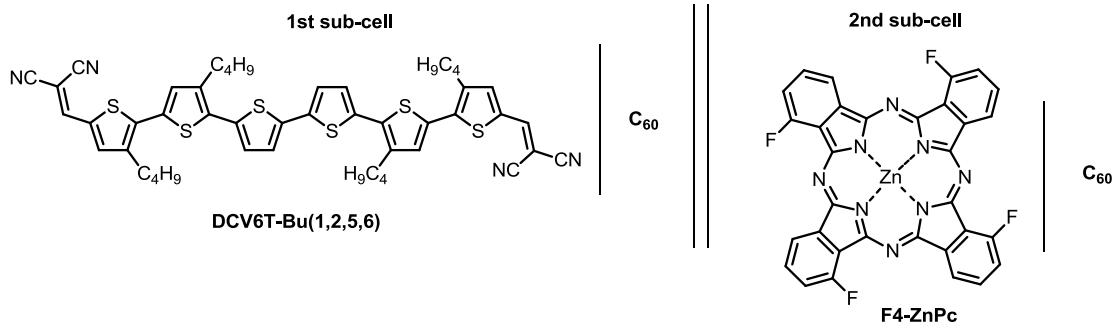

Figure 2.10: Materials for a tandem cell with more than 6% efficiency consisting of two sub-cells.

2.3 Dye-sensitized Solar Cells

The first high efficiency DSSC (PCE 7-8%) was published by Grätzel and O'Regan in 1991.[81] Since then, intense research has been performed in this field and the PCEs were increased up to a certified value of 12.3%.[4] The main construction principle, however, has not changed over the years. DSSCs in general and their fundamental operation principles have been reviewed in a number of articles.[82-90] A DSSC consists of the following components: a transparent conducting oxide substrate as photoanode (e.g., fluorine-doped tin oxide, FTO), a mesoporous semiconductor metal oxide (typically TiO_2 nanoparticles) sensitized by a dye monolayer, an electrolyte layer (liquid or ionic liquid[91-92]) or hole transport material (solid state DSSCs[92-93]), and a counter electrode (typically platinum). The general setup and fundamental processes of a DSSC are shown in **Figure 2.11**. Upon illumination, the sensitizer is excited from the ground state into the excited state (**1**). From the excited state, the sensitizer injects an electron into the conduction band of the TiO_2 (**2**). The electrons percolate through the semiconductor film to the transparent electrode, where they are collected, fed into an

external circuit, and transported to the counter electrode (**3**). There, they reduce the oxidized electrolyte (**4**), which in its reduced form reduces the dye cation (**5**), thus closing the circuit. The main loss mechanisms are the recombination of injected electrons with the oxidized electrolyte (**I**) or with the oxidized dye D^+ (**II**).[88, 94] The maximum voltage produced by the cell is limited by the difference between the chemical potential of the electrons in the TiO_2 nanoparticles (Fermi level) and the chemical potential of the holes in the hole conductor, which corresponds to the Nernst potential for redox electrolytes.[90]

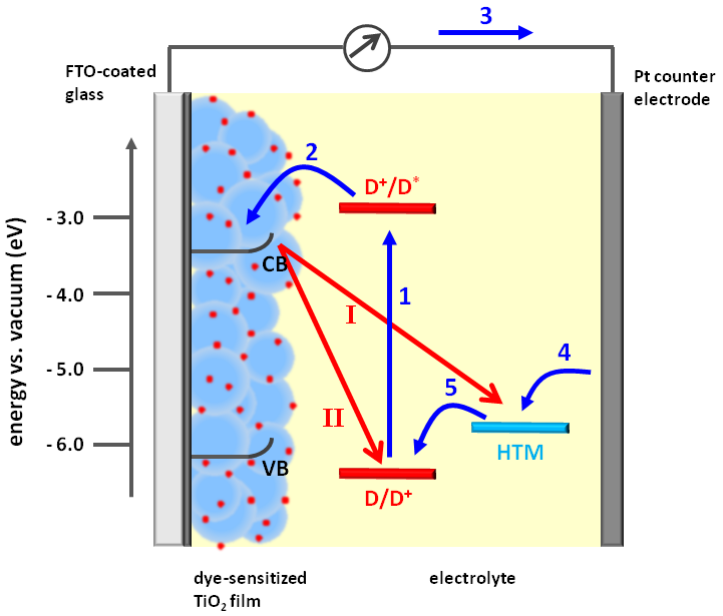

Figure 2.11: Schematic build-up and fundamental processes of a DSSC.

In contrast to inorganic solar cells or organic thin film solar cells, light absorption and charge transport are performed by different materials in a DSSC. Light is absorbed by the dye/sensitizer, while charge transport is accomplished by the semiconducting metal oxide and the electrolyte. Therefore, both fundamental steps can be tuned individually. In 2010, Hagfeldt published an excellent general review on DSSCs, including a discussion of state-of-the-art electrode materials, electrolytes, and hole transport materials.[88] Here, only a short overview of recent developments in the search for efficient sensitizers will be given.

The sensitizers for DSSCs can generally be divided into two groups, metal complexes and metal-free organic dyes. For about 20 years, the most efficient sensitizers were ruthenium complexes with efficiencies of up to 11.5% under AM 1.5 irradiation.[95-98] The best among these ruthenium sensitizers are bipyridine complexes such as **N3**,[97, 99] **N719**[96, 99-100] or **CYC-B11**,[101] or terpyridine complexes such as the "**black dye**"[102-104] (**Figure 2.12**).

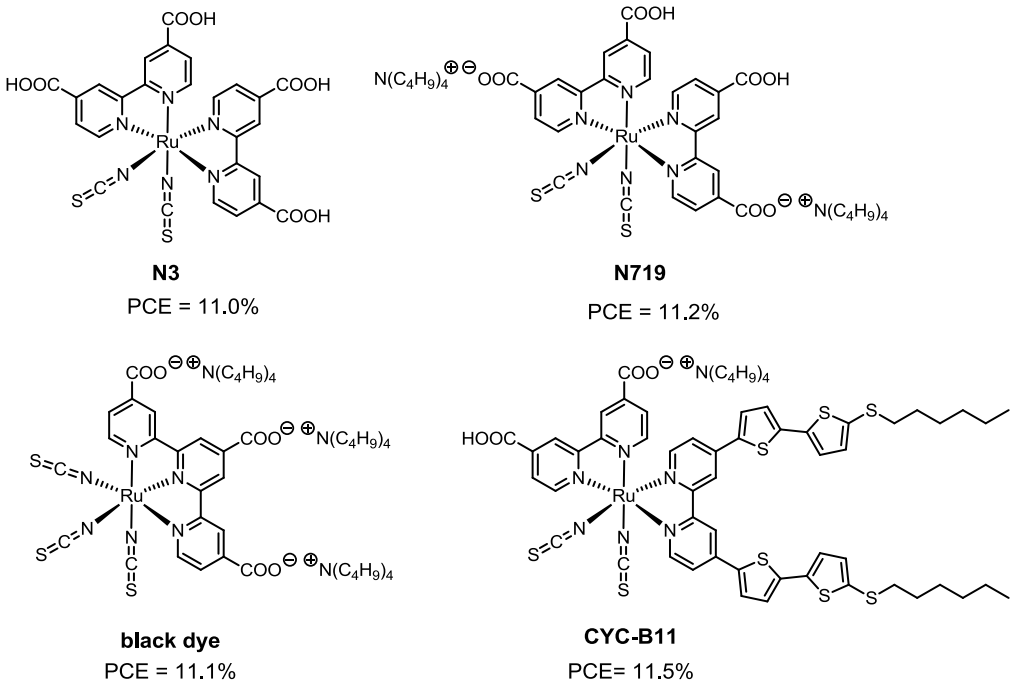

Figure 2.12: Highly efficient ruthenium sensitizers for DSSCs.

In the last few years, porphyrin metal complexes have attracted more and more interest as sensitizers for DSSCs, and very recently, a zinc porphyrin dye established a new record of 12.3% (**Figure 2.13**).[4] In that work, a cobalt(II)/cobalt(III) redox couple was used instead of the commonly used iodide/triiodide couple.

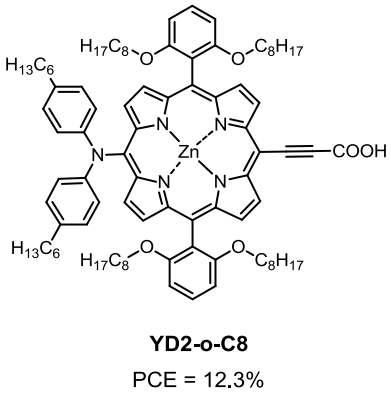

Figure 2.13: Current champion sensitizer for DSSCs.

The PCEs of metal-free organic dyes are somewhat lower (≤ 10%) in comparison to metal complex sensitizers, but they possess advantageous features, such as lower material costs, better tunable absorptions and band gaps by variation of the molecular structure, which typically consists of a π-conjugated donor-acceptor (D-A) system. Various D-π-A-substituted organic dyes have been prepared and used as sensitizers in DSSCs.[105-107] The most efficient organic sensitizers in liquid electrolyte DSSCs showed efficiencies of up to 10.3%, both in devices with the iodide/triiodide redox couple (dye **C229**)[108] and cobalt(II)/cobalt(III) redox couples (dye **C219**)[109] (**Figure 2.14**). **C219** also

attained a remarkable efficiency of 8.9% in a device with an ionic liquid electrolyte. The current record for a solid-state DSSC with an organic sensitizer is 6.08% and was achieved with dye **C220**.[110]

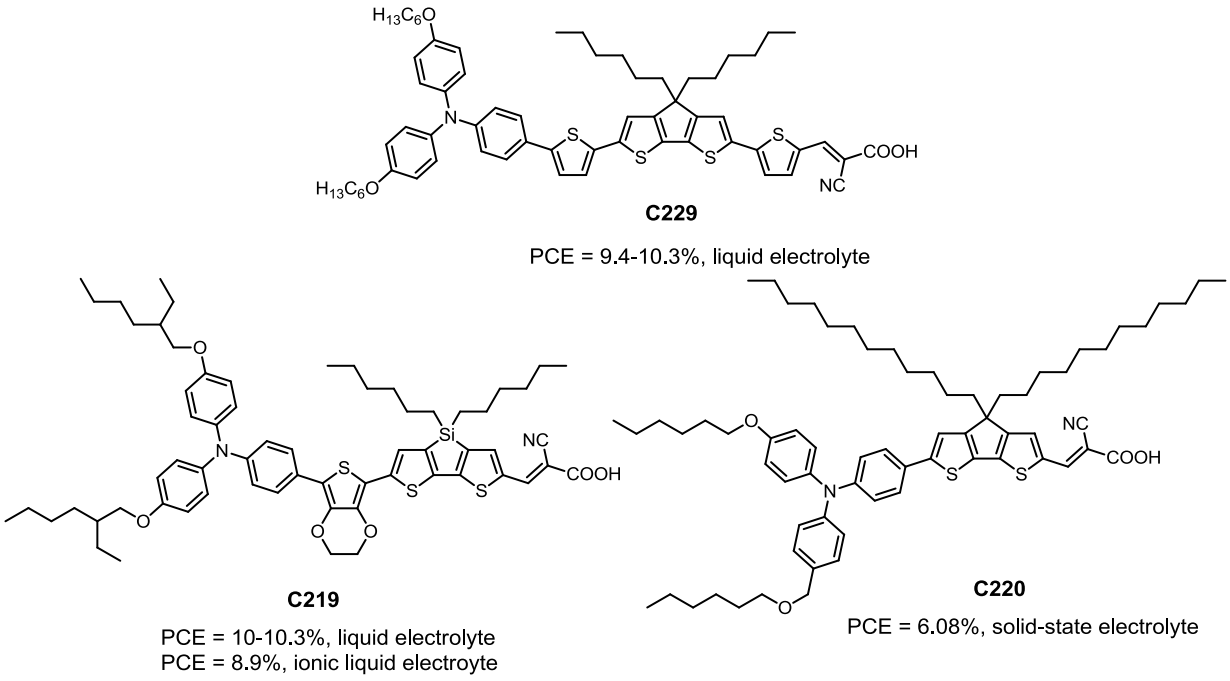

Figure 2.14: Champion molecules for metal-free dye sensitized solar cells.

2.4 Summary

In this chapter, a short overview of the construction and operation principles of different types of organic solar cells was given. Typical characterization parameters were defined and explained. State-of-the-art record materials for different categories of organic solar cells, i.e., small molecule and polymer-based solution- and vacuum-processed solar cells as wells as dye-sensitized solar cells, were presented.

2.5 References

[1] http://www.energymap.info (10/05/2012)

[2] M. A. Green, K. Emery, Y. Hishikawa, W. Warta, E. D. Dunlop, *Prog. Photovolt.: Res. Appl.* **2012**, *20*, 12.

[3] D. Wöhrle, O. R. Hild, *Chem. unserer Zeit* **2010**, *44*, 174.

[4] A. Yella, H.-W. Lee, H. N. Tsao, C. Yi, A. K. Chandiran, M. K. Nazeeruddin, E. W.-G. Diau, C.-Y. Yeh, S. M. Zakeeruddin, M. Grätzel, *Science* **2011**, *334*, 629.

[5] http://www.osa-direct.com/osad-news/tandem-organic-photovoltaic-reaches-106-efficiency-a-worlds-first-for-polymer-organic-photovoltaic-devices.html (10/05/2012)

[6] http://www.heliatek.com/?p=1923 (10/05/2012)

[7] http://www.konarka.com (10/05/2012)

[8] http://www.solarmer.com (10/05/2012)

[9] http://www.samsung.com (10/05/2012)

[10] http://www.g24i.com (10/05/2012)

[11] http://www.heliatek.com/?p=1727 (10/05/2012)

[12] G. Dennler, M. C. Scharber, C. J. Brabec, *Adv. Mater.* **2009**, *21*, 1323.

[13] J. J. M. Halls, J. Cornil, D. A. dos Santos, R. Silbey, D. H. Hwang, A. B. Holmes, J. L. Brédas, R. H. Friend, *Phys. Rev. B* **1999**, *60*, 5721.

[14] S. Barth, H. Bässler, *Phys. Rev. Lett.* **1997**, *79*, 4445.

[15] B. A. Gregg, M. C. Hanna, *J. Appl. Phys.* **2003**, *93*, 3605.

[16] H. Hoppe, N. S. Sariciftci, *J. Mater. Res.* **2004**, *19*, 1924.

[17] B. P. Rand, J. Genoe, P. Heremans, J. Poortmans, *Prog. Photovolt.: Res. Appl.* **2007**, *15*, 659.

[18] S. Karg, W. Riess, V. Dyakonov, M. Schwoerer, *Synth. Met.* **1993**, *54*, 427.

[19] R. O. Loutfy, J. H. Sharp, *J. Chem. Phys.* **1979**, *71*, 1211.

[20] G. Yu, C. Zhang, A. J. Heeger, *Appl. Phys. Lett.* **1994**, *64*, 1540.

[21] K. Walzer, B. Männig, M. Pfeiffer, K. Leo, *Chem. Rev.* **2007**, *107*, 1233.

[22] C. W. Tang, *App. Phys. Lett.* **1986**, *48*, 183.

[23] B. C. Thompson, J. M. J. Fréchet, *Angew. Chem.* **2008**, *120*, 62; *Angew. Chem. Int. Ed.* **2008**, *47*, 58.

[24] T. M. Clarke, J. R. Durrant, *Chem. Rev.* **2010**, *110*, 6736.

[25] M. C. Scharber, D. Mühlbacher, M. Koppe, P. Denk, C. Waldauf, A. J. Heeger, C. J. Brabec, *Adv. Mater.* **2006**, *18*, 789.

[26] J. D. Servaites, M. A. Ratner, T. J. Marks, *Energy Environ. Sci.* **2011**, *4*, 4410.

[27] P. Peumans, A. Yakimov, S. R. Forrest, *J. Appl. Phys.* **2003**, *93*, 3693.

[28] C. J. Brabec, S. Gowrisanker, J. J. M. Halls, D. Laird, S. Jia, S. P. Williams, *Adv. Mater.* **2010**, *22*, 3839.

[29] J. J. M. Halls, C. A. Walsh, N. C. Greenham, E. A. Marseglia, R. H. Friend, S. C. Moratti, A. B. Holmes, *Nature* **1995**, *376*, 498.

[30] G. Yu, A. J. Heeger, *J. Appl. Phys.* **1995**, *78*, 4510.

[31] H. Hoppe, N. S. Sariciftci, *J. Mater. Chem.* **2006**, *16*, 45.

[32] J. Peet, M. L. Senatore, A. J. Heeger, G. C. Bazan, *Adv. Mater.* **2009**, *21*, 1521.

[33] A. J. Moulé, K. Meerholz, *Adv. Funct. Mater.* **2009**, *19*, 3028.

[34] R. Po, M. Maggini, N. Camaioni, *J. Phys. Chem. C* **2009**, *114*, 695.

[35] G. H. Bauer, P. Würfel, in *Organic Photovoltaics* (Eds.: C. J. Brabec, V. Dyakonov, J. Parisi, N. S. Sariciftci), Springer-Verlag, Berlin, Heidelberg, **2003**, pp. 118.

[36] C. J. Brabec, in *Organic Photovoltaics* (Eds.: C. J. Brabec, V. Dyakonov, J. Parisi, N. S. Sariciftci), Springer-Verlag, Berlin, Heidelberg, **2003**, pp. 159.

[37] M. Riede, T. Müller, W. Tress, R. Schüppel, K. Leo, *Nanotechnology* **2008**, *19*, 424001.

[38] C. J. Brabec, A. Cravino, D. Meissner, N. S. Sariciftci, T. Fromherz, M. T. Rispens, L. Sanchez, J. C. Hummelen, *Adv. Funct. Mater.* **2001**, *11*, 374.

[39] V. D. Mihailetchi, P. W. M. Blom, J. C. Hummelen, M. T. Rispens, *J. Appl. Phys.* **2003**, *94*, 6849.

[40] C. M. Ramsdale, J. A. Barker, A. C. Arias, J. D. MacKenzie, R. H. Friend, N. C. Greenham, *J. Appl. Phys.* **2002**, *92*, 4266.

[41] W. J. Potscavage, A. Sharma, B. Kippelen, *Acc. Chem. Res.* **2009**, *42*, 1758.

[42] S. Günes, H. Neugebauer, N. S. Sariciftci, *Chem. Rev.* **2007**, *107*, 1324.

[43] L. Beverina, P. Salice, *Eur. J. Org. Chem.* **2010**, *2010*, 1207.

[44] S. Sreejith, P. Carol, P. Chithra, A. Ajayaghosh, *J. Mater. Chem.* **2008**, *18*, 264.

[45] C. Li, H. Wonneberger, *Adv. Mater.* **2012**, *24*, 613.

[46] G. Bottari, G. de la Torre, D. M. Guldi, T. Torres, *Chem. Rev.* **2010**, *110*, 6768.

[47] A. Mishra, P. Bäuerle, *Angew. Chem.* **2012**, *124*, 2060; *Angew. Chem. Int. Ed.* **2012**, *51*, 2020.

[48] G. Wei, X. Xiao, S. Wang, J. D. Zimmerman, K. Sun, V. V. Diev, M. E. Thompson, S. R. Forrest, *Nano Lett.* **2011**, *11*, 4261.

[49] M. Hirade, C. Adachi, *Appl. Phys. Lett.* **2011**, *99*, 153302.

[50] R. Schüppel, K. Schmidt, C. Uhrich, K. Schulze, D. Wynands, J. L. Brédas, E. Brier, E. Reinold, H. B. Bu, P. Bäuerle, B. Männig, M. Pfeiffer, K. Leo, *Phys. Rev. B* **2008**, *77*, 085311.

[51] F. C. Krebs, *Sol. Energy Mater. Sol. Cells* **2009**, *93*, 394.

[52] B. Walker, C. Kim, T.-Q. Nguyen, *Chem. Mater.* **2010**, *23*, 470.

[53] K. M. Coakley, M. D. McGehee, *Chem. Mater.* **2004**, *16*, 4533.

[54] H. Zhou, L. Yang, W. You, *Macromolecules* **2012**, *45*, 607.

[55] Y. Li, *Acc. Chem. Res.* **2012**, *45*, 723.

[56] F. He, L. Yu, *J. Phys. Chem. Lett.* **2011**, *2*, 3102.

[57] W. Cai, X. Gong, Y. Cao, *Sol. Energy Mater. Sol. Cells* **2010**, *94*, 114.

[58] M. M. Wienk, J. M. Kroon, W. J. H. Verhees, J. Knol, J. C. Hummelen, P. A. van Hal, R. A. J. Janssen, *Angew. Chem.* **2003**, *115*, 3493; *Angew. Chem. Int. Ed.* **2003**, *42*, 3371.

[59] W. Ma, C. Yang, X. Gong, K. Lee, A. J. Heeger, *Adv. Funct. Mater.* **2005**, *15*, 1617.

[60] Y. Kim, S. Cook, S. M. Tuladhar, S. A. Choulis, J. Nelson, J. R. Durrant, D. D. C. Bradley, M. Giles, I. McCulloch, C.-S. Ha, M. Ree, *Nat. Mater.* **2006**, *5*, 197.

[61] G. Li, V. Shrotriya, J. Huang, Y. Yao, T. Moriarty, K. Emery, Y. Yang, *Nat. Mater.* **2005**, *4*, 864.

[62] J. Roncali, *Chem. Rev.* **1997**, *97*, 173.

[63] H. Zhou, L. Yang, A. C. Stuart, S. C. Price, S. Liu, W. You, *Angew. Chem.* **2011**, *123*, 3051; *Angew. Chem. Int. Ed.* **2011**, *50*, 2995.

[64] T.-Y. Chu, J. Lu, S. Beaupré, Y. Zhang, J.-R. Pouliot, S. Wakim, J. Zhou, M. Leclerc, Z. Li, J. Ding, Y. Tao, *J. Am. Chem. Soc.* **2011**, *133*, 4250.

[65] C. M. Amb, S. Chen, K. R. Graham, J. Subbiah, C. E. Small, F. So, J. R. Reynolds, *J. Am. Chem. Soc.* **2011**, *133*, 10062.

[66] Y. Liang, Z. Xu, J. Xia, S.-T. Tsai, Y. Wu, G. Li, C. Ray, L. Yu, *Adv. Mater.* **2010**, *22*, E135.

[67] L. Huo, S. Zhang, X. Guo, F. Xu, Y. Li, J. Hou, *Angew. Chem.* **2011**, *123*, 9871; *Angew. Chem. Int. Ed.* **2011**, *50*, 9697.

[68] Z. He, C. Zhong, X. Huang, W.-Y. Wong, H. Wu, L. Chen, S. Su, Y. Cao, *Adv. Mater.* **2011**, *23*, 4636.

[69] L. Dou, J. You, J. Yang, C.-C. Chen, Y. He, S. Murase, T. Moriarty, K. Emery, G. Li, Y. Yang, *Nat. Photon.* **2012**, *6*, 180.

[70] http://www.osa-direct.com/osad-news/tandem-organic-photovoltaic-reaches-106-efficiency-a-worlds-first-for-polymer-organic-photovoltaic-devices.html ((10/05/2012)

[71] Y. Sun, G. C. Welch, W. L. Leong, C. J. Takacs, G. C. Bazan, A. J. Heeger, *Nat. Mater.* **2012**, *11*, 44.

[72] J. Zhou, X. Wan, Y. Liu, G. Long, F. Wang, Z. Li, Y. Zuo, C. Li, Y. Chen, *Chem. Mater.* **2011**, *23*, 4666.

[73] Y. Matsuo, Y. Sato, T. Niinomi, I. Soga, H. Tanaka, E. Nakamura, *J. Am. Chem. Soc.* **2009**, *131*, 16048.

[74] G. Wei, S. Wang, K. Sun, M. E. Thompson, S. R. Forrest, *Adv. Energy Mater.* **2011**, *1*, 184.

[75] L.-Y. Lin, Y.-H. Chen, Z.-Y. Huang, H.-W. Lin, S.-H. Chou, F. Lin, C.-W. Chen, Y.-H. Liu, K.-T. Wong, *J. Am. Chem. Soc.* **2011**, *133*, 15822.

[76] S.-W. Chiu, L.-Y. Lin, H.-W. Lin, Y.-H. Chen, Z.-Y. Huang, Y.-T. Lin, F. Lin, Y.-H. Liu, K.-T. Wong, *Chem. Commun.* **2012**, *48*, 1825.

[77] V. Steinmann, N. M. Kronenberg, M. R. Lenze, S. M. Graf, D. Hertel, K. Meerholz, H. Bürckstümmer, E. V. Tulyakova, F. Würthner, *Adv. Energy Mater.* **2011**, *1*, 888.

[78] R. Fitzner, E. Reinold, A. Mishra, E. Mena-Osteritz, H. Ziehlke, C. Körner, K. Leo, M. Riede, M. Weil, O. Tsaryova, A. Weiß, C. Uhrich, M. Pfeiffer, P. Bäuerle, *Adv. Funct. Mater.* **2011**, *21*, 897.

[79] M. Riede, C. Uhrich, J. Widmer, R. Timmreck, D. Wynands, G. Schwartz, W.-M. Gnehr, D. Hildebrandt, A. Weiss, J. Hwang, S. Sundarraj, P. Erk, M. Pfeiffer, K. Leo, *Adv. Funct. Mater.* **2011**, *21*, 3019.

[80] http://www.heliatek.com/?p=1923 (10/05/2012)

[81] B. O'Regan, M. Grätzel, *Nature* **1991**, *353*, 737.

[82] L. M. Goncalves, V. d. Z. Bermudez, H. A. Ribeiro, A. M. Mendes, *Energy Environ. Sci.* **2008**, *1*, 655.

[83] F. O. Lenzmann, J. M. Kroon, *Adv. Optoelectron.* **2007**, Article ID 65073.

[84] J. M. Kroon, N. J. Bakker, H. J. P. Smit, P. Liska, K. R. Thampi, P. Wang, S. M. Zakeeruddin, M. Grätzel, A. Hinsch, S. Hore, U. Würfel, R. Sastrawan, J. R. Durrant, E. Palomares, H. Pettersson, T. Gruszecki, J. Walter, K. Skupien, G. E. Tulloch, *Prog. Photovoltaics Res. Appl.* **2007**, *15*, 1.

[85] F.-T. Kong, S.-Y. Dai, K.-J. Wang, *Adv. Optoelectron.* **2007**, Article ID 75384.

[86] M. Grätzel, *J. Photochem. Photobiol. C* **2003**, *4*, 145.

[87] M. Grätzel, *Nature* **2001**, *414*, 338.

[88] A. Hagfeldt, G. Boschloo, L. Sun, L. Kloo, H. Pettersson, *Chem. Rev.* **2010**, *110*, 6595.

[89] B. C. O'Regan, J. R. Durrant, *Acc. Chem. Res.* **2009**, *42*, 1799.

[90] M. Grätzel, *Acc. Chem. Res.* **2009**, *42*, 1788.

[91] M. Gorlov, L. Kloo, *Dalton Trans.* **2008**, 2655.

[92] H. J. Snaith, L. Schmidt-Mende, *Adv. Mater.* **2007**, *19*, 3187.

[93] J.-H. Yum, P. Chen, M. Grätzel, M. K. Nazeeruddin, *ChemSusChem* **2008**, *1*, 699.

[94] J. N. Clifford, E. Martinez-Ferrero, A. Viterisi, E. Palomares, *Chem. Soc. Rev.* **2011**, *40*, 1635.

[95] M. Grätzel, *J. Photochem. Photobiol. A* **2004**, *164*, 3.

[96] M. K. Nazeeruddin, F. De Angelis, S. Fantacci, A. Selloni, G. Viscardi, P. Liska, S. Ito, B. Takeru, M. Grätzel, *J. Am. Chem. Soc.* **2005**, *127*, 16835.

[97] M. K. Nazeeruddin, A. Kay, I. Rodicio, R. Humphry-Baker, E. Müller, P. Liska, N. Vlachopoulos, M. Grätzel, *J. Am. Chem. Soc.* **1993**, *115*, 6382.

[98] N. Robertson, *Angew. Chem.* **2006**, *118*, 2398; *Angew. Chem. Int. Ed.* **2006**, *45*, 2338.

[99] M. Grätzel, *J. Photochem.Photobiol. A* **2004**, *164*, 3.

[100] M. K. Nazeeruddin, R. Splivallo, P. Liska, P. Comte, M. Grätzel, *Chem. Commun.* **2003**, 1456.

[101] C.-Y. Chen, M. Wang, J.-Y. Li, N. Pootrakulchote, L. Alibabaei, C.-h. Ngoc-le, J.-D. Decoppet, J.-H. Tsai, C. Grätzel, C.-G. Wu, S. M. Zakeeruddin, M. Grätzel, *ACS Nano* **2009**, *3*, 3103.

[102] Y. Chiba, A. Islam, Y. Watanabe, R. Komiya, N. Koide, L. Han, *Jpn. J. Appl. Phys.*, *45*, L638.

[103] M. K. Nazeeruddin, P. Péchy, M. Grätzel, *Chem. Commun.* **1997**, 1705.

[104] M. K. Nazeeruddin, P. Pechy, T. Renouard, S. M. Zakeeruddin, R. Humphry-Baker, P. Comte, P. Liska, L. Cevey, E. Costa, V. Shklover, L. Spiccia, G. B. Deacon, C. A. Bignozzi, M. Grätzel, *J. Am. Chem. Soc.* **2001**, *123*, 1613.

[105] H. Imahori, T. Umeyama, S. Ito, *Acc. Chem. Res.* **2009**, *42*, 1809.

[106] A. Mishra, M. K. R. Fischer, P. Bäuerle, *Angew. Chem.* **2009**, *121*, 2510; *Angew. Chem. Int. Ed.* **2009**, *48*, 2474.

[107] M. Wang, M. Xu, D. Shi, R. Li, F. Gao, G. Zhang, Z. Yi, R. Humphry-Baker, P. Wang, S. M. Zakeeruddin, M. Grätzel, *Adv. Mater.* **2008**, *20*, 4460.

[108] Y. Bai, J. Zhang, D. Zhou, Y. Wang, M. Zhang, P. Wang, *J. Am. Chem. Soc.* **2011**, *133*, 11442.

[109] W. Zeng, Y. Cao, Y. Bai, Y. Wang, Y. Shi, M. Zhang, F. Wang, C. Pan, P. Wang, *Chem. Mater.* **2010**, *22*, 1915.

[110] N. Cai, S.-J. Moon, L. Cevey-Ha, T. Moehl, R. Humphry-Baker, P. Wang, S. M. Zakeeruddin, M. Grätzel, *Nano Lett.* **2011**, *11*, 1452.

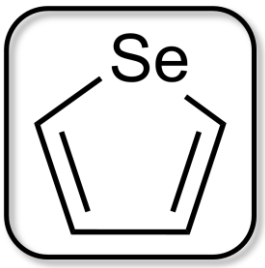

CHAPTER 3

DICYANOVINYL-SUBSTITUTED (CO-)OLIGOMERS BASED ON SELENOPHENE

3.1 General Introduction

In the past five to seven years, acceptor-functionalized oligothiophenes have been widely investigated as electron donor materials for vacuum-processed small molecule solar cells (SMOSC). In this respect, the most promising compounds that have been investigated so far are dicyanovinyl (DCV)-substituted oligothiophenes with the general substitution pattern acceptor-donor-acceptor (A-D-A) (**Figure 3.1**). Due to the A-D-A pattern of the conjugated backbone, those compounds showed strong absorptions at 500-700 nm and reduced band gaps. Furthermore, the DCV groups are stable under vacuum sublimation conditions, a crucial prerequisite for the fabrication of solar cells by vacuum-processing.

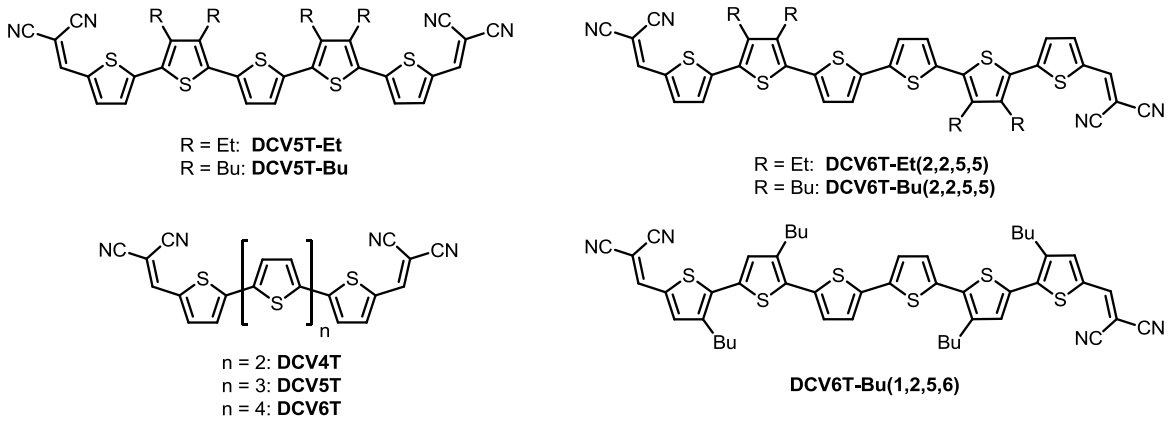

Figure 3.1: Previously synthesized DCV-substituted oligothiophenes.

The first efficient donor of that class of oligothiophenes was the butyl-substituted quinquethiophene **DCV5T-Bu**. In a planar heterojunction (PHJ) solar cell with C_{60} as acceptor this material reached power conversion efficiencies (PCE) of up to 3.4%.[1] Especially the high open circuit voltage (V_{OC}) of almost 1 V was very promising. The external quantum efficiency (EQE) spectrum covered a broad range from 350 nm to 650 nm with a maximum of 48% at 570 nm. A V_{OC} of 1.0-1.1 V seems to be the optimum for this kind of donor materials, since it still allowed sufficient charge separation at the donor-acceptor interface, whereas a further increase in V_{OC} would lead to a decrease in charge separation efficiency.[2]

The corresponding ethyl-derivative **DCV5T-Et**, which only differs in the length of the alkyl chains, attained only an efficiency of 2.5% using the same cell configuration.[3] Due to the identical HOMO energy levels, both compounds produced the same V_{OC} value. The reason for the lower PCE of **DCV5T-Et** was the lower fill factor (FF) of ~40% compared to ~50% for **DCV5T-Bu**. This finding is a consequence of the different alkyl chain lengths, which result in different distances between neighboring molecules, and consequently, differences in hole injection efficiencies and hole mobilities.

The influence of device architecture and morphology on the photovoltaic performance was investigated using several sexithiophene derivatives with different alkyl substitution patterns. With **DCV6T-Et(2,2,5,5)**, different device architectures (PHJ, bulk-heterojunction (BHJ), hybrid-P/BHJ) were tested, and the highest PCE of 2.1% was obtained with the hybrid cell. However, this cell still suffered from transport losses in the mixed layer, which resulted in a low FF of ~42%.[4] Further studies on BHJ solar cells with sexithiophenes **DCV6T-Bu(2,2,5,5)** and **DCV6T-Bu(1,2,5,6)** as donor materials revealed the influence of the substrate temperature on the device performance. X-ray diffraction (XRD) measurements and atomic force microscopy (AFM) showed that a substrate temperature around 90 °C led to an optimal degree of phase separation. Thus, the PCE of **DCV6T-Bu(2,2,5,5)** was raised from 1.6% (30 °C substrate temperature) to 3.8% (90 °C) and the PCE of **DCV6T-Bu(1,2,5,6)** from 2.1% to 4.9%.[5-8] Very recently, it was demonstrated that a substrate temperature of 80 °C resulted in longer charge carrier lifetimes in BHJ devices with quinquethiophene **DCV5T-Bu**.[9]

All these compounds were synthesized by a linear method, i.e., the oligothiophene backbone was synthesized first, then the DCV groups were attached. This method is only suitable for sufficiently soluble compounds, which can be purified by column chromatography, but not for poorly soluble alkyl-free DCV-oligthiophenes. Thus, alkyl-free **DCV*n*Ts** were synthesized by a convergent approach. Twofold C-C cross-coupling of distannylated thiophene or bithiophene with DCV-substituted bromothiophene afforded the corresponding trimer and tetramer, while coupling of the same stannyl building blocks with DCV-substituted bromobithiophene gave the respective pentamer and hexamer.[10] The obtained oligothiophenes were purified by Soxhlet extraction and vacuum sublimation. For **DCV4T** it was possible to grow single crystals by vacuum sublimation and crystal structure analysis revealed the importance of the DCV groups for the molecular ordering in the solid state. The higher homologues of the series (n = 4-6) were implemented in PHJ solar cells, and efficiencies of up to 2.8% (**DCV6T**) were obtained. With **DCV5T**, BHJ devices with different blend layer thicknesses were investigated. The highest PCE of 5.2% was achieved with a 40 nm thick blend layer. This PCE is among the highest values for vacuum-processed single heterojunction organic solar cells.

In a very recent study, a correlation between the crystal packing of three different **DCV4T** derivatives (**Figure 3.2**) and their solar cell performance was investigated. Due to different substituents on the terminal thiophenes the molecular packing of these quaterthiophenes in the crystal structure differed significantly. The different packing behavior also affected the morphology in the blend layer and the three derivatives showed very different PCEs. While the non-alkylated **DCV4T** and ethyl-substituted **DCV4T-Et(1,1,4,4)** only produced PCEs of 1.5% and 2.2%, respectively, the methyl derivative **DCV4T-Me(1,1,4,4)** showed a high PCE of 3.8%.

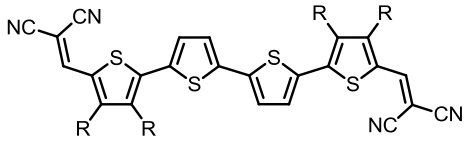

R = H: **DCV4T**
R = Me: **DCV4T-Me(1,1,4,4)**
R = Et: **DCV4T-Et(1,1,4,4)**

Figure 3.2: **DCV4T** derivatives with different alkyl substituents on terminal thiophenes.

Despite the very good performance of DCV-functionalized oligothiophenes, several other terminal acceptor groups have also been used, and the resulting A-D-A oligothiophenes were tested in SMOSCs (**Figure 3.3**).[11] In one investigation, the DCV-protons of **DCV5T-Et** were replaced by methyl or phenyl substituents. While the methyl derivative showed a comparable PCE to **DCV5T-Et**, the phenyl derivative produced a relatively low J_{SC} of 3.5 mA cm^{-2} and FF of 43%, giving rise to a low PCE of 1.5%. This result was ascribed to the non-planarity of the terminal acceptor groups, which caused a highly disordered packing. In another publication, benzothiadiazole- and thiadiazolopyridine-functionalized terthiophenes were synthesized and implemented in PHJ and BHJ solar cells.[12] The absorption maxima of both compounds were blue-shifted compared to **DCV3T** due to the lower acceptor strength of the two acceptors. In contrast to experiences with DCV-substituted oligothiophenes, both compounds showed better PCEs in PHJ devices than in BHJ devices, the reason for that being still unclear. The highest PCE of 3.15% with a high FF of 67% was obtained with a PHJ device containing a 10 nm donor layer of the thiadiazolopyridine derivative. In another series of compounds, the trifluoroacetyl (TFA) group was used as terminal acceptor for A-D-A-D-A type donor materials (**Figure 3.3**) containing a central benzothiadiazole[12] or thienothiadiazole acceptor.[13] The HOMO of the benzothiadiazole-based compounds was below the HOMO of the hole transporting material, which resulted in S-shaped *J-V* curves and low FFs around 30%. Consequently, the obtained PCEs were relatively low (~1.5%).

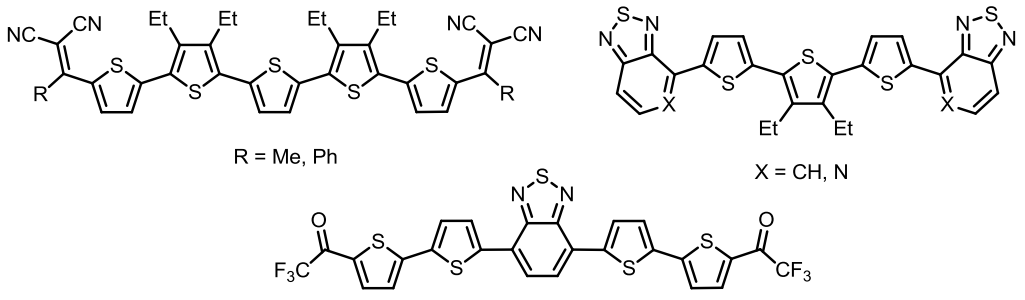

R = Me, Ph

X = CH, N

Figure 3.3: A-D-A and A-D-A-D-A type oligothiophenes with different acceptor groups.

While the DCV group is well established as terminal acceptor unit for oligothiophenes in vacuum-processed solar cells, only a few DCV-substituted oligothiophenes designed for solution-processed solar cells have been reported in the literature (**Figure 3.4**).[14] Among these, only septithiophene

DCN7T was used for the fabrication of solar cells.[15-17] The best efficiency of 3.7% was obtained with a BHJ device containing **DCN7T** as donor and [6,6]-phenyl-C_{61}-butyric acid methyl ester ($PC_{61}BM$) as acceptor in a blend ratio of 1:1.4 w/w. In that case, a very high J_{SC} of 12.4 mA cm^{-2} was obtained, but the FF of 34% was relatively low.

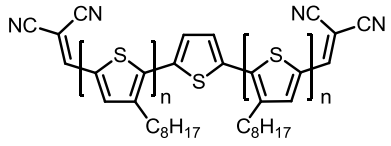

n = 1: **DCN3T**
n = 2: **DCN5T**
n = 3: **DCN7T**

Figure 3.4: DCV-substituted oligothiophenes designed for solution-processes solar cells.

Oligothiophenes with terminal DCV-groups have also been implemented as donor materials in vacuum-processed tandem solar cells. One of the subcells of these tandem cells contained a blend layer of fluorinated zinc phthalocyanine/C_{60} in order to absorb the red part of the solar spectrum. The blend layer of the other subcell consisted of the already described **DCV6T-Bu(1,2,5,6)**/C_{60} and was intended to absorb the green part of the solar spectrum. With this combination of subcells, a certified PCE of 6.07% was achieved.[18] This concept is also suitable for the fabrication of semitransparent solar cells, which produced a PCE of 4.9%.[19]

The previous paragraphs showed that a vast number of terminally acceptor-functionalized oligothiophenes have been used as efficient donor materials in vacuum-processed organic solar cells. Oligoselenophenes, however, have not yet been used in such devices. Oligoselenophenes in general are much less investigated than oligothiophenes. This is mainly due to the less developed chemistry and higher price of selenophene. Therefore, some studies focused only on the theoretical investigation of oligoselenophenes.[20-23] The synthesis of a series of oligoselenophenes up to a hexamer was published by Nakanishi *et al.* in 1997.[24-25] The authors showed that oligoselenophenes could be synthesized by the same C-C cross-coupling reactions as oligothiophenes and that the systematic changes of the optoelectronic properties in a series of oligoselenophenes were similar to those of corresponding oligothiophenes. The investigated oligoselenophenes exhibited red-shifted absorption spectra and lower band gaps compared to their oligothiophene analogs. The solubility decreased drastically with increasing number of selenophenes. Therefore, the synthesis of longer oligomers than a hexamer was not possible. To date, this series remained the only systematically investigated series of oligoselenophenes.

In contrast to oligoselenophene, polyselenophenes have been investigated more thoroughly in recent years, both theoretically and experimentally (see **Chapter 1**). Some promising properties, especially for application in solar cells, were predicted and confirmed by experiments, i.e., lower

band gaps, red-shifted absorption, and better polarizability of the heteroatom compared to polythiophenes.[22-23, 26-30] Due to the predicted favorable properties, several polyselenophenes have been implemented in organic solar cells in the last few years and PCEs of up to 6.87% were achieved.[31-41] Selenophene-containing oligomers, however, have only scarcely been implemented in solar cells. Some selenophene-containing sensitizers for dye-sensitized solar cells were investigated with PCEs similar to their thiophene analogs.[42-43] Furthermore, selenophene- and biselenophene-substituted diketopyrrolopyrroles were used in solution-processed bulk-heterojunction solar cells.[44] PCEs of up to 1.5% were obtained with the biselenophene derivative. Oligoselenophenes longer than a biselenophene have not been used in organic solar cells so far.

Especially the expected lower band gaps and red-shifted absorptions inspired us to synthesize terminally DCV-substituted selenophene-based oligomers for vacuum-processed solar cells. Firstly, we systematically replaced thiophene units in the parent compound **DCV5T-Bu** by selenophene units and investigated the consequences on optoelectronic properties and photovoltaic performance (**Section 3.2**). Then, a series of non-alkylated DCV-substituted oligoselenophenes was synthesized in order to investigate pristine oligoselenophenes and compare their properties to pristine oligothiophenes (**Section 3.3**).

3.2 Dicyanovinyl-substituted Mixed Selenophene-Thiophene Co-oligomers

3.2.1 Introduction

By the time this project was started, the butyl-substituted DCV-quinquethiophene **DCV5T-Bu** was the material in our group that had achieved the highest efficiency of 3.4% in vacuum-processed solar cells. However, the absorption maximum of this material in solution (513 nm) and in thin films (573 nm) did not extend far enough into the red regime of the solar spectrum. Since it had been shown for oligo- and polyselenophenes that their absorptions were red-shifted compared to their thiophene analogs, we intended to synthesize a selenophene analog of **DCV5T-Bu**. Unfortunately, no efficient method for the synthesis of 3,4-dialkylselenophenes was found (see **Section 3.2.3**). Therefore, we changed our strategy and only replaced the non-alkylated thiophenes in **DCV5T-Bu** by selenophenes, hoping that a significant red-shift could already be achieved by this partial substitution. In the end, this approach afforded compounds **1**-**3** (**Figure 3.5**). As a side aspect, compound **4** was synthesized (**Figure 3.6**). In that compound, the central bithiophene unit of **DCV4T-Bu** was replaced by a biselenophene. In the following sections, the synthesis, thermal and optoelectronic properties, and

photovoltaic performance of compounds **1**-**4** are presented and compared to their *all*-thiophene analogs. The consequences of the introduction of selenophenes are discussed in detail.

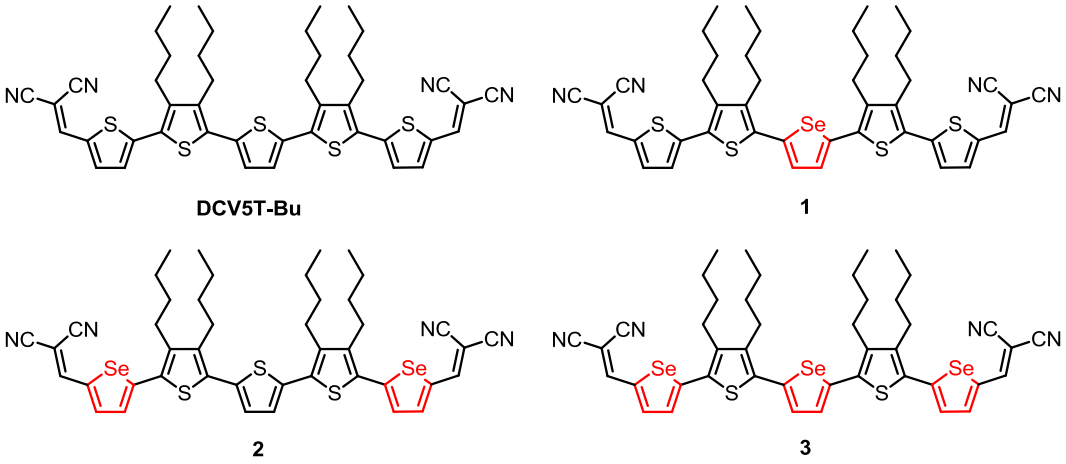

Figure 3.5: Molecular structures of mixed selenophene-thiophene pentamers **1**-**3** and reference compound **DCV5T-Bu**.

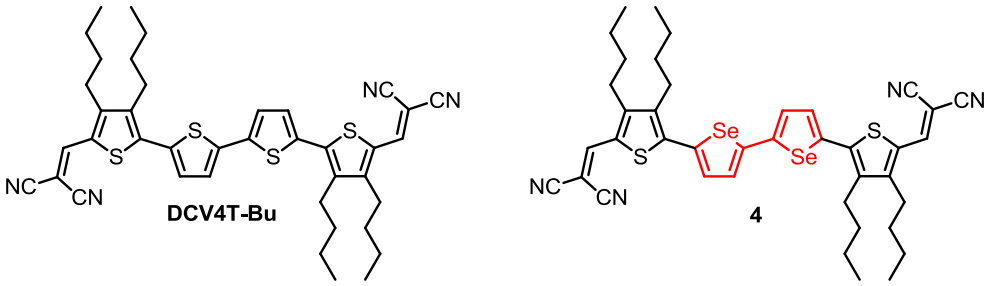

Figure 3.6: Molecular structures of mixed selenophene-thiophene tetramer **4** and reference compound **DCV4T-Bu**.

3.2.2 Synthesis of Co-oligomers 1-4

Two different strategies were applied for the synthesis of the mixed selenophene-thiophene pentamers **1**-**3**. Compounds **1** and **3** were synthesized on a linear route by first building up the complete conjugated backbone (**Scheme 3.1**) and then introducing the DCV acceptor groups (**Scheme 3.2**). The synthesis of pentamer **2** differed in the way that the acceptor groups were introduced. Here, the acceptor groups were already attached to the halogen-functionalized selenophene building block **31,** which then was coupled to the previously synthesized stannylated terthiophene **33**[45] (**Scheme 3.3**). Later on, the DCV-substituted selenophene **31** proved to be a versatile building block for the synthesis of several other DCV-substituted oligomers (see **Section 3.3** and **Chapter 4**).

The synthesis of pentamers **1** and **3** started with the dibromination of selenophene **20** using two equivalents (eq.) NBS in DMF at r.t. In contrast to the established literature synthesis for the resulting 2,5-dibromoselenophene **21**,[24] DMF was used as solvent instead of a chloroform-acetic acid mixture and the yield was increased from 65% to 84%. As a second building block, thiophene boronic ester **23** was synthesized in 72% yield from 3,4-dibutylthiophene **22**[46] by lithiation with *n*-BuLi (1 eq.) at 0 °C and subsequent quenching with 2-isopropoxy-4,4,5,5-tetramethyl-1,3,2-dioxaborolane (ITDB). In the next step, boronic ester **23** was coupled with dibromoselenophene **21** in a Suzuki cross-coupling reaction. A combination of $Pd_2(dba)_3{\cdot}CHCl_3$ (2 mol%) and $HP^tBu_3BF_4$ (4 mol%) was used as catalyst, and aq. K_3PO_4 was chosen as base. With this very active catalytic system,[47] the reaction could be carried out under relatively mild conditions (50 °C, overnight) and the desired trimer **24** was obtained in a good yield of 82% after purification by column chromatography.

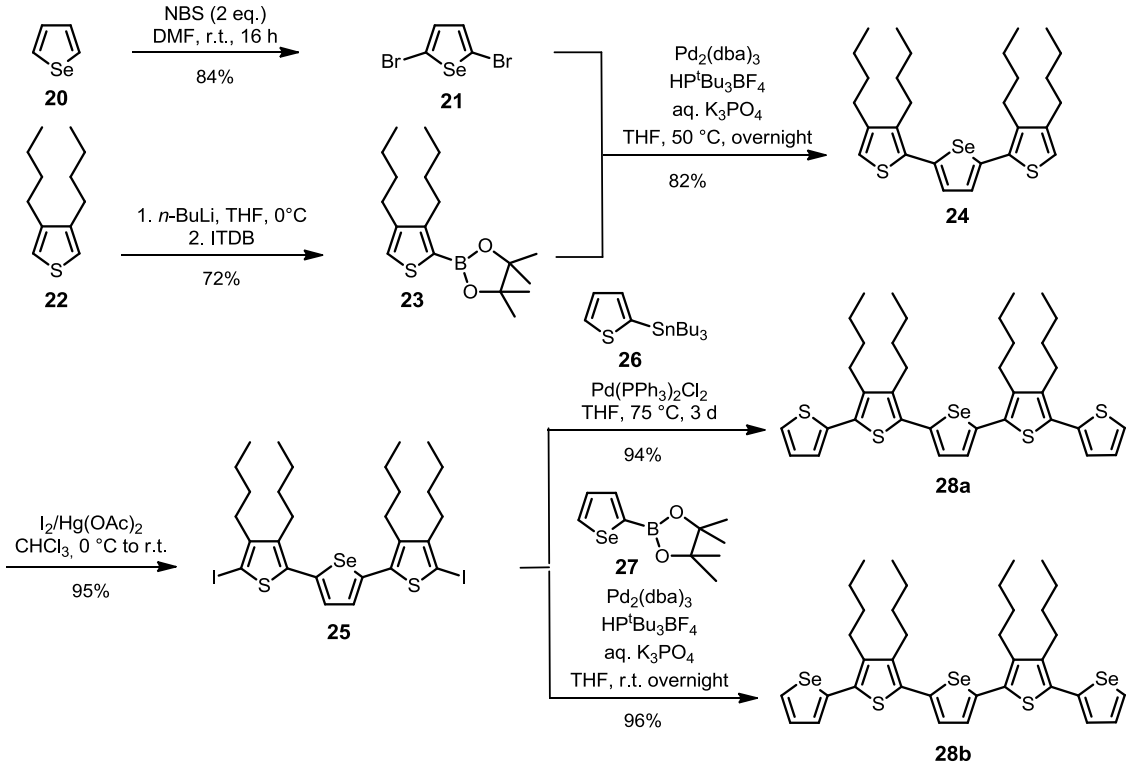

Scheme 3.1: Synthesis of pentamers **28a** and **28b**.

Trimer **24** was diiodinated with iodine/mercury(II) acetate (2 eq.) in chloroform solution to afford the diiodinated trimer **25** in an excellent yield of 95%. From here, the synthetic route split into two pathways, one leading to pentamer **1**, the other leading to pentamer **3**. In order to synthesize pentamer **28a**, diiodo compound **25** was coupled in a Stille cross-coupling with commercially available 2-tributylstannylthiophene **26**. The two reactants were stirred in THF at 75 °C for 3 d with $Pd(PPh)_2Cl_2$ as catalyst, and compound **28a** was obtained in 94% yield after purification on a silica gel column. Pentamer **28b** was synthesized via a Suzuki cross-coupling of diiodinated trimer **25** with

selenophene boronic ester **27**. The latter had been synthesized in 98% yield from selenophene **20** by lithiation with 1 eq. *n*-BuLi in THF at 0 °C and quenching with ITDB. The Suzuki reaction was carried out in THF at r.t. overnight with $Pd_2(dba)_3/HP^tBu_3BF_4$ as catalyst and aq. K_3PO_4 as base. Pentamer **28b** was obtained in an excellent yield of 96% after chromatographic purification. The organometallic reactants in these two cross-couplings were simply chosen due to their availability and not for reactivity reasons. One could also have used a stannylated selenophene or a thiophene boronic ester.

The two pentamers **28a** and **28b** were further functionalized by Vilsmeier-Haack formylation (**Scheme 3.2**). In order to obtain dialdehydes **29a** and **29b**, it was necessary to use 20 eq. of phosphoryl choride/DMF to ensure complete formation of the dialdehydes and to shorten the reaction time. The reactions were carried out in dichloroethane (DCE) at r.t. for 22 h, and the two dialdehydes were obtained in excellent yields of 89% (**29a**) and 94% (**29b**), respectively. Finally, both dialdehydes were reacted with malononitrile in a Knoevenagel condensation using β-alanine as catalyst. A mixture of DCE and EtOH had to be used as solvent because of the low solubility of β-alanine in halogenated solvents. The reactions were carried out under reflux conditions for 24 h, and after purification by column chromatography the desired DCV-substituted pentamers **1** and **3** were both obtained in 79% yield.

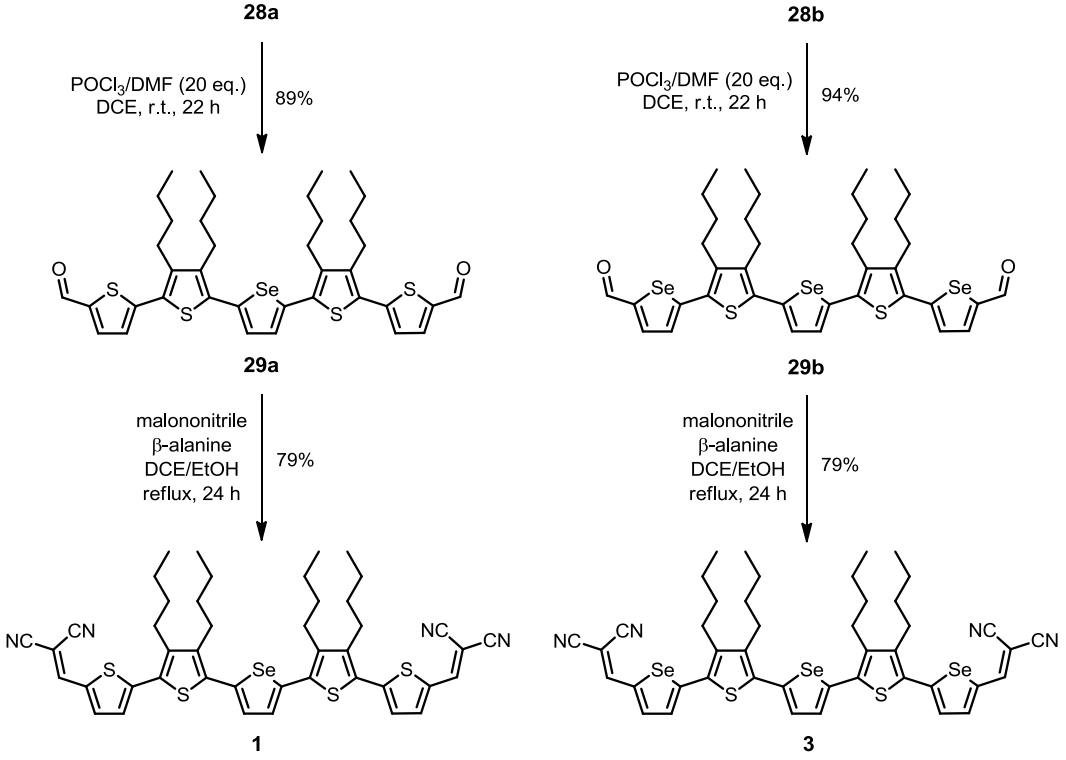

Scheme 3.2: Synthesis of target compounds **1** and **3**.

As mentioned above, pentamer **2** was synthesized by a convergent method (**Scheme 3.3**). First, the distannylated terthiophene **33** was synthesized by lithiation of terthiophene **32** and subsequent quenching with trimethyltin chloride. Terthiophene **32** is literature-known[48] and was synthesized by Nicolas Trinks while he was working on his bachelor thesis in our group.[45] For the lithiation of terthiophene **32**, the addition of *N*,*N*,*N*',*N*'-tetramethylethylenediamine (TMEDA) was necessary to activate the butyllithium because of the bulky butyl groups on the β-positions of trimer **32**. The solution had to be warmed to 50 °C in order to ensure complete formation of the dianion. After quenching with trimethyltin chloride and aqueous work-up distannyl compound **33** was obtained in 83% yield.

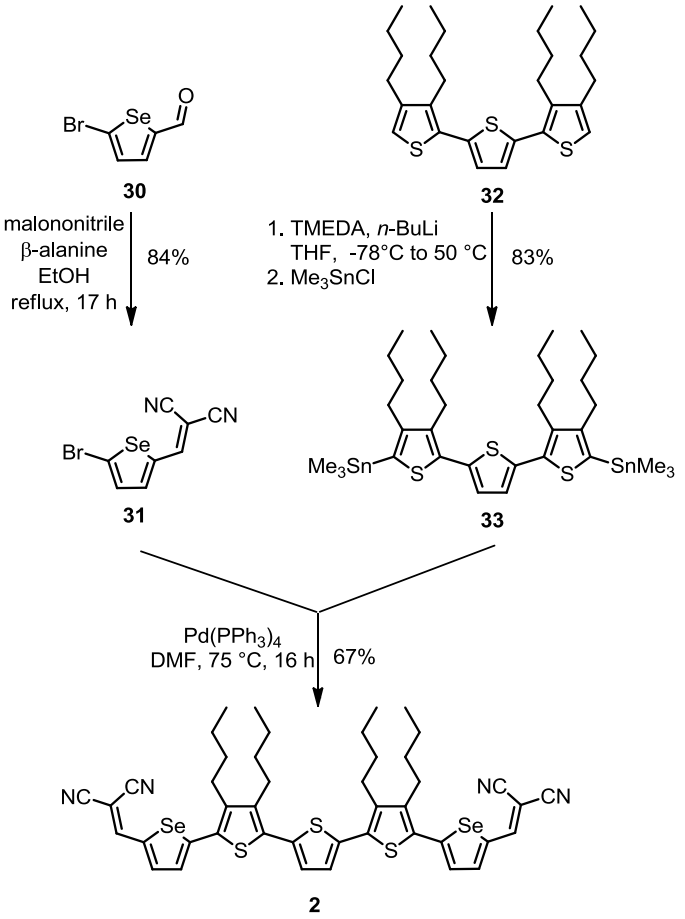

Scheme 3.3: Synthesis of co-oligomer **2**.

The second building block, bromosubstituted DCV-selenophene **31**, was synthesized from 5-bromoselenophene-2-carbaldehyde **30** by Knoevenagel condensation with malononitrile. Unlike the corresponding thiophene, selenophenecarbaldehyde **30** is not commercially available and had to be synthesized according to a literature protocol.[49] The Knoevenagel condensation was carried out in ethanol at 60 °C with β-alanine as catalyst. The product precipitated during the reaction and was filtered off. It was washed with ethanol and no further purification was necessary to obtain the pure

product in 84% yield. In the last step, stannylated terthiophene **33** and bromoselenophene **31** were coupled in a Stille-type cross-coupling reaction with $Pd(PPh_3)_4$ as catalyst. The reaction was carried out in DMF at 75 °C and was complete after 16 h. Pentamer **2** was purified by column chromatography and isolated in 67% yield.

3,4-Dibutylthiophene building block **23**, which was used in the synthesis of pentamers **1**-**3**, also served as starting material for the synthesis of DCV-substituted tetramer **4** (**Scheme 3.4**). For this purpose, it was coupled with 2,2'-dibromoselenophene **34**[24] in a Suzuki cross-coupling. The reaction was carried out using the catalytic system $Pd_2(dba)_3/HP^tBu_3BF_4$ and aq. K_3PO_4 as base in THF at r.t. Tetramer **35** was obtained in 75% yield after stirring for 16 h and chromatographic purification on silica gel. Subsequent Vilsmeier-Haack reaction with $POCl_3$/DMF (20 eq.) in DCE at r.t. afforded dialdehyde **36** in 75% yield. In the last step, **36** was reacted with malononitrile under the usually used Knoevenagel conditions to obtain DCV-substituted co-oligomer **4** in 87% yield.

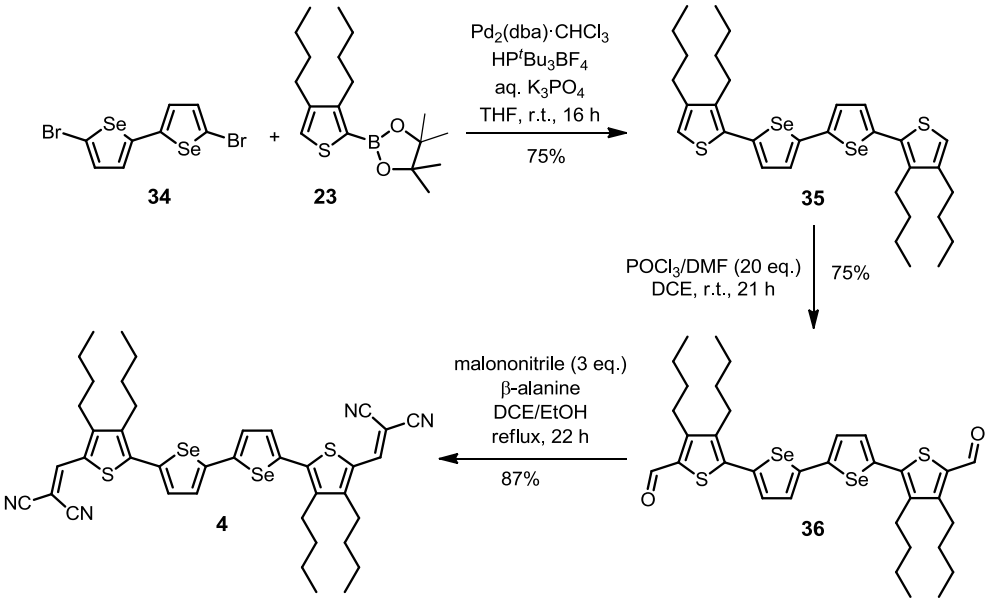

Scheme 3.4: Synthesis of tetramer **4**.

Pentamers **1**-**3** were fully characterized by ^1H and ^{13}C NMR spectroscopy in deuterated chloroform, MALDI-TOF mass spectrometry and elemental analysis. The ^1H NMR spectra of pentamers **1**-**3** showed four signals for the protons of the conjugated backbone (H_a-H_d, **Figure 3.7**), two singlets for H_a and H_d and two doublets for H_b and H_c. If the DCV group was adjacent to selenophene the signal for the DCV proton was slightly shifted downfield (δ_{Ha} = 7.84 ppm) compared to the DCV group being attached to a thiophene (δ_{Ha} = 7.77 ppm). The signals for selenophene protons (X,Y = Se; δ_{Hb} = 7.82 ppm, δ_{Hc} = 7.43 ppm, δ_{Hd} = 7.34-7.35 ppm) were observed downfield-shifted compared to thiophene protons (X,Y = S: δ_{Hb} = 7.69 ppm, δ_{Hc} = 7.29 ppm, δ_{Hd} = 7.19 ppm) which is in accordance with observations on the corresponding parent heterocycles (see **Figure 1.1**).

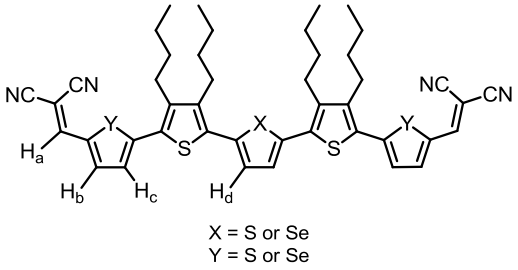

Figure 3.7: Assignment of protons in ^{1}H NMR spectra of pentamers **1**-**3**.

In the ^{13}C NMR spectra 11 signals in the aromatic region (126-155 ppm) were observed for all pentamers corresponding to the carbon atoms of the heteroaromatic rings and one of the DCV carbon atoms. The cyano-substituted carbon atom of the DCV group (~76 ppm) was extremely upfield-shifted due to the strong electron-withdrawing character of the cyano groups. The carbon atoms of the cyano groups appeared as two distinct signals around 114 ppm. In the MALDI-TOF mass spectra pentamers **1**-**3** were clearly identified by their monoisotopic mass peaks at *m/z* = 836.5 (pentamer **1**), 884.2 (pentamer **2**) and 930.5 (pentamer **3**). The elemental analyses were in excellent agreement with the calculated values.

3.2.3 Attempts Towards the Synthesis of 3,4-Dialkylselenophene

As mentioned in the introduction, the synthesis of the *all*-selenophene pentamer **37** (**Figure 3.8**) was not successful because all attempted synthetic methods for the synthesis of 3,4-dialkylated selenophenes either failed or could not be carried out on a larger scale. In this section, these attempts are discussed in detail.

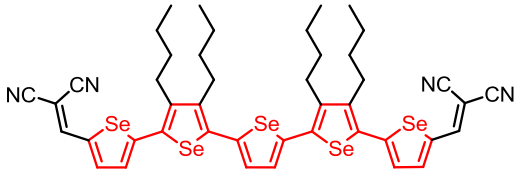

37

Figure 3.8: Attempted *all*-selenophene pentamer **37**.

In the literature, no synthetic methods for the synthesis of 3,4-dialkylated selenophenes (except for 3,4-dimethylselenophene[50]) are described. Therefore, I tried to apply common synthetic pathways for the synthesis of 3,4-dialkylthiophenes to the corresponding selenophenes.

The most common way for the preparation of 3,4-dialkylthiophenes is the Kumada cross-coupling of 3,4-dibromothiophene with alkylmagnesium bromides or chlorides.[46, 51] 3,4-Dibromothiophene can by synthesized from thiophene by tetrabromination with an excess of bromine[52-53] and subsequent

selective reduction at the α-positions with zinc/acetic acid.[53] For selenophene, this route has never been described in the literature. Although 3,4-dibromoselenophene is literature-known,[30, 54-55] it was never used as a reactant in Kumada couplings. Nevertheless, this appeared to be the easiest and fastest method (**Scheme 3.5**).

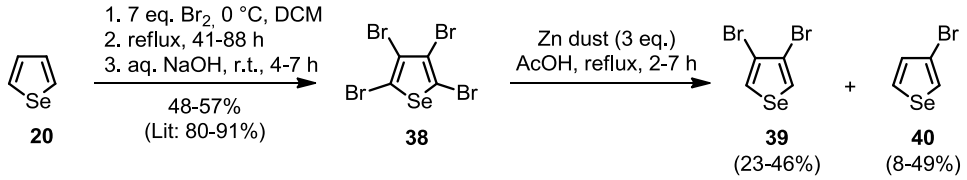

Scheme 3.5: Synthesis of 3,4-dibromoselenophene.

2,3,4,5-Tetrabromoselenophene **38** was prepared according to a literature protocol[55] by bromination of selenophene **20** with excess of bromine (7 eq.). Different reaction times between 41 and 88 h were tested, but the yield always was between 50 and 60%. The literature yield of 80% after 72 h reaction time could never be reached. Very recently, an even higher yield of 91% was reported.[30] It is not clear why these high yields could not be reproduced, maybe the tetrabromoselenophene partly decomposed during work-up. For the subsequent reduction, two methods had been described in the literature. Tetrabromoselenophene was either reduced with zinc in refluxing acetic acid[56] or with *n*-BuLi.[57] For the latter method, however, no detailed reaction conditions or yields were given. Therefore, the first method was tested first. In this case as well, the literature yield of 69% of 3,4-dibromoselenophene **39** was never obtained because the reaction was very difficult to control. When the reaction mixture was refluxed for 3 h, as reported in the literature, a large amount of tetrabromoselenophene **38** (up to 50%) was reisolated besides the desired 3,4-dibromoselenophene **39** (46%) and traces of 3-bromoselenophene **40**. When the reaction was carried out for 7 h, the amount of 3-bromoselenophene **40** increased dramatically to around 50%. Reduction of **38** by lithiation with *n*-BuLi (2 eq.) in THF at -78 °C and subsequent quenching with water resulted in the decomposition of the starting material and no desired product was obtained. Long after this reaction had been carried out, Patra *et al.* reported on the synthesis of 3,4-dibromoselenophene in 81% yield with *n*-BuLi at -78 °C in diethyl ether.[30] The choice of the solvent seems to be crucial for this reaction.

Nevertheless, a sufficient amount of 3,4-dibromoselenophene **39** could be synthesized for the following Kumada reaction (**Scheme 3.6**). In that reaction, butylmagnesium bromide in diethyl ether was added dropwise to a solution of dibromoselenophene **39** and dichloro[1,3-bis(diphenylphosphino)propane]nickel ($Ni(dppp)Cl_2$) as catalyst in diethyl ether at r.t. After complete addition of the Grignard reagent, the reaction was refluxed for 21 h. On a rather small reaction scale (2.3 mmol of **39**), the desired dibutylselenophene **41** was obtained in 53% crude yield. When the reaction was

repeated on a larger scale (30 mmol of **39**), the yield dropped below 10%. Most probably, the reaction temperature was too high in this reaction, which led to homo-coupling of the Grignard reagent and dehalogenation of dibromoselenophene. In 2010, Hollinger *et al.* published the synthesis of 3-hexylselenophene in 50% yield by Kumada coupling of 3-iodoselenophene with hexylmagnesium bromide at 0 °C.[58] This reaction could be successfully reproduced, even with a higher yield (see **Chapter 4**). Apparently, Kumada couplings with selenophene derivatives need to be carried out at lower temperatures than with thiophenes.

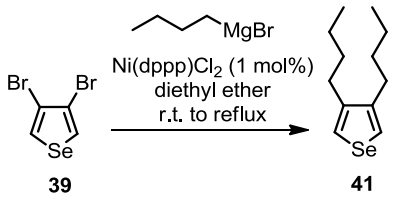

Scheme 3.6: Synthesis of 3,4-dibutylselenophene **41** by Kumada reaction.

Since the overall yield of this synthetic route was relatively low and some of the reactions were very difficult to control and reproduce, I intended to synthesize 3,4-dialkylselenophene by a Hinsberg-analogous ring-closing reaction.[59-60] 3,4-Diethylselenophene **46** was chosen as a target compound because it was reported by Vogel *et al.* as by-product in the synthesis of methyl 3,4-diethyl-selenophene-2-carboxylate **45** (**Scheme 3.7**).[61]

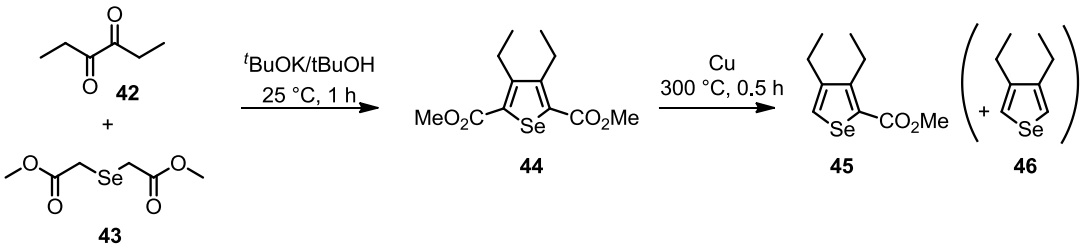

Scheme 3.7: Literature synthesis of 3,4-diethylselenophene-2-carboxylate **45**.[61]

In the first step of the literature procedure, commercially available 3,4-hexandione **42** was reacted with dimethyl 2,2'-selenodiacetate **43** using potassium *tert*-butoxide as a base. The thus obtained dimethyl 3,4-diethylselenophene-2,5-dicarboxylate **44** was decarboxylated with copper at 300 °C to obtain methyl 3,4-diethylselenophene-2-carboxylate **45**. In this reaction, target compound 3,4-diethylselenophene **46** was only obtained as by-product. Unfortunately, no detailed reaction conditions were given in ref. [61]. Nevertheless, this route seemed promising and I tried to prepare dimethyl 2,2'-selenodiacetate **43** according to a literature procedure (**Scheme 3.8**).[57] Therein, methyl chloroacetate was added dropwise to an aqueous solution of sodium hydrogenselenide, which was prepared by addition of sodium borohydride to a dispersion of selenium in water. The preparation of the sodium hydrogenselenide is a very delicate reaction because of vigorous foaming

during the addition of sodium borohydride. Furthermore, it is important that the reaction mixture becomes almost colorless. If it is reddish brown, it contains a lot of sodium diselenide.

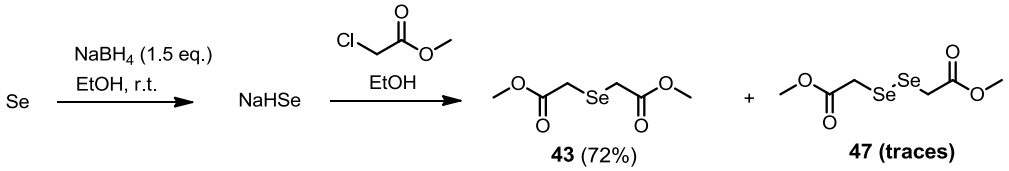

Scheme 3.8: Synthesis of dimethyl 2,2'-selenodiacetate **43.**

Since the reaction was difficult to control in water, the solvent was changed to ethanol according to ref. [62]. In this solvent, the reaction was much less vigorous and easier to control. The second step in the literature procedure, the addition of methyl chloroacetate, also turned out to be problematic. Regardless of the reaction being carried out in water or in ethanol, always a mixture of dimethyl 2,2'-selenodiacetate **43** and dimethyl 2,2'-diselanediyldiacetate **47** was obtained. Apparently, hydrogenselenide was oxidized by methyl chloroacetate to selenium (grey precipitate) and sodium diselenide. This problem was solved by changing the order in which the reactants were added. When the sodium hydrogenselenide solution was added to a solution of methyl chloroacetate in ethanol, the desired product **43** was obtained in 72% yield with only trace amounts of compound **47**. Afterwards, dimethyl selenodiacetate **43** was reacted with 3,4-hexanedione **42** in a Hinsberg reaction (**Scheme 3.9**).

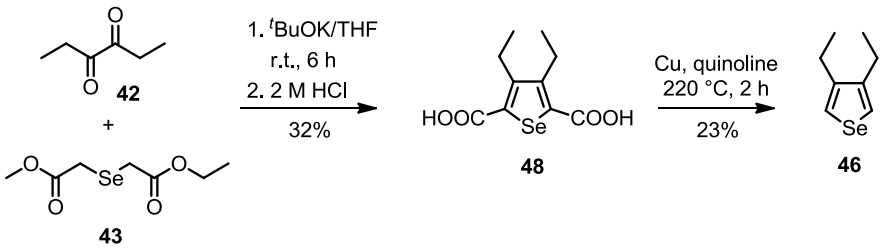

Scheme 3.9: Hinsberg synthesis of 3,4-diethylselenophene.

The reactants were dissolved in THF and potassium *tert*-butoxide was added. The reaction mixture was refluxed for several hours and precipitation with 2 M hydrochloric acid afforded 3,4-diethyl-thiophene-2,5-dicarboxylic acid **48** in 32% yield. No methyl ester was isolated. The resulting carboxylic acid **49** was decarboxylated by a method which is used for the preparation of thieno-[3,2-*b*]thiophene;[63] i.e., heating for 2 h in quinoline at 220 °C in the presence of copper powder. After work-up 3,4-diethylselenophene **46** was obtained in 23% yield.

Due to the low overall yield (calculated with regard to **43**) of only 7%, this did not appear to be a feasible route for the synthesis of several grams of 3,4-dialkylselenophene. Furthermore, several additional steps would have been necessary for the synthesis of 3,4-dibutylselenophene because the

required diketone is not commercially available. Since no suitable method for the preparation of 3,4-dibutylselenophene on a gram-scale was found, the synthesis of quinqueselenophene **37** was discarded.

3.2.4 Thermal Properties of Co-oligomers 1-4

The novel co-oligomers **1**-**4** were designed as donor materials for vacuum-processed organic solar cells, which are usually sublimed at temperatures between 250 °C and 350 °C. Therefore, the thermal stability of these compounds in this temperature range is of crucial importance. Thermal properties were investigated by thermogravimetric analysis (TGA) and differential scanning calorimetry (DSC) under an inert atmosphere at a scan rate of 10 °C min^{-1}.

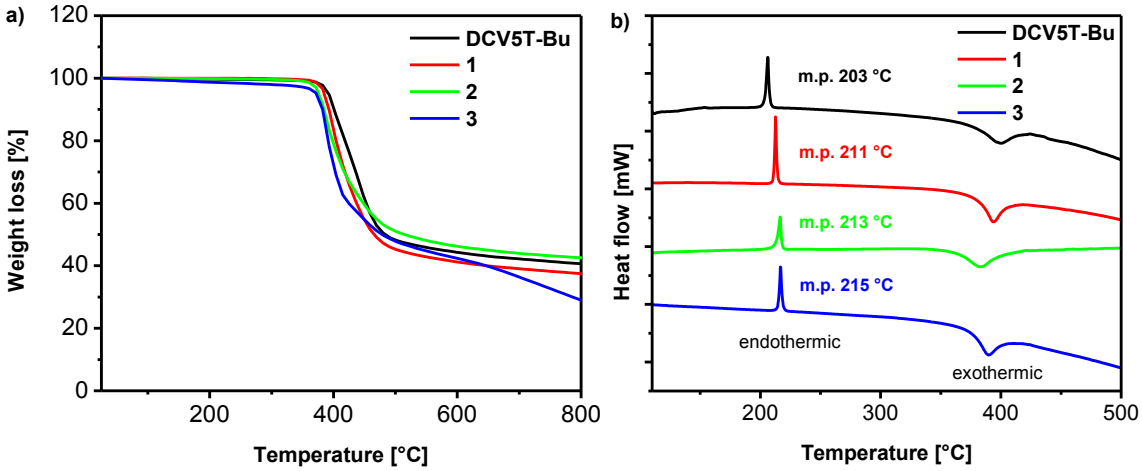

Figure 3.9: (a) TGA thermograms of terminally DCV-substituted pentamers **1**-**3** and **DCV5T** measured under N_2. Conditions: N_2 flow, 50 mL min^{-1}; heating rate, 10 ^{o}C min^{-1}. (b) DSC curves for **1**-**3** in comparison to **DCV5T** measured under argon flow at a heating rate of 10 ^{o}C min^{-1}.

Figure 3.9 shows the DSC and TGA curves for pentamers **1**-**3** compared to **DCV5T-Bu**; **Figure 3.10** shows the DSC curve for tetramer **4** in comparison to **DCV4T-Bu**. From the TGA measurements (**Figure 3.9a**), decomposition temperatures (T_d) with 5% weight loss were determined; in the DSC curves (**Figure 3.9b)**, the melting points manifested as endothermic peaks while beginning decomposition was indicated by an exothermic peak.

The decomposition temperatures for pentamers **1**-**3** and **DCV5T-Bu** lay above 370 °C, thus indicating sufficiently high thermal stability for vacuum sublimation. The T_d slightly decreased with increasing number of selenophenes from 392 °C for **DCV5T-Bu** to 372 °C for pentamer **3**. In contrast, the melting points increased from 203 °C for **DCVT5-Bu** to 215 °C for compound **3**. The exothermic decomposition peaks between 360 °C and 370 °C correspond well with the T_d values from the TGA measurements.

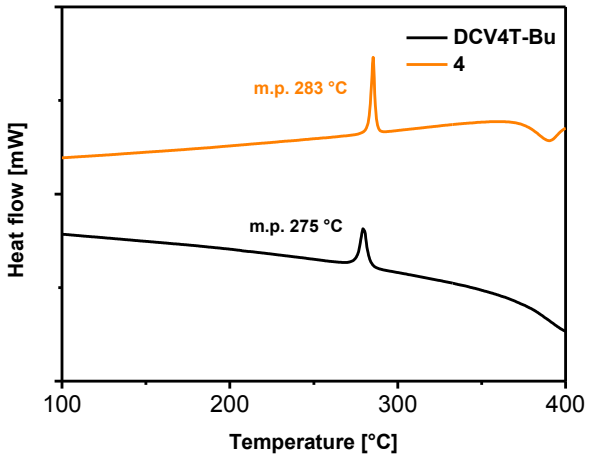

Figure 3.10: DSC curves for tetramer **4** and **DCV4T-Bu** measured under argon flow at a heating rate of 10 ^{o}C min^{-1}.

The melting point of tetramer **4** (283 °C) was slightly higher than the melting point of its *all*-thiophene analog **DCV4T-Bu** (275 °C) due to the replacement of thiophene units by selenophene. In the DSC curve of compound **4**, an exothermic decomposition peak at ~390 °C was visible, for **DCV4T-Bu** no decomposition peak was observed in the temperature range up to 400 °C. This might indicate a slightly higher thermal stability. In summary, it can be stated that the replacement of thiophene by selenophene generally leads to higher melting points, whereas decomposition seems to occur at slightly lower temperatures. The increasing melting points with increasing selenophene content could be a consequence of intermolecular nonbonded Se···Se interactions. It has been shown that the strength of such interactions increases in the order S < Se < Te.[64-65]

3.2.5 Optical Properties of Co-oligomers 1-4

Selenophene-pentamers **1**-**3** and tetramer **4** were investigated by UV-Vis absorption and fluorescence spectroscopy, both in dichloromethane solution (**Figure 3.11**) and in thin films prepared by vacuum deposition on glass substrates (**Figure 3.13**). Their properties were compared to the parent thiophene compounds **DCV5T-Bu** and **DCV4T-Bu** and the data are summarized in **Table 3.1**.

The absorption spectra of pentamers **1**-**3** in solution are structureless with one major absorption maximum between 510 and 535 nm which corresponds to the π-π* (HOMO-LUMO) transition of the conjugated backbone. The bathochromical shift compared to unsubstituted quinquethiophenes or quinqueselenophenes[24, 66] is due to a pronounced lowering of the LUMO energy caused by the electron-withdrawing DCV groups while the HOMO energy levels are lowered to a lesser degree. The position of the absorption maximum shifts to the red with increasing number of selenophene units from 513 nm for **DCV5T-Bu** to 533 nm for compound **3**. The same trend is observed for the emission

maxima, which lie in the range from 677 nm (**DCV5T-Bu**) to 690 nm (**2**). This red-shift is mainly caused by the DCV-substituted selenophenes on the periphery of the molecules. This can be deduced by comparing molecule pairs which only differ in these terminal selenophenes (**DCV5T-Bu** ↔ **2**, **1** ↔ **3**). For each pair, a red-shift of 16-17 nm is observed when the terminal thiophenes are replaced by selenophenes. If one compares pairs which only differ in the central selenophene (**DCV5T-Bu** ↔ **1**, **2** ↔ **3**) only a small red-shift of 3-4 nm is found.

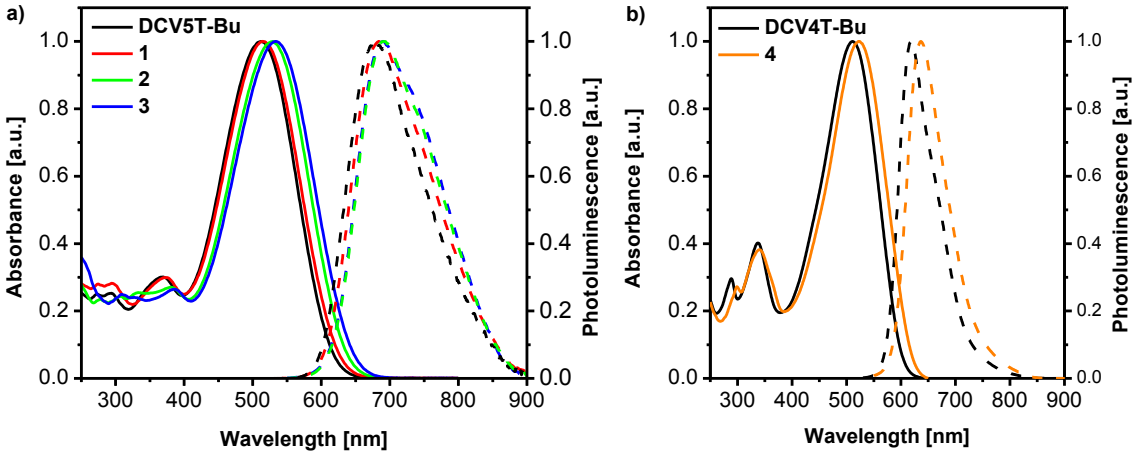

Figure 3.11: Normalized UV-Vis absorption and emission spectra of (a) pentamers **1**-**3** and **DCV5T-Bu** and (b) tetramer **4** and **DCV4T-Bu** in dichloromethane solution.

The molar extinction coefficients of these pentamers also depend on the number of selenophenes in the molecule. In a plot of the extinction coefficients against the number of selenophenes (**Figure 3.12**), an almost perfectly linear increase is observed going from **DCV5T-Bu** ($\lambda_{max,abs}$ = 62,600 L mol^{-1} cm^{-1}; no selenophenes) to pentamer **3** ($\lambda_{max,abs}$ = 66,000 L mol^{-1} cm^{-1}; 3 selenophenes). Since the main absorption band corresponds to a π-π* transition, the corresponding transition dipole moment should be increased by a bigger and better polarizable heteroatom such as selenium. Consequently, the extinction coefficient should be higher with increasing number of selenium atoms in the conjugated backbone. Similar trends have already been observed in the literature.[42-43]

The solution spectra of tetramer **4** and **DCV4T-Bu** (**Figure 3.11b**) show one dominant absorption maximum and one emission maximum, both being structureless. The absorption maximum of **4** is red-shifted by 12 nm compared to **DCV4T-Bu**, the emission maximum is shifted by 18 nm. Except for the red-shift, the spectra look almost identical in solution. In thin films (**Figure 3.13b**), however, the spectra exhibit more differences. The main absorption band of both compounds shows a vibronic fine structure with two peaks of slightly different intensity. For **DCV4T-Bu**, the first maximum (558 nm) is more intense than the second one (600 nm), for compound **4** this is vice-versa (637 vs. 589 nm). The absorption spectrum of **4** is red-shifted by ~35 nm compared to **DCV4T-Bu**. The

emission spectrum of **DCV4T-Bu** is structureless with a maximum at 695 nm, whereas the spectrum of **4** features one maximum at 688 nm and an additional shoulder at 735 nm. This difference in structure of the emission bands and the smaller Stokes shift for **4** compared to **DCV4T-Bu** could be a hint for a higher degree of planarization for tetramer **4** in thin film.

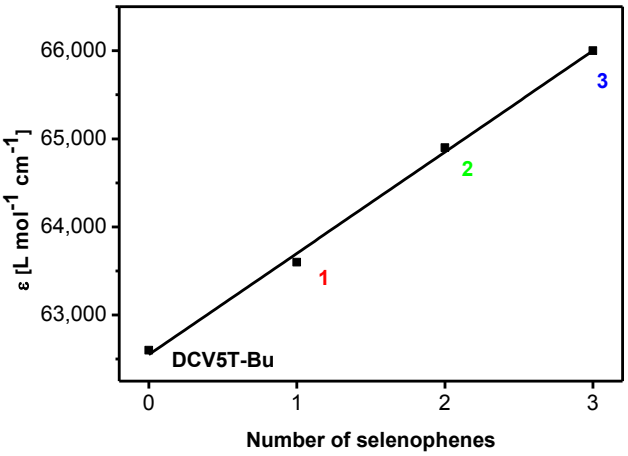

Figure 3.12: Correlation of molar extinction coefficients to number of selenophenes for pentamers **1**-**3** and **DCV5T-Bu**. R-factor for linear fit: R^2 = 0.99966.

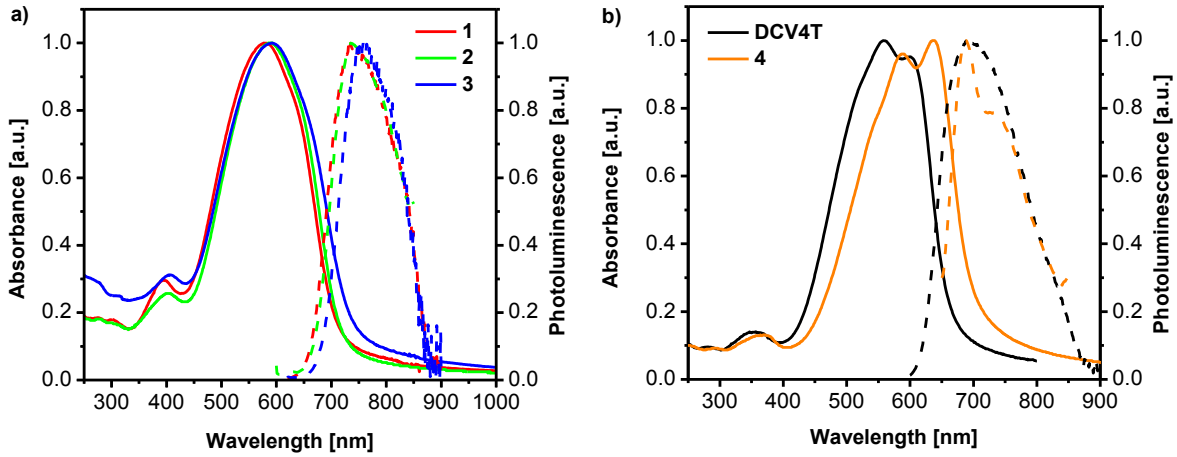

Figure 3.13: Normalized UV-Vis absorption and emission spectra of (a) pentamers **1**-**3** and (b) tetramer **4** in thin films prepared by vacuum sublimation on glass substrates.

The absorption spectra of pentamers **1**-**3** in thin films (**Figure 3.13a**) are broader and batho-chromically shifted by about 60 nm compared to the solution spectra. The reason for this red-shift is planarization and better ordering of the molecules in the solid state giving rise to greater inter-chromophoric interactions. The absorption maxima in thin films are between 573 nm for **DCV5T-Bu** and 592 nm for **3** and follow the same trend as in solution, i.e., red-shift of the maximum with increasing number of selenophenes. From the onset of the absorption maxima in solution and in thin

films, optical band gaps (E_g^{opt}) were calculated for compounds **1**-**4** and the respective reference compounds using the equation E_g^{opt} = 1240 nm / $\lambda_{max,onset}$. The band gaps in thin films, which are between 1.67 eV (**3**) and 1.86 eV (**DCV4T-Bu**), are by 0.20-0.25 eV lower than the band gaps calculated from the solution spectra.

Table 3.1: Optical data of selenophene-thiophene pentamers **1**-**3** and tetramer **4** compared to the parent thiophene compounds **DCV4T-Bu** and **DCV5T-Bu**.

	solution				film		
compound	$\lambda_{max,abs}$ [nm]	ε_{max} [L mol^{-1} cm^{-1}]	$\lambda_{max,em}$ [nm]	E_g^{opt} [eV][a]	$\lambda_{max,abs}$ [nm]	$\lambda_{max,em}$ [nm]	E_g^{opt} [eV][b]
DCV5T-Bu	513	62,600	677	2.02	573	726	1.76
1	516	63,600	684	2.01	577	735	1.74
2	529	64,900	693	1.96	589	737	1.72
3	533	66,000	690	1.93	592	758	1.67
DCV4T-Bu	510	-	618	2.06	558 (600)[c]	695	1.86
4	522	49,700	636	1.97	(589) 637	688 (735)	1.76

[a] Estimated using the onset of the UV-Vis spectra in DCM. [b] Estimated using the onset of the UV-Vis spectra of films prepared by vacuum sublimation. [c] Values in brackets designate additional maxima or shoulders.

The absorption and emission spectra of donor/acceptor blend layers with the investigated pentamers **1**-**3** and **DCV5T-Bu** as donors and C_{60} as acceptor are shown in **Figure 3.14**.

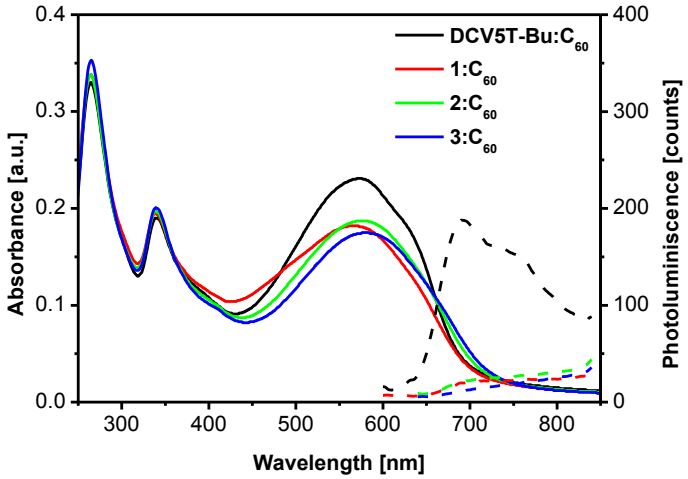

Figure 3.14: UV-Vis absorption and fluorescence spectra of optimized donor-acceptor layers as used in bulk-heterojunction solar cells. Blend layers of all four compounds each with C_{60} in a mixing ratio of 2:1 (v/v) deposited on a heated substrate (90 °C).

These layers were prepared in the same way as the bulk-heterojunction layers in the solar cells which were fabricated with these materials; i.e., the respective donor material was co-deposited with C_{60} (2:1 by volume) on a heated glass substrate (90 °C). Besides the absorption maxima of the donor materials at around 570 nm, these spectra show one additional peak at 340 nm and an increased absorption around 450 nm stemming from the C_{60} absorption. The absorbance of the blend layers with pentamers **1**-**3** is reduced by 20% compared to **DCV5T-Bu** and their emission is almost completely quenched by the acceptor. For **DCV5T-Bu**, however, no complete quenching but only a reduction of the emission by two orders of magnitude was observed. This is a hint for a higher degree of phase separation of donor and acceptor in the case of **DCV5T-Bu** compared to pentamers **1**-**3**. Better phase separation leads to bigger donor and acceptor domains; consequently, not all excitons that are generated in the donor domains reach the C_{60} acceptor domains and the luminescence is not completely quenched.[6]

3.2.6 Electrochemical Properties of Co-oligomers 1-4

The electrochemical properties of pentamers **1**-**3** and **DCV5T-Bu** were investigated by cyclovoltammetry (CV) of the dissolved compounds (**Figure 3.15**) and of films deposited on a platinum electrode (**Figure 3.16**). For the investigation of the dissolved co-oligomers, those were dissolved in dichloromethane ($c \approx 10^{-3}$ mol L^{-1}) with tetrabutylammonium hexafluorophosphate ($TBAPF_6$, 0.1 M) as supporting electrolyte. The data are summarized in **Table 3.2**.

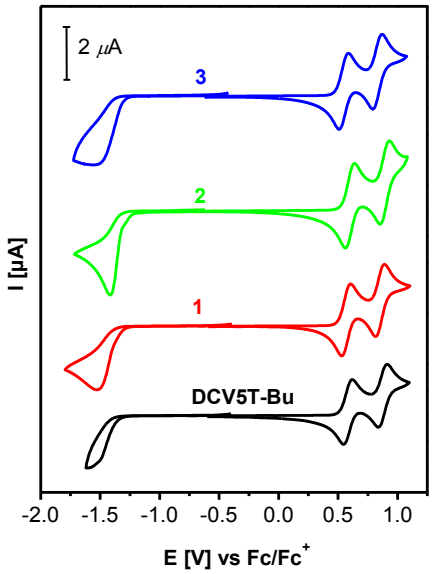

Figure 3.15: Cyclic voltammograms of mixed selenophene-thiophene oligomers **1**-**3** and **DCV5T-Bu**. Measured in DCM/$TBAPF_6$ (0.1 M), $c \approx 10^{-3}$ mol L^{-1}, 295 K, scan rate = 100 mV s^{-1}.

For all compounds two reversible oxidation and one irreversible reduction wave were observed. The first oxidation wave at ~0.60 V and the second oxidation wave at ~0.85 V indicate the formation of stable radical cations and dications. The potentials are only slightly dependant on the number of selenophenes and no clear trend is observable. The irreversible reduction waves at -1.35 V to -1.50 V are due to the irreversible reduction of the DCV groups.

Table 3.2: Electrochemical data of selenophene-thiophene oligomers **1**-**4**, **DCV4T-Bu** and **DCV5T-Bu**.

				solution[a]			*film*[b]		
compound	E^0_{ox1} [V]	E^0_{ox2} [V]	E^0_{red1} [V]	HOMO [eV][c]	LUMO [eV][c]	E_g^{CV} [eV][d]	HOMO [eV][c]	LUMO [eV][c]	E_g^{CV} [eV][d]
DCV5T-Bu	0.58	0.87	-1.50	-5.61	-3.74	1.87	-5.67	-3.75	1.92
1	0.57	0.86	-1.48	-5.60	-3.75	1.85	-5.68	-3.90	1.78
2	0.60	0.89	-1.36	-5.63	-3.80	1.83	-5.64	-3.89	1.75
3	0.55	0.83	-1.45	-5.58	-3.80	1.77	-5.63	-3.85	1.78
DCV4T-Bu	0.76	1.10	-1.49	-5.79	-3.71	2.08	-	-	-
4	0.74	1.03	-1.43	-5.75	-3.75	2.00	-	-	-

[a] Measured in DCM/$TBAPF_6$ (0.1 M), 25 °C, V = 100 mV s^{-1}, vs. Fc^+/Fc. [b] Drop-cast films on platinum electrode measured in acetonitrile solution. [c] E^0 (Fc/Fc^+) set -5.1 eV.[67] [d] Calculated from the difference between the values of $E_{onset, red1}$ and $E_{onset, ox1}$.

For the film measurements, the pentamers were dissolved in DCM and the solution was drop-cast on a platinum working electrode. The resulting thin films were investigated in an acetonitrile solution with 0.1 M $TBAPF_6$ as supporting electrolyte. The obtained cyclovoltammograms are shown in **Figure 3.16**. In contrast to CVs in solution, the two oxidation waves in the film CVs are not of the same intensity. Here, the second oxidation wave is much more intense than the first one. Probably, the molecules dissolve after oxidation to the radical cations and the oxidation to the dication then takes place in solution, which leads to much higher current intensities. In the reductive region, one irreversible reduction was observed for all four compounds, sometimes an additional peak appeared (**Figure 3.16a** and **Figure 3.16d**) when scanning back from negative to more positive potentials. This might be due to the formation of some unknown follow-up products during the irreversible reduction of the DCV groups.

From the onsets of the first oxidation and reduction potential in the solution and film CVs, HOMO and LUMO energy levels were calculated by subtracting the potentials from the vacuum potential (-5.1 eV vs. vacuum) of the Fc/Fc^+ standard.[67] In solution, the HOMO energies of the pentamers are at -5.58 to -5.63 eV and the LUMO energies between -3.74 eV and -3.80 eV. The values in thin films are at -5.63 to –5.68 eV for the HOMO energies and -3.75 to -3.90 eV for the LUMO energies. Thus, the values for both methods are in acceptable agreement. The difference of the respective HOMO

and LUMO energy values for each pentamer corresponds to the electrochemical band gap (E_g^{CV}). The values obtained from the solution measurements gradually decrease with increasing number of selenophenes from 1.87 eV for **DCV5T-Bu** to 1.77 eV for compound **3**. This trend is in good agreement with that observed for the optical band gaps from the solution or thin film spectra. The E_g^{CV} from the thin film CVs do not show such a clear trend but still correspond relatively well with the values in solution.

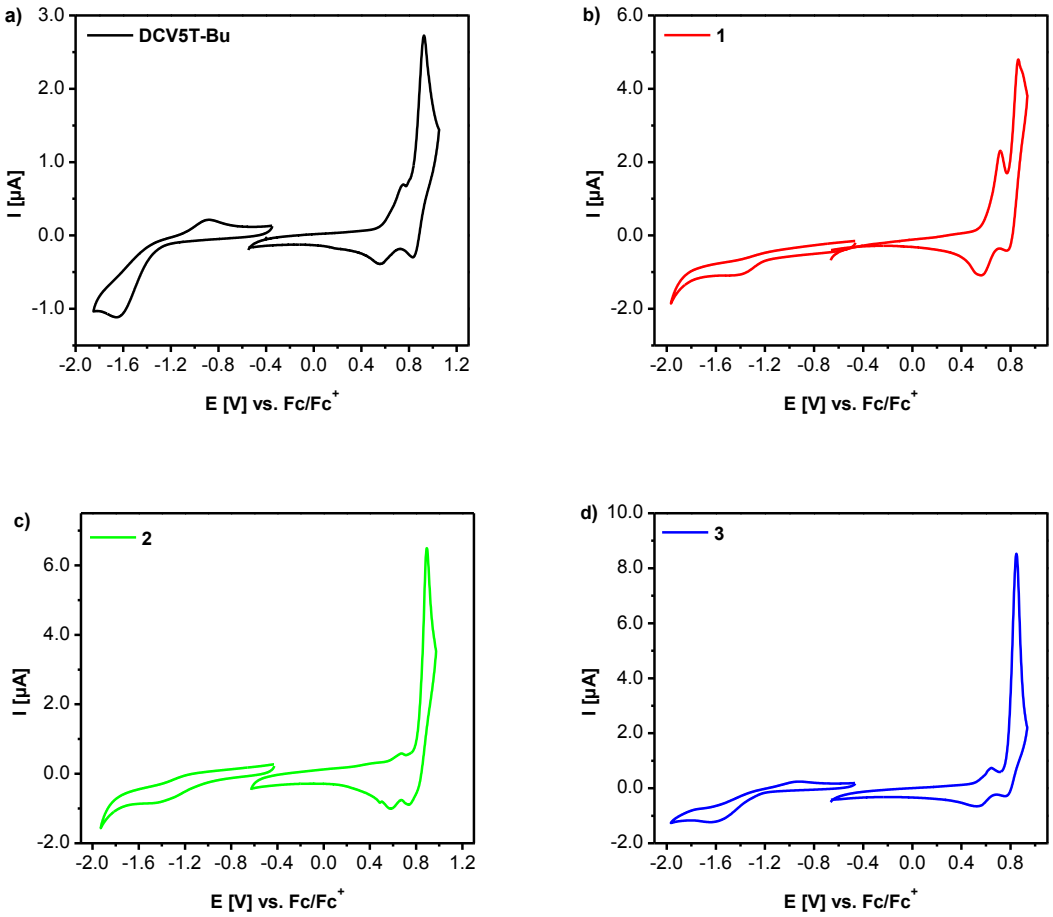

Figure 3.16: Cyclic voltammograms of drop-cast films of **DCV5T** and pentamers **1**-**3** in acetonitrile (295 K, scan rate = 100 mV s^{-1}) with $TBAPF_6$ as supporting electrolyte (0.1 M).

Due to its poor solubility, the electrochemical properties of tetramer **4** were determined by CV and differential pulse voltammetry (DPV) in 1,1,2,2-tetrachloroethane (TCE)/$TBAPF_6$ (0.1 M) at 80 °C. Because of its better solubility, **DCV4T-Bu** was investigated in DCM/$TBAPF_6$ (0.1 M) at room temperature. The voltammograms are depicted in **Figure 3.17**. The CVs of both compounds showed two reversible oxidation waves with similar oxidation potentials. For **DCV4T-Bu,** one irreversible reduction wave was observed due to the irreversible reduction of the DCV groups. The CV of **4** was dominated by a prominent solvent signal in the reductive region and no reduction wave was observed. The DPV, however, clearly shows one reduction peak at -1.43 V. HOMO and LUMO energy

levels were calculated for both compounds from the onsets of the respective first oxidation and reduction potentials. The HOMO of **4** (-5.75 eV) is marginally higher than that of **DCV4T-Bu** (-5.79 eV) while the LUMO of **4** (-3.75 eV) is slightly lower than that of **DCV4T-Bu** (-3.71 eV). Thus, the electrochemical band gap of **4** (2.00 eV) is slightly smaller than that of **DCV4T-Bu** (2.08 eV). This result is in good agreement with the trend for the optical band gaps in solution and in thin film.

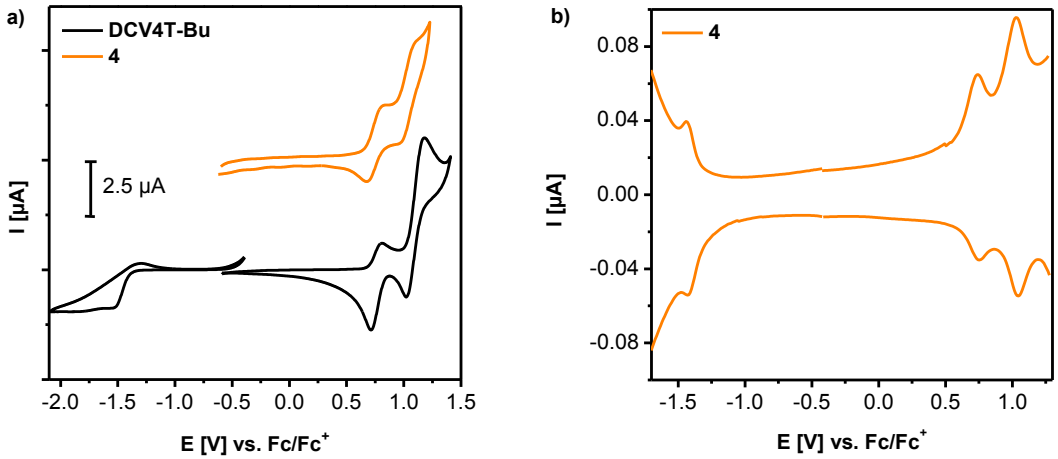

Figure 3.17: (a) Cyclic voltammograms of tetramer **4** and **DCV4T-Bu**. Compound **4** was investigated in TCE/$TBAPF_6$ (0.1 M) at 353 K, **DCV4T-Bu** in DCM/ $TBAPF_6$ (0.1 M) at 293 K; scan rate = 100 mV s^{-1}. (b) Differential pulse voltammogram of **4** under the same conditions as CV.

3.2.7 Photovoltaic Performance of Co-oligomers 1-4

The terminally DCV-substituted thiophene-selenophene pentamers **1**-**3,** tetramer **4** and their thiophene analogs **DCV5T-Bu** and **DCV4T-Bu** were used as electron donor materials in co-evaporated bulk-heterojunction solar cells with fullerene C_{60} as electron acceptor. The cells were prepared by vacuum sublimation following the m-i-p construction principle reported in the literature.[68]

The general device architecture is depicted in **Figure 3.18**. On an indium tin oxide (ITO)-coated glass substrate, first a layer of fullerene C_{60} (15 nm) was deposited, then a mixed donor/acceptor layer (20 nm) was deposited by co-evaporation of the respective DCV-pentamer or tetramer and C_{60} in a ratio of 2:1 by volume, which was found to be optimal for previously reported DCV-derivatives.[5, 10] During the deposition of the mixed layer the substrate was heated to 90 °C. A stronger phase separation was expected from heating of the substrate during the deposition, which should provide better charge transport within the percolation pathways of the mixed layer.[5-6] During the deposition of compound **4** the substrate was only heated to 70 °C because the blend film became too rough at 90 °C. The blend layer was covered with 5 nm of undoped and 50 nm of doped 9,9-bis[4-(*N*,*N*-bis-biphenyl-4-yl-amino)phenyl]-9*H*-fluorene (BPAPF) as hole-transport layer. The undoped BPAPF layer

was introduced to avoid direct contact between the active layer and the doped BPAPF layer, which otherwise could lead to quenching of excitons by the dopants. The thickness of the doped BPAPF layer was chosen to have the active layer approximately in the interference maximum. 10 wt% of NDP9 was used as p-dopant and another layer of NDP9 (1 nm) was used between the hole transport layer (HTL) and the top Au electrode to facilitate charge extraction. The dopant material NDP9 can be used for doping of organic materials with low lying HOMO energy levels and was chosen due to better stability and processability.

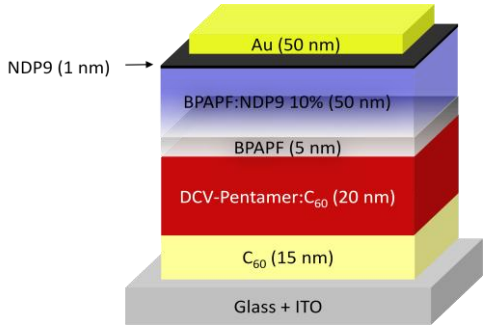

Figure 3.18: General device architecture of investigated BHJ solar cells.

Figure 3.19a shows the *J-V* characteristics of the investigated BHJ solar cells containing DCV pentamers. The active area of the solar cells was approximately 6 mm^2. The photovoltaic parameters of these BHJ devices are summarized in **Table 3.3**. Since the correct active area of especially small organic solar cells is difficult to determine, the *J-V*-characteristics of each solar cell were measured with an aperture mask of 2.76 mm^2 as well. From this measurement, $J_{SC,ap,100}$ normalized to 100 mW cm^{-2} and the PCE were calculated. The mismatch between the spectrum of the sun simulator and AM1.5G was not taken into account.

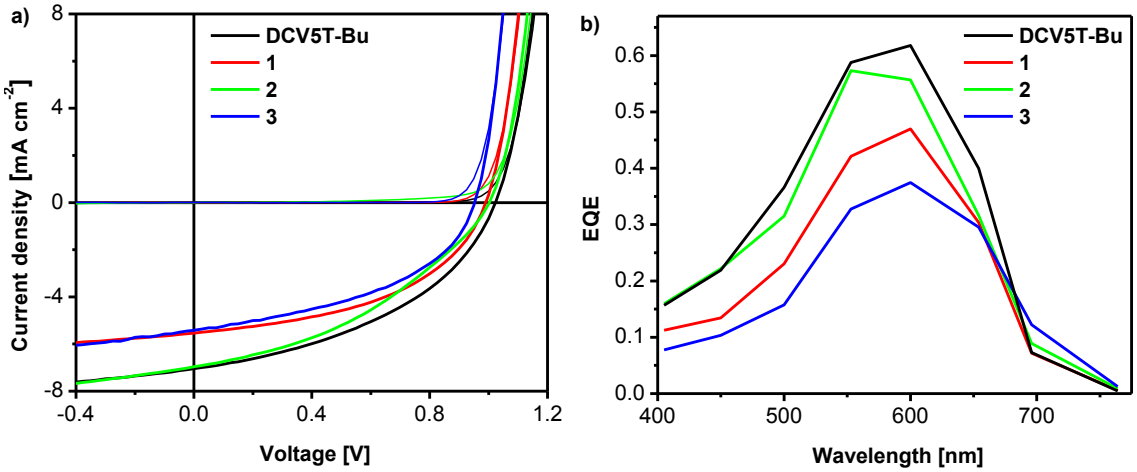

Figure 3.19: a) *J-V*-characteristics of bulk-heterojunction solar cells with DCV-substituted pentamers as donor materials. b) Corresponding EQE spectra of BHJ solar cells.

All devices measured in the dark showed good rectification behavior. The open circuit voltages (V_{OC}) under illumination were in the range of 0.95 to 1.02 V. The obtained high V_{OC} can be ascribed to the large energy difference in the HOMO of the donor and the LUMO of the C_{60} acceptor. Because the LUMO energy level is lowered with increasing selenophene content, V_{OC} decreases from **DCV5T-Bu** to pentamer **3**, i.e., with increasing number of selenophene units.

The short circuit current densities ($J_{SC,ap,100}$) show values in the range of 7.9 to 5.8 mA cm^{-2}. The values match with the external quantum efficiency (EQE) spectra shown in **Figure 3.19b** within the experimental error. The BHJ devices exhibit broad EQE spectra covering the range from 400 to 750 nm, which are in good agreement with the thin film absorption spectra. The J_{SC} values seen in the *J*-*V* curves are further reflected in the EQE spectra, with the **DCV5T**-device showing the best EQE value of about 60% at around 600 nm. The increased J_{SC} value for **DCV5T** is further corroborated by the thin film spectra of the donor:C_{60} blend layers, where **DCV5T** displayed higher absorbance values compared to the selenophene-containing derivatives. Both compounds with a central selenophene unit (**1** and **3**) show a significant decrease in $J_{SC,ap,100}$. This effect has already been observed comparing the absorption in solution and in the blend layers. One possible explanation is a lower degree of phase separation compared to **DCV5T**, giving rise to a lower degree of crystallinity in the DCV-pentamer phase and thus to less intramolecular order resulting in a decrease of absorption in the blended film.

Table 3.3: Photovoltaic parameters of bulk-heterojunction solar cells containing DCV-substituted selenophene-thiophene oligomers **1**-**4**, **DCV4T-Bu** and **DCV5T-Bu**.

compound	J_{SC} [mA cm^{-2}]	V_{OC} [V]	FF [%]	saturation[a]	incident light intensity [mW cm^{-2}]	$J_{SC,ap,100}$ [mA cm^{-2}][b]	PCE [%]
DCV5T-Bu	7.0	1.02	43	1.17	99	7.9	**3.5**
1	5.5	0.99	48	1.14	92	6.5	**3.1**
2	7.0	1.0	39	1.26	101	7.5	**2.9**
3	5.4	0.95	46	1.23	105	5.8	**2.5**
DCV4T-Bu	6.4	0.99	44	1.15	101	7.0	**3.1**
4	4.1	0.97	42	1.15	97	4.8	**2.0**

[a] Defined as $J(-1V)/J_{SC}$. [b] Measured with mask.

In **Table 3.3**, the saturation of the photocurrent with reverse bias is also given. The saturation is defined by the current density under illumination at -1 V bias divided by J_{SC}.[2] The saturation values are between 1.14 and 1.26, which indicates that there is some recombination at short circuit-condition and in reverse bias. A saturation value close to unity corresponds to efficient charge separation and extraction, while a larger value hints for recombination losses and field-dependent

dissociation of charge carriers. Devices with co-oligomers **2** and **3**, containing selenophenes adjacent to the DCV groups, showed a significant increase in saturation. This voltage-dependent recombination of photo-generated charge carriers might be attributed either to a degradation in charge carrier transport in the blend layer or to a decrease of the probability of exciton separation at the donor:acceptor interface.[6]

The PCE decreases almost linearly from 3.5% to 2.5% with increasing number of selenophenes (**Figure 3.20**). In the case of pentamers **1** and **3**, the decrease of PCE is caused by the lower J_{SC}, while in the case of **2**, the decrease of PCE is primarily caused by the lower fill factor. Recently, McCulloch and Durrant *et al.* reported a broad EQE spectrum for a regioregular poly(3-hexylselenophene):$PC_{61}BM$ device compared to the regioregular poly(3-hexylthiophene):$PC_{61}BM$ device, while the peak EQE is significantly lower for the former. The result was ascribed to the relatively lower internal photocurrent generation efficiencies and poor charge transport of the former at the donor:acceptor interface.[32, 69]

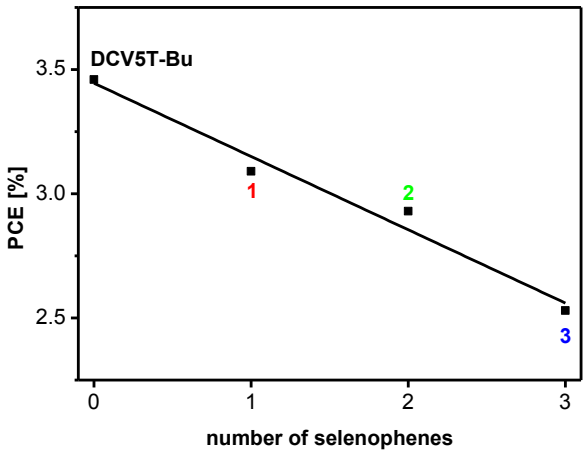

Figure 3.20: Correlation of PCE of co-oligomers **1**-**3** and **DCV5T-Bu** with number of selenophene units. R-factor for linear fit: $R^2 = 0.9652$.

The *J*-*V* curves and EQE spectra of BHJ solar cells with the tetramers **4** and **DCV4T-Bu** are depicted in **Figure 3.21**. The PCE for the **DCV4T-Bu** device is 3.1%, whereas **4** only reaches a PCE of 2.0%. Both devices are characterized by almost the same V_{OC} and FF, but J_{SC} for **DCV4T-Bu** (6.4 mA cm^{-2}) is more than 1.5 times higher than for **4** (4.1 mA cm^{-2}). This increase of J_{SC} is also reflected in the EQE spectra. Although **4** exhibited a red-shifted thin film absorption spectrum, the onsets of the EQE spectra of both compounds differ only marginally; both extend until ~700 nm. However, the EQE values for **DCV4T-Bu** are higher over almost the whole spectral range, with a maximum of ~0.5 around 550 nm. The maximum of **4** only reaches a value of ~0.35 in the region between 550 and 600 nm. As a consequence, the device with **DCV4T-Bu** transforms more photons into electrical current, which

results in a higher J_{SC} value. This finding might be a result of a lower charge separation efficiency in the device with compound **4** due to an increased roughness of the blend layer. Maybe a substrate temperature of 70 °C is still not ideal for devices with tetramer **4,** and lower temperatures may be more favorable for this material.

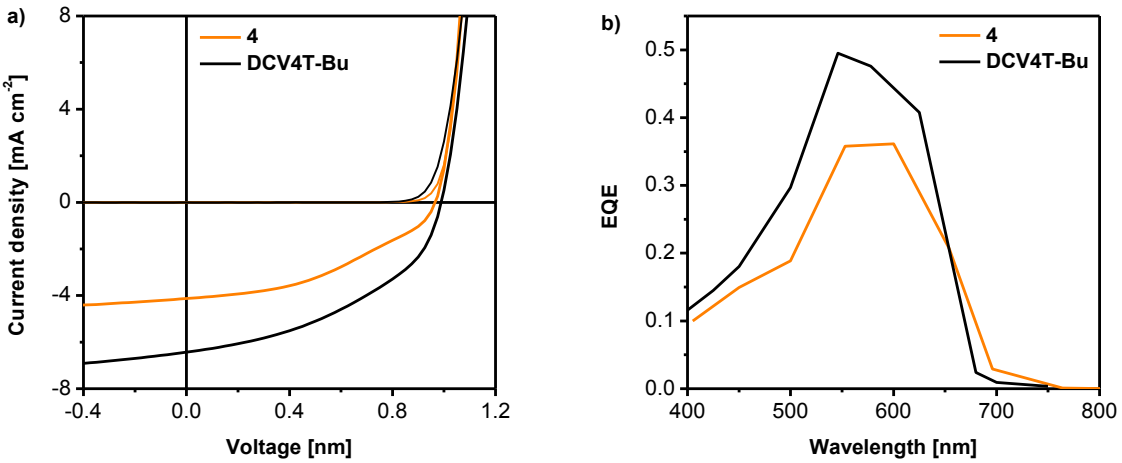

Figure 3.21: (a) *J-V*-characteristics of BHJ cells with tetramers **4** and **DCV4T-Bu** as donor materials. (b) Corresponding EQE spectra of BHJ solar cells.

3.3 Dicyanovinyl-substituted Oligoselenophenes

3.3.1 Introduction

In our group a complete series of DCV-substituted non-alkylated oligothiophenes up to a hexamer was synthesized by a novel convergent synthetic method. The thermal and optoelectronic properties of these compounds have been studied intensively. Furthermore, they were used as donor materials in PHJ and BHJ solar cells. The best efficiency of 5.2% was achieved with quinquethiophene **DCV5T** in a BHJ device with a 40 nm thick blend layer.[10]

As explained in the previous chapter, I did not succeed in synthesizing β-alkylated DCV-substituted oligoselenophenes due to the unavailability of 3,4-dialkylselenophene. Therefore, I turned my focus towards non-alkylated DCV-substituted oligoselenophenes. Oligoselenophenes **5**-**7** (**Figure 3.22**) were synthesized using the above-mentioned convergent method. Additionally, the mixed thiophene-selenophene compound **8** was synthesized by the same method. The reason for the synthesis of this compound was the outstanding solar cell performance of its *all*-thiophene analog. In the following sections, the thermal, optoelectronic, and photovoltaic properties of these oligomers are described and compared to their thiophene analogs. From compound **6**, single crystals were

obtained by vacuum sublimation. The X-ray crystal structure obtained from these crystals was compared to that of the thiophene analog **DCV4T**.

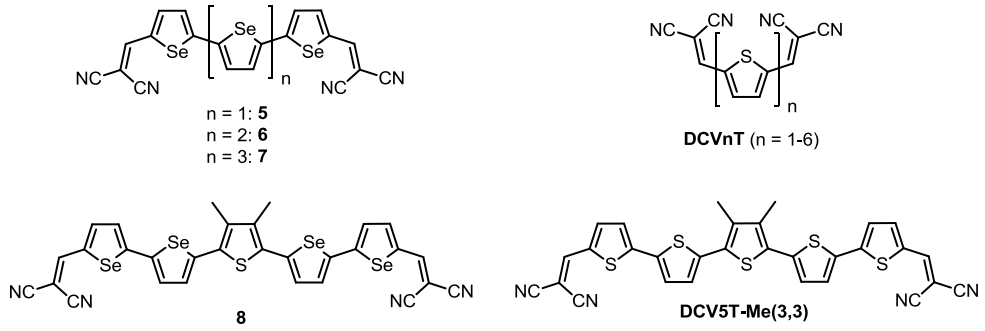

Figure 3.22: Investigated compounds **5**-**8** and their thiophene analogs.

3.3.2 Synthesis of Oligoselenophenes

The shortest oligomer, terselenophene **5**, was synthesized in a linear way starting from terselenophene **51** because compound **5** was expected to be sufficiently soluble for this reaction pathway. Oligomers **6**-**8** were synthesized by the convergent method developed for non-alkylated DCV-oligothiophenes because of their expected poor solubility. The synthesis of compounds **5**-**8** is summarized in **Scheme 3.10**.

The synthesis of DCV-terselenophene **5** started with unsubstituted terselenophene **51**. This was obtained as a side-product during the synthesis of 2,2'-biselenophene via oxidative coupling of α-lithiated selenophene with copper(II) chloride. A systematic synthesis via Stille-type cross-coupling is also known in the literature.[24] Terselenophene **51** was formylated in a Vilsmeier-Haack reaction with $POCl_3$/DMF (20 eq.). After refluxing in DCE for 5 d and subsequent column chromatography, the desired dialdehyde **52** was obtained in 63% yield. The moderate yield was due to the formation of a significant amount of monoaldehyde. Afterwards, dialdehyde **52** was reacted with malononitrile and β-alanine in a Knoevenagel condensation by refluxing the reactants in a DCE/EtOH mixture for 2 d. The target compound **5** was isolated by column chromatography in 72% yield.

Quaterselenophene **6** was synthesized by Stille coupling of distannylated biselenophene **53**[70] with DCV-selenophene **31** using catalytic amounts of $Pd(PPh_3)_2Cl_2$ in DMF at 80 °C. The product was isolated by simple filtration and washing with several solvents in a crude yield of >90%. It was purified by Soxhlet extraction with chlorobenzene for 2-3 weeks to obtain pure quaterselenophene **6** in 80% yield. The synthesis of compounds **7** and **8** was carried out in the same way. Quinqueselenophene **7** was synthesized from distannylated selenophene **54** and DCV-biselenophene **50** while distannylated 3,4-dimethylthiophene **55** was used instead of **54** for the synthesis of

pentamer **8**. Biselenophene **50** was synthesized in high yields from aldehyde **48** by monobromination with NBS in DMF at -25 °C and subsequent Knoevenagel condensation with malononitrile and β-alanine. Distannyl selenophene **54** was prepared from 2,5-dibromoselenophene **21** by lithiation with *n*-BuLi (2 eq.) in diethyl ether at -78 °C and subsequent quenching with trimethyltin chloride in 66% yield. Distannylated 3,4-dimethylthiophene **55** was synthesized by lithiation of 2,5-dibromo-3,4-dimethylthiophene and subsequent quenching with trimethyltin chloride according to a literature procedure.[71] Both Stille couplings afforded the desired products in crude yields of more than 80%, and after Soxhlet extraction with chlorobenzene the target compounds were obtained in 74% (**7**) and 87% (**8**) yield, respectively.

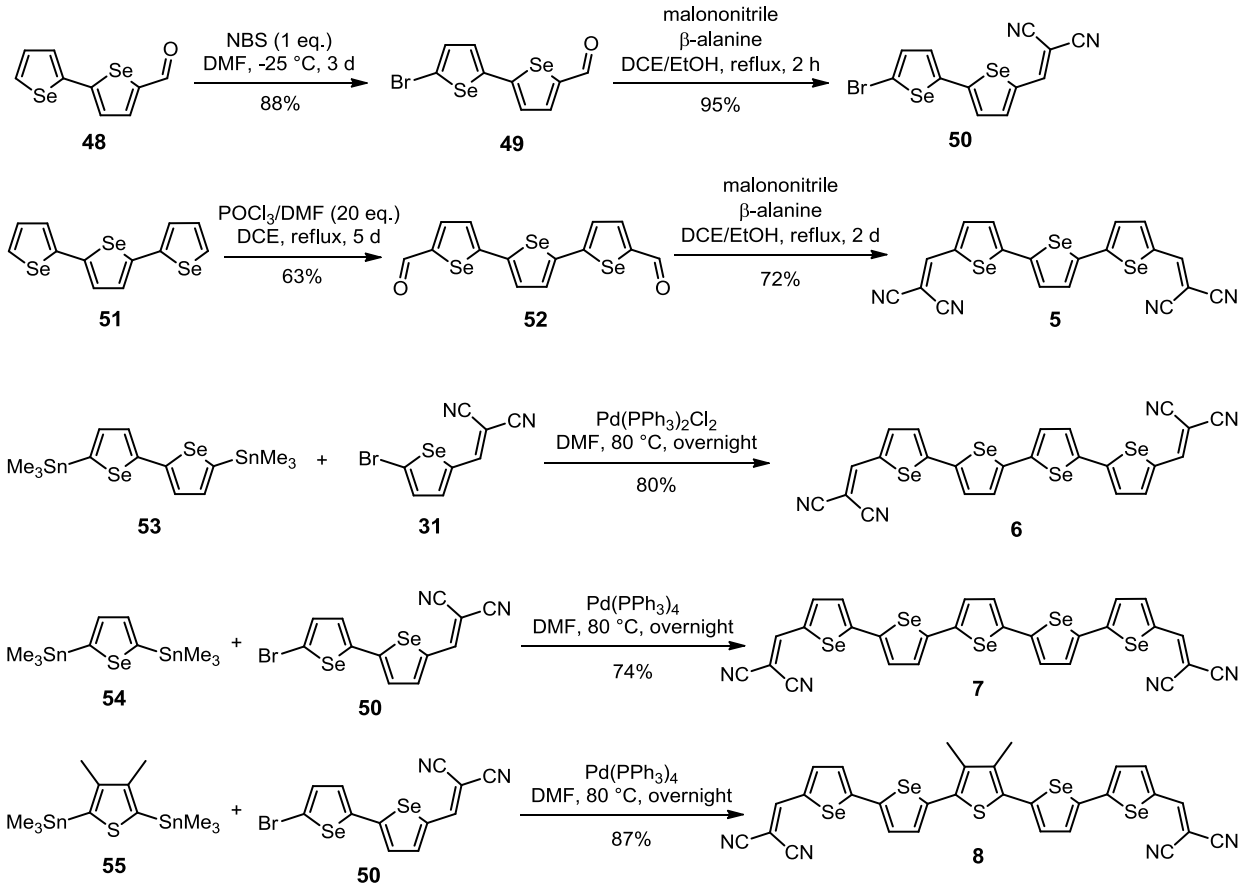

Scheme 3.10: Synthesis of compounds **5**-**8**.

Oligoselenophenes **5**-**7** were characterized by ^{1}H NMR spectroscopy in DMSO-d_6 at elevated temperatures, MALDI-TOF mass spectrometry and elemental analysis. ^{13}C NMR spectroscopy was only possible for trimer **3**, the higher oligomers were not sufficiently soluble. In the ^{1}H NMR spectra the DCV proton was observed at 8.54-8.58 ppm and the selenophene proton adjacent to the DCV group at 8.10-8.11 ppm. The remaining selenophene protons showed chemical shifts of 7.27-7.78 ppm. The MALDI-TOF mass spectra showed very complex isotope patterns due to the large

number of natural isotopes of selenium but the oligomers were clearly identified by their monoisotopic masses: *m/z* = 543.9 (trimer **5**), 671.4 (tetramer **6**) and 799.7 (pentamer **7**).

3.3.3 Thermal Properties of Oligoselenophenes

Oligoselenophenes **5**-**8** were designed for possible application in vacuum-processed solar cells. Therefore, they need to be stable at the usual sublimation temperatures of 250-350 °C. The thermal properties were investigated by DSC under an argon atmosphere (**Figure 3.23a**).

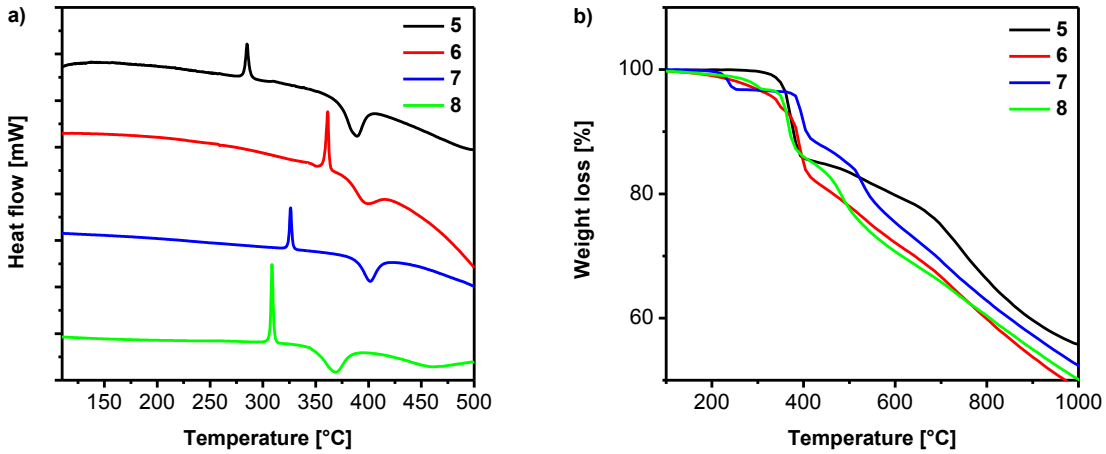

Figure 3.23: (a) DSC curves for compounds **5**-**8** measured under argon flow at a heating rate of 10 °C min^{-1}. (b) TGA thermograms of compounds **5**-**8** measured under N_2. Conditions: N_2 flow, 50 mL min^{-1}; heating rate 10 ^{o}C min^{-1}.

The DSC curve of each compound shows one endothermic peak, indicating the melting point, and one exothermic peak at higher temperatures, indicating beginning decomposition. The melting points of the oligoselenophenes (**5**: 282 °C; **6**: 358 °C; **7**: 324 °C) are higher than those of the corresponding oligothiophenes[10] (**DCV3T**: 265 °C; **DCV4T**: 320 °C; **DCV5T**: 287 °C). The melting points exhibit the same odd-even effect that was found for the analogous oligothiophenes, i.e., the melting point of **6**, which comprises an even number of selenophenes, is significantly higher compared to **5** and **7** with an odd number of selenophenes. The melting point of the mixed pentamer **8** (307 °C) also lies above the melting point of its thiophene analog **DCV5T-Me(3,3)** (301 °C). The decomposition temperatures of compounds **5**-**8** are above 370 °C, ensuring sufficient stability for vacuum sublimation without decomposition. The decomposition behavior was studied in more detail by TGA measurements (**Figure 3.23b**) under a nitrogen atmosphere. The decomposition is indicated by a turning point at ~365-370 °C for oligomers **5**, **6** and **8**, and at 395 °C for quinqueselenophene **7**. The continuous weight loss for all compounds at higher temperatures shows progressing decomposition.

For oligomer **7**, an additional step at around 235 °C is visible. This might be an indication for the loss of some traces of solvent.

3.3.4 Optical Properties of Oligoselenophenes

The optical properties of oligoselenophenes **5**-**7** were investigated by UV-Vis absorption and emission spectroscopy in dichloromethane solution (**Figure 3.24a**). In **Table 3.4** the data are summarized and compared to the data for the corresponding oligothiophenes.

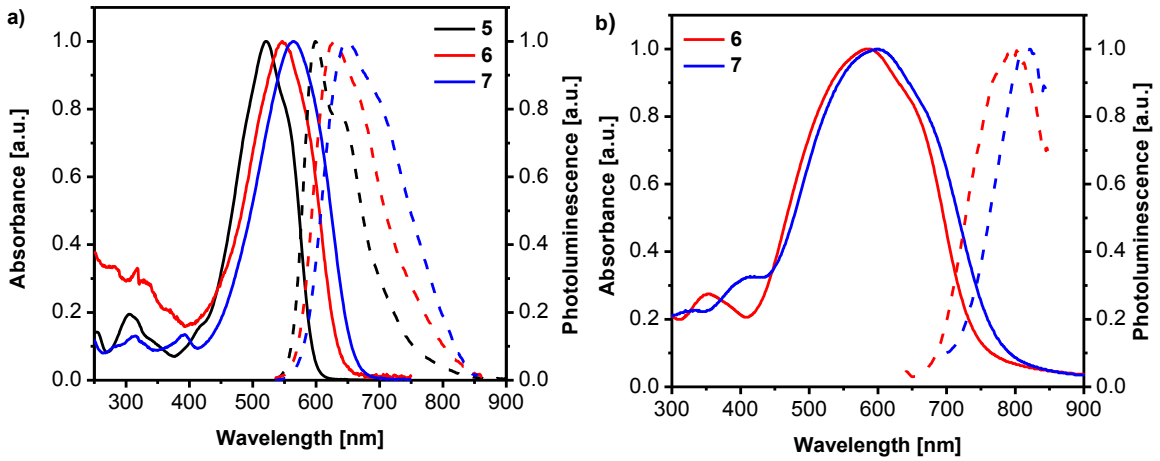

Figure 3.24: (a) UV-Vis absorption and emission spectra of **5**-**7** measured in dichloromethane. (b) UV-Vis absorption and emission spectra of **6** and **7** in thin films deposited by vacuum sublimation.

In the absorption spectrum of trimer **5**, one maximum at 521 nm and a shoulder at around 550 nm are observed. With increasing number of selenophenes, the peak loses its vibronic fine structure and is shifted bathochromically (**6**: 547 nm; **7**: 565 nm) due to extended conjugation. The same loss of structure is observed in the emission spectra. While the emission spectrum of **5** clearly features one maximum at 599 nm and a distinct shoulder at 638 nm, the shoulder almost disappears in the spectra of **6** ($\lambda_{max,em}$ = 654 nm) and **7** ($\lambda_{max,em}$ = 695 nm). Compared to the corresponding oligothiophenes, the absorption maxima are red-shifted by 25-35 nm. For the emission maxima, this trend is slightly more pronounced with shifts between 30 and 45 nm. In contrast to the oligothiophene analogs, no clear trend for the molar extinction coefficients is observed due to the lower solubility of the oligoselenophenes. The extinction coefficients of **5** (ε = 62,200 L mol^{-1} cm^{-1}) and **7** (ε = 63,500 L mol^{-1} cm^{-1}) are in the same region, whereas no extinction coefficient could be determined for **6** because of its very poor solubility.

For oligomers **6** and **7**, thin films were prepared by vacuum sublimation on glass substrates, and their UV-Vis absorption and emission spectra were measured (**Figure 3.24b**). Compared to the solution

spectra, the absorption spectra of thin films are significantly broadened and the maxima are bathochromically shifted by ~30 nm due to planarization and ordering of the molecules in the solid state. The emission maxima are even further red-shifted by 130-140 nm. The broad and red-shifted absorptions result in reduced optical band gaps for **6** and **7** compared to those in solution ($\Delta E_g^{opt} \approx$ 0.29 eV). Both in solution and in thin film, the band gaps of the oligoselenophene derivatives are by 0.1-0.15 eV lower than those of the corresponding oligothiophenes.

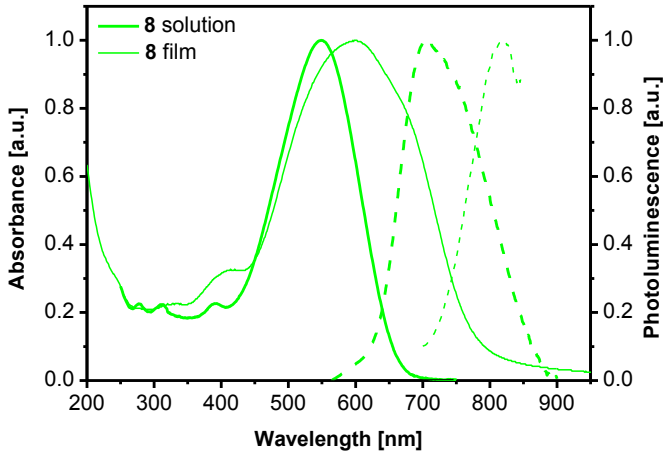

Figure 3.25: UV-Vis absorption and emission spectra of **8** in dichloromethane solution and in thin film.

The UV-Vis absorption and emission spectra of pentamer **8** in dichloromethane solution and in thin films are depicted in **Figure 3.25**, the data are summarized and compared to the thiophene analog **DCV5T-Me(3,3)** in **Table 3.4**.

Table 3.4: Optical data of **5**-**8** compared to the corresponding oligothiophenes.

		solution				*film*		
compound	T_m [a] [°C]	λ_{abs} [nm]	ε [L mol^{-1} cm^{-1}]	λ_{em} [nm]	E_g^{opt} [eV][b]	λ_{abs} [nm]	λ_{em} [nm]	E_g^{opt} [eV][b]
5	282	521	62,200	599	2.08	-	-	-
6	358	547	-[d]	654	1.95	581	797	1.68
7	324	565	63,500	695	1.89	596	822	1.60
DCV3T[c]	265	495	59,300	564	2.20	528	695	1.85
DCV4T[c]	320	518	66,800	612	2.09	560	670	1.78
DCV5T[c]	287	530	73,300	663	2.02	570	767	1.69
8	307	549	61,600	711	1.90	600	822	1.59
DCV5T-Me(3,3)	301	524	63,300	-	1.99	596	-	-

[a] Melting temperature determined from DSC. [b] Estimated using the onset of the UV-Vis spectra in DCM. [c] Values taken from Ref. [10]. [d] Not determined due to low solubility.

Both in solution and in thin films, the absorption spectra exhibit one maximum. In thin films, the maximum is red-shifted by ~50 nm compared to solution, and the absorption band is significantly broader with the indication of a shoulder at higher wavelengths. This hints at planarization of the molecules in the solid state. This red-shift is also observed in the emission spectra, from $\lambda_{max,em}$ = 711 nm in solution to $\lambda_{max,em}$ = 822 nm in thin film. The absorption maximum of **8** in solution is red-shifted by ~25 nm compared to its thiophene analog **DCV5T-Me(3,3)**. Interestingly, there is almost no red-shift of the absorption maximum in thin films.

3.3.5 Electrochemical Properties of Oligoselenophenes

The redox properties of oligomers **5**-**8** were studied by DPV measurements. Terselenophene **5** was investigated at room temperature in dichloromethane solution with 0.1 M $TBAPF_6$ as supporting electrolyte. Due to their poor solubility in dichloromethane, oligomers **6**-**8** were studied in TCE/$TBAPF_6$ solutions at 80 °C. All measurements were carried out with ferrocene as internal standard. The DPVs of oligoselenophenes **5**-**7** are shown in **Figure 3.26**, that of oligomer **8** in **Figure 3.27**. The data are summarized and compared to the corresponding oligothiophenes in **Table 3.5.**

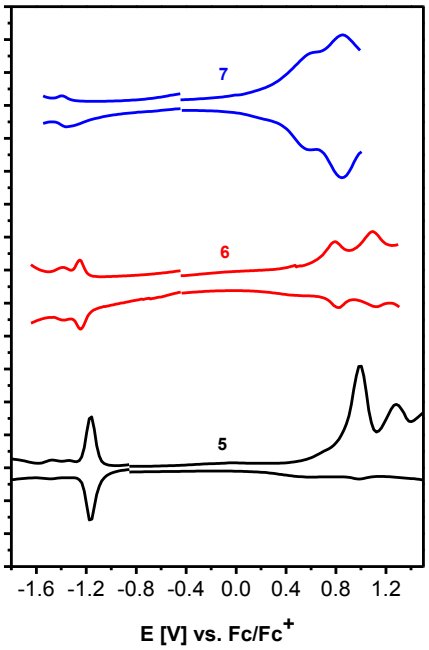

Figure 3.26: Differential pulse voltammograms of **5**-**7** measured in dichloromethane at 25 °C (**5**) or TCE at 80 °C (**6**, **7**). Supporting electrolyte $TBAPF_6$ (0.1 M), scan rate 100 mV s^{-1}, potentials versus Fc/Fc^+.

The DPVs of the oligoselenophenes **5**-**7** exhibit two oxidation potentials and one reduction potential. For **6**, a second reduction potential is visible. The oxidation potentials are shifted to more negative values with increasing chain length of the oligoselenophenes; i.e., the first oxidation potential shifts from 0.99 V for **5** to 0.57 V for **7,** and the second oxidation potential from 1.28 V for **5** to 0.85 V for **7**. This indicates an easier formation of stable radical cations and dications for longer oligoselenophenes due to the extended conjugated system. Compared to the corresponding oligothiophenes, the oxidation potentials are slightly lower by 0.1 V. The reduction potentials also shift to more negative values with increasing number of selenophenes from -1.17 V for **5** to -1.38 V for **7**.

Table 3.5: Electrochemical data of **5**-**8** compared to the corresponding oligothiophenes.

compound	E^0_{ox1} [V]	E^0_{ox2} [V]	E^0_{red1} [V]	HOMO[a] [eV]	LUMO[a] [eV]	E_g^{CV} [eV]
5[b]	0.99	1.28	-1.17	-6.02	-4.00	2.02
6[c]	0.81	1.11	-1.25	-5.81	-3.96	1.85
7[c]	0.57	0.85	-1.38	-5.60	-3.84	1.76
DCV3T[d]	1.06	-	-1.25	-6.09	-3.90	2.19
DCV4T[d]	0.84	1.20	-1.41	-5.85	-3.87	1.98
DCV5T[d]	0.64	0.93	-1.37	-5.62	-3.73	1.89
8	0.53	0.88	-1.44	-5.61	-3.82	1.79
DCV5T-Me(3,3)[e]	0.65	-	-1.50	-5.66	-3.75	1.91

[a] Set Fc/Fc^+ E_{HOMO} = -5.1 eV.[67] [b] Measured in DCM/$TBAPF_6$ (0.1 M), 25 °C, V= 100 mV s^{-1}, vs. Fc/Fc^+. [c] Measured in TCE/$TBAPF_6$ (0.1 M), 80 °C, V= 100 mV s^{-1}, vs. Fc/Fc^+. [d] Values taken from Ref. [10]. [e] According to ref. [72].

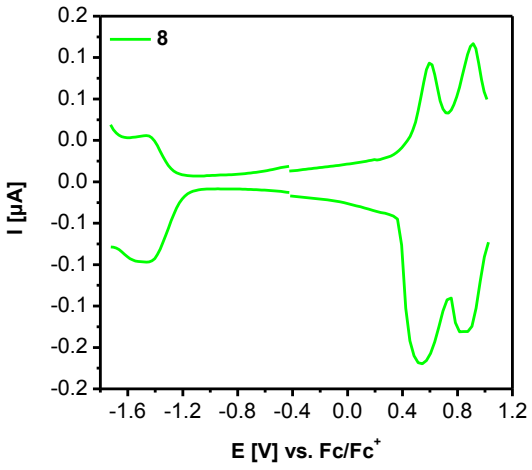

Figure 3.27: DPV of **8** measured in TCE/$TBAPF_6$ (0.1 M) at 80 °C, scan rate 100 mV s^{-1}, potentials vs. Fc/Fc^+.

The DPV of co-oligomer **8** also shows two reversible oxidation waves and one reduction wave. The oxidation potentials are similar to those of **7** but by ~0.1 V lower compared to **DCV5T-Me(3,3)**. Since oligomer **8** only contains one thiophene in the center, it seems reasonable that its electrochemical properties resemble very much those of a pristine oligoselenophene. Consequently, the HOMO and LUMO energy levels of **8** are very close to those of **7** resulting in a very similar electrochemical band gap (**8**: E_g^{CV} = 1.79 eV; **7**: E_g^{CV} = 1.76). Compared to **DCV5T-Me(3,3)** (E_g^{CV} = 1.91 eV), however, the band gap is lowered by 0.12 eV.

From the onset of the first oxidation and reduction potential, HOMO and LUMO energy values were calculated for each compound by subtracting the respective value from the Fc/Fc^+ potential (-5.1 eV vs. vacuum).[67] The difference of the thus determined HOMO and LUMO energy levels is the electrochemical band gap (E_g^{CV}). The HOMO energies rise by ~0.2 eV with increasing number of selenophenes from -6.02 eV for **5** to -5.60 eV for **7**. For the LUMO values, this increase is smaller from -4.00 eV for **5** to -3.84 eV for **7**. Consequently, the electrochemical band gap decreases from 2.02 eV for **5** to 1.76 eV for **7**. Compared to their oligothiophene analogs, the HOMO values of **5**-**7** are relatively similar, whereas the LUMO values are lower by about 0.1 eV. Due to the lower LUMO energies, the electrochemical band gaps of **5**-**7** are 0.1-0.15 eV smaller than the band gaps of **DCVnT**. The fact that the HOMO is only marginally influenced while the LUMO is lowered by the replacement of sulfur by selenium can be understood when the electron density distributions in the frontier orbitals are considered. Semi-empirical AM1-calculations for the oligothiophene series **DCVnT** revealed that the electron density distribution of the HOMO has no coefficient on the heteroatom, whereas the LUMO shows a significant contribution of the heteroatom.[10] When sulfur is replaced by selenium, the HOMO should remain relatively unaffected, but the LUMO should be stabilized by any heteroatom with a lower ionization potential.[73] Thus, the lower ionization potential[74] of selenium (9.75 eV) compared to sulfur (10.36 eV) is the reason for the lower LUMO energies of the investigated oligoselenophenes compared to their thiophene analogs.

Due to the low HOMO energy of -6.02 eV, **5** is expected to show rather n-type semiconducting character and is probably not suitable as donor material in organic solar cells; oligomers **6** (E_{HOMO} = -5.81 eV), **7** (E_{HOMO} = -5.60 eV) and **8** (E_{HOMO} = -5.61 eV) should be suitable p-type materials for solar cells with C_{60} as acceptor. The large difference between the HOMO of **6**-**8** and the LUMO of C_{60} (E_{LUMO} = -4.08 eV)[75] should provide reasonably high open circuit voltages (V_{OC}) as the V_{OC} depends mainly on the energy difference between the LUMO of the acceptor and HOMO of the donor materials.[76-78] Since the HOMO values of **6**-**8** are similar to those of **DCVnT**, the V_{OC} values for the oligoselenophenes are expected to be comparable to those of the corresponding oligothiophenes.

3.3.6 Single Crystal Structure Analysis of Quaterselenophene 6

Lath-like single crystals of DCV-quaterselenophene **6** were obtained after gradient sublimation at $1.75 \cdot 10^{-6}$ mbar and 325 °C. The crystals belong to the monoclinic space group $P2_1/n$, with 4 molecules in the unit cell. The unit cell parameters are: a = 3.92030(10), b = 27.6816(9), c = 22.7887(7) Å, β = 93.181(2)°. **Figure 3.28** shows the molecular structure of **6** in the crystal structure. The crystal structure is isostructural to that of the thiophene analog **DCV4T**.[10] The selenophene units show an *all-trans*-conformation, while the DCV groups are in an *all-cis*-conformation relative to the selenium atoms of the adjacent selenophene ring. The configuration of the molecule is almost planar (rms deviation 0.116 Å) with dihedral angles between the selenophene units below 4.5°. The cyano groups of the DCV groups are slightly twisted out of the molecular plane with nitrogen-plane distances of up to 0.39 Å. The bond lengths of the oligoselenophene backbone are summarized in **Table 3.6** and the inter- and intramolecular non-bonding atom distances shorter than the sum of the corresponding van der Waals radii are collected in **Table 3.7**. The values for the intraring C=C double bonds (1.367–1.381 Å), intraring C–C single bonds (1.402–1.410 Å) and the interring C–C single bonds (1.438–1.446 Å) are comparable with those of the oligothiophene analog **DCV4T**. The C–Se bonds (1.874–1.892 Å), however, are much longer than the C–S bonds (1.730-1.745 Å) in **DCV4T** due to the larger selenium atoms. These values are in good agreement with the values for the respective monomeric selenophene (1.855 Å) and thiophene (1.714 Å).[79-80]

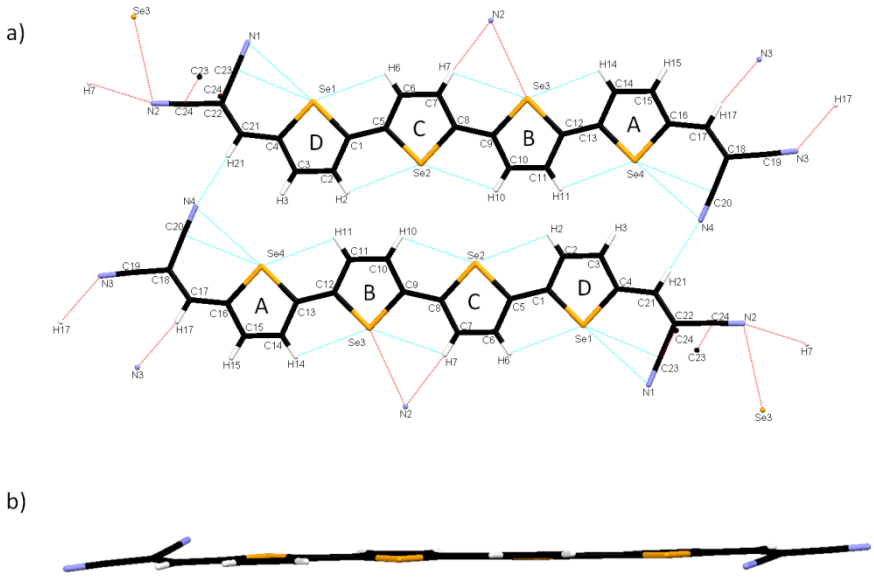

Figure 3.28: (a) Molecular structure of **6** (front view) with atomic numbering scheme. Inter- and intramolecular short contact distances are depicted by red and blue lines, respectively. Torsion angles between adjacent selenophene rings: A-B 178.7 °, B-C 175.5°, C-D 178.4°, N4-A 9.3°, D-N1 6.2° (b) Side view.

The unit cell comprises four molecules divided into two centrosymmetric pairs of antiparallelly arranged molecules (**Figure 3.29**). In the crystal, molecules extend in layers parallel to the (9 3 21) plane, leaving space for channels parallel to [100] that contain disordered molecules (for treatment of the disorder see details in the experimental section). Although the crystal structure resembles that of **DCV4T**, some differences can be recognized by comparison of the intra- and intermolecular short contacts (**Table 3.7** and **Figure 3.28**).

Table 3.6: Bond lengths [Å] in the oligoselenophene moiety in single crystals of compound **6** (Se-C bond lengths are printed in bold).

N1	C23	1.141(4)	C9	Se3	**1.875(2)**
C23	C22	1.427(4)	C9	C10	1.367(3)
N2	C24	1.151(4)	C10	C11	1.405(3)
C24	C22	1.434(4)	C11	C12	1.366(3)
C22	C21	1.363(4)	C12	Se3	**1.880(2)**
C21	C4	1.425(3)	C12	C13	1.439(3)
C4	Se1	**1.883(2)**	C13	Se4	**1.874(2)**
C4	C3	1.381(4)	C13	C14	1.376(2)
C2	C3	1.410(3)	C14	C15	1.402(4)
C2	C1	1.379(4)	C15	C16	1.370(4)
C1	Se1	**1.880(2)**	C16	Se4	**1.892(2)**
C5	C1	1.439(2)	C16	C17	1.414(3)
C5	Se2	**1.875(2)**	C17	C18	1.357(4)
C6	C5	1.370(3)	C18	C19	1.437(3)
C6	C7	1.407(3)	C18	C20	1.439(4)
C7	C8	1.371(4)	C19	N3	1.147(3)
C8	Se2	**1.886(2)**	C20	N4	1.152(4)
C8	C9	1.445(3)			

Table 3.7: Short inter- (left) and intra- (middle and right) molecular contacts [Å] below the sum of the van der Waals radii in single crystals of **6**.

C23…C24[a)]	3.345	Se1…C23	3.116	Se3…H7	2.986
N2…Se3[b)]	3.428	Se1…N1	3.328	Se3…H14	2.952
N2…H7[c)]	2.689	Se1…H6	2.948	Se4…C20	3.147
N3…H17[d)]	2.504	Se2…H2	2.962	Se4…N4	3.319
N4…H21[e)]	2.526	Se2…H10	2.968	Se4…H11	2.967

No intramolecular short contacts between hydrogen and sulfur atoms are observed for **DCV4T,** while each selenium atom in tetramer **6** interacts with the hydrogen atoms of the adjacent selenophene

ring(s). This is a consequence of the larger van der Waals radius of selenium (1.90 Å) compared to sulfur (1.80 Å).[81] In contrast to **DCV4T**, no intermolecular short distances between H2 and H11 are observed. However, there is an additional intermolecular interaction between Se3 and N2. For **DCV4T**, no intermolecular interaction between sulfur and nitrogen atoms was observed. The nitrogen atoms N2-N4 of **6** interact with the hydrogens H7, H17 and H21 via weak nonclassical C-H···N hydrogen bonds. The bond lengths of the hydrogen bonds, especially the N2…H7 bond, are slightly larger compared to **DCV4T**, indicating slightly weaker hydrogen bonding.

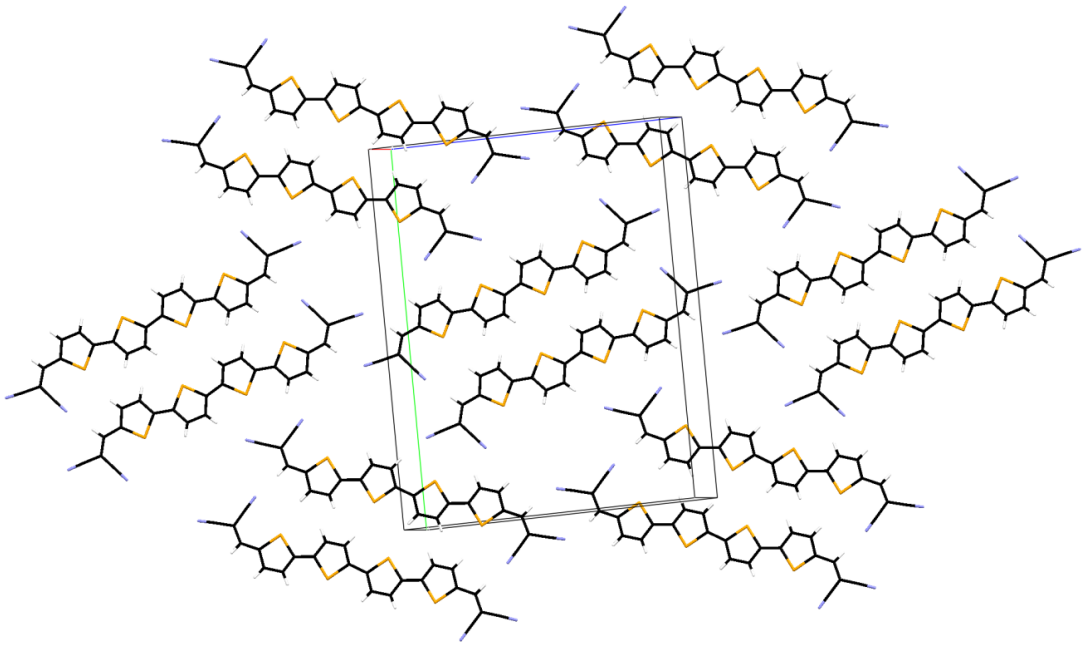

Figure 3.29: Molecular packing of quaterselenophene **6** in the single crystal viewed from the direction normal to the (9 3 21) plane.

DCV-quaterselenophene **6** does not exhibit a herringbone structure in the crystal as observed for the parent 2,2':5',2'':5'',2'''-quaterselenophene.[82] The π-conjugated backbones of the molecules are oriented parallel to one another, as it is seen in the view from the [010] direction (**Figure 3.30**). The intermolecular distances "d" are 3.563 Å compared to 3.512 Å for **DCV4T**, indicating a slightly less compact packing and π–π stacking of the oligoselenophene backbones due to the larger van der Waals radius of selenium compared to sulfur. In the perpendicular direction, the molecules (**Figure 3.30**) are lying in approximate coplanarity with a small offset between neighboring molecules (Δ = 1.085 Å; **Figure 3.30**). As in the case of **DCV4T**, weak nonclassical hydrogen bonding interactions caused by the terminal nitrile residues seem to be the main driving forces for the parallel ordering of the π-conjugated system in **6**. This explains the same packing features of both compounds.

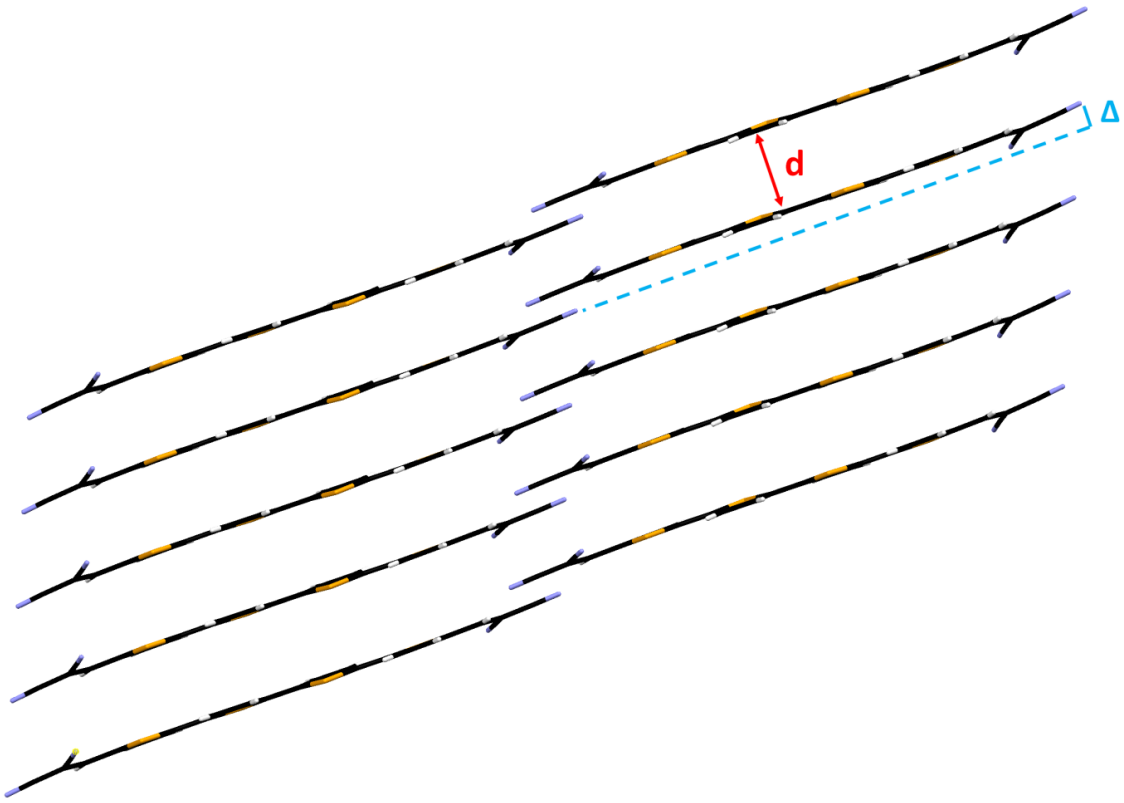

Figure 3.30: Molecular packing of quaterselenophene **6** in the single crystal view from the [010] direction showing the π –π stacking (d) of the molecules.

3.3.7 Photovoltaic Performance of Oligomers 6-8

Terselenophene **5** was not tested as donor material in organic solar cells due to its low-lying HOMO energy level and its possible n-type semiconducting character. Oligoselenophenes **6** and **7**, however, were implemented as donor materials in combination with fullerene C_{60} as electron acceptor, both in planar heterojunction (PHJ) and in bulk-heterojunction (BHJ) solar cells. The devices were fabricated by vacuum sublimation on glass substrates coated with indium tin oxide (ITO). For the PHJ devices, the following layer sequence was used: ITO coated glass, 15 nm C_{60} as acceptor, 6 nm or 10 nm of **6** or **7** as donor, 5 nm undoped 9,9-bis[4-(*N*,*N*-bis-biphenyl-4-ylamino)phenyl]-9*H*-fluorene (BPAPF), 50 nm BPAPF doped with 10 wt% NDP9 as hole transporting layer (HTL), 1 nm NDP9, 50 nm gold as top electrode. For the BHJ devices, a 20 nm or 30 nm mixed donor-acceptor layer was used instead of the pristine donor layer. This layer was prepared by co-evaporation of the respective donor and C_{60} as acceptor on a heated substrate. The device with tetramer **6** was fabricated at a substrate temperature of 70 °C and a blend ratio of 1:1, while pentamer **7** was deposited at 90 °C with a blend ratio of 2:1. These conditions had turned out to be optimal for the corresponding oligothiophenes.[10, 83]

The *J-V* curves of the thus fabricated PHJ and BHJ devices are shown in **Figure 3.31**, the EQE spectra are depicted in **Figure 3.32**. The photovoltaic parameters are summarized in **Table 3.8.** The dark curves in PHJ solar cells showed very good rectification behavior, while larger leakage currents were observed in the BHJ devices. For both device architectures, the layer thicknesses did not significantly influence the overall device efficiencies. J_{SC} increased with increased layer thickness, but the fill factor decreased, leading to an almost unchanged overall efficiency. Pentamer **7** gave better PCEs (PHJ: 3.4%; BHJ: 2.6%) compared to tetramer **6** (PHJ: 2.4%; BHJ: 1.7%). All devices showed a high V_{OC}; when comparing **6** and **7**-based PHJ devices, the V_{OC} decreases from 0.95V to about 0.91V. In this architecture, the change of V_{OC} represents in a first approximation the HOMO energy level difference between the two donor materials in the solid state.[84] This difference can also be expected from the electrochemically determined energy levels ($\Delta E_{HOMO} \approx 0.2$ eV) as shown in **Table 3.5**. One explanation for the deviation of the energetic shift could be that the latter values were obtained for single molecules in solution, whereas the values in the devices were shifted due to molecular packing in the solid state. Since the HOMO values of oligoselenophenes **5**-**7** are very similar to those of **DCVnT**, the V_{OC} values for the oligoselenophenes are comparable to those of the corresponding oligothiophenes.

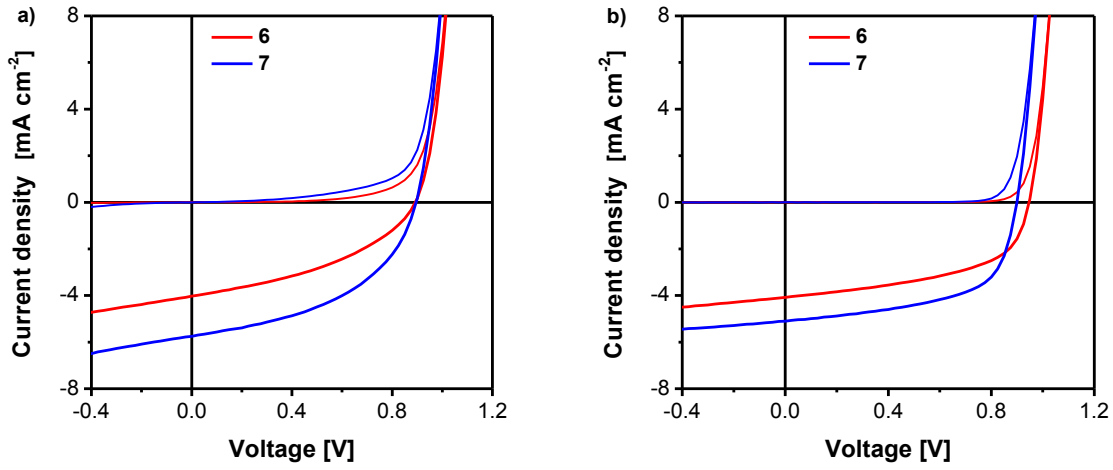

Figure 3.31: *J-V* characteristics of (a) bulk-heterojunction solar cells (20 nm bulk layer) and (b) planar heterojunction solar cells (6 nm donor layer) with **6** and **7** as donor materials.

In PHJ devices, J_{SC} increases with increasing layer thickness from 6 to 10 nm. This result shows that the exciton diffusion length is larger than 6 nm in both materials. The PHJ solar cells with pentamer **7** exhibit slightly higher J_{SC} values of 7.1 mA cm^{-2}. This can be correlated to the EQE spectra of the devices with **7** which are broad and red-shifted compared to tetramer **6**. The spectra for quinqueselenophene **7** show an onset at ~800 nm reaching a maximum of ~0.35, while the maximum for **7** lies below 0.3 with an onset at ~750 nm (**Figure 3.32a**). Thus, more charge carriers are generated in the device with pentamer **7**, leading to an increased photocurrent. PHJ devices with

tetramer **6** show lower FF and larger saturation values compared to the devices with **7**. Both effects originate from a voltage dependent photo-generated charge carrier recombination. One explanation could be an insufficient energetic LUMO offset between **6** and C_{60} leading to inefficient and voltage-dependent exciton separation at this interface. For both compounds, the PHJ devices give better PCEs than the BHJ devices. This difference in performance is mainly due to the slightly increased J_{SC} values and significantly higher FFs for the PHJ devices. This trend is in contradiction to previous results with the corresponding oligothiophenes in which BHJ devices outperformed PHJ solar cells.[10]

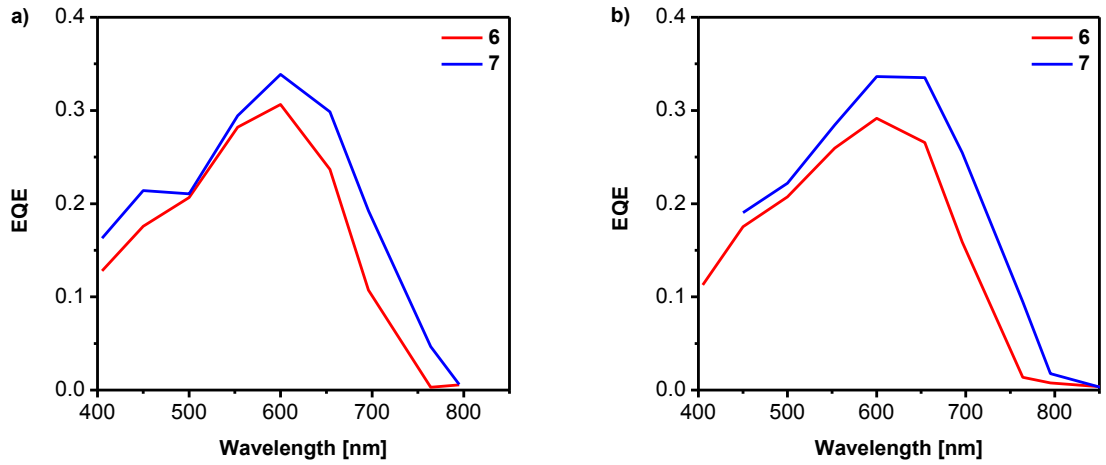

Figure 3.32: EQE spectra of (a) PHJ solar cells and (b) BHJ devices with **6** and **7**.

All BHJ devices show non-ideal rectifying behavior. Increasing the blend layer thickness from 20 to 30 nm only slightly affects the photovoltaic parameters of the BHJ solar cells, which are summarized in **Table 3.8**. Both effects might be a result of strong crystallization and phase separation of the selenophene compounds and C_{60} when deposited on a heated substrate. As a consequence, the generated photocurrent is strongly limited by exciton diffusion, leading to stagnation of J_{SC} with increasing blend layer thickness. At the same time, comparably low FF and high saturation values point towards non-optimal charge carrier transport in these particular blend layers.

Compared to the previously investigated oligothiophenes **DCV4T** and **DCV5T**, the PHJ device efficiencies (6 nm donor layer) of oligoselenophenes **6** and **7** are higher. In the case of the tetramers, the PCE of **6** (2.4%) is twice as high as the PCE for **DCV4T** (1.2%).[10] This is mainly a consequence of the much higher J_{SC} (5.2 vs. 2.9 mA cm^{-2}). For the pentamers, the efficiency increases from 2.6% for **DCV5T** to 3.4% for **7** due to both, higher J_{SC} and FF values. In BHJ devices (20 nm active layer) the PCE for **6** (1.7%) is very similar to that of **DCV4T** (1.5%).[83] However, a considerable decrease of the efficiency was observed for **7** (2.6%) compared to **DCV5T** (3.9%).[10] The main reason for this decrease is the lower FF (0.45 for **7** vs. 0.61 for **DCV5T**), which could be a result of less efficient charge carrier extraction.

Table 3.8: Photovoltaic parameters of PHJ and BHJ solar cells containing **6**-**8**.

compound	device structure	substrate temp. [°C]	layer thickness [nm]	$J_{SC,ap,100}$ [a] [mA cm^{-2}]	V_{OC} [V]	FF	saturation [b]	incident light intensity [mW cm^{-2}]	PCE [%]
6	PHJ	r.t.	6	4.8	0.95	0.53	1.24	96	**2.4**
6	PHJ	r.t.	10	5.3	0.95	0.47	1.30	96	**2.4**
7	PHJ	r.t.	6	6.3	0.90	0.59	1.16	92	**3.3**
7	PHJ	r.t.	10	7.1	0.91	0.53	1.20	92	**3.4**
6	BHJ	70	20	4.6	0.89	0.41	1.44	97	**1.7**
6	BHJ	70	30	4.8	0.88	0.39	1.43	97	**1.6**
7	BHJ	90	20	6.1	0.90	0.47	1.48	105	**2.6**
7	BHJ	90	30	6.4	0.89	0.45	1.45	105	**2.6**
8	BHJ	90	13	6.5	0.86	0.58	1.27	105	**3.2**
DCV5T-Me(3,3)	BHJ	90	30	11.1	0.96	0.66	1.04	115	**6.1**

[a] Measured with mask. [b] Defined as J(-1 V)/J_{SC}.

The *J*-*V* curves and EQE spectra of a BHJ device with co-oligomer **8** are depicted in **Figure 3.33**. The thickness of the blend layer was only 13 nm in this device due to a very low sublimation yield. Therefore, it is difficult to compare the performance of this device with the **DCV5T-Me(3,3)** device in **Table 3.8**, which contains a 30 nm thick blend layer. The poor rectifying behavior of the device measured in the dark and the high saturation factor of 1.27 hint towards a large leakage current, possibly due to the low blend layer thickness.

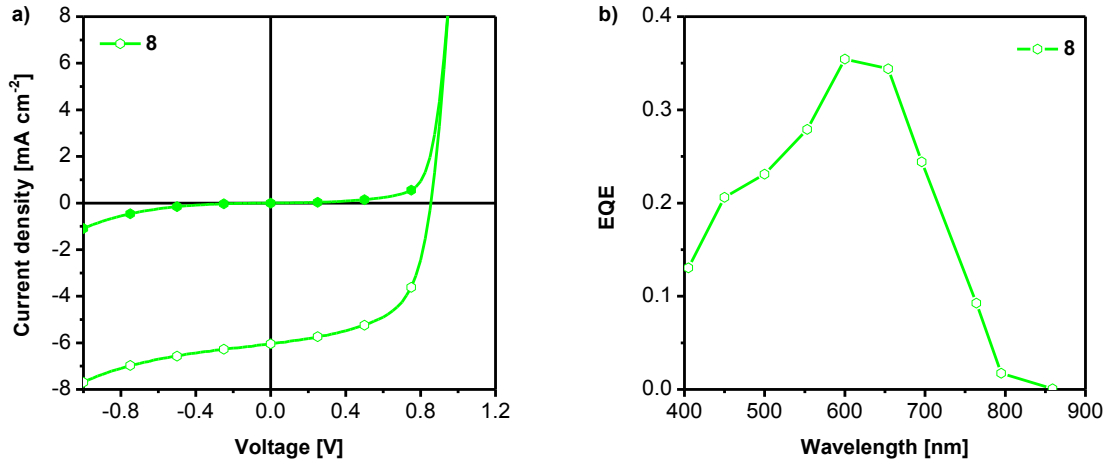

Figure 3.33: *J*-*V* curves (a) and EQE spectra (b) for BHJ solar cells with compound **8**.

The thin blend layer could also be the reason for the rather low J_{SC} (6.5 mA cm^{-2}) compared to that of the **DCV5T-Me(3,3**) device (11.1 mA cm^{-2}). V_{OC} for co-oligomer **8** is by 0.1 eV lower than for

DCV5T-Me(3,3), but still reasonably high and comparable to that of compound **7**. The FF for the device with co-oligomer **8** (0.58) is lower than that of **DCV5T-Me(3,3)** (0.66), but considerably higher than that of **7** (0.45). Thus, the PCE of the device with **8** (3.2%) is only half of the PCE obtained with the *all*-thiophene analog **DCV5T-Me(3,3)** (6.1%), while it is higher than that of quinqueselenophene **7** (2.6%). Most probably, a higher J_{SC} and, as a result, a higher PCE might be achieved if the blend layer thickness could be increased. Unfortunately, the poor sublimation behavior of co-oligomer **8** limits the device performance in this case.

3.4 Summary

In this chapter, the influence of the incorporation of selenophene in DCV-substituted oligomers on the thermal, optical and electrochemical properties and photovoltaic performance was studied. In one series of pentamers (**1**-**3**), the thiophene units in parent **DCV5T-Bu** were subsequently replaced with selenophene units. Pentamers **1** and **3** were prepared by first synthesizing the conjugated backbone and subsequent introduction of the DCV groups. Pentamer **2** was synthesized by cross-coupling of a distannylated terthiophene building block with a brominated DCV-selenophene. All intermediates were obtained in good to excellent yields and the target compounds **1**-**3** could be purified by simple column chromatography. The introduction of selenophene units resulted in increased melting points, bathochromically shifted absorption spectra, lower band gaps and higher molar extinction coefficients, while the electrochemical properties stayed relatively unaffected. We found that the replacement of the thiophenes adjacent to the DCV groups suffices to achieve a considerable red-shift of almost 20 nm. When implemented as donor materials in BHJ solar cells, compounds **1**-**3** attained PCEs of 2.5-3.1% compared to 3.5% for **DCV5T**. The PCE decreased with increasing number of selenophenes, probably due to a lower degree of phase separation in the blend, resulting in recombination losses and lower charger carrier extraction efficiencies.

In a second series of compounds, non-alkylated terminally DCV-substituted oligoselenophenes **5**-**7**, thiophene was completely replaced by selenophene. These oligomers were synthesized by Stille-type cross couplings and the crude products were purified by Soxhlet extraction to obtain the pure oligomers in good yields. The optoelectronic properties and solar cell performance of oligomers **5**-**7** was explored in detail and compared with the corresponding oligothiophenes **DCVnT**. The thermal, optical and electrochemical properties of **5**-**7** exhibited similar chain length dependence as the corresponding oligothiophenes. Red-shifted absorption bands and lowering of the band gap were observed for **5**-**7** in comparison to **DCVnT**. The replacement of sulfur by selenium resulted in a lowering of the LUMO energy level while the HOMO level stayed relatively unaffected. The single

crystal structure of tetramer **6** showed a large resemblance to that of the thiophene tetramer **DCV4T**. The crystal structure analysis further corroborates the important role that the DCV groups play for molecular ordering, whereas the introduction of selenium resulted in increased intermolecular distances. **6** and **7** were implemented as donor materials in vacuum-processed PHJ and BHJ solar cells with C_{60} as acceptor. In PHJ devices, the oligoselenophenes showed higher PCEs than their thiophene analogs, the best efficiency being 3.4% for quinqueselenophene **7**. In BHJ devices, the PCE for **7** was lower than for **DCV5T**, but there is still room for improvement by optimization of the fabrication conditions. Nevertheless, these results demonstrate the successful application of acceptor-functionalized oligoselenophenes as donor materials for efficient SMOSC.

3.5 Experimental Section

Physical measurements and instrumentation.

NMR spectra were recorded on a Bruker AMX 500 (^{1}H NMR: 500 MHz, ^{13}C NMR: 125 MHz) or an Avance 400 spectrometer (^{1}H NMR: 400 MHz, ^{13}C NMR: 100 MHz) at 25 °C unless otherwise noted. Chemical shift values (δ) are expressed in parts per million using residual solvent protons (^{1}H NMR, δ_H = 7.26 for $CDCl_3$, δ_H = 5.32 for CD_2Cl_2, δ_H = 5.92 for $C_2D_2Cl_4$, δ_H = 2.50 for DMSO-d_6; ^{13}C NMR, δ_C = 77.0 for $CDCl_3$, δ_C = 53.84 for CD_2Cl_2) as internal standard. The splitting patterns are designated as follows: s (singlet), d (doublet), t (triplet), q (quartet) and m (multiplet). The assignments are Sel-H (selenophene protons), Th-H (thiophene protons), -CHO (aldehyde protons), DCV-H (dicyanovinyl protons), Bu (butyl protons). Coupling constants (*J*) relate to proton-proton couplings unless otherwise noted. Melting points were determined using a Mettler Toledo DSC 823^e and were not corrected. Elemental analyses were performed on an Elementar Vario EL. Thin layer chromatography was carried out on aluminum plates, pre-coated with silica gel, Merck Si60 F_{254}. Preparative column chromatography was performed on glass columns packed with silica gel, Merck Silica 60, particle size 40 – 43 µm. EI mass spectra were recorded on a Varian Saturn 2000 GC-MS, MALDI-TOF mass spectra on a Bruker Daltonics Reflex III and high resolution MALDI-TOF mass spectra on a Bruker solariX.

Optical measurements in solution were carried out in 1 cm cuvettes with Merck Uvasol grade solvents. Absorption spectra were recorded on a Perkin Elmer Lambda 19 spectrometer and corrected fluorescence spectra were recorded on a Perkin Elmer LS 55 fluorescence spectrometer. Cyclic voltammetry and differential pulse voltammetry experiments were performed with a computer-controlled Autolab PGSTAT30 potentiostat in a three-electrode single-compartment cell with a platinum working electrode, a platinum wire counter electrode, and an Ag/AgCl reference electrode. All potentials were internally referenced to the ferrocene/ferrocenium couple.

X-ray diffraction data of a dark-red single crystal of **6** were collected in a stream of nitrogen at 100(2) K on a Bruker APEX-II CCD area detector diffractometer using graphite-monochromated Mo K_α radiation. Absorption correction based on a semi-empirical method was performed with the SADABS algorithm.[85] The structure was solved by direct methods with SHELXS-97,[86] revealing all atoms of the selenophene backbone. Additional atoms were located from difference Fourier maps during refinement on F^2 with SHELXL-97.[86] In the structure, voids in the asymmetric unit with a volume of ca. 97 Å^3 are present. These voids represent ca. 17% of the overall volume and are filled with heavily disordered molecules of **6**, clearly discernible from the smeared electron density (maximum electron density within the voids 11.2 e^-). It was not possible to resolve this disorder satisfactorily. Therefore, all electron density associated with peaks in these voids was eventually omitted by applying the PLATON/SQUEEZE option.[87] For the final model, all non-H atoms were refined anisotropically. H atoms were placed in calculated positions riding the parent C atom with C—H distance constraints of 0.95 Å, and with U_{iso}(H) = 1.2U_{eq}(C).

Compound **6**: $C_{24}H_{10}N_4Se_4$, M_r = 670.20, dark-red lath, 0.65 × 0.24 × 0.10 mm^3, monoclinic, $P2_1/n$, a = 3.9203(1) Å, b = 27.6816(9) Å, c = 22.7887(7) Å, β = 93.181(2) °, V = 2469.22(13) Å^3 , Z = 4, μ = 5.961 mm^{-1} , dx = 1.803 g·cm^{-3}, T = 100(2) K. 49820 reflections collected (ϑ_{max} = 38.1°) and merged to 13421 independent data (R_{int} = 0.050); final R indices: $R_1(I > 2\sigma(I))$ = 0.0481, wR_2 (all) = 0.1109.

Detailed crystallographic data for the structure of **6** have been deposited with the Cambridge Crystallographic Data Centre as supplementary publication CCDC 874137.

Thin Film and Device Fabrication

Thin films and heterojunction solar cell devices were prepared by thermal vapor deposition in ultra high vacuum at a base pressure of 10^{-7} mbar onto the substrate at room temperature. Thin films for absorption and emission measurements were prepared on quartz substrates, solar cells on tin-doped indium oxide (ITO) coated glass (Thin Film Devices, USA, sheet resistance of 30 Ω sq.$^{-1}$). Layer thicknesses were determined during evaporation by using quartz crystal monitors calibrated for the respective material. The thin films prepared for absorption and emission measurements were approximately 30 nm thick. Thin film absorption spectra were recorded on a Shimadzu UV-2101/3101 UV-Vis spectrometer. The thin film emission spectra were recorded with an Edinburgh Instruments FSP920 fluorescence spectrometer. Bulk-heterojunction solar cells were prepared layer by layer without breaking the vacuum. The layer structure of the bulk-heterojunction solar cells is as follows: ITO/15 nm C_{60}/20 or 30 nm blend layer of respective donor material and C_{60} (ratio 2:1 in volume) prepared by coevaporation deposited on heated substrate (70 or 90 °C)/5 nm BPAPF/50 nm BPAPF doped with 10 wt% NDP9 (purchased from Novaled AG, Dresden, Germany)/1 nm NDP9/50 nm gold. Planar heterojunction devices were built up as follows: ITO/15 nm C_{60}/6 nm or

10 nm donor layer of respective donor material/5 nm BPAPF/50 nm BPAPF doped with 10 wt% NDP9/1 nm NDP9/50 nm gold.

Photovoltaic Characterization

J–V and EQE measurements were carried out in a glove box with nitrogen atmosphere. *J–V* characteristics were measured using a source-measure unit (Keithley SMU 2400) and an AM 1.5G sun simulator (KHS Technical Lighting SC1200). The illumination intensity was monitored with a silicon photodiode (Hamamatsu S1337) which was calibrated at Fraunhofer ISE. The mismatch between the spectrum of the sun simulator and the AM 1.5G spectrum was not taken into account. For well defined active solar cell areas, aperture masks (2.76 mm²) were used. Simple EQE measurements were carried out using the sun simulator in combination with color filters for monochromatic illumination.

Materials

THF (Merck) was dried under reflux over sodium/benzophenone (Merck). DMF (Merck) was dried under reflux over phosphorous pentoxide (Merck). DCM, DCE, $CHCl_3$, *n*-hexane and diethyl ether were purchased from Merck and distilled prior to use. All synthetic steps were carried out under an argon atmosphere (except Knoevenagel condensations). Selenophene **20** was purchased from Molekula, $HP^tBu_3BF_4$ from Alfa Aesar and potassium carbonate from ABCR. *n*-Butyl lithium (1.6 N in *n*-hexane) and $Pd_2(dba)_3{\cdot}CHCl_3$ were purchased from Acros. *N*-Bromosuccinimide, iodine, mercury(II) acetate, phosphoryl chloride and β-alanine were purchased from Merck. Malononitrile, trimethyltin chloride, 2-isopropoxy-4,4,5,5-tetramethyl[1,3,2]dioxaborolane (ITDB) and 2-(tributylstannyl)-thiophene **26** were purchased from Aldrich.

3,4-Dibutylthiophene **22**,[46] 5-bromoselenophene-2-carbaldehyde **30**,[49] 3,4,3'',4''-tetrabutyl-2,2':5',2''-terthiophene **32**,[48] 5,5'-dibromo-2,2'-biselenophene **34**,[24] 2,2'-biselenophene-5-carbaldehyde **48**,[24] and 5,5'-bis(trimethylstannyl)-2,2'-biselenophene **53**[70] were synthesized according to literature procedures. 2,2':5',2''-Terselenophene **51** was obtained as a by-product in 12% yield during the synthesis of 2,2'-biselenophene according to ref. [24].

2,5-Dibromoselenophene (21).

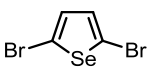

In the absence of light, selenophene **20** (4.02 g, 30.7 mmol) was dissolved in dry DMF (25 mL) and the solution was degassed. NBS (10.9 g, 61.2 mmol) was added in four portions within 30 min; afterwards, the orange solution was stirred at r.t. for 18 h. The reaction mixture was poured into ice-

water (100 mL) and extracted with DCM (3 × 100 mL). The combined organic phases were washed with brine (100 mL), water (2 × 100 mL) and dried over Na_2SO_4. Removal of the solvent yielded 10.1 g of an orange liquid, which was purified by column chromatography (silica; *n*-hexane). The pure product (7.46 g, 25.8 mmol, 84%) was obtained as a colorless liquid.

^{1}H NMR (400 MHz, $CDCl_3$): δ = 7.00 (s, 2H, H-3,4).

^{13}C NMR (100 MHz, $CDCl_3$): δ = 132.98 (C-3,4), 115.60 (C-2,5).

MS (EI): *m/z* = 290 (100, $M+H^+$).

Analytical data were in accordance with literature data.[24]

2-(3,4-Dibutylthien-2-yl)-4,4,5,5-tetramethyl-1,3,2-dioxaborolane (23).

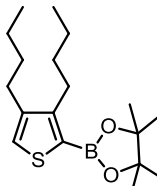

In a flame-dried three-necked flask (with septum, thermometer and argon valve), 3,4-dibutylthiophene **22** (12.6 g, 63.0 mmol) was dissolved under argon in 110 mL of dry THF. The solution was cooled in an ice/NaCl bath below -10 °C and *n*-BuLi (1.6 M in hexane, 39.5 mL, 63.2 mmol) was added dropwise within 1 h so the temperature did not rise above -10 °C. Afterwards, the orange solution was stirred at -10 °C for 30 min and at r.t. for 1 h. The pale yellow solution was again cooled below -10 °C and ITDB (11.7 g, 62.9 mmol) was added within 20 min at such a rate that the temperature did not rise above -10 °C. The mixture was stirred for 30 min at -10 °C and 1 h at r.t. It was poured into an ice-cold sat. $NaHCO_3$ solution (200 mL) and *rapidly* extracted with ice-cold diethyl ether (2 × 200 mL). The combined organic layers were dried over Na_2SO_4 and the solvent was removed in vacuum. The crude product (22.7 g) was purified by vacuum distillation ($2.0\text{-}3.0\cdot10^{-2}$ mbar) to obtain the pure product **23** (14.7 g, 45.5 mmol, 72%) as a colorless liquid.

Bp.: 123-126 °C ($3.0\cdot10^{-2}$ mbar).

^{1}H NMR (400 MHz, $CDCl_3$): δ = 7.17 (s, 1H, Th-H), 2.82 (t, ^3J = 7.6 Hz, 2H, α-Bu), 2.54 (t, ^3J = 7.8 Hz, 2H, α-Bu), 1.65-1.57 (m, 2H, β-Bu), 1.50-1.35 (m, 6H, β-Bu + γ-Bu), 1.33 (s, 12H, $-CH_3$), 0.95 (t, ^3J = 7.6 Hz, 3H, δ-Bu), 0.94 (t, ^3J = 7.6 Hz, 3H, δ-Bu).

Analytical data were in agreement with literature data.[88]

2,5-Bis(3,4-dibutylthien-2-yl)selenophene (24).

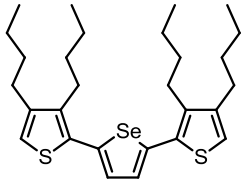

In a Schlenk tube and under argon, 2,5-dibromoselenophene **21** (3.99 g, 13.8 mmol) and boronic ester **23** (10.4 g, 32.3 mmol) were dissolved in degassed THF (40 mL), $Pd_2(dba)_3$ (243 mg, 266 µmol, 2 mol%) and $HP^tBu_3BF_4$ (154 mg, 545 µmol, 4 mol%) were added, the solution was degassed again and 20 mL (40.0 mmol) of an aq. K_3PO_4 solution (2 M) was added. The solution was stirred at 50 °C for 22 h. THF was evaporated, 50 mL of water was added and the mixture was extracted with DCM (3 × 50 mL). The combined organic layers were dried over Na_2SO_4 and the solvent was removed in vacuum. The crude product was purified by column chromatography (flash silica; *n*-hexane) to obtain the pure product **24** (5.86 g, 11.3 mmol, 82%) as an off-white solid.

Mp.: 56 °C.

^{1}H NMR (400 MHz, $CDCl_3$): δ = 7.21 (s with ^{77}Se-satellites, $^3J_{Se\text{-}H}$ = 5.2 Hz, 2H, Sel-H), 6.85 (s, 2H, Th-H), 2.71 (t, ^3J = 7.8 Hz, 4H, α-Bu), 2.54 (t, ^3J = 7.8 Hz, 4H, α-Bu), 1.69–1.62 (m, 4H, β-Bu), 1.58–1.50 (m, 4H, β-Bu), 1.49–1.40 (m, 8H, γ-Bu), 0.98 (t, ^3J = 7.4 Hz, 6H, δ-Bu), 0.96 (t, ^3J = 7.4 Hz, 6H, δ-Bu).

^{13}C NMR (100 MHz, $CDCl_3$): δ = 143.61, 141.70, 138.50, 133.26, 127.81, 118.94, 32.76, 31.84, 28.93, 27.64, 23.01, 22.69, 14.02, 13.92.

Elemental analysis: calc. (%) for $C_{28}H_{40}S_2Se$: C 65.71, H 7.76, S 12.34; found: C 65.91, H 7.69, S 12.22.

MS (EI): *m/z* = 521 (100, M^+), 478 (12, M-C_2H_5).

2,5-Bis(3,4-dibutyl-5-iodothien-2-yl)selenophene (25).

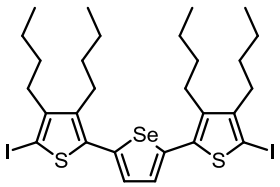

Trimer **24** (2.89 g, 5.56 mmol) was dissolved in dry chloroform (100 mL) and the solution was degassed. At 0 °C, mercury(II) acetate (3.72 g, 11.7 mmol) was added, the solution was stirred at 0 °C for 15 min and then overnight at r.t. The orange solution was cooled back to 0 °C, and iodine (2.96 g, 11.7 mmol) was added. The solution became greenish blue, was stirred at 0 °C for 30 min and then at r.t. for 4 h. The resulting solid was filtered off, washed thoroughly with chloroform, and the filtrate

was washed with sodium disulfite solution (100 mL). The aqueous phase was extracted with chloroform and DCM. The combined organic layers were dried over Na_2SO_4 and the solvent was removed in vacuum. The crude product was purified by column chromatography (flash silica; *n*-hexane). The pure product **25** (4.06 g, 5.26 mmol, 95%) was obtained as a yellow solid.

Mp.: 96 °C.

^{1}H NMR (400 MHz, $CDCl_3$): δ = 7.15 (s, 2H, Sel-H), 2.73 (virtual t, 4H, α-Bu), 2.53 (virtual t, 4H, α-Bu), 1.55-1.39 (m, 16 H, β-Bu + γ-Bu), 0.98 (t, ^3J = 7.0 Hz, 6H, δ-Bu), 0.94 (t, ^3J = 7.2 Hz, 6H, δ-Bu).

^{13}C NMR (100 MHz, $CDCl_3$): δ = 147.59, 140.91, 138.39, 138.13, 128.22, 74.29, 33.05, 32.08, 31.05, 28.40, 22.93, 22.86, 13.93, 13.86.

MS (MALDI-TOF): *m/z* [M^+] = 772.0 (calc. for $C_{28}H_{38}I_2S_2Se$: 771.97).

Elemental analysis: calc. (%) for $C_{28}H_{38}I_2S_2Se$: C 43.59, H 4.96, S 8.31; found: C 43.44, H 4.88, S 8.44.

4,4,5,5-Tetramethyl-2-(selenophen-2-yl)-1,3,2-dioxaborolane (27).

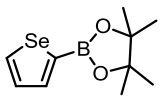

Selenophene **20** (3.04 g, 23.2 mmol) was dissolved under argon in dry THF (30 mL) and the solution was cooled to -78 °C. At this temperature, *n*-BuLi (1.6 M in hexane, 14.8 mL, 23.7 mmol) was added dropwise during 20 min. The yellow solution was stirred at -78 °C for 1 h. ITDB (4.47 g, 24.1 mmol) was added dropwise during 20 min and the turbid mixture was allowed to slowly warm to r.t. It became yellow and clear and was stirred at r.t. for 16 h. The solvent was removed in vacuum (not to dryness) and a sat. NH_4Cl solution (30 mL) was added. It was extracted with DCM (3 × 30 mL), the combined organic layers were washed with brine (50 mL) and water (50 mL) and dried over Na_2SO_4. Removal of the solvent afforded the crude product as an orange oil, which quickly crystallized. The resulting yellowish crystals were dried in high vacuum and 5.60 g (21.8 mmol, 94%) of pure boronic ester **27** were obtained.

^{1}H NMR (400 MHz, $CDCl_3$): δ = 8.37 (dd with ^{77}Se-satellites, ^3J = 5.2 Hz, ^4J = 0.8 Hz, $^2J_{H\text{-}Se}$ = 45.2 Hz, 1H, Sel-H-5), 7.95 (dd with ^{77}Se-satellites, ^3J = 3.6 Hz, ^4J = 0.8 Hz, $^2J_{H\text{-}Se}$ = 13.6 Hz, 1H, Sel-H-3), 7.46 (dd, ^3J = 5.2 Hz, ^3J = 3.6 Hz, 1H, Sel-H-4), 1.35 (s, 12H, $-CH_3$).

^{13}C NMR (100 MHz, $CDCl_3$): δ = 139.56, 137.63, 130.96, 84.09, 24.77.

MS (EI): *m/z* = 258 ($M+H^+$, 100).

Elemental analysis: calc. (%) for $C_{10}H_{15}BO_2Se$: C 46.73, H 5.88; found C 46.66, H 5.83.

2,5-Bis(3,4-dibutyl-2,2'-bithien-5-yl)selenophene (28a).

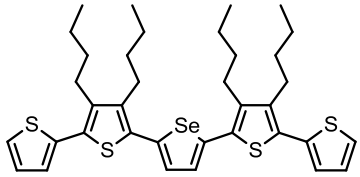

In a Schlenk tube and under argon, diiodo trimer **25** (1.41 g, 1.84 mmol) and 2-(tributylstannyl)-thiophene **26** (2.76 g, 7.18 mmol) were dissolved in dry degassed THF (20 mL). $Pd(PPh_3)_2Cl_2$ (51.5 mg, 73.5 µmol, 4 mol%) and cesium fluoride (550 mg, 3.62 mmol) were added, the solution was degassed and stirred at 75 °C for 90 h. THF was evaporated, water (50 mL) was added and the mixture was extracted with DCM (3 × 50 mL). The combined organic layers were washed with water (50 mL), dried over Na_2SO_4 and the solvent was removed. The crude product was purified by column chromatography (flash silica; *n*-hexane/DCM 9:1). The pure product **28a** (1.18 g, 1.73 mmol, 94%) was obtained as an orange solid.

Mp.: 102 °C.

^{1}H NMR (400 MHz, $CDCl_3$): δ = 7.32 (d, ^3J = 5.2 Hz, 2H, Th-H), 7.25 (s, 2H, Sel-H), 7.15 (d, ^4J = 2.8 Hz, 2H, Th-H), 7.07 (dd, ^3J = 5.2 Hz, ^4J = 3.6 Hz, 2H, Th-H), 2.75-2.68 (m, 8H, α-Bu), 1.63-1.39 (m, 16H, β-Bu + γ-Bu), 0.98 (t, ^3J = 7.2 Hz, 6H, δ-Bu), 0.96 (t, ^3J = 7.6 Hz, 6H, δ-Bu).

^{13}C NMR (100 MHz, $CDCl_3$): δ = 140.93, 140.20, 139.74, 136.10, 132.10, 129.84, 127.90, 127.36, 125.83, 125.31, 33.01, 32.90, 28.11, 27.84, 23.10, 23.00, 13.90, 13.87.

MS (MALDI-TOF): *m/z* [M^+] = 684.2 (calc. for $C_{36}H_{44}S_4Se$: 684.15).

Elemental analysis: calc. (%) for $C_{36}H_{44}S_4Se$: C 63.22, H 6.48, S 18.75; found: C 63.34, H 6.37, S 18.63.

2,5-Bis[3,4-dibutyl-5-(selenophen-2-yl)thien-2-yl]selenophene (28b).

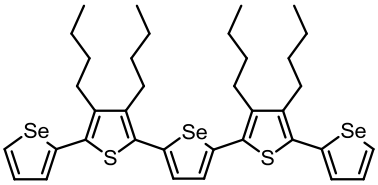

Diiodo compound **25** (1.47 g, 1.90 mmol) and boronic ester **27** (1.23 g, 4.79 mmol) were dissolved in dry THF (22 mL) and the solution was degassed. $Pd_2(dba)_3{\cdot}CHCl_3$ (39 mg, 37.7 µmol, 2 mol%) and $HP^tBu_3BF_4$ (21.8 mg, 75.1 µmol, 4 mol%) were added, the solution was degassed again and 5.8 mL (11.6 mmol) of a degassed 2 M aq. K_3PO_4 solution was added. The reaction mixture was stirred at r.t. overnight. THF was evaporated, the residue was redissolved in DCM and water (50 mL) was added.

The organic layers were separated and the aqueous layer was extracted with DCM (2 × 50 mL). The combined organic layers were dried over Na_2SO_4 and the solvent was removed. The crude product was purified by column chromatography (flash silica; *n*-hexane/DCM 9:1) to obtain product **28b** (1.42 g, 1.82 mmol, 96%) as an orange solid.

Mp.: 110 °C.

^{1}H NMR (400 MHz, $CDCl_3$): δ = 8.00 (dd with ^{77}Se-satellites, ^3J = 4.4 Hz, ^4J = 2.4 Hz, $^2J_{H\text{-}Se}$ = 47.0 Hz, 2H, Sel-H), 7.32-7.28 (m, 4H, Sel-H), 7.25 (s with ^{77}Se-satellites, $^3J_{H\text{-}Se}$ = 5.2 Hz, 2H, Sel-H), 2.75-2.67 (m, 8H, α-Bu), 1.62-1.41 (m, 16H, β-Bu + γ-Bu), 0.97 (t, ^3J = 7.2 Hz, 6H, δ-Bu), 0.96 (t, ^3J = 7.2 Hz, 6H, δ-Bu).

^{13}C NMR (100 MHz, $CDCl_3$): δ = 141.01, 140.87, 139.89, 139.83, 132.23, 132.11, 130.95, 129.82, 127.96, 127.90, 33.00, 32.92, 28.16, 27.91, 23.10, 23.02, 13.90, 13.87.

MS (MALDI-TOF): *m/z* [M^+] = 778.1 (calc. for $C_{36}H_{44}S_2Se_3$: 778.04).

Elemental analysis: calc. (%) for $C_{36}H_{44}S_2Se_3$: C 55.59, H 5.70, S 8.25; found: C 55.79, H 5.52, S 8.29.

5',5''-(Selenophene-2,5-diyl)bis(3',4'-dibutyl-2,2'-bithiophene-5-carbaldehyde) (29a).

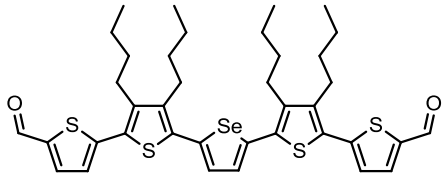

DMF (1.29 g, 17.6 mmol) and $POCl_3$ (2.70 g, 17.6 mmol) were dissolved under argon in DCE (12 mL) and the solution was stirred at r.t. for 2 h. Pentamer **28a** (600 mg, 0.88 mmol) was dissolved under argon in DCE (15 mL) and the Vilsmeier reagent was added. The solution turned from yellow to deeply red. It was stirred at r.t. for 21 h. 50 mL of a sat. $NaHCO_3$ solution was added and the mixture was stirred for 1.5 h at r.t. It was extracted with DCM (3 × 50 mL), the combined organic layers were washed with water (50 mL), dried over Na_2SO_4 and the solvent was removed. The crude product was purified by column chromatography (flash silica; traces of monoaldehyde eluted with DCM, dialdehyde eluted with DCM/EtOAc 95:5). The pure product **29a** (578 mg, 0.78 mmol, 89%) was obtained as a red solid.

Mp.: 96 °C.

^{1}H NMR (400 MHz, $CDCl_3$): δ = 9.89 (s, 2H, -CHO), 7.71 (d, ^3J = 4.0 Hz, 2H, Th-H), 7.30 (s, 2H, Sel-H), 7.25 (d, ^3J = 4.0 Hz, 2H, Th-H), 2.80-2.71 (m, 8H, α-Bu), 1.62-1.43 (m, 16H, β-Bu + γ-Bu), 0.98 (t, ^3J = 7.2 Hz, 12H, δ-Bu).

^{13}C NMR (100 MHz, $CDCl_3$): δ = 182.61, 146.19, 142.68, 142.14, 140.93, 140.54, 136.87, 134.23, 128.94, 128.61, 126.90, 32.92, 32.53, 28.14, 28.04, 23.05, 23.01, 13.86.

MS (MALDI-TOF): *m/z* [M^+] = 739.5 (calc. for $C_{38}H_{44}O_2S_4Se$: 740.14).

Elemental analysis: calc. (%) for $C_{38}H_{44}O_2S_4Se$: C 61.68, H 5.99, S 17.33; found: C 61.79, H 5.98, S 17.51.

5,5'-[5,5'-(Selenophene-2,5-diyl)bis(3,4-dibutylthiophene-5,2-diyl)]bis(selenophene-2-carbaldehyde) (29b).

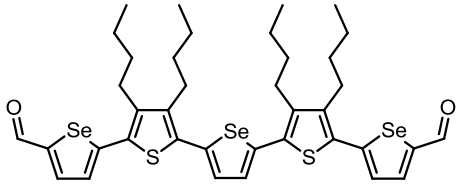

DMF (945 mg, 12.9 mmol) and $POCl_3$ (1.99 g, 13.0 mmol) were dissolved under argon in DCE (10 mL) and the solution was stirred at r.t. for 2 h. Compound **28b** (502 mg, 0.65 mmol) was dissolved under argon in DCE (15 mL) and the Vilsmeier reagent was added. The solution turned from yellow to deeply red. It was stirred at r.t. for 22 h. 50 mL of a sat. $NaHCO_3$ solution was added and the mixture was stirred for 2 h at r.t. It was extracted with DCM (3 × 50 mL), the combined organic layers were washed with water (50 mL), dried over Na_2SO_4 and the solvent was removed. The crude product was purified by column chromatography (flash silica; traces of monoaldehyde eluted with DCM, dialdehyde eluted with DCM/EtOAc 95:5). The pure dialdehyde **29b** (507 mg, 0.61 mmol, 94%) was obtained as a red solid.

Mp.: 107 °C.

^{1}H NMR (400 MHz, $CDCl_3$): δ = 9.78 (s with ^{77}Se-satellites, $^3J_{H\text{-}Se}$ = 4.4 Hz, 2H, -CHO), 7.94 (d, ^3J = 4.2 Hz, 2H, Sel-H), 7.43 (d, ^3J = 4.2 Hz, 2H, Sel-H), 7.31 (s, 2H, Sel-H), 2.78-2.71 (m, α-Bu), 1.63-1.43 (m, 16H, β-Bu + γ-Bu), 0.98 (t, ^3J = 7.0 Hz, 12H, δ-Bu).

^{13}C NMR (100 MHz, $CDCl_3$): δ = 183.98, 151.11, 148.21, 142.50, 140.90, 140.65, 139.83, 134.22, 131.66, 128.62, 128.03, 32.93, 32.57, 28.31, 28.10, 23.08, 23.06, 13.87, 13.86.

MS (MALDI-TOF): *m/z* [M^+] = 834.5 (calc. for $C_{38}H_{44}O_2S_2Se_3$: 834.03).

Elemental analysis: calc. (%) for $C_{38}H_{44}O_2S_2Se_3$: C 54.74, H 5.32, S 7.69; found: C 54.81, H 5.32, S 7.78.

2-[(5-Bromoselenophen-2-yl)methylene]malononitrile (31).

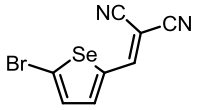

5-Bromoselenophene-2-carbaldehyde **30** (2.15 g, 9.04 mmol), malononitrile (1.50 g, 22.7 mmol) and β-alanine (53.0 mg, 0.59 mmol) were dissolved in ethanol (30 mL) and the solution was stirred at 60 °C for 15 h. The mixture was cooled to r.t. and the resulting solid was filtered off. It was washed with ethanol and dried in high vacuum to obtain the pure product **31** (2.16 mg, 7.56 mmol, 84%) as yellow crystals.

Mp.: 183 °C.

^{1}H NMR (400 MHz, $CDCl_3$): δ = 7.83 (d with ^{77}Se-satellites, ^{4}J = 0.6 Hz, $^{3}J_{Se\text{-}H}$ = 8.1 Hz, DCV-H), 7.59 (dd, ^{3}J = 4.3 Hz, ^{4}J = 0.6 Hz, Sel-H-3), 7.43 (d, ^{3}J = 4.3 Hz, Sel-H-4).

^{13}C NMR (100 MHz, $CDCl_3$): δ = 153.23, 142.45, 141.94, 134.11, 131.93, 113.49, 113.39, 78.44.

MS (EI): *m/z* = 288 (79, M^+), 286 (100, M^+), 207 (71, M-Br), 205 (32, M-Br).

Elemental analysis: calc. (%) for $C_8H_3BrN_2Se$: C 33.60, H 1.06, N 9.80; found: C 33.75, H 1.13, N 10.00.

5,5''-Bis(trimethylstannyl)-3,4,3'',4''-tetrabutyl-2,2':5',2''-terthiophene (33).

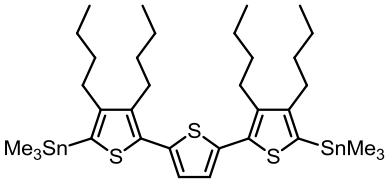

Terthiophene **32** (2.00 g, 4.23 mmol) was dissolved under argon in dry THF (12 mL) and dry *n*-hexane (7 mL) and TMEDA was added. The solution was stirred at r.t. for 30 min. At -78 °C, *n*-BuLi (1.6 M in hexane, 6.25 mL, 10.0 mmol) was added dropwise within 30 min, the solution was warmed to r.t. and then stirred at 50 °C for 25 min. A solution of Me_3SnCl (2.00 g, 10.0 mmol) in abs. THF (7 mL) was added at -78 °C and the mixture was stirred at r.t. for 3 d. A sat. NH_4Cl solution (120 mL) was added and the mixture was extracted with diethyl ether (3 × 150 mL), the combined organic layers were dried over $MgSO_4$ and the solvent was removed. After drying in high vacuum, product **33** (2.82 g, 3.50 mmol, 83%) was obtained as an orange oil. It was used without further purification.

^{1}H NMR (400 MHz, $CDCl_3$): δ = 7.03 (s, 2H, Th-H), 2.73 (t, 4H, ^{3}J = 7.9 Hz, α-Bu), 2.55 (t, 4H, ^{3}J = 7.5 Hz, α-Bu), 1.58-1.38 (m, 16H, β-Bu + γ-Bu), 0.97 (t, 6H, ^{3}J = 7.2 Hz, δ-Bu), 0.97 (t, 6H, ^{3}J = 7.2 Hz, δ-Bu), 0.39 (s, 18H, Me).

^{13}C NMR (100 MHz, $CDCl_3$): δ = 151.29, 139.86, 136.79, 136.52, 125.45, 34.96, 33.02, 31.51, 27.73, 23.19, 23.11, 13.99, 13.89, 7.81.

MS (MALDI-TOF): *m/z* [M^+] = 798.1 (calc. for $C_{34}H_{56}S_3Sn_2$: 798.2).

2,2'-{[5',5'''-(Selenophene-2,5-diyl)bis(3',4'-dibutyl-2,2'-bithien-5',5-diyl)]bis(methanylylidene)}dimalononitrile (1).

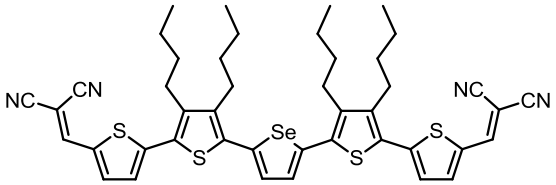

Dialdehyde **29a** (275 mg, 0.372 mmol), malononitrile (73.4 mg, 1.11 mmol) and β-alanine (4.00 mg, 44.9 µmol) were dissolved in a DCE/ethanol mixture (25 mL, 1:1 v/v) and the solution was refluxed for 24 h. The solvent was evaporated and the residue was purified by column chromatography (flash silica; DCM). The pure product **1** (245 mg, 0.293 mmol, 79%) was obtained as a green solid with a metallic sheen.

Mp.: 211 °C.

^{1}H NMR (400 MHz, $CDCl_3$): δ = 7.77 (s, 2H, DCV-H), 7.69 (d, ^3J = 4.4 Hz, 2H, Th-H), 7.34 (s, 2H, Sel-H), 7.29 (d, ^3J = 4.4 Hz, 2H, Th-H), 2.84-2.79 (m, 4H, α-Bu), 2.77-2.72 (m, 4H, α-Bu), 1.63-1.44 (m, 16H, β-Bu + γ-Bu), 1.00 (t, ^3J = 7.2 Hz, 6H, δ-Bu), 0.99 (t, ^3J = 6.8 Hz, 6H, δ-Bu).

^{13}C NMR (100 MHz, $CDCl_3$): δ = 149.89, 148.35, 144.11, 141.01, 139.17, 135.53, 133.96, 129.00, 128.60, 126.14, 114.40, 113.53, 75.80, 32.87, 32.41, 28.05, 23.04, 23.01, 13.86.

MS (MALDI-TOF): *m/z* [M^+] = 836.5 (calc. for $C_{44}H_{44}N_4S_4Se$: 836.16).

Elemental analysis: calc. (%) for $C_{44}H_{44}N_4S_4Se$: C 63.21, H 5.30, N 6.70; found: C 63.15, H 5.15, N 6.78.

2,2'-{[5,5'-(3,3'',4,4''-Tetrabutyl-2,2':5',2''-terthien-5,5''-diyl)bis(selenophene-5,2-diyl)]bis(methanylylidene)}dimalononitrile (2).

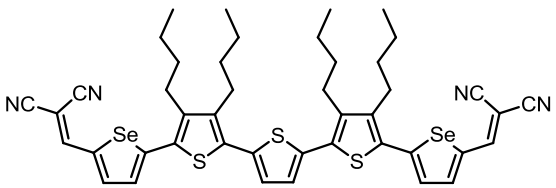

In a Schlenk tube, DCV-substituted bromoselenophene **31** (322 mg, 1.13 mmol) and distannyl terthiophene **33** (300 mg, 0.376 mmol) were dissolved under argon in dry DMF (4 mL) and the mixture was degassed. $Pd(PPh_3)_4$ (4 mg, 3 µmol) was added, the mixture was degassed again and stirred at 75 °C for 3 d. Water (30 mL) was added and the mixture was extracted with DCM (30 mL). The organic layer was dried over Na_2SO_4 and the solvent was removed in vacuum. The crude product was purified by column chromatography (silica; DCM/*n*-hexane 4:1) to obtain pure product **2** (223 mg, 0.253 mmol, 67%) as a green solid.

Mp.: 213 °C.

^{1}H-NMR ($CDCl_3$, 400 MHz): δ = 7.84 (s with ^{77}Se-satellites, $^3J_{Se\text{-}H}$ = 9.0 Hz, 2H, DCV-H), 7.82 (d, ^3J = 4.5 Hz, 2H, Sel-H), 7.43 (d, ^3J = 4.5 Hz, 2H, Sel-H), 7.19 (s, 2H, Th-H), 2.83-2.73 (m, 8H, α-Bu), 1.63-1.55 (m, 8H, β-Bu), 1.54-1.45 (m, 8H, γ-Bu), 1.00 (t, ^3J = 7.5 Hz ,6H, δ-Bu), 0.99 (t, ^3J = 7.5 Hz ,6H, δ-Bu).

^{13}C-NMR ($CDCl_3$, 125 MHz, 320 K): δ = 154.61, 152.79, 143.82, 142.99, 141.60, 138.94, 136.17, 133.36, 131.51, 127.55, 127.10, 114.25, 113.92, 76.13, 32.79, 32.45, 28.59, 28.01, 23.04, 22.99, 13.78, 13.73.

MS (MALDI-TOF): *m/z* [M^+] = 884.2 (calc. for $C_{44}H_{44}N_4S_3Se_2$: 884.1).

Elemental analysis: calc. (%) for $C_{44}H_{44}N_4S_3Se_2$: C 59.85, H 5.02, N 6.35; found: C 59.97, H 5.14, N 6.47.

2,2'-({5,5'-[5,5'-(Selenophene-2,5-diyl)bis(3,4-dibutylthien-5,2-diyl)]bis(selenophene-5,2-diyl)}bis(methanylylidene))dimalononitrile (3).

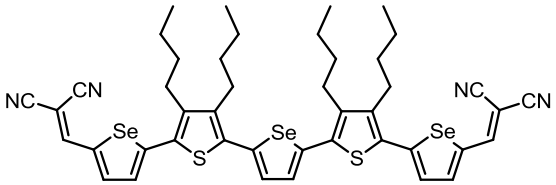

Dialdehyde **29b** (236 mg, 0.283 mmol), malononitrile (58.2 mg, 0.881 mmol) and β-alanine (2.20 mg, 24.7 µmol) were dissolved in a DCE/ethanol mixture (20 mL, 1:1 v/v) and the solution was refluxed for 24 h. The solvent was evaporated and the residue was purified by column chromatography (flash silica; DCM). The pure product **3** (208 mg, 0.224 mmol, 79%) was obtained as a green solid with a metallic luster.

Mp.: 215 °C.

^{1}H NMR (400 MHz, $CDCl_3$): δ = 7.84 (s, 2H, DCV-H), 7.82 (d, ^3J = 4.4 Hz, 2H, Sel-H), 7.43 (d, ^3J = 4.4 Hz, 2H, Sel-H), 7.35 (s, 2H, Sel-H), 2.81-2.73 (m, 8H, α-Bu), 1.63-1.44 (m, 16H, β-Bu + γ-Bu), 1.00 (t, ^3J = 7.2 Hz, 6H, δ-Bu), 0.99 (t, ^3J = 7.2 Hz, 6H, δ-Bu).

^{13}C NMR (100 MHz, $CDCl_3$): δ = 154.59, 152.97, 143.98, 143.40, 141.19, 140.99, 138.99, 135.72, 131.36, 129.03, 127.29, 114.39, 114.02, 75.50, 32.86, 32.33, 28.60, 28.11, 23.05, 13.87, 13.80.

MS (MALDI-TOF): *m/z* [M^+] = 930.5 (calc. for $C_{44}H_{44}N_4S_2Se_3$: 930.05).

Elemental analysis: calc. (%) for $C_{44}H_{44}N_4S_2Se_3$: C 56.83, H 4.77, N 6.03; found: C 56.94, H 4.77, N 5.97.

5,5'-Bis(3,4-dibutylthien-2-yl)-2,2'-biselenophene (35).

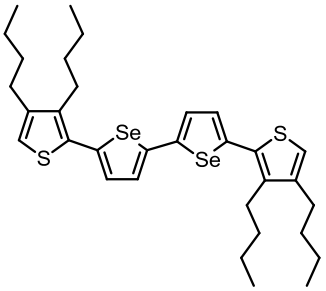

5,5'-Dibromo-2,2'-biselenophene **34** (300 mg, 0.70 mmol) and thienyl boronic ester **23** (832 mg, 1.70 mmol) were dissolved under argon in THF (5 mL) and the solution was degassed. $Pd_2(dba)_3 \cdot CHCl_3$ (52.5 mg, 57.0 µmol) and $HP^tBu_3BF_4$ (24.4 mg, 84.0 µmol) were added and the solution was degassed again. A 2 M aq. potassium phosphate solution (1.11 mL) was added, and the mixture was stirred at r.t. for 16 h and then at 50 °C for 1 h. Water (30 mL) was added and the mixture was extracted with DCM (3 x 30 mL). The combined organic layers were dried over Na_2SO_4 and the solvent was evaporated. The crude product was purified by column chromatography (flash silica; *n*-hexane/DCM 9:1) to afford pure product **35** (297 mg, 0.54 mmol, 75%) as a yellow solid.

Mp.: 127 °C.

^{1}H-NMR (400 MHz, $CDCl_3$): δ = 7.19 (d, ^3J = 4.0 Hz, 2H, Sel-H), 7.15 (d, ^3J = 4.0 Hz, 2H, Sel-H), 6.85 (s, 2H, Th-H), 2.70 (t, ^3J = 8.1 Hz, 4H, α-Bu), 2.53 (t, ^3J = 7.6 Hz, 4H, α-Bu), 1.68-1.60 (m, 4H, β-Bu), 1.56-1.39 (m, 12H, β-Bu + γ-Bu), 0.98 (t, ^3J = 7.2 Hz, 6H, δ-Bu), 0.96 (t, ^3J = 7.2 Hz, 6H, δ-Bu).

^{13}C-NMR (400 MHz, $CDCl_3$): δ = 144.07, 143.72, 140.73, 138.71, 133.15, 128.30, 126.57, 126.57, 31.83, 32.69, 27.62, 22.68, 14.02, 13.93.

MS (MALDI-TOF): *m/z* [M^+] = 650.0 (calc. for $C_{32}H_{42}S_2Se_2$: 650.1).

Elemental analysis: calc. (%) for $C_{32}H_{42}S_2Se_2$: C 59.25, H 6.53, S 9.89; found: C 59.37, H 6.40, S 9.76.

5,5'-(2,2'-Biselenophene-5,5'-diyl)bis(3,4-dibutylthiophene-2-carbaldehyde) (36).

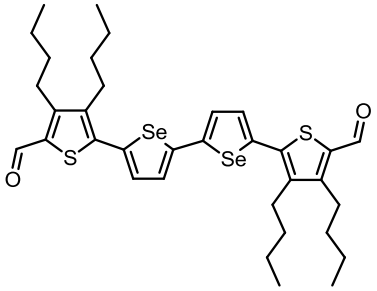

Phosphoryl chloride (0.63 mL, 1.06 g, 6.91 mmol) and DMF (510 mg, 6.91 mmol) were dissolved under argon in DCE (10 mL) and the solution was stirred at r.t. for 2 h. A solution of tetramer **35** (224 mg, 0.345 mmol) in DCE (11 mL) was added to this mixture and it turned purple. The reaction mixture was stirred at r.t. for 21 h, a sat. $NaHCO_3$ solution (20 mL) was added and stirring was continued for 1.5 h. It was extracted with diethyl ether (3 x 20 mL), the combined organic layers were washed with water (40 mL), dried over Na_2SO_4 and the solvent was removed in vacuum. The crude product was purified by column chromatography (flash silica; DCM to DCM/EtOAc 9:1) and product **36** (182 mg, 0.258 mmol, 75%) was obtained as shiny red crystals.

Mp.: 178 °C.

^{1}H-NMR (400 MHz, $CDCl_3$): δ = 10.01 (s, 2H, -CHO), 7.36 (d, ^3J = 4.0 Hz, 2H, Sel-H), 7.28 (d, ^3J = 4.0 Hz, 2H, Sel-H), 2.89 (t, ^3J = 8.0 Hz, 4H, α-Bu), 2.73 (t, ^3J = 7.6 Hz, 4H, α-Bu) 1.65-1.42 (m, 16H, β-Bu + γ-Bu), 0.98 (t, ^3J = 7.2 Hz, 12H, δ-Bu).

^{13}C-NMR (100 MHz, $CDCl_3$): δ = 182.02, 153.11, 145.74, 142.94, 139.40, 136.02, 130.38, 127.45, 34.58, 32.70, 27.25, 27.11, 22.98, 22.83, 13.84.

MS (MALDI-TOF): *m/z* [M^+] = 706.2 (calc. for $C_{34}H_{42}O_2S_2Se_2$: 706.1).

Elemental analysis: calc. (%) for $C_{34}H_{42}O_2S_2Se_2$: C 57.94, H 6.01, S 9.10; found: C 58.11, H 5.94, S 8.86.

2,2'-[5,5'-(2,2'-Biselenophene-5,5'-diyl)bis(3,4-dibutylthien-5,2-diyl)]bis(methan-1-yl-1-ylidene)dimalononitrile (4).

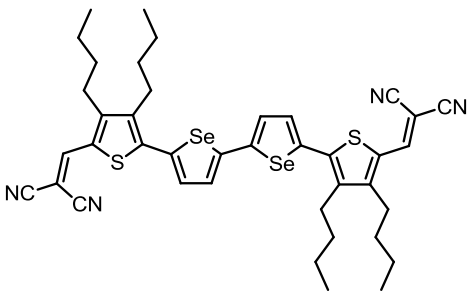

Dialdehyde **36** (117 mg, 116 µmol), malononitrile (34 mg, 0.55 mmol) and β-alanine (1.25 mg, 14 µmol) were dissolved in a DCE/ethanol mixture (15 mL, 1:1 v/v) and the mixture was refluxed for 22 h. The solvent was removed in vacuum, the resulting green solid was washed with ethanol and dried in high vacuum. The pure product **4** (116 mg, 0.145 mmol) was obtained in 87% yield.

Mp.: 283 °C.

^{1}H-NMR (500 MHz, 373 K, $C_2D_2Cl_4$): δ = 7.77 (s, 2H, DCV-H), 7.43 (d, ^3J = 4.1 Hz, 2H, Sel-H), 7.41 (d, ^3J = 4.1 Hz, 2H, Sel-H), 2.75 (t, ^3J = 6.4 Hz, 4H, α-Bu), 2.70 (t, ^3J = 6.4 Hz, 4H, α-Bu), 1.57-1.48 (m, 8H, β-Bu), 1.47-1.41 (m, 8H, γ-Bu), 0.98 (t, ^3J = 7.4, Hz, 6H, δ-Bu), 0.96 (t, ^3J = 7.4 Hz, 6H, δ-Bu).

^{13}C NMR: Solubility not sufficient.

HR-MS (MALDI-TOF): *m/z* [M^+] = 800.1177 (calc. for $C_{40}H_{42}N_4S_2Se_2$: 800.1186).

5'-Bromo-2,2'-biselenophene-5-carbaldehyde (49).

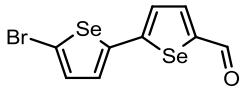

2,2'-Biselenophene-5-carbaldehyde **48** (1.29 g, 4.47 mmol) was dissolved in DMF (10 mL) and NBS (800 mg, 4.49 mmol) was dissolved in 5 mL DMF. The solutions were put in the freezer for 3 h, mixed together and put back in the freezer for 3 d. The resulting orange crystals (780 mg) were filtered off and washed with methanol. The filtrate was put in the freezer over the weekend. The resulting precipitate was filtered off and another 280 mg of a yellow solid were obtained. Water was added to the filtrate and the mixture was extracted with DCM (3 × 25 mL). The combined organic layers were washed with water (3 × 20 mL), dried over Na_2SO_4 and the solvent was removed. The resulting solid was washed with methanol and dried in high vacuum to afford 385 mg of a yellow solid. All fractions contained pure product **49** and were combined to obtain an overall yield of 1.45 g (3.94 mmol, 88%).

Mp.: 153 °C.

^{1}H NMR (400 MHz, CD_2Cl_2): δ = 9.71 (s, 1H, -CHO), 7.87 (d, ^3J = 4.0 Hz, 1H, Sel-H-4), 7.28 (d, ^3J = 4.0 Hz, 1H, Sel-H-3), 7.23 (d, ^3J = 4.0 Hz, 1H, Sel-H-3'), 7.17 (d, ^3J = 4.0 Hz, 1H, Sel-H-4').

^{13}C NMR (100 MHz, $CDCl_3$): δ = 183.88, 153.47, 147.85, 140.12, 134.10, 128.92, 127.23, 117.92.

MS (EI): m/z = 368 (100, M^+), 339 (16, M-CHO), 260 (32, M-CHO-Br).

Elemental analysis: calc. (%) for $C_9H_5BrOSe_2$: C 29.46, H 1.37; found: C 29.58, H 1.41.

2-[(5'-Bromo-2,2'-biselenophen-5-yl)methylene]malononitrile (50).

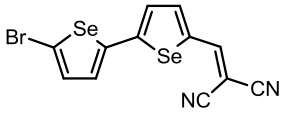

Aldehyde **49** (1.40 g, 3.82 mmol), malononitrile (763 mg, 11.5 mmol) and β-alanine (33 mg, 0.37 mmol) were suspended in an ethanol/DCE mixture (1:1 v/v, 15 mL) and the mixture was stirred at 80 °C for 2 h. The resulting red crystals were filtered off, washed with methanol and dried in high vacuum to afford 1.51 g (3.63 mmol, 95%) of product **50**.

Mp.: 208 °C.

^{1}H NMR (400 MHz, CD_2Cl_2): δ = 7.87 (s, 1H, DCV-H), 7.77 (d, ^{3}J = 4.3 Hz, 1H, Sel-H), 7.29-7.26 (m, 3H, Sel-H).

^{13}C NMR (100 MHz, CD_2Cl_2): δ = 156.74, 154.04, 144.93, 144.79, 138.84, 135.21, 130.51, 127.62, 119.92, 114.71, 114.41, 77.14.

MS (EI): *m/z* = 418 (100, M^+), 337 (21, M-Br).

Elemental analysis: calc. (%) for $C_{12}H_5BrN_2Se_2$: C 34.73, H 1.21, N 6.75; found: C 34.89, H 1.31, N 6.80.

(2,2':5',2''-Terselenophene)-5,5''-dicarbaldehyde (52).

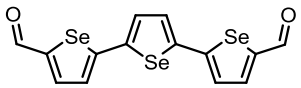

DMF (2.29 g, 31.3 mmol) was dissolved under argon in DCE (30 mL) and $POCl_3$ (4.72 g, 30.8 mmol) was added slowly at 0 °C. The mixture was stirred at r.t. for 2 h. It was added to a solution of 2,2':5',2''-terselenophene **51** (595 mg, 1.53 mmol) in DCE (30 mL) and the resulting red mixture was refluxed for 5 d. A sat. $NaHCO_3$ solution (150 mL) was added and the mixture was stirred for 1.5 h. It was extracted with DCM (5 × 200 mL). The combined organic layers were dried over Na_2SO_4 and the solvent was removed. The crude product was purified by column chromatography (flash silica; mono-aldehyde eluted with DCM, dialdehyde eluted with DCM/EtOAc 8:2). The pure product **52** (426 mg, 0.957 mmol, 63%) was obtained as an orange solid.

Mp.: 215 °C.

^{1}H NMR (400 MHz, $CDCl_3$): δ = 9.76 (s with ^{77}Se-satellites, $^{3}J_{Se-H}$ = 4.6 Hz, 2H, -CHO), 7.90 (d, ^{3}J = 4.0 Hz, 2H, H-4,4''), 7.40 (s, 2H, H-3',4'), 7.38 (d, ^{3}J = 4.0 Hz, 2H, H-3,3'').

^{13}C NMR (100 MHz, $CDCl_3$): δ = 184.14, 153.60, 148.71, 145.20, 140.43, 130.37, 128.02.

MS (MALDI-TOF): *m/z* [M^+] = 445.9 (calc. for $C_{14}H_8O_2Se_3$: 445.8).

Elemental analysis: calc. (%) for $C_{14}H_8O_2Se_3$: C 37.78, H 1.81; found: C 38.03, H 2.12.

2,2'-[2,2':5',2''-Terselenophene-5,5''-diylbis(methanylylidene)]dimalononitrile (5).

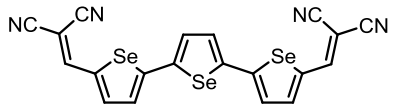

[2,2':5',2''-Terselenophene]-5,5''-dicarbaldehyde **52** (392 mg. 0.881 mmol), malononitrile (400 mg, 6.05 mmol) and β-alanine (10.8 mg, 0.121 mmol) were dissolved in a DCE/EtOH mixture (75 mL, 2:1 v/v) and the mixture was refluxed for 43 h. The mixture was cooled to r.t. and the solvent was reduced to half of its volume. The resulting solid was filtered off and washed thoroughly with ethanol, methanol and diethyl ether to obtain 390 mg of crude product. It was recrystallized from chlorobenzene (80 mL) and the resulting blackish crystals were filtered off, washed with ethanol and methanol and dried in high vacuum. 343 mg (0.634 mmol, 72%) of pure product **5** was obtained.

Mp.: 282 °C.

^{1}H NMR (500 MHz, DMSO-d_6, 360 K): δ = 8.55 (s, 2H, DCV-H), 8.11 (dd, ^3J = 4.5 Hz, ^4J = 0.5 Hz, 2H, Sel-H-4,4''), 7.78 (s, 2H, Sel-H-3',4'), 7.68 (d, ^3J = 4.5 Hz, 2H, Sel-H-3,3'').

^{13}C NMR (125 MHz, DMSO-d_6, 360 K): δ = 154.28, 154.12, 144.54, 144.10, 138.55, 131.56, 128.21, 113.68, 113.41, 74.83.

MS (MALDI-TOF): *m/z* [M^+] = 543.9 (calc. for $C_{20}H_8N_4Se_3$: 543.8).

Elemental analysis: calc. (%) for $C_{20}H_8N_4Se_3$: C 44.39, H 1.49, N 10.35; found: C 44.19, H 1.62, N 10.45.

2,2'-[2,2':5',2'':5'',2'''-Quaterselenophene-5,5'''-diylbis(methanylylidene)]dimalononitrile (6).

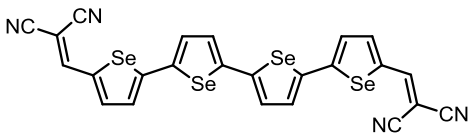

In a Schlenk tube, 5,5'-bis(trimethylstannyl)-2,2'-biselenophene **53** (396 mg, 0.676 mmol) and DCV-selenophene **31** (482 mg, 1.69 mmol) were dissolved in dry DMF (6 mL) and the solution was degassed. $Pd(PPh_3)_2Cl_2$ (23.5 mg, 33.5 µmol) was added, the solution was degassed again and stirred at 80 °C for 3 d. The solution was cooled to r.t. and the resulting solid was filtered off. It was washed with THF and methanol and dried in high vacuum to obtain product **6** as a green solid (364 mg,

0.543 mmol, 80%). The compound was further purified by Soxhlet extraction with chlorobenzene for 3 weeks.

Mp.: 358 °C.

^{1}H NMR (500 MHz, DMSO-d_6, 360 K): δ = 8.54 (s, 2H, DCV-H), 8.11 (d, ^3J = 4.5 Hz, 2H, Sel-H), 7.75 (d, ^3J = 4.5 Hz, 2H, Sel-H), 7.64 (d, ^3J = 4.5 Hz, 2H, Sel-H), 7.55 (d, ^3J = 4.5 Hz, 2H, Sel-H).

^{13}C NMR: Solubility not sufficient.

MS (MALDI-TOF): *m/z* [M^+] = 671.4 (calc. for $C_{24}H_{10}N_4Se_4$: 671.8).

Elemental analysis: calc. (%) for $C_{24}H_{10}N_4Se_4$: C 43.01, H 1.50, N 8.36; found: C 43.33, H 1.71, N 8.55.

2,5-Bis(trimethylstannyl)selenophene (54).

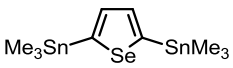

2,5-Dibromoselenophene **21** (3.09 g, 10.7 mmol) was dissolved under argon in dry diethyl ether (50 mL) and the solution was cooled to -78 °C. *n*-BuLi (1.6 M in hexane, 14.0 mL, 22.3 mmol) was added dropwise within 10 min and the mixture was stirred below -70 °C for 50 min. Trimethyltin chloride (4.69 g, 23.5 mmol, dissolved in 5 mL diethyl ether) was added and stirring was continued for 1.5 h. The mixture was poured into a sat. $NaHCO_3$ solution (80 mL) and extracted with diethyl ether (100 mL). The combined organic layers were dried over Na_2SO_4 and the solvent was removed to obtain 4.78 g of an off-white solid. The crude product was washed with methanol to obtain **54** as white crystals (3.24 g, 7.09 mmol, 66%).

^{1}H NMR (400 MHz, $CDCl_3$): δ = 7.68 (s, 2H, Sel-H), 0.37 (s with Sn-satellites, $^2J_{H\text{-}Sn}$ = 56 Hz, 18 H, Sn-CH_3).

^{13}C NMR (100 MHz, $CDCl_3$): δ = 150.16, 138.68, -7.79.

MS (EI): *m/z* = 444 (100, M-CH_3).

Elemental analysis: calc. (%) for $C_{10}H_{10}SeSn_2$: C 26.30, H 4.41; found: C 26.42, H 4.30.

2,2'-[2,2':5',2'':5'',2''':5''',2'''':5'''',2''''-Quinqueselenophene-5,5''''-diylbis(methanylylidene)]-dimalononitrile (7).

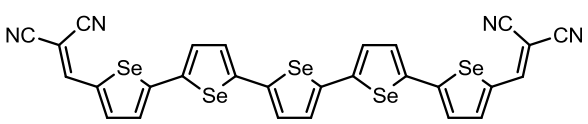

In a Schlenk tube, 2,5-bis(trimethylstannyl)selenophene **54** (201 mg, 0.440 mmol), biselenophene **50** (384 mg, 0.925 mmol) and $Pd(PPh_3)_4$ (27 mg, 23.4 µmol, 5 mol%) were dissolved in dry DMF (12 mL) and the solution was degassed. It was stirred at 80 °C for 20 h. The resulting solid was filtered off, washed with THF and methanol and dried in high vacuum to obtain 317 mg of a green solid. It was further purified by Soxhlet extraction with chlorobenzene for 4 d to afford 260 mg (0.325 mmol, 74%) of pure product **7**.

Mp.: 324 °C.

^{1}H NMR (500 MHz, DMSO-d_6, 340K): δ = 8.58 (s, 2H, DCV-H), 8.10 (d, ^3J = 4.5 Hz, 2H, Sel-H), 7.76 (d, ^3J = 4.5 Hz, 2H, Sel-H), 7.63 (d, ^3J = 4.5 Hz, 2H, Sel-H), 7.50 (s, 2H, Sel-H-3'',4''), 7.48 (d, ^3J = 4.0 Hz, 2H, Sel-H).

^{13}C NMR: Solubility not sufficient.

MS (MALDI-TOF): *m/z* [M^+] = 799.7 (calc. for $C_{28}H_{12}N_4Se_5$: 799.7).

Elemental analysis: calc. (%) for $C_{28}H_{12}N_4Se_5$: C 42.08, H 1.51, N 7.01; found: C 42.08, H 1.60, N 6.89.

2,2'-[5',5''-(3,4-Dimethylthien-2,5-diyl)bis(2,2'-biselenophene-5',5-diyl)]bis(methan-1-yl-1-ylidene)dimalononitrile (8).

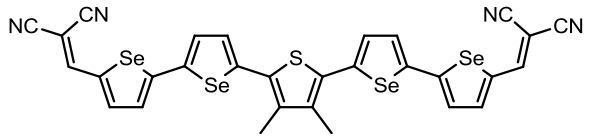

In a Schlenk tube, (3,4-dimethylthien-2,5-diyl)bis(trimethylstannane) **55** (300 mg, 0.685 mmol), biselenophene **50** (598 mg, 1.44 mmol) and $Pd(PPh_3)_4$ (42 mg, 36.4 µmol, 4 mol%) were dissolved in dry DMF (20 mL) and the solution was degassed. It was stirred at 80 °C for 17 h. The resulting solid was filtered off, washed with THF and methanol and dried in high vacuum to obtain 495 mg of a green solid. It was further purified by Soxhlet extraction with chlorobenzene for 5 d to afford 465 mg (0.596 mmol, 87%) of pure product **8**.

Mp.: 307 °C.

^{1}H NMR (500 MHz, $C_2D_2Cl_4$, 340K): δ = 7.75 (s, 2H, DCV-H), 7.73 (d, ^3J = 4.5 Hz, 2H, Sel-H), 7.49 (d, ^3J = 4.0 Hz, 2H, Sel-H), 7.29 (d, ^3J = 4.0 Hz, 4H, Sel-H), 2.32 (s, 6H, -CH_3).

^{13}C NMR: Solubility not sufficient.

MS (MALDI-TOF): *m/z* [M^+] = 781.9 (calc. for $C_{30}H_{16}N_4SSe_4$: 781.8).

Elemental analysis: calc. (%) for $C_{30}H_{16}N_4SSe_4$: C 46.17, H 2.07, N 7.18; found: C 46.35, H 2.16, N 6.93.

3.6 References

[1] K. Schulze, C. Uhrich, R. Schüppel, K. Leo, M. Pfeiffer, E. Brier, E. Reinold, P. Bäuerle, *Adv. Mater.* **2006**, *18*, 2872.

[2] R. Schüppel, K. Schmidt, C. Uhrich, K. Schulze, D. Wynands, J. L. Brédas, E. Brier, E. Reinold, H. B. Bu, P. Bäuerle, B. Männig, M. Pfeiffer, K. Leo, *Phys. Rev. B* **2008**, *77*, 085311.

[3] K. Schulze, M. Riede, E. Brier, E. Reinold, P. Bäuerle, K. Leo, *J. Appl. Phys.* **2008**, *104*, 074511.

[4] D. Wynands, B. Männig, M. Riede, K. Leo, E. Brier, E. Reinold, P. Bäuerle, *J. Appl. Phys.* **2009**, *106*, 054509.

[5] D. Wynands, M. Levichkova, K. Leo, C. Uhrich, G. Schwartz, D. Hildebrandt, M. Pfeiffer, M. Riede, *Appl. Phys. Lett.* **2010**, *97*, 073503.

[6] D. Wynands, M. Levichkova, M. Riede, M. Pfeiffer, P. Bäuerle, R. Rentenberger, P. Denner, K. Leo, *J. Appl. Phys.* **2010**, *107*, 014517.

[7] M. Levichkova, D. Wynands, A. A. Levin, K. Walzer, D. Hildebrandt, M. Pfeiffer, V. Janonis, M. Pranaitis, V. Kažukauskas, K. Leo, M. Riede, *Org. Electron.* **2011**, *12*, 2243.

[8] A. A. Levin, M. Levichkova, D. Hildebrandt, M. Klisch, A. Weiss, D. Wynands, C. Elschner, M. Pfeiffer, K. Leo, M. Riede, *Thin Solid Films* **2012**, *520*, 2479.

[9] H. Ziehlke, L. Burtone, C. Körner, R. Fitzner, E. Reinold, P. Bäuerle, K. Leo, M. Riede, *Org. Electron.* **2011**, *12*, 2258.

[10] R. Fitzner, E. Reinold, A. Mishra, E. Mena-Osteritz, H. Ziehlke, C. Körner, K. Leo, M. Riede, M. Weil, O. Tsaryova, A. Weiß, C. Uhrich, M. Pfeiffer, P. Bäuerle, *Adv. Funct. Mater.* **2011**, *21*, 897.

[11] A. Mishra, C. Uhrich, E. Reinold, M. Pfeiffer, P. Bäuerle, *Adv. Energy Mater.* **2011**, *1*, 265.

[12] S. Steinberger, A. Mishra, E. Reinold, J. Levichkov, C. Uhrich, M. Pfeiffer, P. Bäuerle, *Chem. Commun.* **2011**, *47*, 1982.

[13] S. Steinberger, A. Mishra, E. Reinold, E. Mena-Osteritz, H. Müller, C. Uhrich, M. Pfeiffer, P. Bäuerle, *J. Mater. Chem.* **2012**, *22*, 2701.

[14] Y. Liu, J. Zhou, X. Wan, Y. Chen, *Tetrahedron* **2009**, *65*, 5209.

[15] Y. Liu, X. Wan, B. Yin, J. Zhou, G. Long, S. Yin, Y. Chen, *J. Mater. Chem.* **2010**, *20*, 2464.

[16] B. Yin, L. Yang, Y. Liu, Y. Chen, Q. Qi, F. Zhang, S. Yin, *Appl. Phys. Lett.* **2010**, *97*, 023303.

[17] D. Demeter, T. Rousseau, P. Leriche, T. Cauchy, R. Po, J. Roncali, *Adv. Funct. Mater.* **2011**, *21*, 4379.

[18] M. Riede, C. Uhrich, J. Widmer, R. Timmreck, D. Wynands, G. Schwartz, W.-M. Gnehr, D. Hildebrandt, A. Weiss, J. Hwang, S. Sundarraj, P. Erk, M. Pfeiffer, K. Leo, *Adv. Funct. Mater.* **2011**, *21*, 3019.

[19] J. Meiss, T. Menke, K. Leo, C. Uhrich, W.-M. Gnehr, S. Sonntag, M. Pfeiffer, M. Riede, *Appl. Phys. Lett.* **2011**, *99*, 043301.

[20] S. Millefiori, A. Alparone, *Synth. Met.* **1998**, *95*, 217.

[21] S. S. Zade, M. Bendikov, *Chem. Eur. J.* **2008**, *14*, 6734.

[22] S. S. Zade, N. Zamoshchik, M. Bendikov, *Chem. Eur. J.* **2009**, *15*, 8613.

[23] S. S. Zade, N. Zamoshchik, M. Bendikov, *Acc. Chem. Res.* **2011**, *44*, 14.

[24] H. Nakanishi, S. Inoue, T. Otsubo, *Mol. Cryst. Liq. Cryst.* **1997**, *296*, 335.

[25] S. Inoue, H. Nakanishi, K. Takimiya, Y. Aso, T. Otsubo, *Synth. Met.* **1997**, *84*, 341.

[26] M. Heeney, W. Zhang, D. J. Crouch, M. L. Chabinyc, S. Gordeyev, R. Hamilton, S. J. Higgins, I. McCulloch, P. J. Skabara, D. Sparrowe, S. Tierney, *Chem. Commun.* **2007**, 5061.

[27] A. Patra, Y. H. Wijsboom, S. S. Zade, M. Li, Y. Sheynin, G. Leitus, M. Bendikov, *J. Am. Chem. Soc.* **2008**, *130*, 6734.

[28] Y. H. Wijsboom, A. Patra, S. S. Zade, Y. Sheynin, M. Li, L. J. W. Shimon, M. Bendikov, *Angew. Chem.* **2009**, *121*, 5551; *Angew. Chem. Int. Ed.* **2009**, *48*, 5443.

[29] L. Li, J. Hollinger, A. A. Jahnke, S. Petrov, D. S. Seferos, *Chem. Sci.* **2011**, *2*, 2306.

[30] A. Patra, Y. H. Wijsboom, G. Leitus, M. Bendikov, *Chem. Mater.* **2011**, *23*, 896.

[31] R. Yang, R. Tian, J. Yan, Y. Zhang, J. Yang, Q. Hou, W. Yang, C. Zhang, Y. Cao, *Macromolecules* **2004**, *38*, 244.

[32] A. M. Ballantyne, L. Chen, J. Nelson, D. D. C. Bradley, Y. Astuti, A. Maurano, C. G. Shuttle, J. R. Durrant, M. Heeney, W. Duffy, I. McCulloch, *Adv. Mater.* **2007**, *19*, 4544.

[33] D. S. Chung, H. Kong, W. M. Yun, H. Cha, H.-K. Shim, Y.-H. Kim, C. E. Park, *Org. Electron.* **2010**, *11*, 899.

[34] F. Qiao, X. Hou, Y. Lu, H. Chen, A. Liu, X. Hu, N. Siu Choon, *Sol. Energy Mater. Sol. Cells* **2010**, *94*, 442.

[35] A. Maurano, C. G. Shuttle, R. Hamilton, A. M. Ballantyne, J. Nelson, W. Zhang, M. Heeney, J. R. Durrant, *J. Phys. Chem. C* **2011**, *115*, 5947.

[36] S. D. Oosterhout, M. M. Wienk, M. Al-Hashimi, M. Heeney, R. A. J. Janssen, *J. Phys. Chem. C* **2011**, *115*, 18901.

[37] M. I. Ozkut, S. Atak, A. M. Onal, A. Cihaner, *J. Mater. Chem.* **2011**, *21*, 5268.

[38] D. Bhattacharyya, K. K. Gleason, *J. Mater. Chem.* **2012**, *22*, 405.

[39] W.-H. Lee, S. K. Lee, S. K. Son, J.-E. Choi, W. S. Shin, K. Kim, S.-H. Lee, S.-J. Moon, I.-N. Kang, *J. Polym. Sci., Part A* **2012**, *50*, 551.

[40] M. Shahid, R. S. Ashraf, Z. Huang, A. J. Kronemeijer, T. McCarthy-Ward, I. McCulloch, J. R. Durrant, H. Sirringhaus, M. Heeney, *J. Mater. Chem.* **2012**, DOI: 10.1039/c2jm31189e.

[41] H. A. Saadeh, L. Lu, F. He, J. E. Bullock, W. Wang, B. Carsten, L. Yu, *ACS Macro Lett.* **2012**, 361.

[42] F. Gao, Y. Cheng, Q. Yu, S. Liu, D. Shi, Y. Li, P. Wang, *Inorg. Chem.* **2009**, *48*, 2664.

[43] R. Li, X. Lv, D. Shi, D. Zhou, Y. Cheng, G. Zhang, P. Wang, *J. Phys. Chem. C* **2009**, *113*, 7469.

[44] K. A. Mazzio, M. Yuan, K. Okamoto, C. K. Luscombe, *ACS Appl. Mater. Interfaces* **2011**, *3*, 271.

[45] N. Trinks, Bachelor thesis, Ulm University (Ulm), **2010**.

[46] K. Tamao, S. Kodama, I. Nakajima, M. Kumada, A. Minato, K. Suzuki, *Tetrahedron* **1982**, *38*, 3347.

[47] G. C. Fu, *Acc. Chem. Res.* **2008**, *41*, 1555.

[48] J. Krömer, P. Bäuerle, *Tetrahedron* **2001**, *57*, 3785.

[49] D. N. Antonov, L. I. Belen'kii, S. Gronowitz, *J. Heterocycl. Chem.* **1995**, *32*, 53.

[50] G. Barbey, G. Dian, N. Merlet, F. Outurquin, C. Paulmier, *Synthesis* **1989**, 181.

[51] C. W. Spangler, M. He, *J. Chem. Soc., Perkin Trans. 1* **1995**, 715.

[52] J. M. Tour, R. Wu, *Macromolecules* **1992**, *25*, 1901.

[53] K. Van De Wetering, C. Brochon, C. Ngov, G. Hadziioannou, *Macromolecules* **2006**, *39*, 4289.

[54] R. B. Helmholdt, E. J. Sonneveld, C. M. L. V. Velde, F. Blockhuys, A. T. H. Lenstra, H. J. Geise, R. Peschara, *Acta Crystallogr., Sect. B* **2007**, *63*, 783.

[55] D. T. Tùng, A. Villinger, P. Langer, *Adv. Synth. Catal.* **2008**, *350*, 2109.

[56] C. Paulmier, J. Morel, P. Pastour, *Bull. Soc. Chim. de France* **1969**, 2511.

[57] R. Ketcham, A. B. Hörnfeldt, S. Gronowitz, *J. Org. Chem.* **1984**, *49*, 1117.

[58] J. Hollinger, A. A. Jahnke, N. Coombs, D. S. Seferos, *J. Am. Chem. Soc.* **2010**, *132*, 8546.

[59] S. Gronowitz, in *Thiophene and Its Derivatives, Part 1* (Ed.: S. Gronowitz), Wiley-Interscience, New York, **1985**, pp. 34.

[60] R. J. Mullins, D. R. Williams, in *Name Reactions in Heterocyclic Chemistry* (Eds.: J. J. Li, E. J. Corey), Wiley & Sons, Hoboken, NJ, **2005**, pp. 199.

[61] E. Vogel, C. Fröde, A. Breihan, H. Schmickler, J. Lex, *Angew. Chem.* **1997**, *109*, 2722; *Angew. Chem. Int. Ed.* **1997**, *36*, 2609.

[62] D. L. Klayman, T. S. Griffin, *J. Am. Chem. Soc.* **1973**, *95*, 197.

[63] L. S. Fuller, B. Iddon, K. A. Smith, *J. Chem. Soc., Perkin Trans. 1* **1997**, 3465.

[64] C. Bleiholder, D. B. Werz, H. Köppel, R. Gleiter, *J. Am. Chem. Soc.* **2006**, *128*, 2666.

[65] J. H. Schulte, D. B. Werz, F. Rominger, R. Gleiter, *Organic & Biomolecular Chemistry* **2003**, *1*, 2788.

[66] T. Otsubo, K. Takimiya, in *Handbook of Thiophene-Based Materials: Applications in Organic Electronics and Photonics* (Ed.: I. F. Perepichka, Perepichka, D. F.), Wiley-VCH, Weinheim, **2009**, pp. 321.

[67] C. M. Cardona, W. Li, A. E. Kaifer, D. Stockdale, G. C. Bazan, *Adv. Mater.* **2011**, *23*, 2367.

[68] J. Drechsel, B. Männig, D. Gebeyehu, M. Pfeiffer, K. Leo, H. Hoppe, *Org. Electron.* **2004**, *5*, 175.

[69] T. M. Clarke, A. M. Ballantyne, S. Tierney, M. Heeney, W. Duffy, I. McCulloch, J. Nelson, J. R. Durrant, *J. Phys. Chem. C* **2010**, *114*, 8068.

[70] D. J. Crouch, P. J. Skabara, M. Heeney, I. McCulloch, D. Sparrowe, S. J. Coles, M. B. Hursthouse, *Macromol. Rapid Commun.* **2008**, *29*, 1839.

[71] H. Ziehlke, R. Fitzner, C. Körner, R. Gresser, E. Reinold, P. Bäuerle, K. Leo, M. K. Riede, *J. Phys. Chem. A* **2011**, *115*, 8437.

[72] R. Fitzner, E. Mena-Osteritz, A. Mishra, G. Schulz, E. Reinold, M. Weil, C. Körner, H. Ziehlke, C. Elschner, K. Leo, M. Riede, M. Pfeiffer, C. Uhrich, P. Bäuerle, *J. Am. Chem. Soc.* **2012**, submitted.

[73] H. O. Villar, P. Otto, M. Dupuis, J. Ladik, *Synth. Met.* **1993**, *59*, 97.

[74] D. R. Lide, in *CRC Handbook of Chemistry and Physics*, 84 ed., Boca Rato, Florida, **2003**.

[75] Q. Xie, F. Arias, L. Echegoyen, *J. Am. Chem. Soc.* **1993**, *115*, 9818.

[76] C. J. Brabec, A. Cravino, D. Meissner, N. S. Sariciftci, T. Fromherz, M. T. Rispens, L. Sanchez, J. C. Hummelen, *Adv. Funct. Mater.* **2001**, *11*, 374.

[77] M. C. Scharber, D. Mühlbacher, M. Koppe, P. Denk, C. Waldauf, A. J. Heeger, C. J. Brabec, *Adv. Mater.* **2006**, *18*, 789.

[78] M. Riede, T. Müller, W. Tress, R. Schüppel, K. Leo, *Nanotechnology* **2008**, *19*, 424001.

[79] J. Schatz, in *Science of Synthesis, Vol. 9*, **2000**, p. 287.

[80] J. Schatz, in *Science of Synthesis, Vol. 9*, **2000**, p. 423.

[81] A. Bondi, *J. Phys. Chem.* **1964**, *68*, 441.

[82] H. Nakanishi, S. Inoue, Y. Aso, T. Otsubo, *Synth. Met.* **1999**, *101*, 639.

[83] R. Fitzner, C. Elschner, M. Weil, C. Uhrich, C. Körner, M. Riede, K. Leo, M. Pfeiffer, E. Reinold, E. Mena-Osteritz, P. Bäuerle, *Adv. Mater.* **2012**, *24*, 675.

[84] C. Uhrich, D. Wynands, S. Olthof, M. K. Riede, K. Leo, S. Sonntag, B. Männig, M. Pfeiffer, *J. Appl. Phys.* **2008**, *104*, 043107.

[85] Sheldrick, G.M. (2008). SADABS. University of Göttingen, Germany.

[86] G. M. Sheldrick, *Acta Cryst. A* **2008**, *64*, 112.

[87] A. L. Spek, *Acta Cryst. D* **2009**, *65*, 148.

[88] M. Mutschler, Diploma thesis, Ulm University (Ulm), **2009**.

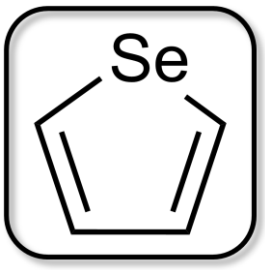

CHAPTER 4

DICYANOVINYL-SUBSTITUTED DICHALCOGENOPHENOPYRROLE-BASED CO-OLIGOMERS

4.1 General Introduction

In the previous chapter, terminally DCV-substituted oligoselenophenes were presented as donor materials for small molecule organic solar cells (SMOSC). The motivation for the synthesis of these compounds was to obtain donor materials with red-shifted absorption spectra compared to previously synthesized oligothiophene analogs. Although a certain red-shift of 20-30 nm was achieved, an even more pronounced red-shift would be desirable to absorb more photons in the red and near-infrared region of the solar spectrum. One way to achieve this goal could be the introduction of a stronger donor moiety into the oligothiophene/oligoselenophene backbone. Therefore, we planned to use *N*-alkylated 4*H*-dithieno[3,2-*b*:2',3'-*d*]pyrrole (DTP) as donor moiety, which has been widely investigated as donor building block for donor-acceptor polymers in the past few years due to its excellent electron donating abilities, exceeding those of other commonly used donor building blocks.[1] Later on, we extended this approach to 4*H*-diselenopheno-[3,2-*b*:2',3'-*d*]pyrrole (DSP)-based compounds. In contrast to DTP, there is only one report on the synthesis and characterization of a DSP derivative so far.[2]

Some DTP-based polymers have been implemented as p-type semiconducting materials in organic field effect transistors (OFET),[3-8] organic light emitting diodes (OLED),[9] and organic solar cells (OSC). Most of the polymers used in OSCs only gave power conversion efficiencies (PCE) below 2%. Due to their relatively high-lying HOMO energy levels the resulting V_{OC} values were only in the range of 0.38-0.55 V.[6-7, 10-13] The best DTP-containing donor-acceptor polymers attained PCEs of 2-3% (**Figure 4.1**).

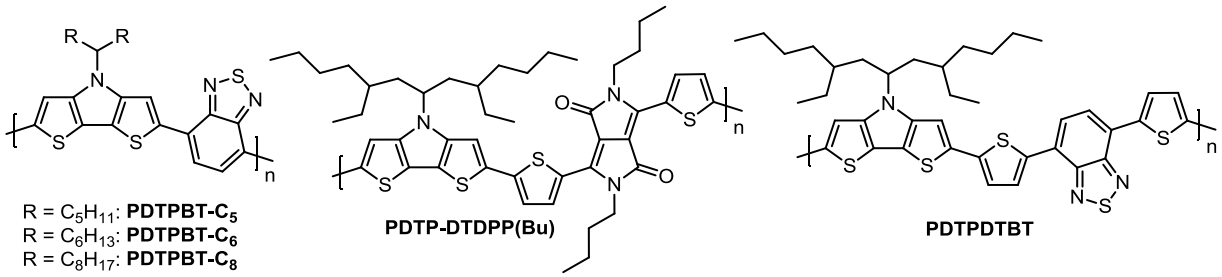

Figure 4.1: Dithienopyrrole-based donor-acceptor polymers with PCEs > 2%.

The highest PCE of 2.80% (J_{SC} = 11.9 mA cm^{-2}, V_{OC} = 0.54 V, FF = 0.44) was obtained with a blend layer of **PDTPBT-C$_5$**/$PC_{61}BM$ (D:A ratio 1:3 w/w). The performance of this polymer exceeded those of its analogs with longer alkyl chains (**PDTPBT-C$_6$** and **PDTPBT-C$_8$**) due to a more uniform morphology of the blend film, which led to an increased V_{OC}.[14] The structurally similar copolymer **PDTPDTBT** showed comparable V_{OC} (0.52 V) and FF (0.44) values in a blend with $PC_{61}BM$, but J_{SC} was lower (9.47 mA cm^{-2}) resulting in a PCE of only 2.18%.[15] With dithienopyrrole-diketopyrrolopyrrole copolymer **PDTB-DTDPP(Bu)**, a PCE of 2.71% was obtained in a blend with $PC_{71}BM$ (D:A ratio 1:2

w/w). In combination with $PC_{61}BM$, the PCE decreased to 2.34%. This device exhibited a very broad absorption in the range of 500-1100 nm and a high J_{SC} of 14.87 mA cm^{-2}, but the PCE was limited by the low V_{OC} of 0.38 V.[16]

Due to its electron-donating properties and planar structure, DTP was also used as core unit for several oligomers (**Figure 4.2**). These oligomers showed bathochromically shifted absorption spectra, higher exctinction coefficients, lower band gaps and higher fluorescence quantum yields (up to 66%) compared to simple quaterthiophenes.[17-19] DFT calculations revealed only negligible electron density on the nitrogen in the HOMO electron density distribution, while the nitrogen atom contributed significantly to the electron distribution of the LUMO. Therefore, the nitrogen atom (and substituents at this atom) exerts only an inductive effect on the HOMO energy level, while the LUMO is influenced by mesomeric and inductive effects.[17] Furthermore, it was found that alkyl chains at the β-positions of the thiophenes adjacent to the DTP caused a blue-shift of the absorption maximum compared to compounds without these substituents. This was explained by distortion of the conjugated backbone due to alkyl-sulfur interactions, leading to a shorter conjugation length.[18-19]

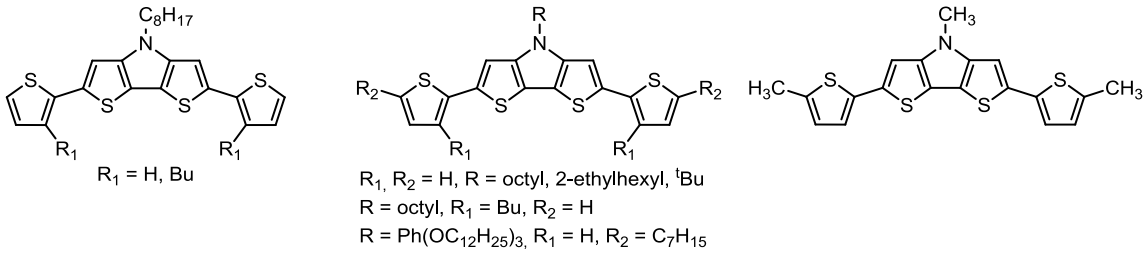

Figure 4.2: DTP-based oligomers.

Until today there are only a few rare examples for the application of DTP-based oligomers in organic electronic devices such as OFETs,[20] DSSCs,[21] or SMOSCs[22] (**Figure 4.3**). Compounds **S3** and **S4** were used as sensitizers in DSSCs and gave PCES of 3.70% (**S3**) and 1.24% (**S4**). These efficiencies are rather moderate compared to the best dyes in the literature, which attain PCEs over 10%. Their IPCE spectra were broad and extended up to 750-800 nm, but the device performance suffered from dye aggregation on the TiO_2 photoanode and the high HOMO energy levels of these compounds.[21]

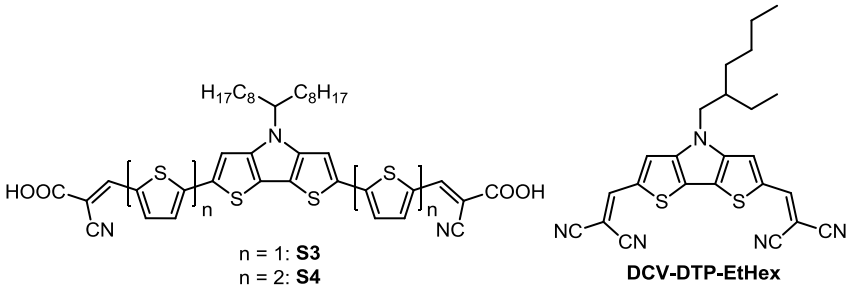

Figure 4.3: DTP-based oligomers used in organic solar cells.

The DCV-substituted compound **DCV-DTP-EtHex** was tested as donor material in PHJ solar cells with C_{60} as acceptor. The donor layer was deposited both from solution and by vacuum-sublimation, but only very poor PCEs of 0.24% and 0.09% were obtained.[22]

Three routes have been reported in the literature for the synthesis of *N*-alkylated DTPs. The first approach consisted of *N*-alkylation of the parent DTP with alkyl bromides (**Scheme 4.1**).[23] DTP had first been synthesized in 1983 by thermal decomposition of 3-azido-2,2'-bithiophene.[24] The main drawback of this approach is the lengthy synthesis of the parent DTP, which takes four steps from 2,3-dibromothiophene.

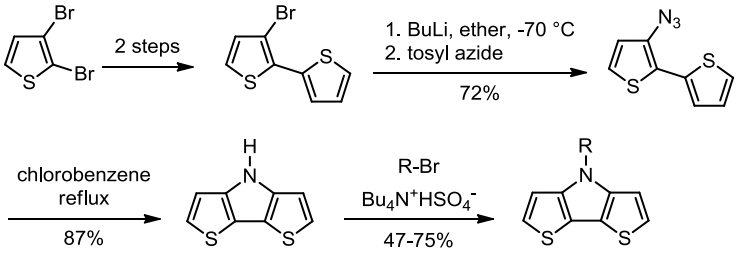

Scheme 4.1: First synthesis of *N*-alkylated DTPs.

In 2003, Ogawa and Rasmussen reported on an improved synthetic route for *N*-alkylated DTPs with only two or three steps starting from 3-bromothiophene (**Scheme 4.2**).[25] The latter was reacted with alkyl amines in a Buchwald-Hartwig reaction to form a mixture of secondary and tertiary thienyl amines. The secondary amines were transformed into tertiary amines by a second Buchwald-Hartwig reaction with 3-bromothiophene. The synthesis of the amines had already been published in 2001.[26] The ring closure of the tertiary amines was carried out in a one-pot reaction consisting of bromination with NBS and subsequent coupling with copper.

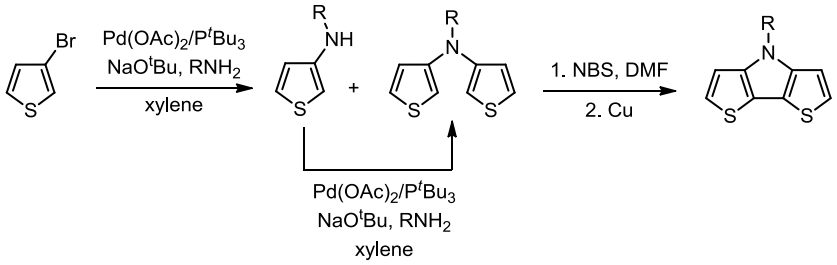

Scheme 4.2: Synthesis of *N*-alkylated DTPs via ring closure of tertiary thienyl amines.

This method definitely brought an improvement compared to the first approach; however, it still possessed some major drawbacks. Firstly, the secondary and tertiary amines are rather unstable and cannot be stored for a longer time. Secondly, scaling up of the reactions proved to be difficult due to a significant drop in yields. The most important disadvantage is the linear reaction sequence. In order to introduce a new alkyl substituent, the whole sequence has to be repeated from the beginning.

In 2005, Koeckelberghs *et al.* published a third approach for the synthesis of *N*-alkylated DTPs (**Scheme 4.3**). They reacted 3,3'-dibromo-2,2'-bithiophene with alkyl amines under Buchwald-Hartwig conditions and screened different palladium sources, ligands and solvents. The best yields were obtained with a combination of $Pd_2(dba)_3{\cdot}CHCl_3$ and BINAP in toluene. The use of a chelating ligand was crucial in order to suppress β-hydride elimination.[27-29] With this method, a variety of alkyl substituents was introduced in good to excellent yields.[30] While 3,3'-dibromo-2,2'-bithiophene had been synthesized before by various methods,[31-33] Evenson and Rasmussen published in 2010 an optimized synthesis of DTP which started from 3-bromothiophene. Lithiation with LDA, transmetallation with $ZnCl_2$ and oxidative coupling with $CuCl_2$ provided the desired bithiophene in 85-90% yield. Thus, a versatile method was found to synthesize *N*-alkylated DTPs in only two steps from 3-bromothiophene in good overall yields.[34]

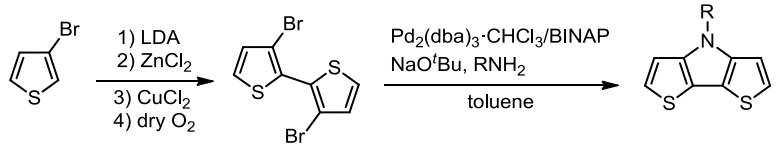

Scheme 4.3: Synthesis of *N*-alkylated DTPs by Buchwald-Hartwig reaction of 3,3'dibromo-2,2'-bithiophene with alkyl amines.

While DTP derivatives are well-established building blocks in the literature, only one DSP derivative was described in a publication of Marder *et al.* from 2010.[2] Therein, diselenophenopyrrole was synthesized by a method similar to that of Koeckelberghs *et al.* (**Scheme 4.4**). First, the authors synthesized a TMS-protected 3,3'-dibromo-2,2'-biselenophene, then this building block was reacted with an aromatic amine in a Buchwald-Hartwig reaction. In this publication, the optical and electrochemical properties of this novel DSP compound were investigated but no further application was presented. No *N*-alkylated diselenophenopyrroles are known in the literature so far.

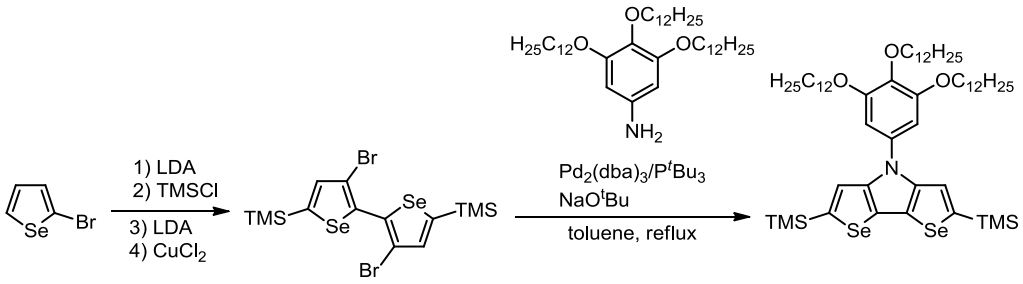

Scheme 4.4: Literature synthesis of a diselenophenopyrrole.

In this chapter, the synthesis of vacuum-processable and solution-processable co-oligomers containing the strong donors DTP or DSP and strong terminal DCV acceptor group are presented. The thermal, optical, and electrochemical properties of these co-oligomers were investigated.

Furthermore, they were implemented as donor materials in organic solar cells. However, the performance of these devices cannot be discussed in this thesis for confidentiality reasons.

4.2 Vacuum-processable Co-Oligomers with a Dichalcogenophenopyrrole Core

4.2.1 Introduction

When I designed the target compounds for vacuum-processing, I wanted to avoid longer alkyl chains in order to limit the molecular weight and to incorporate as few insulating side groups as possible. Taking these considerations into account, I designed the following lead structure: A DTP or DSP core with a short alkyl chain or an aryl substituent at the nitrogen, on both α-positions functionalized with a DCV-substituted thiophene or selenophene. Due to previous results by Heliatek, *N*-propyl and *N*-phenyl-functionalized core units were used (**Figure 4.4**).

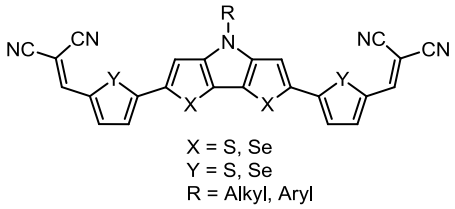

Figure 4.4: Lead structure for vacuum-processable DTP-based and DSP-based co-oligomers.

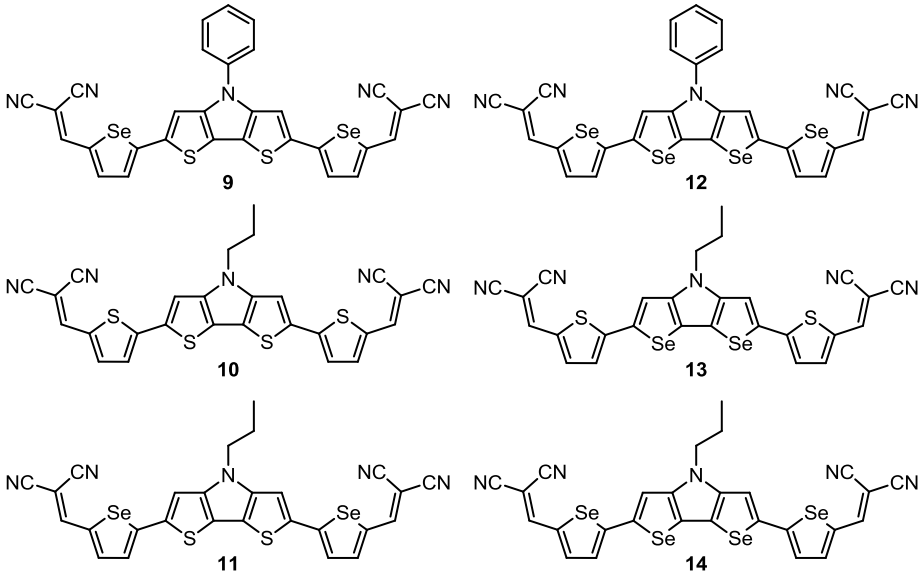

Figure 4.5: Investigated vacuum-processable co-oligomers with a DTP or DSP core.

Following this lead structure, three oligomers with a DTP core (**9**-**11**) and three oligomers with a DSP core (**12**-**14**) were synthesized, their thermal and optoelectronic properties were investigated, and they were implemented as donor materials in vacuum-processed BHJ solar cells (**Figure 4.5**). By introduction of the DSP unit, which was expected to be a stronger donor than DTP, and replacement of the terminal thiophene units by selenophene, I intended to obtain co-oligomers with stronger red-shifted absorption spectra compared to the all-thiophene co-oligomer **10**.

4.2.2 Synthesis of Vacuum-processable Co-oligomers

The synthesis of co-oligomers **9**-**14** was carried out in a convergent way because of the expected poor solubility of the target compounds. The retrosynthetic analysis of the lead structure revealed the two possible approaches **A** and **B** (**Scheme 4.5**). In both approaches, the target compound was synthesized by C-C cross-coupling of a dichalcogenophenopyrrole building block and a DCV-substituted thiophene or selenophene unit. Stille-type cross-coupling was chosen as C-C coupling method because excellent results had been achieved with it in the synthesis of other DCV-functionalized oligomers used in SMOSCs.[35-36]

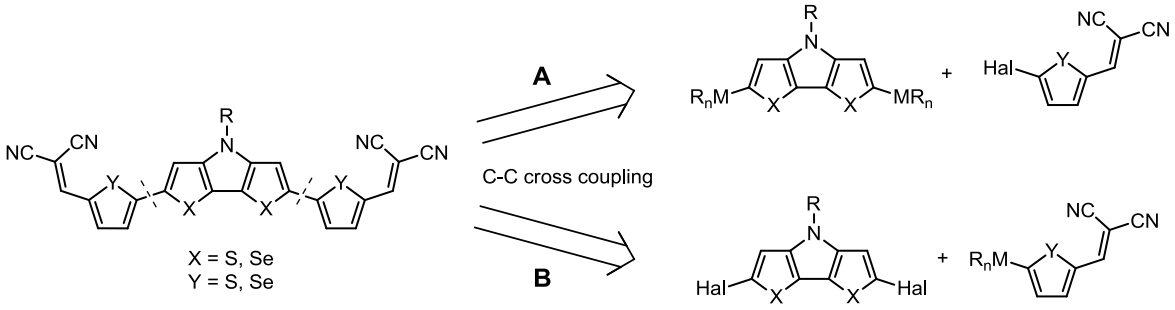

Scheme 4.5: Retrosynthesis of dichalcogenophenopyrrole-based compounds.

The difference in the two routes is the functionalization of the respective building blocks. In route **A**, a bis-organometallated dichalcogenophenopyrrole is coupled with a halogenated DCV-thiophene or selenophene, respectively. In route **B**, the reactivity of the building blocks is inverted, i.e., a dihalogenated dichalcogenophenopyrrole is coupled with an organometallated DCV-thiophene/ selenophene. At first glance, the first route seems to be more promising due to the easier synthesis of both building blocks, the stannylated dichalcogenophenopyrrole and the halogenated thiophene/selenophene. The second route requires a metallated DCV-compound, whose synthesis is challenging due to the base lability of the DCV group. Therefore, route **A** was chosen for the synthesis of compounds **9**-**12**. However, this route was not viable for compound **13** and **14** because the required stannylated diselenophenopyrrole building block could not be synthesized due to ring-

opening of one selenophene ring during lithiation (*vide infra*). Hence, route **B** had to be taken for these two compounds.

4.2.2.1 Synthesis of Dithienopyrrole Co-oligomers

The dithienopyrrole building blocks were synthesized according to the method developed by Koeckelberghs *et al.*[30, 37] because it allowed the introduction of different aliphatic and aromatic substituents at the nitrogen atom while using only one starting material, 3,3'-dibromobithiophene **56** (**Scheme 4.6**). Bithiophene **56** was synthesized according to a literature procedure from 3-bromothiophene by lithiation with LDA, transmetallation with zinc(II) chloride, and subsequent oxidative coupling with copper(II) chloride in 90% yield.[34]

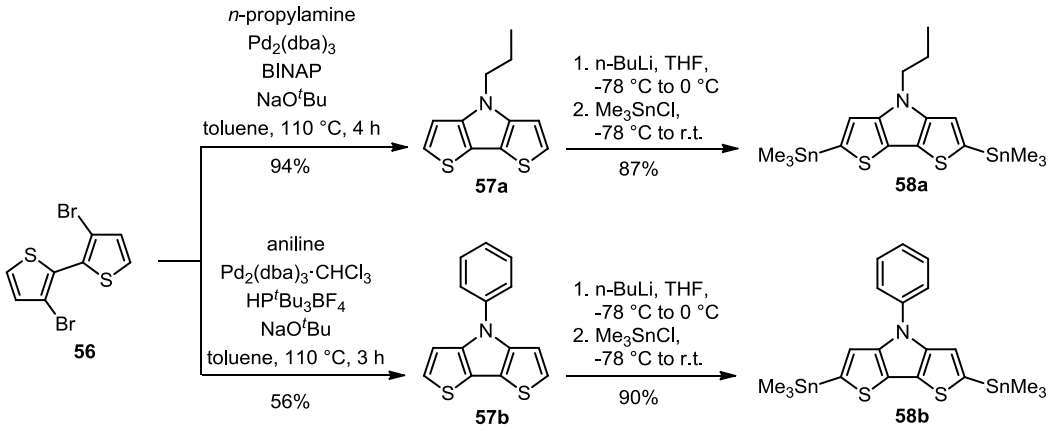

Scheme 4.6: Synthesis of distannylated dithienopyrroles **58a-b**.

For the subsequent Buchwald-Hartwig amination, the choice of the catalyst ligand was crucial. If aliphatic amines were used, a chelating ligand such as (2,2'-bis(diphenylphosphino)-1,1'-binaphthyl) (BINAP) was necessary in order to suppress β-hydride elimination. With aromatic amines, however, this ligand only afforded low yields. In that case, the tris(*tert*-butyl)phosphine (P^tBu_3) ligand gave the best results. Thus, *N*-propyldithienopyrrole **57a** was synthesized in 94% yield by reacting bithiophene **56** and *n*-propylamine with $Pd_2(dba)_3$/BINAP as catalyst and sodium *tert*-butylate as base in toluene at 110 °C for 4 h. The reaction should be carried out in a closed reaction vessel because of the high volatility of propylamine. For the synthesis of *N*-phenyldithienopyrrole **57b**, only the ligand of the catalyst system was changed from BINAP to P^tBu_3 and aniline was used as amine. After 3 h reaction time and column chromatography on silica gel, **57b** was isolated in 56% yield. In this case, the lower yield was probably due to an insufficient reaction time. The dithienopyrrole compounds **57a**-**b** were stannylated by lithiation with *n*-BuLi (2.5 eq.) in THF and subsequent quenching with trimethyltin chloride (2.5 eq.). In order to obtain the dilithiated dithienopyrrole, it is important to work in a relatively concentrated solution (ca. 0.3 mol L^{-1} of **57a**-**b**) and to warm up the reaction from -78 °C to

0 °C. The quenching reagent should be added at -78 °C; then, the reaction can be warmed to room temperature. If these rules are followed, one obtains almost exclusively the distannylated dithienopyrrole with only small amounts of monostannylated compound. The desired distannylated dithienopyrroles were obtained in 87% (**58a**) and 90% (**58b**) yield, respectively. In a previous publication, it was recommended to work under dilute conditions at concentrations around 0.01 mol L^{-1},[19] but according to our observations the yields decreased under more diluted conditions.

In the last step, the stannyl building blocks **58a** and **58b** were coupled with either bromo-substituted DCV-selenophene **31** or DCV-thiophene **59** (synthesis of DCV-building blocks see **Chapter 3**). The reactions were carried out with $Pd(PPh_3)_4$ in concentrated THF or DMF solutions at 80 °C overnight (**Scheme 4.7**). The desired product precipitated and could simply be filtered off. If some monocoupling product was left, it could easily be removed by washing the crude product with THF and methanol. Further purification by Soxhlet extraction with chlorobenzene afforded the target compounds **9**-**11** in yields of 90% (**9**), 83% (**10**) and 60% (**11**).

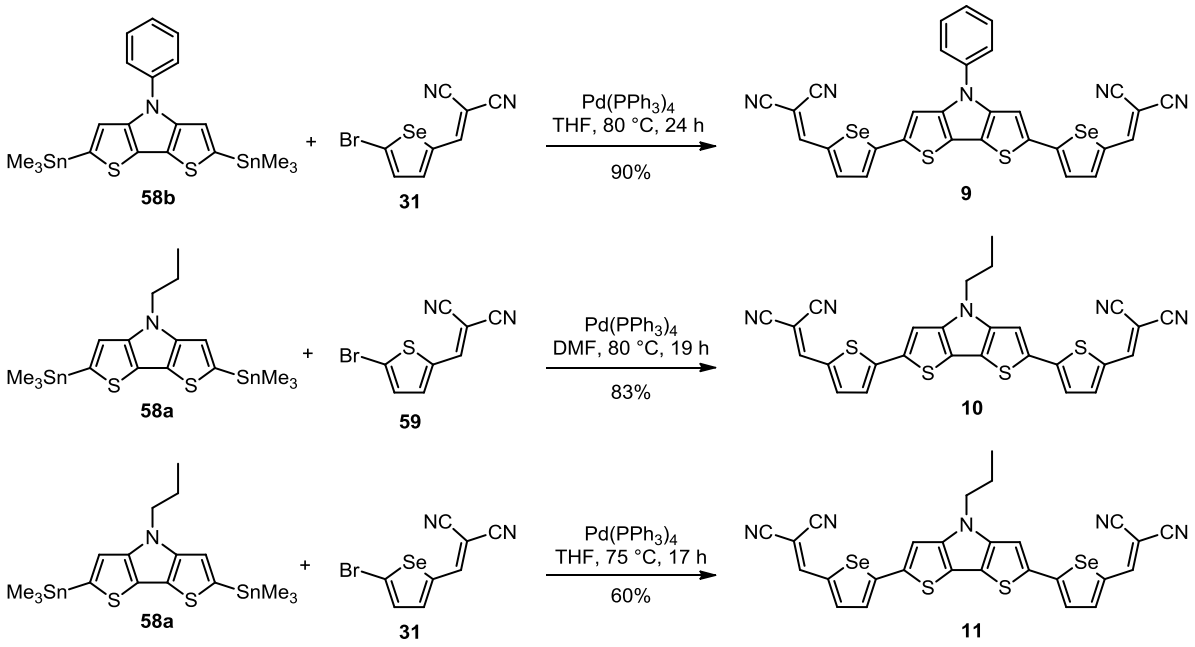

Scheme 4.7: Synthesis of target compounds **9**-**11** by Stille-type cross-coupling.

4.2.2.2 Synthesis of Diselenophenopyrrole Co-oligomers

For the synthesis of the diselenophenopyrrole core (**Scheme 4.8**), the literature protocol developed by Marder *et al.*[2] was slightly varied. Instead of (3,3'-dibromo-[2,2'-biselenophene]-5,5'-diyl)bis(trimethylsilane), the corresponding diiodo biselenophene **62** was used. Due to previous

experiences with β-halogenated selenophenes, a better reactivity in cross-coupling reactions was expected for the diiodo compound compared to the dibromo derivative.

The synthesis of biselenophene **62** started with selenophene **20**, which was transformed into (5-iodoselenophen-2-yl)trimethylsilane **61** in a one-pot reaction. First, it was lithiated with *n*-BuLi (1 eq.) at -78 °C and quenched with trimethylsilyl chloride (1 eq.) to obtain the TMS-protected selenophene **60**. This was lithiated *in situ* with a second equivalent of *n*-BuLi and quenched with iodine. After work-up and distillation, compound **61** was obtained in 53% yield over two steps. Iodoselenophene **61** was further lithiated with LDA to induce a base-catalyzed halogen dance reaction,[2, 38] which led to the formation of [3-iodo-5-(trimethylsilyl)-selenophen-2-yl]lithium. In order to obtain full conversion in the halogen dance reaction, it was important to work below -60 °C and to add the base very slowly within 3-4 hours. The lithiated species was oxidatively coupled with copper(II) chloride to afford compound **62**.

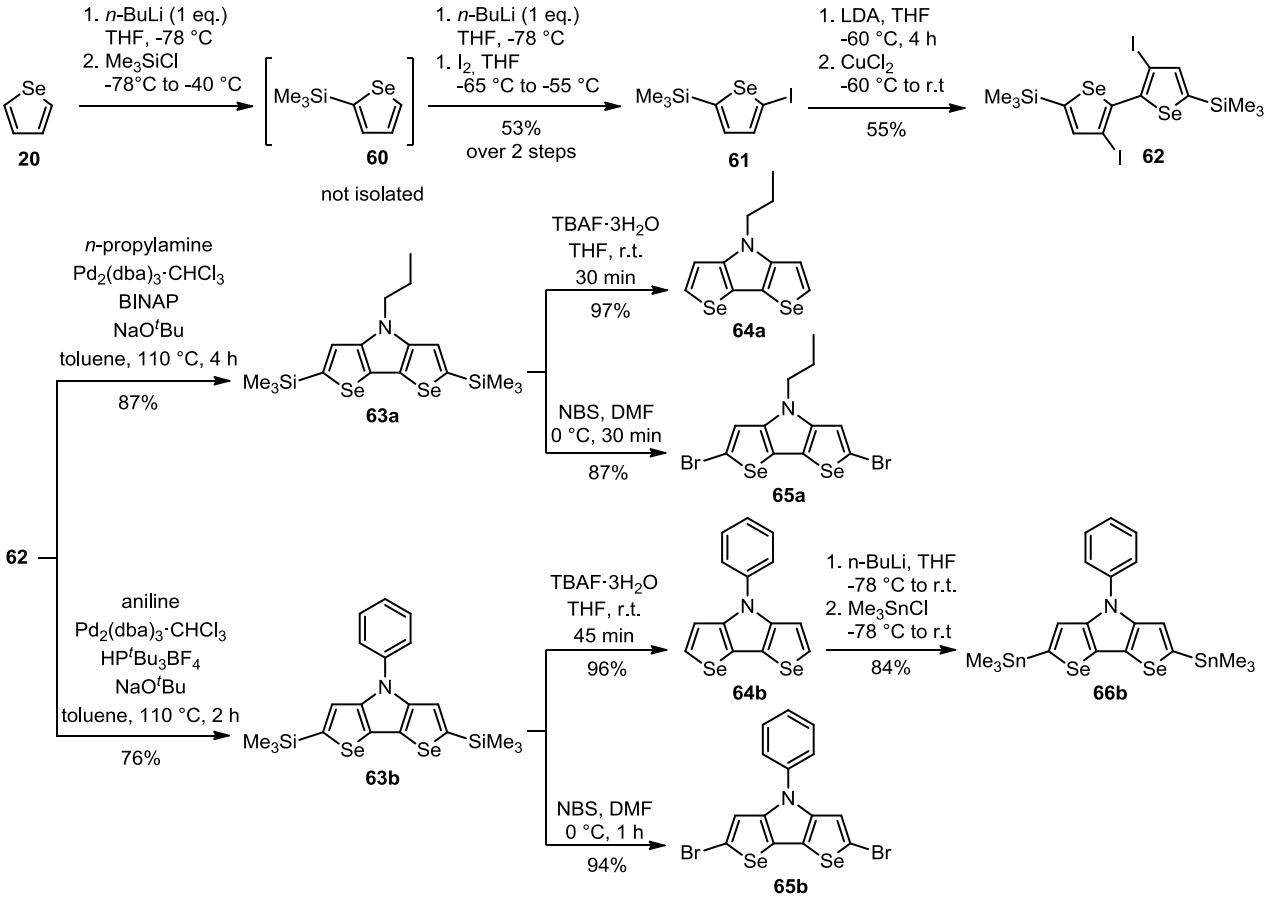

Scheme 4.8: Synthesis of *N*-propyl- and *N*-phenyldiselenophenopyrrole as well as their dibromo and distannyl derivatives.

TMS-protected diiodo biselenophene **62** was purified by column chromatography on basic alumina (on silica gel, the TMS groups were cleaved off) and subsequent precipitation with ethanol. Thus,

pure biselenophene **62** was obtained in 55% yield. The purity of this compound was of crucial importance since even minor impurities significantly lowered the product yields of the subsequent Buchwald-Hartwig reactions. Those reactions were carried out as explained before for the dithienopyrroles, using $Pd_2(dba)_3$/BINAP as catalyst for aliphatic amines and $Pd_2(dba)_3/P^tBu_3$ for aromatic amines. Here, the choice of the base was important as well. When potassium *tert*-butylate was used instead of sodium *tert*-butylate, the yields decreased drastically to about 15%. The reactions were carried out in toluene at 110 °C, and after 2-4 h the desired diselenophenopyrroles **63a** and **63b** were isolated in 87% and 76% yield, respectively. They were purified by column chromatography on basic alumina in order to preserve the TMS protecting groups. The TMS-protected compounds **63a** und **63b** were transformed into the corresponding dibromo derivatives **65a** and **65b** with NBS (2.2 eq.) in DMF at 0 °C. The reactions were complete after 30-60 min. While dibromo derivative **65b** was very stable and was isolated in an excellent yield of 94%, dibromo compound **65a** tended to polymerize in solution, especially in the presence of light and at temperatures above 40 °C. A similar instability had been reported for dibrominated *N*-alkylated DTPs.[39-40] When compound **65a** was handled carefully, i.e., in the absence of light and no elevated temperatures during work-up, it was obtained in 87% yield. Both compounds needed to be purified on basic alumina because of decomposition on silica gel. In order to obtain the deprotected diselenophenopyrroles **64a** and **64b**, the TMS groups were cleaved off with tetrabutylammonium fluoride (TBAF) in THF at r.t. Usually, a reaction time of 30-45 min was sufficient to obtain full conversion. After purification by column chromatography on silica gel, compounds **64a** and **64b** were obtained in almost quantitative yields of 97% and 96%, respectively.

In the following step, I intended to stannylate the diselenophenopyrroles **64a** and **64b** as described above for the corresponding dithienopyrroles. In the case of the phenyl derivative **64b**, the stannylation worked reasonably well and distannylated diselenophenopyrrole **66b** was obtained in 84% crude yield as determined from ^{1}H NMR spectra. It contained about 20% of monostannylated product, but it was used in the Stille coupling without further purification. In the case of the propyl derivative **64a**, the stannylation and especially the lithiation step proved to be much more difficult. During lithiation with *n*-butyllithium, one of the selenophene rings was opened, and after quenching with water the main product of the reaction was the ring-opened 4*H*-selenopheno[3,2-*b*]pyrrole **67** (E = H) (**Scheme 4.9**). Most probably, stannylated ring-opening products were formed as well, but these could not be unambiguously identified in the NMR spectra.

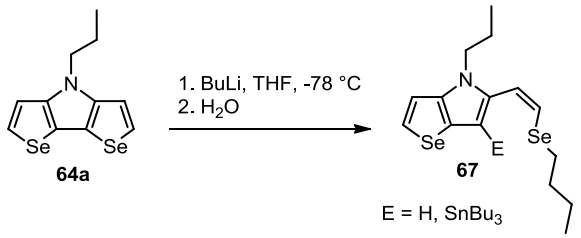

Scheme 4.9: Unexpected ring-opening reaction during the lithiation of propyl-DSP **64a**.

This reaction also occurred during the lithiation of the phenyl-substituted diselenophenopyrrole, but in this case it was only a minor side-reaction and the desired distannylated product was still obtained in reasonably good yields. The structure of the unexpected ring-opened product **67** is deduced from ^{1}H NMR and GC-MS data. The detected mass of 375 u (calc. exact mass of **67** with E = H: 375.1 u) as well as the signal patterns in the NMR spectrum (**Figure 4.6**) strongly hint at the proposed structure. The two doublets at 7.60 and 7.16 ppm (**A**) were assigned to the protons at the preserved selenophene ring and the singlet at 6.74 ppm (**C**) corresponds to the pyrrole proton. The two doublets 6.80 and 6.55 ppm (**B**), with a coupling constant of 10.4 Hz, were assigned to the two olefinic protons of compound **67**. The coupling constant is a good indication for a *cis*-configured double bond. In the aliphatic region, the signals of a butyl group (**E**) in addition to the propyl group (**D**) are clearly visible.

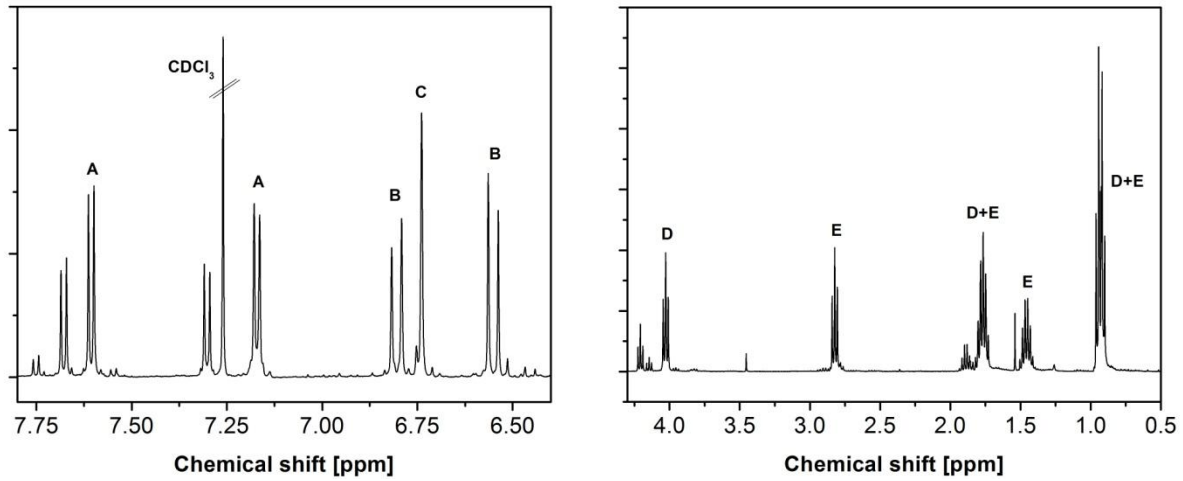

Figure 4.6: (a) Aromatic and (b) aliphatic region of the ^{1}H NMR spectrum of ring-opening product **67**.

Similar ring-opening products have been reported in the literature,[41-43] and the proposed ring-opening mechanism is shown in **Scheme 4.10**.

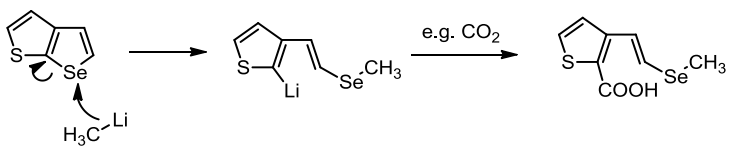

Scheme 4.10: Mechanism of ring cleavage of selenophenes by organolithium reagents as proposed in Ref. [42].

In order to avoid the undesired ring-opening reaction, various reaction conditions were screened for the lithiation (**Table 4.1**). At first, the lithiation was carried out under the usual conditions which were used for the DTP compounds, i.e., lithiation with *n*-BuLi at -78 °C and warming up to at least 0 °C before quenching with trimethyltin chloride. When these conditions were applied for propyl-DSP **64a**, the main product of the reaction was the ring-opening product **67** (E = $SnBu_3$), together with some unreacted starting material. The reaction was repeated several times, each time warming up to a lower temperature (0 °C, -20 °C, -40 °C). However, the ring-opening product was always the main product and the distannylated compound only was formed if the reaction was warmed above -40 °C. Therefore, lithiation with *n*-BuLi could not be applied in this case. In order to explore if a stronger lithiation reagent would lithiate the diselenophenopyrrole faster and thus suppress the undesired ring-opening reaction, the reaction was also carried out with *n*-BuLi/TMEDA and *tert*-BuLi. Unfortunately, only ring-opening products were obtained in both cases, not even traces of distannylated DSP were found. Consequently, the last possibility was to use a milder lithiation reagent such as LDA. The reaction was carried out with this reagent twice; once it was warmed up to 0 °C and once to r.t. with reaction times of up to 5 h. In the first case, only starting material was isolated; in the second case, a 1:1 mixture of starting material and an unknown stannylated product was obtained.

Table 4.1: Reaction conditions for attempted stannylation of *N*-propyldiselenophenopyrrole.

lithiation reagent	temperature [° C]	time [min]	products
n-BuLi	-78 to r.t.	105	starting material + ring-opening product
n-BuLi	-78 to 0	120	distannyl compound + ring-opening product
n-BuLi	-78 to -40	210	traces of distannyl compound + stannylated ring-opening product
n-BuLi	-78 to -20	240	mixture of ring-opening products
n-BuLi / TMEDA	-78 to 0	90	only ring-opening product
tert-BuLi	-78 to r.t.	90	mixture of ring-opening products
LDA	-78 to 0	180	only starting material
LDA	-60 to r.t.	300	starting material + unknown product (ca. 1:1)

Due to these problems during lithiation, the synthetic strategy for the *N*-propyldiselenopheno-pyrrole-based compounds was changed and synthetic approach **B** was followed, i.e., Stille cross-coupling of a dihalogenated DSP with a stannylated DCV-thiophene/selenophene. As halogenated building block dibromodiselenophenopyrrole **65a** can be used. The problem of this route was the stannylated DCV-compound. In the literature, there is no example for an organometallic derivative of a DCV-substituted thiophene and only one example for a compound that is at least similar; the latter

was described in a patent by *Sony* (**Scheme 4.11**).[44] In this patent, 5-(tributylstannyl)thiophene-2-carbaldehyde was reacted with ethyl 2-cyanoacetate in a Knoevenagel condensation to obtain the corresponding condensation product without the stannyl group being cleaved off. However, the synthesis of the aldehyde was not described. In another patent, a similar aldehyde with an additional methyl group was synthesized from its acetal by acidic deprotection with 1 N hydrochloric acid in THF.[45] According to this patent, the stannyl group remained unaffected under these acidic conditions.

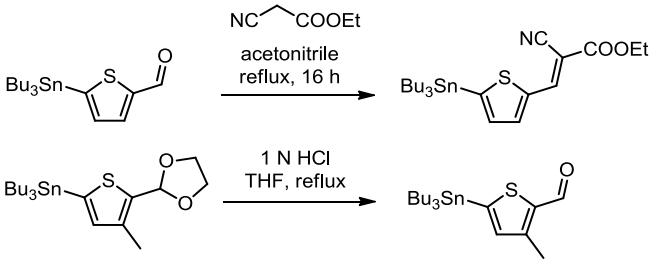

Scheme 4.11: Literature synthesis of a stannylated thiophenecyanoacrylic acid ester.

Encouraged by these literature procedures, I tried to synthesize DCV compound **70a** starting from the protected stannylated thiophenecarbaldehyde **68**[46-47] (**Scheme 4.12**). It was deprotected with 1 N HCl in refluxing THF, and after 10 min the acetal was completely cleaved while only some percent of the stannyl groups were also cleaved off. Longer reaction times should be avoided to prevent further cleavage of the stannyl groups. Thus, aldehyde **69a** was obtained in 91% crude yield. Subsequent Knoevenagel condensation with malononitrile and β-alanine in acetonitrile under reflux conditions afforded the desired DCV compound **70a** in 72% yield. The compound can easily be purified by column chromatography on silica gel without cleavage of the stannyl group. This is rather untypical for stannylated thiophenes and probably due to the electron-withdrawing DCV group which renders the thiophene less electron-rich.

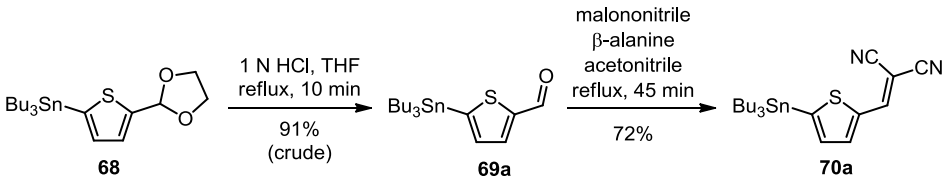

Scheme 4.12: Synthesis of stannylated DCV-thiophene **70a**.

Because the synthesis of the protected aldehyde **68** consists of another two steps, thus rendering the synthesis of compound **70a** a four-step synthesis, I tried to find a more direct route with fewer steps (**Scheme 4.13**). This route started with commercially available 2-tributylstannylthiophene **71a**, which was lithiated with LDA at temperatures below -60 °C and quenched with DMF to obtain the stannylated aldehyde **69a**. The temperature needed to be kept below -60 °C; otherwise, a significant

amount of the stannyl groups was cleaved off. Thus, aldehyde **69a** was obtained in 21% yield. With the corresponding selenophene compound **71b**, the reaction worked better and aldehyde **69b** was obtained in 70% yield. For both aldehydes, the subsequent Knoevenagel condensation afforded the desired DCV-substituted thiophene **70a** and selenophene **70b** in almost identical yields of 73% and 72%, respectively.

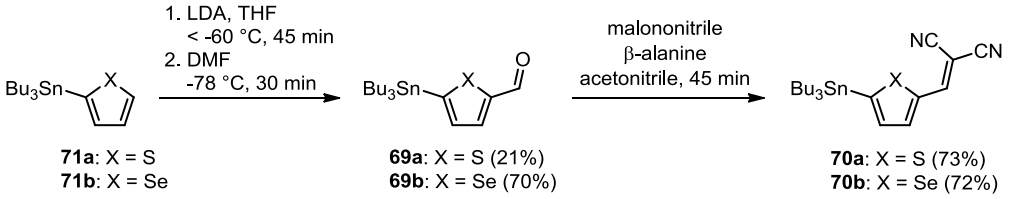

Scheme 4.13: Synthesis of stannylated DCV-thiophene **70a** and DCV-selenophene **70b**.

Building blocks **70a** and **70b** were then used to synthesize the target compounds **13** and **14** (**Scheme 4.14**). The *N*-phenyl derivative **12** was synthesized by retrosynthetic approach **A**, i.e., by Stille coupling of distannylated diselenophenopyrrole **66b** with brominated DCV-selenophene **31**. The reaction was carried out in DMF at 80 °C for 22 h using the standard catalyst $Pd(PPh_3)_4$, and co-oligomer **12** was obtained in 59% yield after filtering, washing and Soxhlet extraction. For co-oligomers **13** and **14**, route **B** was chosen since the distannylated *N*-propyldiselenophenopyrrole was not available. Thus, co-oligomer **14** was synthesized by Stille coupling of dibromo-DSP **65a** with selenophenyl stannane **70b** using the standard catalyst $Pd(PPh_3)_4$. The reaction was carried out in THF at 80 °C for 23 h, and product **14** was isolated in 62% yield.

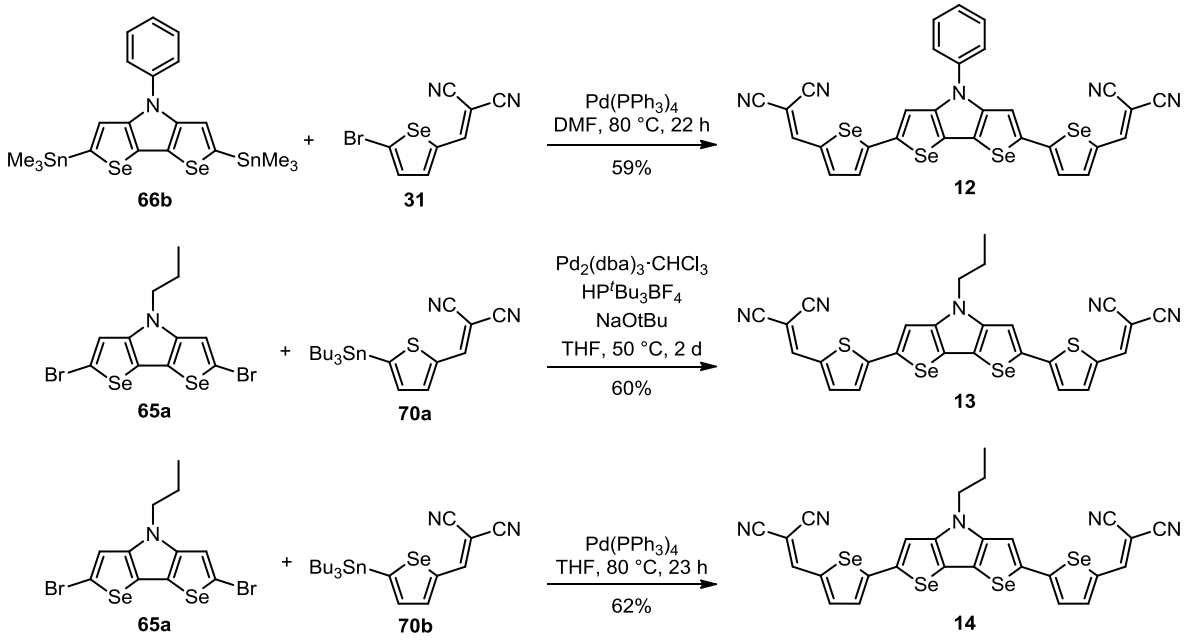

Scheme 4.14: Synthesis of target compounds **12**-**14**.

When dibromo-DSP **65a** was reacted with thienyl stannane **70a** under the same conditions, target molecule **13** was obtained, but it was contaminated with side-product **72**, containing two DSP moieties (**Figure 4.7**). Presumably, this product was formed by oxidative homocoupling of compound **65a** and subsequent reaction with stannane **70a**. This side-product could not be separated by Soxhlet extraction due to its similar solubility. Separation by column chromatography on silica gel with DCM as eluent was possible but very tedious because of the low solubility of both compounds **13** and **72**.

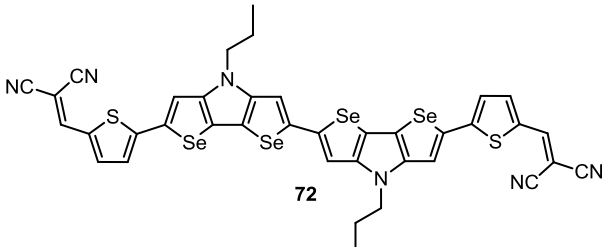

72

Figure 4.7: Undesired side-product occurring during the synthesis of compound **13**.

Therefore, several attempts were made to find optimized reaction conditions for the exclusive formation of co-oligomer **13** (see bachelor thesis Eduard Brier[48]). At first, cesium fluoride was added to activate the stannyl compound; however, the stannane seemed to decompose under these conditions and no product was obtained. Then, the catalyst was changed to the more active system $Pd_2(dba)_3{\cdot}CHCl_3/HP^tBu_3BF_4$ with traces of NaO^tBu to deprotonate the phosphonium salt. In DMF no product was obtained with this catalyst system. In THF three different temperatures were tested, and 50 °C turned out to be the optimal temperature resulting in a yield of 62%. At 80 °C, the yield was slightly lower (57%), and at r.t. almost no product was obtained.

Due to the low solubility of co-oligomers **9**-**14**, ^{1}H NMR spectra had to be recorded in $C_2D_2Cl_4$ at 80-100 °C and ^{13}C NMR spectra could not be measured even with a high number of scans. Due to the symmetry of the molecules the ^{1}H NMR spectra for all co-oligomers showed four signals for the protons in the conjugated backbone (H_a-H_d, **Figure 4.8**).

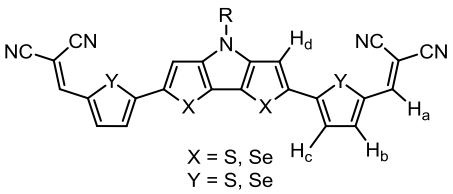

Figure 4.8: Assignment of proton signals in ^{1}H NMR spectra of co-oligomers **9**-**14**.

The DCV proton (H_a) appeared as a singlet between 7.68 and 7.75 ppm. If the DCV group was adjacent to a selenophene unit H_a appeared at slightly downfield-shifted compared to the DCV group being adjacent to a thiophene unit. The chalcogenophene protons H_b and H_c appeared as doublets with a coupling constant of ~4.5 Hz. If Y = Se the signals for H_b (7.71-7.74 ppm) and H_C (7.30-7.40

ppm) were shifted downfield compared to Y = S (δ_{Hb} = 7.56-7.58 ppm, δ_{Hc} = 7.19-7.28 ppm), which is typical for selenophene protons compared to thiophene protons (see **Figure 1.1**). When DSP was used as a core unit the proton of this building block (H_d) was also shifted downfield (δ_{Hd} = 7.45-7.52 ppm) compared to DTP as a core unit (δ_{Hd} = 7.26-7.34 ppm).

The compounds were further characterized by MALDI-TOF mass spectrometry and elemental analysis. In the MALDI-TOF spectra the compounds were clearly identified by their monoisotopic mass peaks; m/z = 667.3 (co-oligomer **9**), 537.1 (**10**), 633.0 (**11**), 761.0 (**12**), 632.9 (**13**) and 726.8 (**14**). With increasing selenophene content a more complicated isotope pattern was observed due to the six natural isotopes of selenium.

4.2.3 Thermal Properties of Co-oligomers 9-14

The thermal properties of co-oligomers **9**-**14** were investigated by Differential Scanning Calorimetry (DSC) (**Figure 4.9**). The melting points are summarized in **Table 4.2**. The DSC curves of all co-oligomers showed one endothermic peak, indicating the melting point, and one relatively well-defined exothermic decomposition peak at higher temperatures but very close to the melting peak. Directly after melting the compounds seem to decompose in a defined way, most probably by cleavage of the DCV groups.

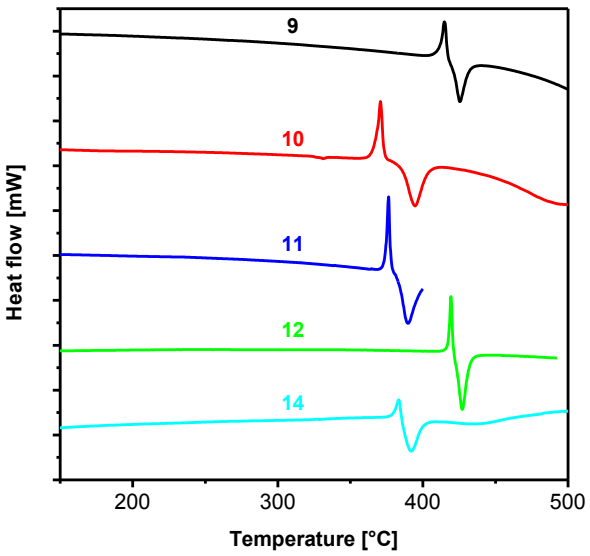

Figure 4.9: DSC curves for co-oligomers **9**-**14** measured at a heating rate of 10 °C min^{-1} under argon flow.

The melting points of the diselenophenopyrrole co-oligomers **12**-**14** are somewhat higher than those of the dithienopyrrole co-oligomers **9**-**11** but only by few degrees (~5 °C). Furthermore, the melting

points of the *N*-phenyl derivatives **9** (412 °C) and **12** (414 °C) are significantly higher than those of the *N*-propyl derivatives **10**, **11**, **13** and **14** (~365-380 °C). The phenyl ring possibly induces stronger intermolecular interactions due to π-π stacking, thus increasing the melting temperature.

4.2.4 Optical Properties of Co-oligomers 9-14

The optical properties of co-oligomers **9**-**14** were investigated by UV-Vis absorption and emission spectroscopy, both in dichloromethane solution (**Figure 4.10**) and in thin films prepared by vacuum deposition (**Figure 4.11**). The resulting data are summarized in **Table 4.2**.

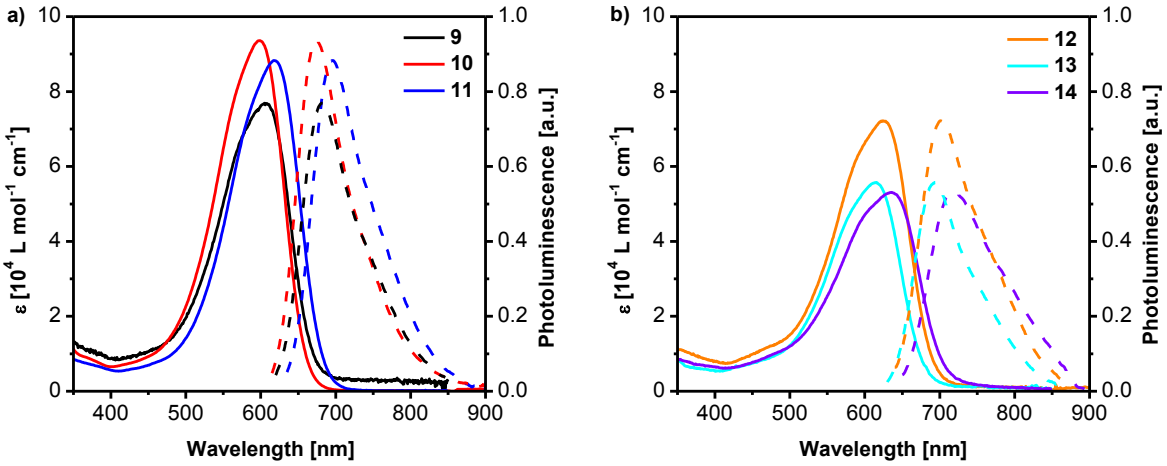

Figure 4.10: UV-Vis absorption spectra and emission spectra of (a) dithienopyrrole co-oligomers **9**-**11** and (b) diselenophenopyrrole co-oligomers **12**-**14** measured in dichloromethane solution.

In solution, the absorption and emission spectra of all compounds show one maximum without structure. At the lower wavelength edge, the indication of a shoulder is observed. The absorption maxima lie in the range of 600-640 nm and the emission maxima between 670 and 720 nm. Compared to comparable oligomers without terminal DCV groups,[18-19] the absorption spectra of **9**-**14** are bathochromically shifted by about 200 nm. Compared to compound **S3** (see general introduction), containing weaker electron accepting cyanoacrylic acid groups instead of DCV groups, the shift is about 40-80 nm.[21] The absorption maxima of the diselenophenopyrrole-based co-oligomers **12**-**14** are red-shifted ($\Delta\lambda \approx 17$ nm) compared to their dithienopyrrole analogs **9**-**11**. A similar red-shift ($\Delta\lambda \approx 20$ nm) is observed when the terminal thiophenes are replaced by selenophenes (compare **10**↔**11** and **13**↔**14**). This has already been observed in the series of thiophene-selenophene pentamers described in **Chapter 3**. When comparing corresponding phenyl- and propyl substituted compounds (**9** and **11**; **12** and **14**), the phenyl derivatives exhibit blue-shifted absorption maxima ($\Delta\lambda \approx 12$-14 nm) compared to the propyl derivatives. Considering only the propyl

derivatives, the molar extinction coefficients of the DTP compounds **10** and **11** are significantly higher than those of the DSP compounds **13** and **14** with a difference of 35,000 to 38,000 L mol^{-1} cm^{-1}. For the phenyl derivatives, only a small difference of ~4,000 L mol^{-1} cm^{-1} in the molar extinction coefficients is observed. The optical band gaps of **9**-**14** calculated from the onset of the absorption band are between 1.75 eV and 1.89 eV. As a consequence of their red-shifted absorption maxima, the band gaps of the DSP-based compounds are slightly lower compared to their DTP analogs.

Table 4.2: Optical data of co-oligomers **9**-**14**.

		solution				*film*	
compound	T_m [°C][a]	λ_{abs} [nm]	ε_{max} [L mol^{-1} cm^{-1}]	λ_{em} [nm]	E_g^{opt} [eV][b]	λ_{abs} [nm]	E_g^{opt} [eV][c]
9	412	607	76,900	683	1.86	(638)[d], 680	1.54
10	367	598	93,600	668	1.89	637, (670)	1.56
11	374	619	88,300	685	1.82	(660), 700	1.52
12	414	624	72,200	701	1.80	662, (705)	1.52
13	-	615	55,700	694	1.83	(661), 701	1.52
14	380	638	53,100	719	1.75	(682), 726	1.44

[a] Melting temperature determined from DSC. [b] Estimated using the onset of the UV-Vis spectra in DCM. [c] Estimated using the onset of the UV-Vis spectra of films prepared by vacuum sublimation. [d] Values in brackets indicate a second absorption maximum.

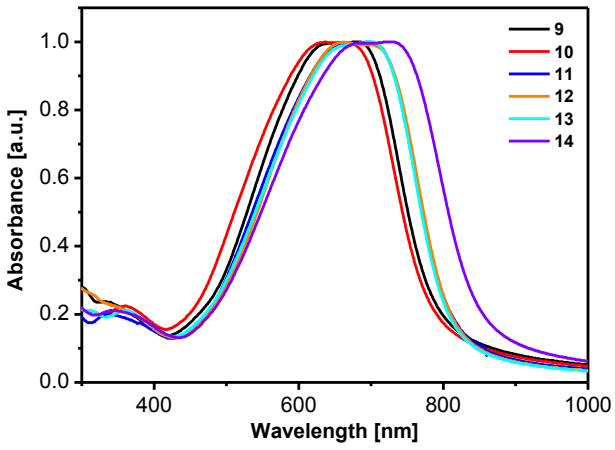

Figure 4.11: Normalized UV-Vis absorption spectra of **9**-**14** in vacuum-deposited thin films.

In thin films, the absorptions spectra of all compounds are considerably broadened and red-shifted compared to solution (**Figure 4.11**). Two maxima of almost identical intensity are observed; between these maxima, the absorbance only decreases marginally, thus forming an absorption plateau over a range of ~30-40 nm. The same trends as in solution are observed; i.e., the replacement of dithienopyrrole by diselenophenopyrrole as well as the replacement of the terminal thiophenes by

selenophenes leads to a red-shifted absorption, whereas the phenyl derivatives show blue-shifted absorption spectra compared to their propyl analogs. The optical band gaps determined from the thin film spectra are between 1.56 eV and 1.44 eV (**Table 4.2**).

4.2.5 Electrochemical Properties of Co-oligomers 9-14

The electrochemical properties of co-oligomers **9**-**14** were investigated in 1,1,2,2-tetrachlorethane (TCE)/$TBAPF_6$ (0.1 M) at 80 °C due to their poor solubility. Since the cyclovoltammograms (CV) were dominated by the solvent signal when going to negative potentials, differential pulse voltammograms (DPV) were used to determine the oxidation and reduction potentials of **9**-**14**. The DPVs are depicted in **Figure 4.12** and the data derived from them are summarized in **Table 4.3**.

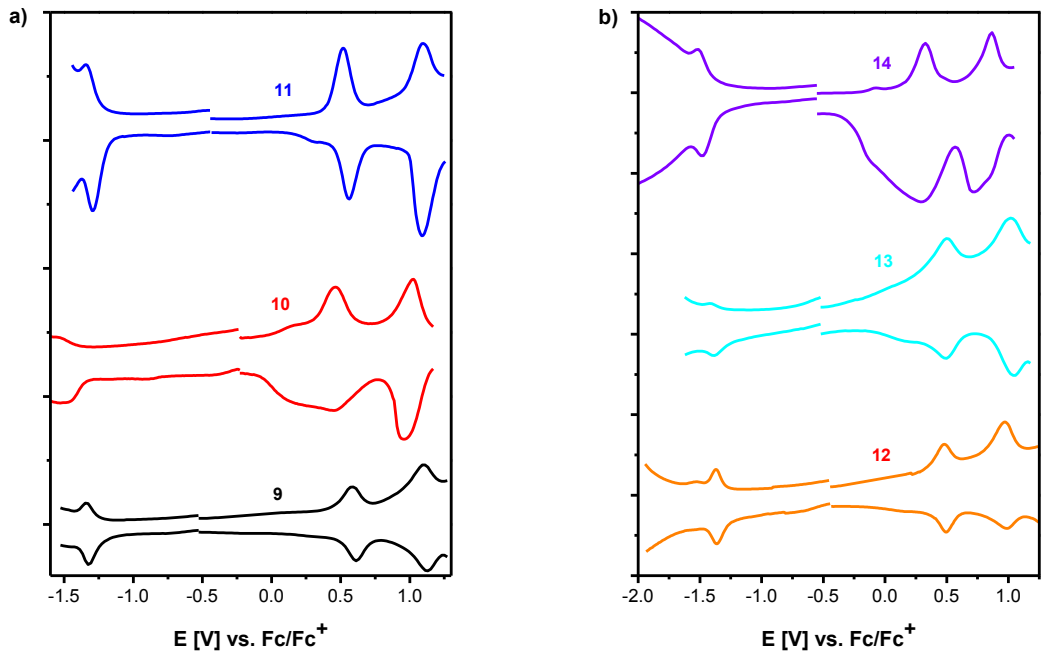

Figure 4.12: Differential pulse voltammograms (DPV) of (a) co-oligomers **9**-**11** and (b) **12**-**14** measured in $TCE/TBAPF_6$ (0.1 M), scan rate 100 mV s^{-1} , potentials versus Fc/Fc^+, measured at 80 °C.

All co-oligomers exhibit two reversible oxidation waves, indicating the formation of radical cations and dications, and one reduction wave, stemming from the reduction of the DCV groups. Co-oligomers **9**-**13** show first oxidation potentials of 0.47-0.60 V and second oxidation potentials of 0.98-1.12 V. The oxidation potentials of **14** are significantly lower (E^0_{ox1} = 0.32 V, E^0_{ox2} = 0.87 V). The oxidation potentials of the phenyl derivatives are generally higher than those of the propyl derivatives. When comparing corresponding DTP and DSP-based co-oligomers (**9** ↔ **12**, **11** ↔ **14**),

the DSP derivatives possess lower oxidation potentials than the DTP compounds. Apparently, DSP shows stronger electron donor properties compared to DTP due to the larger and better polarizable selenium atoms. The oxidation potential difference is more pronounced for the propyl derivatives **11** and **14** ($\Delta E^0_{Ox} \approx 0.2$ V) than for the phenyl derivatives **9** and **12** ($\Delta E^0_{Ox} = 0.11$-0.14 V). However, the oxidation potentials of **10** and **13** are almost identical, although they differ in the core unit. These trends are also reflected in the HOMO energy levels, which were calculated from the onset of the first oxidation potential obtained from cyclovoltammetry. Oligomer **9** exhibits the lowest HOMO energy (-5.59 eV), while oligomer **14** shows the highest HOMO energy (-5.33 eV). Since the reduction potentials could not be detected by CV and the determination of onset potentials from DPV is difficult, the LUMO energy level for each compound was calculated from its HOMO energy by addition of the respective optical band gap. The estimated LUMO energy levels are in the range from -3.84 to -3.58 eV.

Table 4.3: Electrochemical data of co-oligomers **9**-**14**.

compound	E^0_{ox1} [V]	E^0_{ox2} [V]	E^0_{red1} [V]	E_{HOMO} [eV][a]	E_{LUMO} [eV][b]
9	0.60	1.12	-1.34	-5.59	-3.84
10	0.47	1.01	-1.53	-5.47	-3.58
11	0.53	1.07	-1.32	-5.56	-3.74
12	0.49	0.98	-1.37	-5.54	-3.74
13	0.49	1.03	-1.40	-5.52	-3.69
14	0.32	0.87	-1.49	-5.33	-3.58

Measured in TCE/$TBAPF_6$ (0.1 M), 80 °C, V= 100 mV s^{-1}, vs. Fc^+/Fc. [a] Calculated from the onset of the first oxidation potential, vs. $E^0_{Fc/Fc+}$ = -5.1 eV vs vacuum.[49] [b] Calculated from $E_{HOMO} + E_g^{opt}$.

4.2.6 Photovoltaic Performance of Co-oligomers 9-14

Co-oligomers **9**-**14** were implemented as donor materials in vacuum-processed BHJ solar cells. For reasons of confidentiality no further details can be given here.

4.3 Solution-processable Co-oligomer

4.3.1 Introduction

In the past few years, significant progress has been made in the solution-processing of small molecule organic solar cells,[50] leading to a current record PCE of 6.7%.[51] Compared to vacuum-processing, solution-processing offers the advantage that the donor materials are not sublimed but deposited from solution. As a consequence, the molecular weight is not limited and thermally labile functional groups can be incorporated. The major prerequisite for solution-processable donor compounds is sufficiently high solubility in the solvents used for the preparation of the blend layers. Therefore, it is usually inevitable to decorate the conjugated backbone of oligothiophenes or oligoselenophenes with longer alkyl chains or other solubilizing side groups.

Since the co-oligomers presented in **Section 4.2** attained very high PCEs in vacuum-processed BHJ devices, we intended to implement compounds with the same conjugated backbone in solution-processed solar cells. Co-oligomers **9**-**14** are hardly soluble in common organic solvents; therefore, they could not be used directly but needed to be modified by the introduction of alkyl side chains. First, I planned to introduce a longer alkyl chain at the nitrogen of the DTP or DSP core. However, first tests with *all*-thiophene compounds revealed that this did not sufficiently increase the solubility. Therefore, it was necessary to incorporate further alkyl chains at the thiophenes or selenophenes next to the core unit. Taking these considerations into account, I designed the *all*-selenophene co-oligomer **15**, bearing a 2-ethylhexyl chain at the DSP nitrogen and hexyl chains at the β-positions of the selenophenes adjacent to the DSP core (**Figure 4.13**). The optoelectronic properties of **15** were investigated and it was implemented as donor material in solution-processed BHJ solar cells.

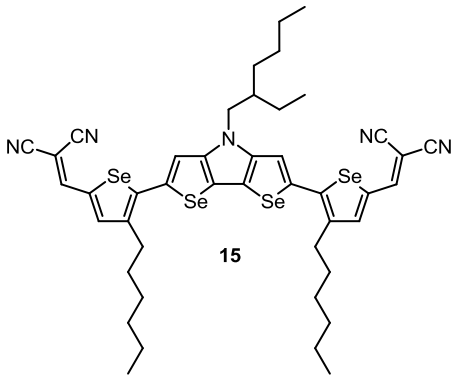

15

Figure 4.13: Solution-processable DSP-based donor compound.

4.3.2 Synthesis of Co-oligomer 15

Target compound **15** was synthesized from two building blocks, distannylated diselenophenopyrrole **75** and 2-bromo-3-hexylselenophene **79** (**Scheme 4.15**). The synthesis of distannyl DSP **75** started with TMS-protected diiodobiselenophene **62**, which was reacted with 2-ethylhexylamine in a Buchwald-Hartwig amination. Since an aliphatic amine was used, a combination of $Pd_2(dba)_3{\cdot}CHCl_3$ and BINAP served as catalytic system (see **4.2.2.1**). The reaction was carried out as described for compound **57a**, and after column chromatography on basic alumina TMS-protected diselenophenopyrrole **73** was obtained in an excellent yield of 90%. The TMS groups were cleaved off with $TBAF{\cdot}3H_2O$ in THF at r.t. to afford deprotected diselenophenopyrrole **74** in 88% yield after purification on silica gel. Diselenophenopyrrole **74** was distannylated by lithiation with *n*-BuLi and subsequent quenching with Me_3SnCl. The crude stannylated product **75** was obtained in 98%. It was used directly without further purification.

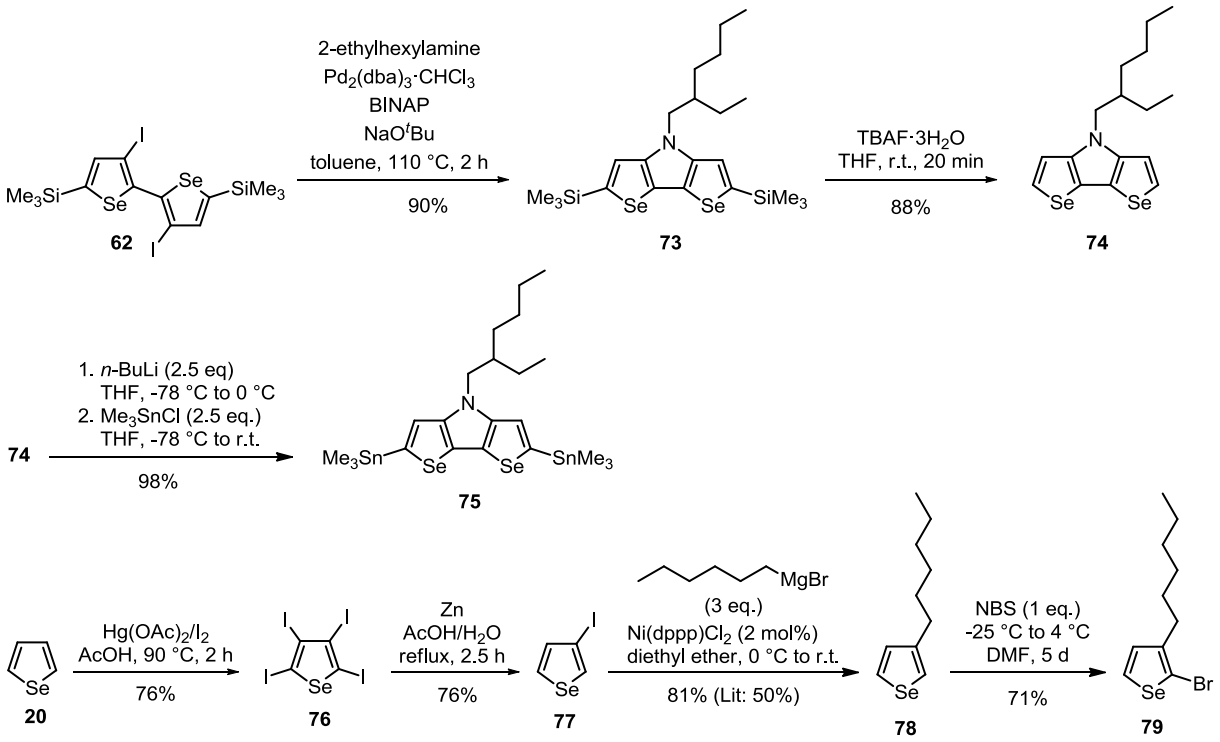

Scheme 4.15: Synthesis of building blocks **75** and **79**.

The synthesis of 2-bromo-3-hexylselenophene **79** started with selenophene **20**, which was first tetraiodinated, then reduced to 3-iodoselenophene according to a literature procedure.[52] For the iodination, stoichiometric amounts of mercury acetate and iodine were necessary, which is the major drawback of this reaction. However, this reaction proceeded more smoothly and faster than the previously described tetrabromination and tetraiodoselenophene **76** was obtained in 76% yield. Tetraiodoselenophene **76** was reduced to 3-iodoselenophene **77** with zinc in an acetic acid/water

mixture. After distillation, the desired product **77** was obtained in a good yield of 76%. The subsequent Kumada coupling with hexylmagnesium bromide was carried out according to a literature procedure.[53] In that reaction, 3-iodoselenophene **77** was reacted with hexylmagnesium bromide in diethyl ether using Ni(dppp)Cl_2 as catalyst. When the reaction was carried out in THF instead of diethyl ether, the main product was 3,3'-biselenophene, i.e., the homocoupling product of 3-iodoselenophene. The Grignard reagent had to be added at 0 °C and full conversion was only obtained when it was added in two portions, with 1.5 eq. Grignard reagent and 1 mol% Ni(dppp)Cl_2 for each addition. The reaction mixture was stirred at r.t. overnight and after distillation, 3-hexyl-selenophene **78** was obtained in 81% yield. It was monobrominated with 1 eq. NBS in DMF at -25 °C. The reaction was carried out at -25 °C for one day and at 4 °C for four days. Under these conditions, the bromination occurred selectively at the 2-position and 2-bromo-3-hexylselenophene **79** was obtained in 71% after column chromatography.

The two building blocks **75** and **79** were coupled in a Stille-type cross-coupling with Pd(PPh_3)$_2Cl_2$ in DMF at 100 °C (**Scheme 4.16**). The coupling product **80** was obtained in 52% yield after column chromatography. Co-oligomer **80** was formylated by a Vilsmeier-Haack reaction with 20 eq. DMF/$POCl_3$ in DCM at r.t. to obtain dialdehyde **81** in 41% yield after chromatographic purification. The final Knoevenagel condensation with malononitrile was carried out under the usual conditions (catalyst β-alanine, DCE/EtOH, 80 °C). The desired DCV-substituted co-oligomer **15** was purified by column chromatography with DCM to afford 84% of pure product.

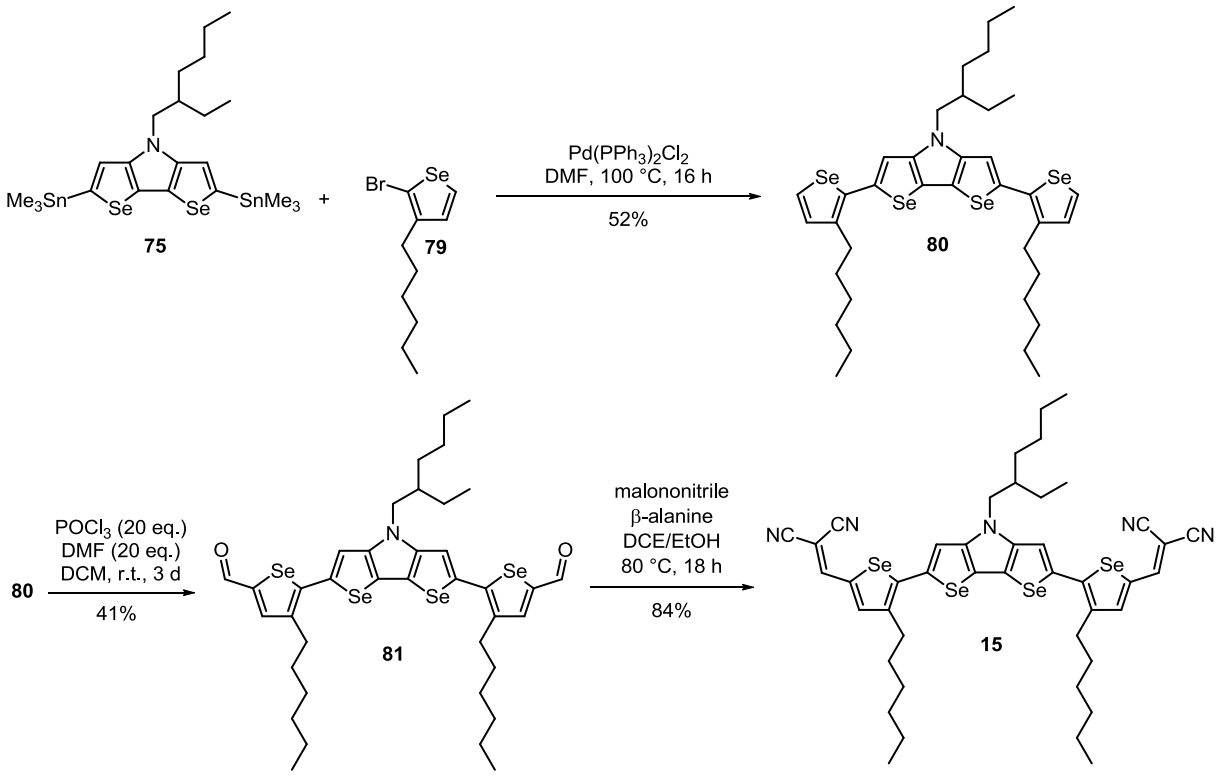

Scheme 4.16: Synthesis of target compound **15**.

4.3.3 Optical and Electrochemical Properties of Co-oligomer 15

Co-oligomer **15** was investigated by UV-Vis absorption and fluorescence spectroscopy in dichloromethane solution and in thin film. The films were prepared by spin-coating from chloroform solution. The spectra are shown in **Figure 4.14** and compared to co-oligomer **14**. The data for both compounds are summarized in **Table 4.4**.

In solution, both co-oligomers exhibit one major absorption and emission maximum. The absorption maximum of **15** ($\lambda_{max,abs}$ = 608 nm) is hypsochromically shifted compared to **14** ($\lambda_{max,abs}$ = 638 nm) although they possess the same conjugated backbone. Furthermore, the shape of the absorption band of **15** is more Gaussian-like than that of **14**, the latter featuring a slight shoulder towards lower wavelengths and a very steep slope on the higher wavelength side. In contrast, the emission spectra of both compounds are almost identical, exhibiting a maximum at ~720 nm, i.e., the Stokes shift is smaller for **14** than for **15**. The reason for these observations is the additional hexyl chains at the β-positions of the selenophenes adjacent to the DSP core in compound **15**. Due to their steric hindrance, they cause a distortion of the conjugated backbone and, consequently, a slightly shorter conjugation length.[18-19] This gives rise to a bathochromic shift of the absorption maximum of **15** compared to **14**. Furthermore, the ground state structure of **15** is expected to be less planar than that of **14**, leading to more structural rearrangement during photoexcitation. This is the reason for the larger Stokes shift of compound **15**. The higher molar exctinction coefficient of **15** (ε_{max} = 70,300 L mol^{-1} cm^{-1}) compared to **14** (ε_{max} = 53,100 L mol^{-1} cm^{-1}) is probably due to solubility problems in the case of **14**. Even after ultrasonication for several hours, co-oligomer **14** was not completely dissolved and the determined molar exctinction coefficient is probably too low.

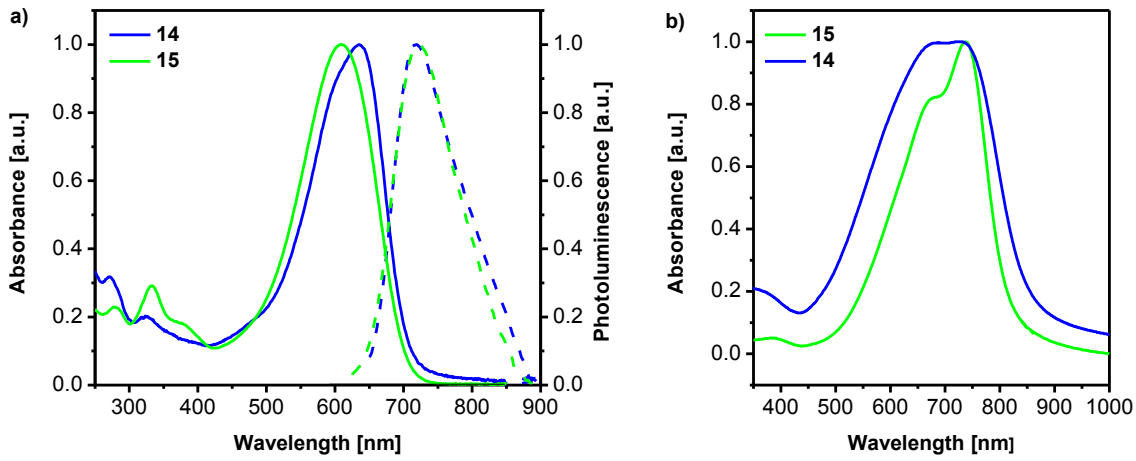

Figure 4.14: UV-Vis absorption and emission spectra of co-oligomers **15** and **14** in (a) dichloromethane solution and (b) thin films.

Table 4.4: Thermal and optical data of co-oligomer **15** compared to **14**.

		solution				*film*	
compound	T_m [°C][a]	$\lambda_{max\,abs}$ [nm]	ε_{max} [L mol^{-1} cm^{-1}]	$\lambda_{max\,em}$ [nm]	E_g^{opt} [eV][b]	λ_{abs} [nm]	E_g^{opt} [eV][c]
14	380	638	53,100	719	1.75	(682),[d] 726	1.44
15	218	608	70,300	723	1.77	(680), 738	1.52

[a] Melting temperature determined from DSC. [b] Estimated using the onset of the UV-Vis spectra in DCM. [c] Estimated using the onset of the UV-Vis spectra of films prepared by vacuum sublimation. [d] Values in brackets designate a second maximum.

In thin films, the absorption spectra of **14** and **15** are red-shifted and broadened compared to the solution spectra. For **15**, one maximum at 738 nm and a shoulder at 680 nm is observed, whereas **14** exhibits two maxima (682 and 726 nm) of almost identical intensity. In contrast to the solution spectra, the positions of the maxima of **14** and **15** in the thin film spectra only differ by few nanometers due to planarization of the conjugated backbone in the solid state. The spectrum of **14** is significantly broader than that of **15**, possibly due to better ordering and stacking of the molecules when processed by vacuum sublimation compared to solution-processing. Furthermore, the long alkyl chains in compound **15** also lead to a less dense and more disordered packing in the solid state.

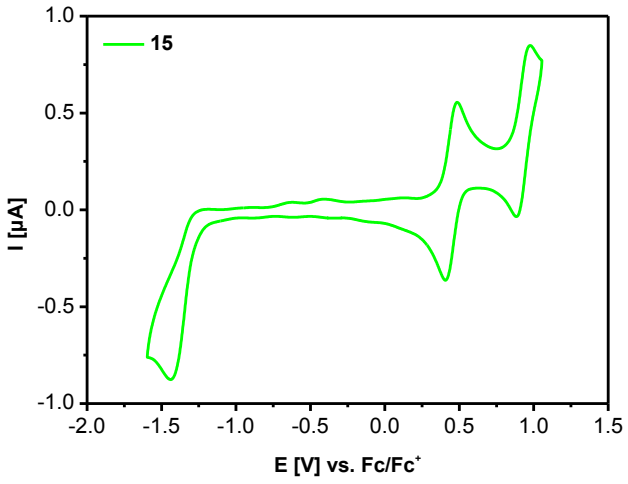

Figure 4.15: Cyclovoltammogram of compound **15** measured in DCM/TBAPF$_6$ (0.1 M), 298 K, scan rate 100 mV s^{-1}, vs. Fc/Fc$^+$.

The electrochemical properties of co-oligomer **15** were investigated by cyclovoltammetry in dichloromethane/TBAPF (0.1 M) at room temperature (**Figure 4.15** and **Table 4.5**). Two reversible oxidation waves, corresponding to the formation of radical cations and dications, and one irreversible reduction wave, generated by the reduction of the DCV groups, were observed. From the onset of the first oxidation potential, a HOMO energy level of -5.47 eV vs. vacuum was calculated.

For better comparability with co-oligomer **14**, the LUMO energy was calculated by addition of the optical band gap to the HOMO energy, leading to a LUMO energy level of -3.70 eV vs. vacuum. The frontier orbital energies of **15** are by 0.12-0.15 eV lower than those of **14**, presumably due to a stabilizing inductive effect of the longer alkyl chain at the nitrogen atom.

Table 4.5: Electrochemical data of compound **15** compared to **14**.

compound	E^0_{ox1} [V]	E^0_{ox2} [V]	E^0_{red1} [V]	E_{HOMO} [eV][a]	E_{LUMO} [eV][b]
14	0.32	0.87	-1.49	-5.33	-3.58
15	0.45	0.93	-1.36	-5.47	-3.70

[a] Calculated from the onset of the first oxidation potential, vs. $E^0_{Fc/Fc+}$ = -5.1 eV vs vacuum.[49] [b] Calculated from $E_{HOMO} + E_g^{opt}$.

4.3.4 Photovoltaic Performance of Co-oligomer 15

Co-oligomer **15** was used as donor for solution-processed BHJ solar cells in combination with $PC_{61}BM$ as acceptor. The devices (**Figure 4.16**) were fabricated by spin-coating of a poly(3,4-ethylenedioxy-thiophene) poly(styrenesulfonate) (PEDOT-PSS) solution onto ITO-coated glass substrates and subsequent spin-coating of a solution of **15** and $PC_{61}BM$ in different solvents. The aluminum top electrode was deposited by thermal evaporation. Chloroform, chlorobenzene (CB) and 1,1,2,2-tetrachloroethane (TCE) were used as solvents for the donor/acceptor solution (ratio 1:2 w/w). The solutions were warmed to 60 °C and deposited on pre-heated substrates (60 °C). With chloroform, a second D:A ratio (1:1 w/w) and spin-coating at r.t. was tested. The photovoltaic parameters of all devices are summarized in **Table 4.6**.

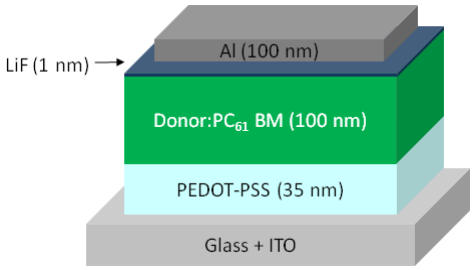

Figure 4.16: Device architecture of solution-processed BHJ solar cells.

The *J-V* curves for devices prepared from different solvents are depicted in **Figure 4.17a,** the EQE spectrum for a representative device is shown in **Figure 4.17b**. The *J-V* curves are representative for all devices since the general shape depended only marginally on the fabrication conditions. In the

dark, all devices exhibit poor rectification behavior due to a large leakage current in the negative bias regime caused by a poor quality of the blend films. This leakage current results in a very poor saturation behavior of the devices under illumination. The best device attain a PCE of 0.64%, the lowest value is 0.30%. Most of the devices exhibit PCEs in the range of 0.5-0.6%, with J_{SC} ~2.0-2.5 mA cm^{-2}, V_{OC} ~0.7-0.9 V, and fill factors around 0.3. The choice of solvent only has a minor influence on the device performance, but chloroform seems to be slightly better than chlorobenzene and tetrachloroethane.

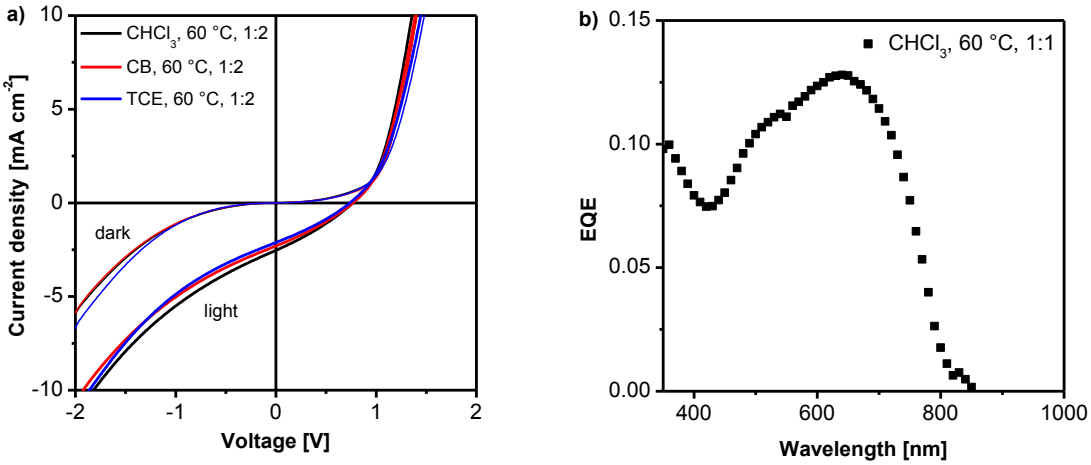

Figure 4.17: (a) *J-V* curves for solution-processed BHJ solar cells with **15**/$PC_{61}BM$ (1:2, w/w) deposited from chloroform, chlorobenzene (CB) and 1,1,2,2-tetrachlorethane (TCE) solutions. (b) Representative EQE spectrum.

The solubility of co-oligomer **15** was comparable in all tested solvents. Due to the slightly better performance, chloroform was used for further optimizations. However, variation of spin-coating temperature (60 °C and room temperature), blend layer thickness (varied by spin-coating speed) and donor:acceptor ratio (1:1 and 1:2 w/w) did not significantly change the overall device performance. It was not possible to deduce clear relations between device performance and fabrication conditions. With some devices annealing experiments were carried out. Annealing at 80 °C and 95 °C for one minute showed no improvement of the device performance, annealing at 95 °C for 2 min led to a significant decrease of the PCE.

In summary, co-oligomer **15** possesses promising optical and electrochemical properties, but its performance in solution-processed solar cells was relatively poor, at least under the fabrication conditions which I used. Presumably, the solubility is still not sufficient for the formation of a favorable blend morphology during solution-processing.

Table 4.6: Photovoltaic parameters for BHJ solar cells with compound **15**.

solvent	temperature [°C]	D:A ratio	concentration [mg mL^{-1}]	speed [rpm]	J_{SC} [mA cm^{-2}]	V_{OC} [V]	FF [%]	PCE [%]
$CHCl_3$	r.t.	1:2	15.0	1000	2.51	0.86	0.29	0.62
				1250	2.51	0.83	0.29	0.60
				1500	2.69	0.72	0.30	0.58
$CHCl_3$	60	1:1	12.5	1000	1.43	0.85	0.25	0.30
				1250	2.27	0.87	0.30	0.60
				1500	2.27	0.90	0.31	0.64
$CHCl_3$	60	1:2	12.5	1000	2.27	0.85	0.28	0.54
				1250	2.32	0.74	0.29	0.50
				1500	2.51	0.72	0.30	0.54
$CHCl_3$	60	1:2	15.0	1500	2.34	0.78	0.29	0.53
				2000	2.54	0.77	0.30	0.58
				3000	2.33	0.83	0.29	0.56
CB	60	1:2	20.0	750	1.58	0.88	0.28	0.38
				1000	2.23	0.76	0.30	0.50
				1250	2.30	0.77	0.30	0.52
TCE	60	1:2	20.0	750	1.86	0.89	0.27	0.45
				1000	2.12	0.74	0.30	0.46
				1250	2.00	0.73	0.30	0.43

4.4 Summary

In this chapter, the synthesis of terminally DCV-substituted co-oligomers with a dithienopyrrole or a diselenophenopyrrole core was presented. Diselenophenopyrrole is still a rather unexplored building block in the literature; therefore, the synthesis of this building block and its derivatives was not always straight-forward. Especially the synthesis of *N*-propyl diselenophenopyrrole proved to be more difficult than expected. The stannylation of this building block was not successful due to an unexpected ring-opening reaction during lithiation. Despite some synthetic problems three dithienopyrrole-based and three diselenophenopyrrole-based co-oligomers **9**-**14** for vacuum-processable solar cells were synthesized and their thermal and optoelectronic properties were investigated. The absorption range could be tuned by the selenophene content, i.e., with increasing selenophene units, the absorption spectra were bathochromically shifted. Co-oligomers **9**-**14** were implemented as donor materials in vacuum-processed BHJ solar cells, but the results cannot be disclosed for reasons of confidentiality. A corresponding co-oligomer **15** for solution-processed solar cells was synthesized as well. Co-oligomer **15** contained the same conjugated backbone as **14** but

longer alkyl chains in order to improve solubility. It showed promising optoelectronic properties, but its performance in solution-processed BHJ solar cells was relatively poor with a maximum PCE of 0.64%. The PCE only depended to a small degree on the fabrication conditions such as solvent, donor/acceptor ratio and layer thickness. However, there could be some room for optimization by the use of additives.

4.5 Experimental Section

Physical measurements and instrumentation

NMR spectra were recorded on a Bruker AMX 500 (^{1}H NMR: 500 MHz, ^{13}C NMR: 125 MHz) or an Avance 400 spectrometer (^{1}H NMR: 400 MHz, ^{13}C NMR: 100 MHz) at 25 °C unless otherwise noted. Chemical shift values (δ) are expressed in parts per million using residual solvent protons (^{1}H NMR, δ_H = 7.26 for $CDCl_3$, δ_H = 5.92 for $C_2D_2Cl_4$, δ_H = 2.50 for DMSO-d_6, δ_H = 5.32 for CD_2Cl_2; ^{13}C NMR, δ_C = 77.0 for $CDCl_3$) as internal standard. The splitting patterns are designated as follows: s (singlet), d (doublet), t (triplet), q (quartet) and m (multiplet). Unless otherwise noted, coupling constants (*J*) are proton-proton coupling constants. The assignments are Sel-H (selenophene protons), Th-H (thiophene protons), DSP-H (diselenophenopyrrole protons), DTP-H (dithienopyrrole protons), -CHO (aldehyde protons), DCV-H (dicyanovinyl protons), Hex (hexyl protons). Melting points were determined using a Mettler Toledo DSC 823^e and were not corrected. Elemental analyses were performed on an Elementar Vario EL. Thin layer chromatography was carried out on aluminum plates, pre-coated with silica gel, Merck Si60 F_{254}. Preparative column chromatography was performed on glass columns packed with silica gel, Merck Silica 60, particle size 40 – 43 µm. EI mass spectra were recorded on a Varian Saturn 2000 GC-MS, MALDI-TOF mass spectra on a Bruker Daltonics Reflex III and Hi-Res MALDI-TOF mass spectra on a Bruker solariX.

Optical measurements in solution were carried out in 1 cm cuvettes with Merck Uvasol grade solvents. Absorption spectra were recorded on a Perkin Elmer Lambda 19 spectrometer and corrected fluorescence spectra were recorded on a Perkin Elmer LS 55 fluorescence spectrometer. Cyclic voltammetry and differential pulse voltammetry experiments were performed with a computer-controlled Autolab PGSTAT30 potentiostat in a three-electrode single-compartment cell with a platinum working electrode, a platinum wire counter electrode, and an Ag/AgCl reference electrode. All potentials were internally referenced to the ferrocene/ferrocenium couple.

Thin Film Fabrication

Thin films were prepared by thermal vapor deposition in ultra high vacuum at a base pressure of 10^{-7} mbar onto quartz substrates at room temperature. Layer thicknesses were determined during evaporation by using quartz crystal monitors calibrated for the respective material. The thin films prepared for absorption and emission measurements are approximately 30 nm thick. Thin film absorption spectra were recorded on a Shimadzu UV-2101/3101 UV-Vis spectrometer, the emission spectra were recorded with an Edinburgh Instruments FSP920 fluorescence spectrometer.

Device Fabrication and Photovoltaic Characterization

The solution-processed photovoltaic devices were prepared by spin-coating PEDOT:PSS (Clevios P, VP Al4083) onto pre-cleaned, patterned indium tin oxide (ITO) substrates (15 Ω $sq.^{-1}$). The photoactive layer was deposited by spin-coating from chloroform, chlorobenzene or 1,1,2,2-tetrachloroethane solutions with a total concentration of 12.5 mg/mL ($CHCl_3$, 60 °C), 15.0 mg/mL ($CHCl_3$, r.t.) or 20.0 mg/mL (CB and TCE, 60 °C). The blend layer thickness was varied using different spin-coating speeds. The counter electrode of LiF (1 nm) and aluminum (100 nm) was deposited by vacuum evaporation at < $2 \cdot 10^{-6}$ torr. The active area of the cell was 0.2 cm^2. *J-V* characteristics were measured under ca. 100 mW cm^{-2} simulated sunlight from a tungsten-halogen lamp (Philips Brilliantline Pro) filtered by an Edmund Optics NT54-047 UV filter and a Hoya LB 120 filter. Spectral response was measured with a Keithley 2400 source meter, using monochromatic light from a 300 W xenon lamp in combination with a monochromator (Oriel, Cornerstone 260). A calibrated Si cell was used as reference. The device was kept behind a quartz window in an argon filled container.

Materials

THF (Merck) was dried under reflux over sodium/benzophenone (Merck). DMF (Merck) was dried under reflux over phosphorous pentoxide (Merck). Toluene, diethyl ether, *n*-propylamine and diisopropylamine (all Merck) were dried under reflux over calcium hydride. Acetonitrile, chlorobenzene, DCM, DCE, ethanol, methanol, *n*-hexane, diethyl ether, aniline, and trimethylsilyl chloride were purchased from Merck and distilled prior to use. Copper(II) chloride was dried at 200 °C under reduced pressure. All synthetic steps were carried out under an argon atmosphere (except Knoevenagel condensations). Selenophene **20** was purchased from Molekula, $HP^tBu_3BF_4$ and BINAP from Alfa Aesar. *n*-Butyllithium (1.6 N in *n*-hexane), $Ni(dppp)Cl_2$, $Pd_2(dba)_3 \cdot CHCl_3$, $Pd(PPh_3)_4$ and $Pd(PPh_3)_2Cl_2$ were purchased from Acros. Ammonium chloride, β-alanine, 1-bromohexane, *N*-bromosuccinimide, 2-ethylhexylamine, iodine, mercury(II) acetate, phosphoryl chloride, sodium carbonate, sodium bicarbonate, sodium thiosulfate, sodium *tert*-butylate, sodium sulfate,

TBAF·3H_2O, and zinc dust were purchased from Merck. Malononitrile, trimethyltin chloride and 2-(tributylstannyl)thiophene **71a** were purchased from Aldrich.

2-[(5-Bromoselenophen-2-yl)methylene]malononitrile **31** and 2-[(5-bromothien-2-yl)methylene]-malononitrile **59** were synthesized as described in **Chapter 3**. 3,3'-Dibromo-2,2'-bithiophene **56**,[34] 4-propyl-4*H*-dithieno[3,2-*b*:2',3'-*d*]pyrrole **57a**,[54] and 2-(tributylstannyl)selenophene **71b**[55] were synthesized according to literature procedures.

4-Phenyl-4*H*-dithieno[3,2-*b*:2',3'-*d*]pyrrole (57b).

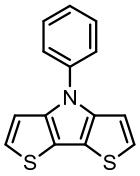

3,3'-Dibromo-2,2'-bithiophene **56** (702 mg, 2.17 mmol), $Pd_2(dba)_3$·$CHCl_3$ (75.3 mg, 72.8 µmol), $HP^tBu_3BF_4$ (39.5 mg, 136 µmol) and NaO^tBu (528 mg, 5.49 mmol) were dissolved in dry degassed toluene (12 mL), the mixture was degassed and stirred at r.t. for 15 min. Aniline (630 mg, 6.76 mmol) was added and the mixture was stirred at 110 °C for 3 h. Water (30 mL) was added, the mixture was extracted with DCM (2 × 40 mL), the combined organic layers were dried over Na_2SO_4 and the solvent was removed. The crude product was purified by column chromatography (flash silica; *n*-hexane/DCM 3:1) to obtain pure product **57b** (309 mg, 1.21 mmol, 56%) as slightly yellow crystals.

Mp.: 127 °C.

^{1}H NMR (400 MHz, $CDCl_3$): δ = 7.62-7.58 (m, 2H, Ph-H), 7.56-7.51 (m, 2H, Ph-H), 7.34 (tt, ^3J = 7.4 Hz, ^4J = 1.2 Hz, 1H, Ph-H), 7.18 (s, 4H, Th-H).

^{13}C NMR (100 MHz, $CDCl_3$): δ = 143.92, 139.85, 129.76, 125.97, 123.44, 122.59, 116.88, 112.24.

MS (EI): *m/z* = 255 (100, M^+).

Elemental analysis: calc. (%) for $C_{14}H_9NS_2$: C 65.85, H 3.55, N 5.49, S 25.11; found: C 66.10, H 3.61, N 5.48, S 24.97.

4-Propyl-2,6-bis(trimethylstannyl)-4*H*-dithieno[3,2-*b*:2',3'-*d*]pyrrole (58a).

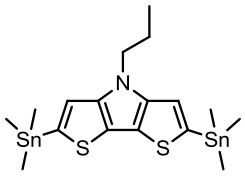

4-Propyl-4*H*-dithieno[3,2-*b*:2',3'-*d*]pyrrole **57a** (510 mg, 2.30 mmol) was dissolved under argon in dry THF (7.5 mL) and the solution was cooled to -70 °C. *n*-BuLi (1.6 M in hexane, 3.10 mL, 4.96 mmol) was added dropwise within 10 min. The mixture was stirred below -70 °C for 30 min and warmed to r.t. within 30 min. A white solid precipitated and the solution was yellow. The mixture was cooled back to -25 °C and Me_3SnCl (1.02 g, 5.12 mmol, dissolved in 1.5 mL THF) was added in one portion. The mixture became clear and was warmed to r.t. within 2 h. *n*-Hexane (25 mL) was added and lithium chloride precipitated. The organic layer was washed with water (3 × 20 mL), dried over Na_2SO_4 and the solvent was removed in vacuum. The crude product was dried in high vacuum to obtain a gray solid (1.10 g, 2.01 mmol, 87%), which was used in the next step without further purification.

^{1}H NMR (400 MHz, $CDCl_3$): δ = 7.01 (s, 2H, DTP-H), 4.16 (t, ^3J = 7.0 Hz, 2H, α-Pr), 1.97-1.88 (m, 2H, β-Pr), 0.97 (t, ^3J = 7.6 Hz, 3H, γ-Pr), 0.40 (s with Sn-satellites, $^2J_{Sn119-H}$ = 57.6 Hz, $^2J_{Sn117-H}$ = 55.2 Hz, 18H, Sn-CH_3).

^{13}C NMR (100 MHz, $CDCl_3$): δ = 147.86, 135.58, 117.90, 49.07, 23.76, 11.70, -8.10.

MS (MALDI-TOF): *m/z* [M^+] = 547.0 (calc. for $C_{20}H_{25}NS_2Sn_2$: 547.0).

4-Phenyl-2,6-bis(trimethylstannyl)-4*H*-dithieno[3,2-*b*:2',3'-*d*]pyrrole (58b).

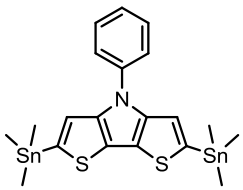

4-Phenyl-4*H*-dithieno[3,2-*b*:2',3'-*d*]pyrrole **57b** (264 mg, 1.03 mmol) was dissolved under argon in dry THF (4.2 mL) and the solution was cooled to -78 °C. *n*-BuLi (1.6 M in hexane, 1.65 mL, 2.64 mmol) was added dropwise within 10 min. The mixture was stirred at -78 °C for 1 h and at 0 °C for 1 h. The mixture became solid. It was cooled back to -78 °C and Me_3SnCl (548 mg, 2.75 mmol, dissolved in 0.6 mL THF) was added dropwise. The mixture became clear and was stirred at -78 °C for 30 min and 3 h at r.t. A sat. Na_2CO_3 solution (10 mL) was added and the mixture was extracted with DCM (3 × 15 mL). The combined organic layers were washed with water (15 mL) and the solvent was removed to obtain the crude product **58b** as a grayish solid (544 mg, 0.94 mol, 91%). It was directly used in the next step without further purification.

^{1}H NMR (400 MHz, $CDCl_3$): δ = 7.63 (d, ^3J = 8.6 Hz, 2H, Ph-H), 7.55 (t, ^3J = 8.2 Hz, 2H, Ph-H), 7.33 (t, ^3J = 8.8 Hz, 1H, Ph-H), 7.17 (s with Sn-satellites, $^3J_{Sn-H}$ = 13.4 Hz, 2H, DTP-H), 0.40 (s with Sn-satellites, $^2J_{Sn-H}$ = 57.6 Hz, 18H, Sn-CH_3).

^{13}C NMR (100 MHz, $CDCl_3$): δ = 146.78, 140.34, 136.59, 129.70, 125.64, 122.75, 122.43, 119.03, -8.09 ($^2J_{Sn119-C}$ = 185 Hz, $^2J_{Sn117-C}$ = 177 Hz).

MS (MALDI-TOF): *m/z* [M^+] = 581.1 (calc. for $C_{20}H_{25}NS_2Sn_2$: 580.9).

(5-Iodoselenophen-2-yl)trimethylsilane (61).

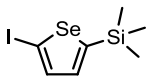

Selenophene **20** (5.48 g, 41.8 mmol) was dissolved under argon in dry THF (30 mL) and *n*-BuLi (2.5 M, 16.8 mL, 42.0 mmol) was added dropwise at -78 °C. The solution was stirred at -78 °C for 45 min. Me_3SiCl (5.50 mL, 43.0 mmol) was added and stirring was continued for 1 h (solution warmed up to ca. -40 °C). The solution was cooled back to - 78 °C and another portion of *n*-BuLi (2.5 M, 17.3 mL, 43.3 mmol) was added. After stirring for 1 h at - 78 °C, a solution of iodine (10.6 g, 41.8 mmol) in THF (20 mL) was added dropwise at -65 to -55 °C within 15 min. The solution was stirred for another 1 h, and remaining iodine was destroyed with a $Na_2S_2O_3$ solution (15 mL). THF was evaporated, water (75 mL) was added and the mixture was extracted with diethyl ether (3 × 75 mL). The combined organic layers were dried over Na_2SO_4 and the solvent was removed to obtain an orange oil (13.18 g). It was purified by Kugelrohr distillation to obtain pure product **61** (7.25 g, 22.0 mmol, 53%) as a yellow liquid.

Bp.: 113 °C ($6\cdot10^{-2}$ mbar). GC-purity ~93%.

^{1}H NMR (400 MHz, $CDCl_3$): δ = 7.55 (d, ^3J = 3.7 Hz, 1H, Sel-H), 7.13 (d, ^3J = 3.7 Hz, 1H, Sel-H), 0.31 (s, 9H, Si-CH_3).

^{13}C NMR (100 MHz, $CDCl_3$): δ = 156.43, 141.60, 137.87, 79.77, 0.21.

MS (EI): *m/z* = 330 (37, M^+), 328 (19, M^+), 315 (100, M-CH_3), 313 (39, M-CH_3).

(3,3'-Diiodo-2,2'-biselenophene-5,5'-diyl)bis(trimethylsilane) (62).

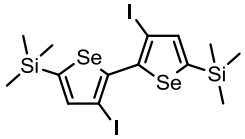

Diisopropylamine (7.06 g, 69.8 mmol) was dissolved in abs. THF (40 mL) and *n*-BuLi (1.6 M in hexane, 41.6 mL, 66.5 mmol) was added dropwise at 0 °C. The solution was stirred at 0 °C for 45 min. (5-iodoselenophen-2-yl)trimethylsilane **61** (21.0 g, 63.8 mmol) was dissolved under argon in abs. THF

(250 mL), the LDA solution was added dropwise at -60 °C within 1.75 h and the reaction mixture was stirred for 2 h below -60 °C. $CuCl_2$ (8.68 g, 64.6 mmol) was added and stirring was continued below -65 °C for 1 h. Afterwards, the mixture was stirred at r.t. overnight. The solvent was removed completely and the residue was filtered over an alumina column (basic Al_2O_3 with 10% H_2O; *n*-hexane). The resulting solid was redissolved in several mL *n*-hexane, and ethanol was added until a yellow solid precipitated. The yellow solid was filtered off, washed with ethanol and methanol and dried in high vacuum to obtain the pure product **62** (11.38 g, 17.3 mmol, 55%) as a pale yellow solid.

Mp.: 106 °C.

^{1}H NMR (400 MHz, $CDCl_3$): δ = 7.49 (s with ^{77}Se-satellites, $^3J_{Se\text{-}H}$ = 8.5 Hz, 2H, SeI-H), 0.34 (s, 18H, Si-CH_3).

^{13}C NMR (100 MHz, $CDCl_3$): δ = 153.31, 146.16, 144.28, 87.22, 0.05.

MS (MALDI-TOF): *m/z* [M^+] = 657.9 (calc. for $C_{14}H_{20}I_2Se_2Si_2$: 657.8).

Elemental analysis: calc. (%) for $C_{14}H_{20}I_2Se_2Si_2$: C 25.62, H 3.07; found: C 25.48, H 2.92.

4-Propyl-2,6-bis(trimethylsilyl)-4*H*-diselenopheno[3,2-*b*:2',3'-*d*]pyrrole (63a).

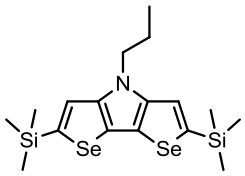

Biselenophene **62** (1.15 g, 1.75 mmol), NaO^{t}Bu (585 mg, 6.09 mmol), $Pd_2(dba)_3{\cdot}CHCl_3$ (70.0 mg, 67.7 µmol) and BINAP (150 mg, 241 µmol) were dissolved under argon in dry toluene (12 mL), the solution was degassed and stirred at r.t. for 20 min. *n*-Propylamine (380 mg, 6.43 mmol) was added and the mixture was stirred at 110 °C for 4 h. Water (20 mL) was added and the mixture was extracted with DCM (2 × 20 mL). The combined organic layers were dried over Na_2SO_4 and the solvent was removed in vacuum. The resulting brown oil was purified by column chromatography (basic Al_2O_3 with 10% H_2O; *n*-hexane). The pure product **63a** (703 mg, 1.53 mmol, 87%) was obtained as an off-white solid.

Mp.: 116 °C.

^{1}H NMR (400 MHz, $CDCl_3$): δ = 7.39 (s with ^{77}Se-satellites, $^3J_{Se\text{-}H}$ = 9.9 Hz, 2H, SeI-H), 4.20 (t, ^3J = 7.1 Hz, 2H, α-Pr), 1.90 (sextet, ^3J = 7.3 Hz, 2H, β-Pr), 0.98 (t, ^3J = 7.4 Hz, 3H, γ-Pr), 0.35 (s, 18H, Si-CH_3).

^{13}C NMR (100 MHz, $CDCl_3$): δ = 147.95, 144.36, 120.85, 120.10, 49.17, 24.06, 17.67, 0.29.

MS (EI): *m/z* = 460 (100, M^+), 447 (39).

Elemental analysis: calc. (%) for $C_{17}H_{27}NSe_2Si_2$: C 44.44, H 5.92, N 3.05; found: C 44.26, H 5.96, N 3.12.

4-Phenyl-2,6-bis(trimethylsilyl)-4*H*-diselenopheno[3,2-*b*:2',3'-*d*]pyrrole (63b).

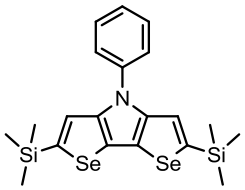

$Pd_2(dba)_3{\cdot}CHCl_3$ (37.4 mg, 36.2 µmol), $HP^tBu_3BF_4$ (19.2 mg, 66.2 µmol) and some mg of NaO^tBu were dissolved in dry degassed toluene (11 mL), the mixture was degassed and stirred at r.t. for 45 min. Biselenophene **62** (700 mg, 1.07 mmol), NaO^tBu (261 mg, 2.72 mmol) and aniline (303 mg, 3.25 mmol) were added and the mixture was stirred at 110 °C for 2.5 h. Water (20 mL) was added and the mixture was extracted with DCM (3 × 20 mL). The combined organic layers were dried over Na_2SO_4 and the solvent was removed. The crude product was purified by column chromatography (basic Al_2O_3 with 10% H_2O; *n*-hexane). The pure product **63b** (402 mg, 0.81 mmol, 76%) was obtained as a yellow solid.

Mp.: 139 °C.

^{1}H NMR (400 MHz, $CDCl_3$): δ = 7.56 (d, 4H, Ph-H), 7.47 (s with ^{77}Se-satellites, $^3J_{Se\text{-}H}$ = 10.3 Hz, 2H, Sel-H), 7.42-7.35 (m, 1H, Ph-H), 0.33 (s, 18H, Si-CH_3).

^{13}C NMR (100 MHz, $CDCl_3$): δ = 147.58, 145.53, 140.23, 129.72, 126.51, 124.25, 123.23, 121.07, 0.24.

MS (EI): *m/z* = 496 (100, M^+), 494 (84, M^+), 481 (25, M-CH_3), 480 (26, M-CH_3).

Elemental analysis: calc. (%) for $C_{20}H_{25}NSe_2Si_2$: C 48.67, H 5.11, N 2.84; found: C 48.53, H 5.14, N 2.99.

4-Propyl-4*H*-diselenopheno[3,2-*b*:2',3'-*d*]pyrrole (64a).

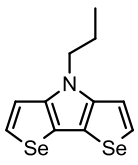

TMS-protected diselenophenopyrrole **63a** (900 mg, 1.96 mmol) was dissolved in THF (15 mL) and TBAF·3H_2O (1.32 g, 4.18 mmol) was added. The mixture was stirred at r.t. for 1.5 h (reaction complete after 30 min according to GC). The solvent was removed in vacuum and the crude product was purified by column chromatography (silica; *n*-hexane/DCM 3:2). The product was obtained as an orange oil. Methanol (1 mL) was added and the mixture was ultrasonicated for several minutes. An

orange solid precipitated, the solvent was removed in vacuum and the solid was dried in high vacuum to obtain the pure product **64a** (600 mg, 1.90 mmol, 97%) as a slightly orange solid.

Mp.: 61 °C.

^{1}H NMR (400 MHz, $CDCl_3$): δ = 7.68 (d with ^{77}Se-satellites, $^2J_{Se\text{-}H}$ = 47.3 Hz, ^3J = 5.7 Hz, 2H, Sel-H), 7.30 (d, ^3J = 5.7 Hz, 2H, Sel-H), 4.21 (t, ^3J = 7.0 Hz, 2H, α-Pr), 1.89 (sextet, ^3J = 7.2 Hz, 2H, β-Pr), 0.94 (t, ^3J = 7.4 Hz, 3H, γ-Pr).

^{13}C NMR (100 MHz, $CDCl_3$): δ = 145.03, 125.55, 116.09, 114.39, 49.22, 23.99, 11.63.

MS (EI): *m/z* = 317 (95, M^+), 288 (94), 286 (100), 208 (49).

Elemental analysis: calc. (%) for $C_{11}H_{11}NSe_2$: C 41.92, H 3.52, N 4.44; found: C 42.16, H 3.45, N 4.66.

4-Phenyl-4*H*-diselenopheno[3,2-*b*:2',3'-*d*]pyrrole (64b).

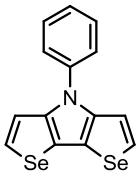

TMS-protected diselenophenopyrrole **63b** (400 mg, 0.81 mmol) was dissolved in THF (15 mL) and TBAF·3H_2O (560 mg, 1.77 mmol) was added. The mixture became brownish and was stirred at r.t. for 45 min. Water (20 mL) was added and the mixture was extracted with DCM (2 × 25 mL). The combined organic layers were dried over Na_2SO_4 and the solvent was removed. The crude product was purified by column chromatography (silica; *n*-hexane/DCM 3:2) to obtain product **64b** as an off-white solid (272 mg, 0.78 mmol, 96%).

Mp.: 118 °C.

^{1}H NMR (400 MHz, $CDCl_3$): δ = 7.71 (d with ^{77}Se-satellites, $^2J_{Se\text{-}H}$ = 47.4 Hz, ^3J = 5.8 Hz, 2H, Sel-H), 7.57-7.50 (m, 4H, Ph-H), 7.39 (d, ^3J = 5.8 Hz, 2H, Sel-H), 7.37-7.34 (m, 1H, Ph-H).

^{13}C NMR (100 MHz, $CDCl_3$): δ = 144.57, 139.91, 129.68, 126.58, 126.32, 123.92, 118.45, 115.49.

MS (EI): *m/z* = 351 (100, M^+), 271 (36), 191 (29).

Elemental analysis: calc. (%) for $C_{14}H_9NSe_2$: C 48.16, H 2.60, N 4.01; found: C 48.30, H 2.65, N 4.21.

2,6-Dibromo-4-propyl-4*H*-diselenopheno[3,2-*b*:2',3'-*d*]pyrrole (65a).

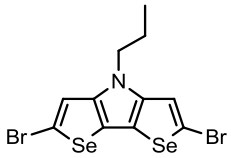

In the absence of light, diselenophenopyrrole **63a** (702 mg, 1.53 mmol) was dissolved in DMF (4 mL). At 0 °C, a solution of NBS (598 mg, 3.36 mmol) in DMF (4 mL) was added dropwise and the solution was stirred at 0 °C for 30 min. The solution became dark. It was diluted with DCM and a sat. $NaHCO_3$ solution was added. The layers were separated and the aqueous layer was extracted with DCM (2×). The combined organic layers were washed with water (2×) and the solvent was removed in vacuum. The crude product was purified by column chromatography (basic Al_2O_3 with 10% H_2O; *n*-hexane/DCM 1:1). The pure product **65a** (623 mg, 1.32 mmol, 87%) was obtained as a dark solid.

Mp.: Decomposition >134 °C.

^{1}H NMR (400 MHz, CD_2Cl_2): δ = 7.33 (s, 2H, Sel-H), 4.08 (t, ^3J = 7.0 Hz, 2H, α-Pr), 1.85-1.75 (m, 2H, β-Pr), 0.87 (t, ^3J = 7.4 Hz, 3H, γ-Pr).

^{13}C NMR (100 MHz, $CDCl_3$): δ = 141.68, 118.48, 110.44, 100.38, 49.65, 24.24, 11.59.

MS (EI): *m/z* = 477 (50, M^+), 475 (100, M^+), 474 (96, M^+), 443 (17, M-C_2H_5), 359 (18).

Elemental analysis: calc. (%) for $C_{11}H_9Br_2NSe_2$: C 27.94, H 1.92, N 2.96; found: C 28.20, H 2.17, N 3.12.

2,6-Dibromo-4-phenyl-4*H*-diselenopheno[3,2-*b*:2',3'-*d*]pyrrole (65b).

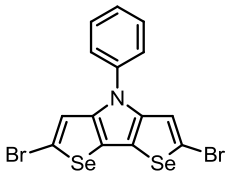

In the absence of light, diselenophenopyrrole **63b** (239 mg, 0.48 mmol) was dissolved in DMF (8 mL). At 0 °C, a solution of NBS (188 mg, 1.08 mmol) in DMF (8 mL) was added dropwise and stirring was continued at this temperature for 30 min. The mixture was stirred at r.t. overnight (reaction complete after 1 h according to GC). A sat. $NaHCO_3$ (20 mL) solution was added and the mixture was extracted with DCM (3 × 20 mL). The combined organic layers were washed with a sat. $NaHCO_3$ solution (20 mL) and water (2 × 20 mL), dried over Na_2SO_4 and the solvent was removed in vacuum. The crude product was purified by column chromatography (short column; basic Al_2O_3 with 10% H_2O, *n*-hexane/DCM 1:1). Product **65b** (230 mg, 0.45 mmol, 94%) was obtained as a slightly orange solid.

Mp.: Decomposition >193 °C.

^{1}H NMR (400 MHz, $CDCl_3$): δ = 7.55-7.51 (m, 2H, Ph-H), 7.46-7.43 (m, 2H, Ph-H), 7.39 (tt, ^3J = 7.2 Hz, ^4J = 1.2 Hz, 1H, Ph-H), 7.35 (s, 2H, Sel-H).

^{13}C NMR (100 MHz, $CDCl_3$): δ = 141.04, 139.06, 129.88, 127.35, 124.12, 113.06, 118.78, 111.12.

MS (EI): *m/z* = 508 (79, M^+), 428 (16, M-Br), 349 (23, M-2Br), 269 (17) 208 (25).

Elemental analysis: calc. (%) for $C_{14}H_7Br_2NSe_2$: C 33.17, H 1.39, N 2.76; found: C 33.28, H 1.60, N 2.95.

4-Phenyl-2,6-bis(trimethylstannyl)-4*H*-diselenopheno[3,2-*b*:2',3'-*d*]pyrrole (66b).

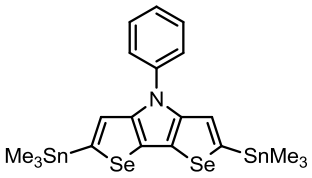

4-Phenyl-4*H*-diselenopheno[3,2-*b*:2',3'-*d*]pyrrole **64b** (205 mg, 0.59 mmol) was dissolved under argon in dry THF (1.9 mL) and the mixture was cooled to -60 °C. *n*-BuLi (1.6 M in hexane, 0.82 mL, 1.31 mmol) was added dropwise and the mixture was allowed to slowly warm to r.t. within 2 h. An off-white precipitate was formed. The solution was cooled back to -50 °C and a solution of Me_3SnCl (281 mg, 1.41 mmol) in THF (0.3 mL) was added in one portion. The solution was allowed to warm to r.t. within 3.5 h. After 2 h, another portion of Me_3SnCl (197 mg, 0.99 mmol, in 0.2 mL THF) was added. The mixture was diluted with *n*-hexane (25 mL) and washed with water (2 × 15 mL). The combined organic layers were dried over Na_2SO_4 and the solvent was removed in vacuum. The resulting beige-brown solid (334 mg, 84%) was dried in high vacuum. It contained ~70% distannylated product **66b**, but it was used without further purification in the next step.

^{1}H NMR (400 MHz, $CDCl_3$): δ = 7.60-7.52 (m, 4H, Ph-H), 7.45 (s, 2H, DSP-H), 7.39-7.35(m, 1H, Ph-H), 0.38 (s, 18H, Sn-CH_3).

^{13}C NMR (100 MHz, $CDCl_3$): δ = 147.45, 142.07, 140.31, 129.65, 126.31, 124.13, 122.67, -7.82.

MS (MALDI-TOF): *m/z* [M^+] = 675.1 (calc. for $C_{20}H_{25}NSe_2Sn_2$: 674.8).

2-{[5-(Tributylstannyl)thien-2-yl]methylene}malononitrile (70a).

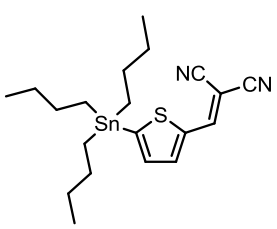

5-(Tributylstannyl)thiophene-2-carbaldehyde **69a** (2.067 g, 3.61 mmol), malononitrile (517 mg, 7.83 mmol) and β-alanine (11.2 mg, 0.13 mmol) were dissolved in acetonitrile and heated to 80 °C for 50 min (the reaction was completed after 30 min according to GC). Water was added and the mixture was extracted twice with DCM. The combined organic layers were washed with water twice, dried over Na_2SO_4 and the solvent was removed to obtain an orange liquid. The crude product was purified by column chromatography (flash silica; short column; *n*-hexane/DCM 100:0 to 0:100). The pure product **70a** (1.19 g, 2.65 mmol, 73%) was obtained as a yellow liquid.

^{1}H NMR (400 MHz, $CDCl_3$): δ = 7.85 (s, 1H, DCV-H), 7.84 (d, ^3J = 3.6 Hz, 1H, Th-H-4), 7.30 (d with Sn-satellites, $^2J_{Sn-H}$ = 18.4 Hz, ^3J = 3.6 Hz, 1H, Th-H-3), 1.60-1.52 (m, 6H, Sn-β-Bu), 1.38-1.29 (m, 6H, Sn-γ-Bu), 1.18 (t, ^3J = 8.0 Hz, 6H, Sn-α-Bu), 0.90 (t, ^3J = 7.2 Hz, 6H, Sn-δ-Bu).

^{13}C NMR (100 MHz, $CDCl_3$): δ = 156.16, 149.83, 140.71, 138.14, 136.84, 114.33, 113.41, 28.21, 27.15, 13.59, 11.23.

MS (EI): *m/z* = 449 (1, M^+), 394 (93), 338 (100), 281 (77), 252 (20), 227 (11).

Elemental analysis: calc. (%) for $C_{20}H_{30}N_2SSn$: C 53.47, H 6.73, N 6.24, S 7.14; found: C 53.35, H 6.56, N 6.42, S 6.93.

5-(Tributylstannyl)selenophene-2-carbaldehyde (69b).

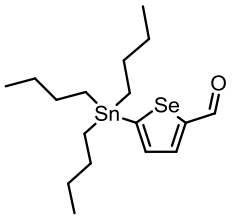

Tributylstannylselenophene **71b** (5.02 g, 12.0 mmol) was dissolved under argon in dry THF (20 mL) and the mixture was cooled to -78 °C. A solution of LDA (prepared from 4.7 mL *n*-BuLi (1.6 M in hexane) and 1.8 mL diisopropylamine in 8 mL THF) was added dropwise during 10 min. The orange solution was stirred at -78 °C for 40 min. DMF (985 mg, 13.5 mmol) was added in one portion and the mixture was stirred at -78 °C for another 30 min. It was quenched with a sat. NH_4Cl solution (40 mL) and extracted with diethyl ether (3 × 40 mL). The combined organic layers were dried over Na_2SO_4 and the solvent was removed in vacuum to obtain product **69b** (5.18 g, 11.6 mmol, 97%) as an orange oil. It was directly used in the next step without further purification.

^{1}H NMR (400 MHz, $CDCl_3$): δ = 9.82 (s, 1H, -CHO), 8.07 (d, ^3J = 3.6 Hz, 1H, Sel-H-3), 7.59 (d, ^3J = 3.6 Hz, 1H, Sel-H-4), 1.61-1.53 (m, 6H, Sn-β-Bu), 1.39-1.29 (m, 6H, Sn-γ-Bu), 1.15 (t, ^3J = 8.2 Hz, 6H, Sn-α-Bu), 0.90 (t, ^3J = 7.4 Hz, 6H, Sn-δ-Bu).

^{13}C NMR (100 MHz, $CDCl_3$): δ = 183.14, 154.69, 138.84, 138.78, 138.63, 28.88, 27.22, 13.62, 11.28.

MS (EI): *m/z* = 449 (7, M^+), 391 (17, M-Bu), 334 (23, M-2Bu), 277 (100, M-3Bu).

2-{[5-(Tributylstannyl)selenophen-2-yl]methylene}malononitrile (70b).

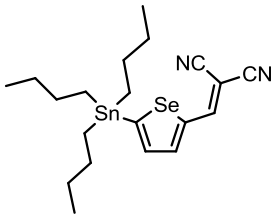

5-(Tributylstannyl)selenophene-2-carbaldehyde **69b** (3.61 g, 8.06 mmol), malononitrile (1.48 g, 22.5 mmol) and β-alanine (33.0 mg, 0.37 mmol) were dissolved in acetonitrile (20 mL) and heated to 80 °C for 45 min (reaction complete after 30 min according to GC). Water was added and the mixture was extracted with DCM (3 × 40 mL). The combined organic layers were dried over Na_2SO_4 and the solvent was removed to obtain a red oil. The crude product was purified by column chromatography (flash silica; short column; *n*-hexane/DCM 3:1). The pure product **70b** (2.87 g, 5.79 mmol, 72%) was obtained as a yellow liquid.

^{1}H NMR (400 MHz, $CDCl_3$): δ = 7.94 (d, ^3J = 3.6 Hz, 1H, Sel-H-4), 7.91 (s, 1H, DCV-H), 7.61 (d with Sn-satellites, $^2J_{Sn\text{-}H}$ = 12.4 Hz, ^3J = 3.6 Hz, 1H, Sel-H-3), 1.59-1.52 (m, 6H, Sn-β-Bu), 1.38-1.29 (m, 6H, Sn-γ-Bu), 1.18 (t, ^3J = 8.2 Hz, 6H, Sn-α-Bu), 0.90 (t, ^3J = 7.4 Hz, 6H, Sn-δ-Bu).

^{13}C NMR (100 MHz, $CDCl_3$): δ = 165.75, 152.68, 144.96, 142.84, 138.57, 114.29, 113.67, 28.83 ($^3J_{Se\text{-}C}$ = 22 Hz), 27.16 ($^2J_{Se\text{-}C}$ = 60 Hz), 13.58, 11.46 ($^1J_{Se\text{-}C}$ = 345 Hz).

MS (EI): *m/z* = 496 (4, M^+), 440 (88), 382 (15), 327 (38), 292 (100).

Elemental analysis: calc. (%) for $C_{20}H_{30}N_2SeSn$: C 48.42, H 6.09, N 5.65; found: C 48.67, H 5.92, N 5.92.

2,2'-{[5,5'-(4-Phenyl-4*H*-dithieno[3,2-*b*:2',3'-*d*]pyrrole-2,6-diyl)bis(selenophene-5,2-diyl)]bis(methanylylidene)}dimalononitrile (9).

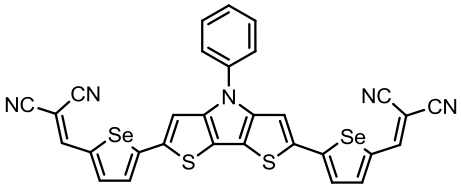

In a Schlenk tube, stannylated dithienopyrrole **58b** (306 mg, 0.527 mmol) and bromoselenophene **31** (376 mg, 1.31 mmol) were dissolved in dry degassed THF (2 mL) and the solution was degassed.

$Pd(PPh_3)_4$ (15.0 mg, 13.0 µmol, 2 mol%) was added, the mixture was degassed again and stirred at 80 °C for 24 h. After cooling to r.t. the resulting solid was filtered off and washed with THF and methanol. The green product **9** (315 mg, 0.473 mmol, 90%) was dried in high vacuum. The product was further purified by Soxhlet extraction with chlorobenzene for 9 d and obtained as green powder after removal of the solvent.

Mp.: 412 °C.

^{1}H NMR (500 MHz, 340 K, DMSO-d_6): δ = 8.56 (s, 2H, DCV-H), 8.11 (d, ^3J = 4.0 Hz, 2H, Sel-H), 7.87 (s, 2H, DTP-H), 7.78-7.75 (m, 3H, Ph-H + Sel-H), 7.68-7.65 (m, 2H, Ph-H), 7.51-7.48 (m, 2H, Ph-H).

MS (MALDI-TOF): *m/z* [M^+] = 667.3 (calc. for $C_{30}H_{13}N_5S_2Se_2$: 666.9).

Elemental analysis: calc. (%) for $C_{30}H_{13}N_5S_2Se_2$: C 54.14, H 1.97, N 10.52, S 9.64; found: C 54.15, H 2.10, N 10.40, S 9.54.

2,2'-{[5,5'-(4-Propyl-4*H*-dithieno[3,2-*b*:2',3'-*d*]pyrrole-2,6-diyl)bis(thien-5,2-diyl)]bis(methanylylidene)}dimalononitrile (10).

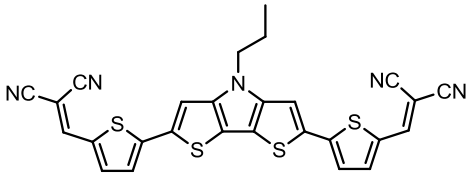

In a Schlenk tube, stannylated dithienopyrrole **58a** (350 mg, 80%, 0.512 mmol) and bromothiophene **59** (360 mg, 1.51 mmol) were dissolved under argon in dry DMF (5 mL) and the solution was degassed. $Pd(PPh_3)_4$ (22.0 mg, 19.0 µmol) was added, the solution was degassed again and then stirred at 80 °C for 19 h. After cooling to r.t. the mixture was filtered and the resulting solid was washed with little THF until the washing water turned from purple to blue. The now green solid was washed with methanol, dried in high vacuum and further purified by Soxhlet extraction with chlorobenzene. The pure product **10** (228 mg, 0.424 mmol, 83%) was obtained as green needles.

Mp.: 367 °C.

^{1}H NMR (500 MHz, 340 K, $C_2D_2Cl_4$): δ = 7.69 (s, 2H, DCV-H), 7.58 (d, ^3J = 3.6 Hz, 2H, Th-H), 7.31 (s, 2H, DTP-H), 7.28 (d, ^3J = 3.6 Hz, 2H, Th-H), 4.15 (t, 2H, ^3J = 5.8 Hz, α-Pr), 1.93 (q, ^3J = 6.0 Hz, 2H, β-Pr), 0.98 (t, 3H, ^3J = 5.8 Hz, γ-Pr).

MS (MALDI-TOF): *m/z* [M^+] = 537.1 (calc. for $C_{27}H_{15}N_5S_4$: 537.0).

Elemental analysis: calc. (%) for $C_{27}H_{15}N_5S_4$: C 60.31, H 2.81, N 13.02, S 23.85; found: C 60.11, H 3.01, N 13.23, S 24.08.

2,2'-[5,5'-(4-Propyl-4*H*-dithieno[3,2-*b*:2',3'-*d*]pyrrole-2,6-diyl)bis(selenophene-5,2-diyl)]bis(methan-1-yl-1-ylidene)dimalononitrile (11).

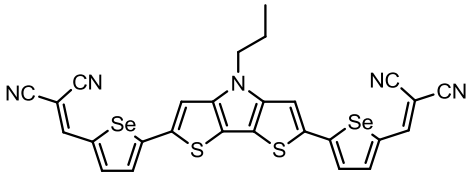

In a Schlenk tube, stannylated dithienopyrrole **58a** (273 mg, 0.50 mmol) and bromoselenophene **31** (428 mg, 1.50 mmol) were dissolved under argon in dry THF (4 mL) and the solution was degassed. $Pd(PPh_3)_4$ (8.8 mg, 7.6 µmol) was added, the solution was degassed again and then stirred at 75 °C for 17 h. After cooling to r.t. the mixture was filtered and the resulting solid was washed with little THF until the washing water turned from purple to blue. The now green solid was washed with methanol and dried in high vacuum to obtain 266 mg of crude product. This was further purified by Soxhlet extraction with chlorobenzene. The pure product **11** (192 mg, 0.30 mmol, 60%) was obtained as green needles.

Mp.: 374 °C.

^{1}H NMR (500 MHz, 373 K, DMSO-d_6): δ = 7.74 (s, 2H, DCV-H), 7.74 (d, 2H, ^3J = 3.6 Hz, Sel-H), 7.40 (d, 2H, ^3J = 3.6 Hz, Sel-H), 7.26 (s, 2H, DTP-H), 4.14 (t, 2H, ^3J = 5.8 Hz, α-Pr), 1.95 (q, ^3J = 5.8 Hz, 2H, β-Pr), 1.00 (t, 3H, ^3J = 5.8 Hz, γ-Pr).

MS (MALDI-TOF): *m/z* [M^+] = 633.0 (calc. for $C_{27}H_{15}N_5S_2Se_2$: 632.9).

Elemental analysis: calc. (%) for $C_{27}H_{15}N_5S_2Se_2$: C 51.35, H 2.39, N 11.09, S 10.16; found: C 51.66, H 2.49, N 11.14, S 10.01.

2,2'-[5,5'-(4-Phenyl-4*H*-diselenopheno[3,2-*b*:2',3'-*d*]pyrrole-2,6-diyl)bis(selenophene-5,2-diyl)]bis(methan-1-yl-1-ylidene)dimalononitrile (12).

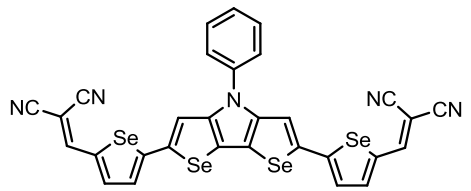

In a Schlenk tube, stannane **66b** (310 mg, 70%, 0.32 mmol) and bromoselenophene **31** (350 mg, 1.22 mmol) were dissolved under argon in dry DMF (4 mL) and the solution was degassed. $Pd(PPh_3)_4$ (7.8 mg, 6.78 µmol, 2 mol%) was added and the mixture was stirred at 80 °C for 22 h. After some minutes, the mixture became very viscous and more DMF (4 mL) was added. After cooling to r.t. the resulting solid was filtered off, washed with THF, methanol and DCM and dried in high vacuum. The

crude product (220 mg) was purified by Soxhlet extraction with chlorobenzene for 4 d to obtain pure product **12** (143 mg, 0.19 mmol, 59%) as a greenish solid.

Mp. 417 °C.

^{1}H NMR (500 MHz, 373 K, $C_2D_2Cl_4$): δ = 7.72 (s, 2H, DCV-H), 7.71 (d, ^3J = 4.4 Hz, 2H, Sel-H), 7.63-7.59 (m, 2H, Ph-H), 7.50-7.48 (m, 2H, Ph-H), 7.45 (s, 2H, DSP-H), 7.31 (d, ^3J = 4.4 Hz, 2H, Sel-H).

MS (MALDI-TOF): *m/z* [M^+] = 761.1 (calc. for $C_{30}H_{13}N_5Se_4$: 760.8).

Elemental analysis: calc. (%) for $C_{30}H_{13}N_5Se_4$: C 47.45, H 1.73, N 9.22; found: C 47.26, H 1.99, N 9.34.

2,2'-{[5,5'-(4-Propyl-4*H*-diselenopheno[3,2-*b*:2',3'-*d*]pyrrole-2,6-diyl)bis(thien-5,2-diyl)]bis(methanylylidene)}dimalononitrile (13).

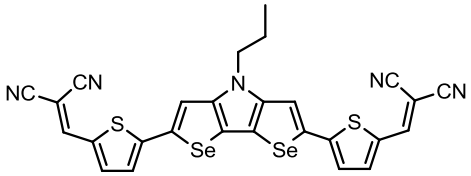

$Pd_2(dba)_3{\cdot}CHCl_3$ (4.4 mg, 4.23 µmol), $HP^tBu_3BF_4$ (3.1 mg, 11.0 µmol) and NaO^tBu (1.2 mg, 13 µmol) were dissolved under argon in THF (2 mL) and the solution was degassed. Dibromodiselenopheno-pyrrole **65a** (100 mg, 0.211 mmol) and thienylstannane **70a** (237 mg, 0.529 mmol) were added and the solution was degassed again. The reaction mixture was stirred at 50 °C overnight. More stannane **70a** (100 mg, 0.223 mmol) was added and stirring was continued for 2 h. The crude product was filtered off, washed with methanol and pure product **13** (93 mg, 0.147 mmol, 70%) was obtained as a green solid.

^{1}H NMR (500 MHz, $C_2D_2Cl_4$, 350 K): δ = 7.68 (s, 2H, DCV-H), 7.56 (d, 2H, ^3J = 4.5 Hz, Sel-H), 7.52 (s, 2H, DSP-H), 7.19 (d, 2H, ^3J = 4.5 Hz, Sel-H), 4.19 (t, 2H, ^3J = 5.6 Hz, α-Pr), 1.94-1.87 (m, 2H, β-Pr), 0.98 (t, 3H, ^3J = 5.8 Hz, γ-Pr).

HR-MS (MALDI-TOF): *m/z* [M^+] = 632.90943 (calc. for $C_{27}H_{15}N_5S_2Se_2$: 632.90962).

2,2'-{[5,5'-(4-Propyl-4*H*-diselenopheno[3,2-*b*:2',3'-*d*]pyrrole-2,6-diyl)bis(selenophene-5,2-diyl)]bis(methanylylidene)}dimalononitrile (14).

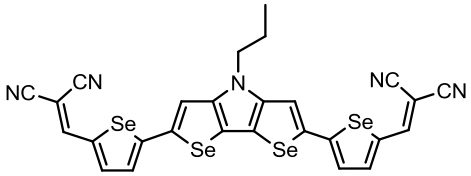

In a Schlenk tube, dibromodiselenophenopyrrole **65a** (200 mg, 0.423 mmol) and selenophenyl-stannane **70b** (619 mg, 1.25 mmol) were dissolved in dry degassed THF (5 mL) and the solution was degassed. $Pd(PPh_3)_4$ (13.4 mg, 11.6 µmol, 3 mol%) was added, the mixture was degassed again and stirred at 80 °C for 23 h. After cooling to r.t. the resulting solid was filtered off and washed with THF and methanol. The green product **14** (190 mg, 0.262 mmol, 62%) was dried in high vacuum. The product was further purified by Soxhlet extraction with chlorobenzene for 4 d.

Mp.: 380 °C.

^{1}H NMR (500 MHz, 360 K, $C_2D_2Cl_4$): δ = 7.73 (s, 2H, DCV-H), 7.71 (d, 2H, ^3J = 4.5 Hz, Sel-H), 7.46 (s, 2H, DSP-H), 7.30 (d, 2H, ^3J = 4.5 Hz, Sel-H), 4.18 (t, 2H, ^3J = 6.2 Hz, α-Pr), 1.96-1.88 (m, 2H, β-Pr), 1.00 (t, 3H, ^3J = 6.0 Hz, γ-Pr).

MS (MALDI-TOF): *m/z* [M^+] = 726.8 (calc. for $C_{27}H_{15}N_5Se_4$: 726.8).

Elemental analysis: calc. (%) for $C_{27}H_{15}N_5Se_4$: C 44.71, H 2.08, N 9.66; found: C 44.50, H 2.23, N 9.42.

4-(2-Ethylhexyl)-2,6-bis(trimethylsilyl)-4*H*-diselenopheno[3,2-*b*:2',3'-*d*]pyrrole (73).

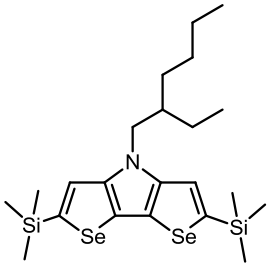

Biselenophene **62** (2.52 g, 3.84 mmol), NaO^{t}Bu (910 mg, 9.47 mmol), $Pd_2(dba)_3{\cdot}CHCl_3$ (148 mg, 143 µmol) and BINAP (237 mg, 381 µmol) were dissolved under argon in dry toluene (15 mL), the solution was degassed and stirred for 20 min. 2-Ethylhexylamine (1.31 g, 10.1 mmol) was added and the mixture was stirred at 110 °C for 2 h. Water (20 mL) was added and the mixture was extracted with DCM (3 × 20 mL). The combined organic layers were dried over Na_2SO_4 and the solvent was removed in vacuum. The resulting brown oil was purified by column chromatography (alumina 10% H_2O, *n*-hexane). The pure product **73** (1.83 g, 3.45 mmol, 90%) was obtained as a yellow solid.

^{1}H NMR (400 MHz, $CDCl_3$): δ =7.35 (s with ^{77}Se-satellites, $^3J_{Se-H}$ = 10 Hz, 2H, Sel-H), 4.14-4.03 (m, 2H, N-CH_2), 1.95-1.91 (m, 1H, N-CH_2-C*H*), 1.42-1.23 (m, 8H, -CH_2-), 0.92 (t, ^3J = 7.4 Hz, 3H, -CH_3), 0.89 (t, ^3J = 7.2 Hz, 3H, -CH_3), 0,35 (s, 18H, Si-CH_3).

^{13}C NMR (100 MHz, $CDCl_3$): δ = 148.29, 144.21, 120.76, 120.25, 51.32, 40.56, 30.42, 28.36, 28.36, 23.95, 23.00, 14.06, 10.71, 0.26.

MS (MALDI-TOF): *m/z* [M^+] = 530.6 (calc. for $C_{22}H_{37}NSe_2Si_2$: 531.1).

Elemental analysis: calc. (%) for $C_{22}H_{37}NSe_2Si_2$: C 49.89, H 7.04, N 2.64; found: 49.92, H 6.81, N 2.55.

4-(2-Ethylhexyl)-4*H*-diselenopheno[3,2-*b*:2',3'-*d*]pyrrole (74).

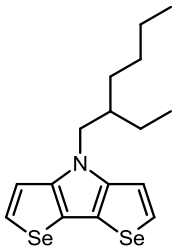

TMS-protected diselenophenopyrrole **73** (1.52 g, 2.88 mmol) was dissolved in THF (20 mL) and TBAF·$3H_2O$ (1.92 g, 6.07 mmol) was added. The solution was stirred at r.t. for 30 min. The solvent was evaporated to dryness and the crude product was purified by column chromatography (silica; *n*-hexane/DCM 3:2) to obtain product **74** as a pale yellow solid (979 mg, 2.54 mmol, 88%).

Mp.: 41 °C.

^{1}H NMR (400 MHz, $CDCl_3$): δ = 7.67 (d with ^{77}Se-satellites, $^2J_{Se\text{-}H}$ = 47.2 Hz, ^3J = 5.6 Hz, 2H, α-DSP-H), 7.28 (d, ^3J = 5.6 Hz, 2H, β-DSP-H), 4.15-4.03 (m, 2H, N-CH_2-), 1.96-1.87 (m, 1H, N-CH_2-C<u>H</u>-$(CH_2)_2$-), 1.39-1.22 (m, 8H, -CH_2-), 0.90 (t, ^3J = 7.2 Hz, 3H, -CH_3), 0.88 (t, ^3J = 7.2 Hz, 3H, -CH_3).

^{13}C NMR (100 MHz, $CDCl_3$): δ = 145.30, 125.45 ($^1J_{Se\text{-}C}$ = 56 Hz), 115.98, 114.53, 51.54, 40.65, 30.60, 28.64, 24.00, 22.97, 14.03, 10.68.

MS (EI): *m/z* = 387 (100, M^+), 386 (68, M^+), 385 (100, M^+), 384 (82, M^+), 383 (65, M^+), 285 (M-C_7H_{17}).

Elemental analysis: calc. (%) for $C_{16}H_{21}NSe_2$: C 49.88, H 5.49, N 3.64; found: 49.73, H 5.30, N 3.45.

4-(2-Ethylhexyl)-2,6-bis(trimethylstannyl)-4*H*-diselenopheno[3,2-*b*:2',3'-*d*]pyrrole (75).

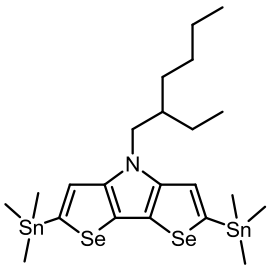

4-(2-Ethylhexyl)-4*H*-diselenopheno[3,2-*b*:2',3'-*d*]pyrrole **74** (202 mg, 524 µm) was dissolved under argon in dry THF (2.2 mL) and the solution was cooled to -78 °C. *n*-BuLi (1.6 M in hexane, 0.82 mL, 1.31 mmol) was added dropwise within 10 min. The red solution was stirred at -78 °C for 1 h and at

0 °C for 1 h. The mixture became blue. It was cooled back to -78 °C and Me_3SnCl (260 mg, 1.30 mmol, dissolved in 0.3 mL THF) was added dropwise. The mixture became orange and clear, was stirred at -78 °C for 1 h and 3 h at r.t. A sat. Na_2CO_3 solution (10 mL) was added and the mixture was extracted with DCM (2 × 15 mL). The combined organic layers were washed with water (15 mL) and the solvent was removed. The crude product **75** (390 mg, 0.520 mmol, 99%) was used without further purification.

^{1}H NMR (400 MHz, $CDCl_3$): δ = 7.33 (s, 2H, DSP-H), 4.15-4.03 (m, 2H, N-CH_2-), 1.98-1.91 (m, 1H, N-CH_2-C<u>H</u>-$(CH_2)_2$-), 1.44-1.21 (m, 8H, -CH_2-), 0.92 (t, ^3J = 7.6 Hz, 3H, -CH_3), 0.89 (t, ^3J = 7.2 Hz, 3H, -CH_3), 0.39 (s, 18H, Sn-CH_3).

^{13}C NMR (100 MHz, $CDCl_3$): δ = 148.32, 140.78, 121.91, 121.13, 67.96, 51.41, 40.55, 30.43, 28.41, 25.59, 23.96, 23.01, 14.08, 10.71, -7.85.

MS (MALDI-TOF): *m/z* [M^+] = 711.1 (calc. for $C_{22}H_{37}NSe_2Sn_2$: 710.9).

2,3,4,5-Tetraiodoselenophene (76).

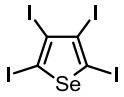

To a white suspension of selenophene **20** (10.3 g, 78.4 mmol), acetic acid (400 mL) and mercury acetate (100 g, 314 mmol) heated at 90 °C, iodine (79.6 g, 314 mmol) was added in portions over 15 min. The mixture became purple and an orange precipitate formed. Heating was continued for 2 h (the purple color disappeared), the reaction was slowly cooled to r.t., water (300 mL) was added and the mixture was stirred for 30 min. It was stored in the refrigerator overnight, filtered, the solids were collected and treated with a potassium iodide solution (ca. 2 M, 700 mL) for 3 h with constant stirring. The off-white solid was filtered off and dried in high vacuum to obtain 37.8 g (59.6 mmol, 76%) of tetraiodoselenophene **76**.

^{1}H NMR (400 MHz, DMSO-d_6): no signal.

^{13}C NMR (100 MHz, DMSO-d_6): δ = 110.11 (C-3,4), 92.03 (C-2,5).

MS (EI): *m/z* = 636 (100, M^+).

Analytical data were in accordance with literature data.[52]

3-Iodoselenophene (77).



Tetraiodoselenophene **76** (17.0 g, 26.8 mmol) was suspended in 80% acetic acid (340 mL) and the mixture was degassed. Zinc dust (5.38 g, 82.2 mmol) was added in 5 portions while heating to 110 °C. The mixture was refluxed for 2.5 h. Water (300 mL) was added and the mixture was extracted with diethyl ether (2 × 300 mL). The combined organic layers were washed with water (2 × 200 mL), a sat. $NaHCO_3$ solution (2 x 250 mL + addition of solid $NaHCO_3$) and again water, then they were dried over Na_2SO_4 and the solvent was removed. The crude product (6.77 g) was purified by Kugelrohr distillation (130 °C, 7 mbar) to afford pure product **77** (5.25 g, 20.4 mmol, 76%).

Bp.: 130 °C (7 mbar).

^{1}H NMR (400 MHz, $CDCl_3$): δ = 8.10 (dd with ^{77}Se-satellites, $^2J_{Se-H}$ = 46.0 Hz, ^4J = 2.4 Hz, ^4J = 1.0 Hz, 1H, H-2), 7.86 (dd with ^{77}Se-satellites, $^2J_{Se-H}$ = 46.8 Hz, ^3J = 5.6 Hz, ^4J = 2.4 Hz, 1H, H-5), 7.32 (dd, ^3J = 5.6 Hz, ^4J = 1.0 Hz, 1H, H-4).

^{13}C NMR (100 MHz, $CDCl_3$): δ = 137.32 (C-4), 132.29 (C-5), 132.09 (C-2), 78.48 (C-3).

MS (EI): *m/z* = 258 (100, M^+), 131 (21, M-I).

Analytical data were in accordance with literature data.[53]

3-Hexylselenophene (78).



A hexylmagnesium bromide solution was prepared from 1-bromohexane (13.7 g, 82.8 mmol) and magnesium (2.08 g, 85.7 mmol) in dry Et_2O (80 mL). The mixture was refluxed for 2 h. 3-iodoselenophene **77** (6.89 g, 26.8 mmol) was dissolved under argon in dry Et_2O (50 mL) and the solution was cooled with an ice-bath. Ni(dppp)Cl_2 (144 mg, 266 µmol) was added, then 40 mL of the Grignard solution was added dropwise within 25 min. The solution was allowed to warm to r.t. within 1 h. Another portion of catalyst (74 mg, 137 µmol) was added, the solution was cooled to 0 °C and another 20 mL of Grignard solution was added dropwise within 5 min. The solution was allowed to warm to r.t. within 3 h. After 3 h, another portion of catalyst (75 mg, 138 µmol) and Grignard

solution (20 mL) was added and the mixture was stirred at r.t. overnight. The reaction mixture was quenched with 2 M HCl (15 mL) and water (50 mL) was added. The phases were separated and the aqueous phase was extracted with diethyl ether (2 × 75 mL). The combined organic layers were washed with a sat. Na_2CO_3 solution (100 mL), water (2 × 75 mL) and dried over Na_2SO_4. The solvent was removed in vacuum to afford a brown oil. It was further purified by Kugelrohr distillation ($1.2 \cdot 10^{-2}$ mbar, 117 °C) to obtain pure product **78** (4.67 g, 21.7 mmol, 81%) as a pale yellow liquid.

Bp.: 117 °C ($1.2 \cdot 10^{-2}$ mbar).

^{1}H NMR (400 MHz, $CDCl_3$): δ = 7.92 (dd with ^{77}Se-satellites, $^2J_{Se-H}$ = 46.4 Hz, ^3J = 5.2 Hz, ^4J = 2.4 Hz, 1H, H-5), 7.54 (dd with ^{77}Se-satellites, $^2J_{Se-H}$ = 48.4 Hz, ^4J = 2.4 Hz, ^4J = 1.2 Hz, 1H, H-2), 7.22 (dd, ^3J = 5.2 Hz, ^4J = 1.2 Hz, 1H, H-4), 2.61 (t, ^3J = 7.8 Hz, 2H, α-Hex), 1.66-1.58 (m, 2H, β-Hex), 1.38-1.24 (m, 6H, γ,δ,ε-Hex), 0.89 (t, ^3J = 7.2 Hz, 3H, -CH_3).

^{13}C NMR (100 MHz, $CDCl_3$): δ = 145.25, 131.42, 129.60, 123.74, 31.90, 31.68, 30.34, 29.00, 22.61, 14.10.

MS (EI): *m/z* = 216 (64, M^+), 214 (37, M^+), 145 (100, M-C_5H_{11}).

Analytical data were in accordance with literature data.[53]

2-Bromo-3-hexylselenophene (79).

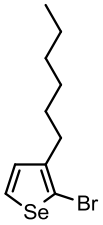

3-Hexylselenophene **78** (1.29 g, 4.81 mmol) was dissolved in DMF (10 mL) and NBS (852 mg, 4.79 mmol) in 5 mL DMF. The solutions were put in the freezer (-25 °C) for 4 h, combined, put back in the freezer for 16 h and in the refrigerator for 5 d. The orange solution was poured into a sat. Na_2CO_3 solution (50 mL) and extracted with DCM (3 × 30 mL). The combined organic layers were washed with water (3 × 25 mL), dried over Na_2SO_4 and the solvent was removed. The crude product was purified by column chromatography (flash silica; *n*-hexane). The pure product **79** (1.00 g, 3.40 mmol) was obtained as a pale yellow liquid.

^{1}H NMR (400 MHz, $CDCl_3$): δ = 7.84 (d with ^{77}Se-satellites, $^2J_{Se-H}$ = 45.6 Hz, ^3J = 6.0 Hz, 1H, Sel-H-5), 7.02 (d, ^3J = 6.0 Hz, 1H, Sel-H-4), 2.54 (t, ^3J = 7.6 Hz, 2H, α-Hex), 1.60-1.52 (m, 2H, β-Hex), 1.37-1.26 (m, 6H, γ,δ,ε-Hex), 0.89 (t, ^3J = 7.0 Hz, 2H, -CH_3).

^{13}C NMR (100 MHz, $CDCl_3$): δ = 144.25, 131.18, 129.98, 111.09, 31.62, 30.64, 29.60, 28.88, 22.59, 14.09.

MS (EI): *m/z* = 296 (24, M^+), 294 (24, M^+), 292 (21, M^+), 225 (46, M-C_5H_{11}), 223 (60, M-C_5H_{11}), 221 (27, M-C_5H_{11}), 144 (100, M-C_5H_{11}-Br).

Elemental analysis: calc. (%) for $C_{10}H_{15}BrSe$: C 40.84, H 5.14; found: C 41.19, H 4.85.

4-(2-Ethylhexyl)-2,6-bis(3-hexylselenophen-2-yl)-4*H*-diselenopheno[3,2-*b*:2',3'-*d*]pyrrole (80).

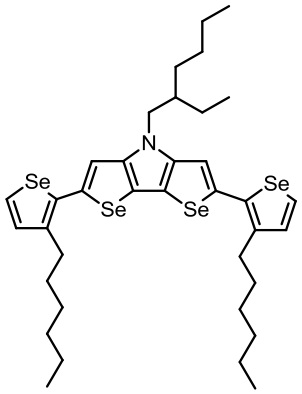

Diselenophenopyrrole **75** (330 mg, 464 µmol) and 2-bromo-3-hexylselenophene **79** (330 mg, 1.12 mmol) were dissolved under argon in dry DMF (8 mL) and the solution was degassed. $Pd(PPh_3)_2Cl_2$ (12.8 mg, 18.2 µmol) was added, the solution was degassed again and stirred at 100 °C for 16 h. The mixture was diluted with DCM (40 mL) and washed with water (3×). The solution was dried over Na_2SO_4 and the solvent was removed in vacuum. The crude product was purified by column chromatography (flash silica; *n*-hexane/DCM 8:2) and the pure product **80** (195 mg, 240 µmol, 52%) was obtained as a yellow oil.

^{1}H NMR (400 MHz, $CDCl_3$): δ = 7.83 (d with ^{77}Se-satellites, $^2J_{Se\text{-}H}$ = 44.8 Hz, ^3J = 5.4 Hz, 2H, α-Sel-H), 7.23 (d, ^3J = 5.4 Hz, 2H, β-Sel-H), 7.16 (s, 2H, DSP-H), 4.12-4.01 (m, 2H, N-CH_2-), 2.77 (t, ^3J = 7.4 Hz, 4H, α-Hex), 1.97-1.87 (m, 1H, N-CH_2-C*H*-$(CH_2)_2$-), 1.70-1.60 (m, 4H, β-Hex), 1.40-1.22 (m, 20 H, -CH_2-), 0.94-0.84 (m, 12H, -CH_3).

^{13}C NMR (100 MHz, $CDCl_3$): δ = 144.17, 140.78, 138.59, 138.06, 133.54, 128.69, 117.15, 113.00, 51.48, 40.70, 31.72, 31.00, 30.67, 30.52, 29.36, 28.67, 24.06, 23.01, 22.66, 14.10, 14.06, 10.73.

MS (MALDI-TOF): *m/z* [M^+] = 813.2 (calc. for $C_{36}H_{49}NSe_4$: 813.1).

Elemental analysis: calc. (%) for $C_{36}H_{49}NSe_4$: C 53.27, H 6.09, N 1.73; found: C 53.16, H 6.21, N 1.76.

5,5'-[4-(2-Ethylhexyl)-4*H*-diselenopheno[3,2-*b*:2',3'-*d*]pyrrole-2,6-diyl]bis(4-hexylselenophene-2-carbaldehyde) (81).

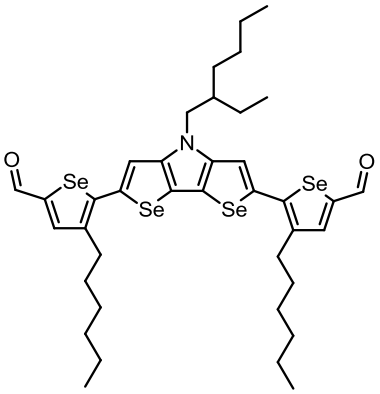

DMF (303 mg, 4.15 mmol) and $POCl_3$ (603 mg, 3.93 mmol) were dissolved under argon in dry DCM (10 mL) and the solution was stirred at r.t. for 2 h. Compound **80** (158 mg, 195 µmol, dissolved in 8 mL DCM) was added and the mixture was stirred at r.t. for 3 d. A sat. Na_2CO_3 solution (10 mL) was added and the mixture was stirred for 4 h. The phases were separated and the aqueous phase was extracted with DCM (2 × 20 mL). The solvent was removed and the crude product was purified by column chromatography (flash silica; DCM) to afford pure product **81** (70.0 mg, 80.7 µmol, 41%) as a greenish solid.

Mp.: 174 °C.

^{1}H NMR (400 MHz, $CDCl_3$): δ = 9.71 (s, 2H, -CHO), 7.89 (s, 2H, Sel-H), 7.33 (s, 2H, DSP-H), 4.17-4.06 (m, 2H, N-CH_2-), 2.83 (t, ^3J = 8.2 Hz, 4H, α-Hex), 1.95-1.87 (m, 1H, N-CH_2-C*H*-$(CH_2)_2$-), 1.75-1.67 (m, 4H, β-Hex), 1.46-1.25 (m, 20 H, -CH_2-), 0.94 (t, ^3J = 7.4 Hz, 3H, -CH_3), 0.91-0.86 (m, 9H, -CH_3).

^{13}C NMR (100 MHz, $CDCl_3$): δ = 183.73, 149.48, 145.60, 145.26, 143.33, 141.33, 137.63, 119.06, 114.15, 51.57, 40.74, 31.64, 30.72, 30.66, 29.29, 28.64, 24.04, 22.97, 22.62, 14.07, 14.03, 10.70.

MS (MALDI-TOF): *m/z* [M^+] = 869.3 (calc. for $C_{38}H_{49}NO_2Se_4$: 869.0).

Elemental analysis: calc. (%) for $C_{38}H_{49}NO_2Se_4$: C 52.60, H 5.69, N 1.61; found: C 52.78, H 5.58, N 1.57.

2,2'-({5,5'-[4-(2-Ethylhexyl)-4*H*-diselenopheno[3,2-*b*:2',3'-*d*]pyrrole-2,6-diyl]bis(4-hexylselenophene-5,2-diyl)}bis(methanylylidene))dimalononitrile (15).

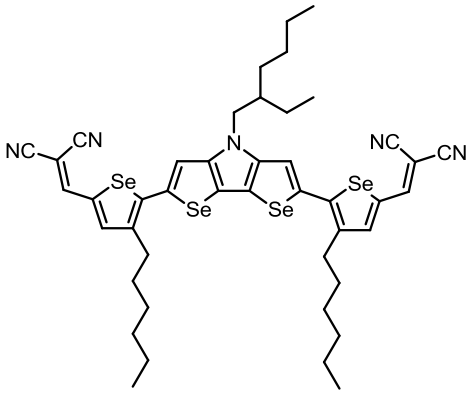

Dialdehyde **81** (58 mg, 66.9 µmol), malononitrile (15.7 mg, 238 µmol) and β-alanine (0.9 mg, 10.1 µmol) were dissolved in a DCE/ethanol mixture (1:1 v/v, 8 mL) and the solution was stirred at 80 °C for 18 h. The solvent was removed in vacuum and the residue was purified by column chromatography (flash silica; DCM). The pure product **15** (54.0 mg, 56.0 µmol, 84%) was obtained as a green solid.

Mp.: 218 °C.

^{1}H NMR (400 MHz, $CDCl_3$): δ = 7.75 (s, 2H, Sel-H), 7.72 (s, 2H, DCV-H), 7.42 (s, 2H, DSP-H), 4.19-4.08 (m, 2H, N-CH_2-), 2.84 (t, ^{3}J = 7.6 Hz, 4H, α-Hex), 1.98-1.91 (m, 1H, N-CH_2-C*H*-$(CH_2)_2$-), 1.74-1.66 (m, 4H, β-Hex), 1.43-1.25 (m, 20 H, -CH_2-), 0.93 (t, ^{3}J = 7.2 Hz, 3H, -CH_3), 0.91-0.86 (m, 9H, -CH_3).

^{13}C NMR (100 MHz, $CDCl_3$): δ = 153.20, 152.59, 147.39, 146.39, 141.07, 137.36, 136.11, 120.71, 114.88, 114.52, 114.02, 75.51, 51.95, 40.59, 31.64, 30.57, 30.47, 29.36, 28.56, 24.06, 23.04, 22.65, 14.11, 14.07, 10.81.

MS (MALDI-TOF): *m/z* [M^+] = 963.4 (calc. for $C_{44}H_{49}N_5Se_4$: 963.1).

Elemental analysis: calc. (%) for $C_{44}H_{49}N_5Se_4$: C 54.84, H 5.12, N 7.27; found: C 55.01, H 5.25, N 7.23.

4.6 References

[1] H. Zhou, L. Yang, W. You, *Macromolecules* **2012**, *45*, 607.

[2] Y. A. Getmanenko, P. Tongwa, T. V. Timofeeva, S. R. Marder, *Org. Lett.* **2010**, *12*, 2136.

[3] J. Liu, R. Zhang, G. Sauvé, T. Kowalewski, R. D. McCullough, *J. Am. Chem. Soc.* **2008**, *130*, 13167.

[4] W. Zhang, J. Li, L. Zou, B. Zhang, J. Qin, Z. Lu, Y. F. Poon, M. B. Chan-Park, C. M. Li, *Macromolecules* **2008**, *41*, 8953.

[5] X. Zhan, Z. Tan, E. Zhou, Y. Li, R. Misra, A. Grant, B. Domercq, X.-H. Zhang, Z. An, X. Zhang, S. Barlow, B. Kippelen, S. R. Marder, *J. Mater. Chem.* **2009**, *19*, 5794.

[6] S. Zhang, Y. Guo, H. Fan, Y. Liu, H.-Y. Chen, G. Yang, X. Zhan, Y. Liu, Y. Li, Y. Yang, *J. Polym. Sci. Part A: Polym. Chem.* **2009**, *47*, 5498.

[7] X. Zhang, T. T. Steckler, R. R. Dasari, S. Ohira, W. J. Potscavage, S. P. Tiwari, S. Coppée, S. Ellinger, S. Barlow, J.-L. Brédas, B. Kippelen, J. R. Reynolds, S. R. Marder, *J. Mater. Chem.* **2010**, *20*, 123.

[8] T. L. Nelson, T. M. Young, J. Liu, S. P. Mishra, J. A. Belot, C. L. Balliet, A. E. Javier, T. Kowalewski, R. D. McCullough, *Adv. Mater.* **2010**, *22*, 4617.

[9] S. J. Evenson, M. J. Mumm, K. I. Pokhodnya, S. C. Rasmussen, *Macromolecules* **2011**, *44*, 835.

[10] M. Zhang, H. Fan, X. Guo, Y. He, Z. Zhang, J. Min, J. Zhang, G. Zhao, X. Zhan, Y. Li, *Macromolecules* **2010**, *43*, 5706.

[11] R. S. Ashraf, J. Gilot, R. A. J. Janssen, *Sol. Energy Mater. Sol. Cells* **2010**, *94*, 1759.

[12] E. Zhou, K. Tajima, C. Yang, K. Hashimoto, *J. Mater. Chem.* **2010**, *20*, 2362.

[13] K. M. Noone, E. Strein, N. C. Anderson, P.-T. Wu, S. A. Jenekhe, D. S. Ginger, *Nano Lett.* **2010**, *10*, 2635.

[14] W. Yue, Y. Zhao, S. Shao, H. Tian, Z. Xie, Y. Geng, F. Wang, *J. Mater. Chem.* **2009**, *19*, 2199.

[15] E. Zhou, M. Nakamura, T. Nishizawa, Y. Zhang, Q. Wei, K. Tajima, C. Yang, K. Hashimoto, *Macromolecules* **2008**, *41*, 8302.

[16] E. Zhou, Q. Wei, S. Yamakawa, Y. Zhang, K. Tajima, C. Yang, K. Hashimoto, *Macromolecules* **2010**, *43*, 821.

[17] S. Barlow, S. A. Odom, K. Lancaster, Y. A. Getmanenko, R. Mason, V. Coropceanu, J.-L. Brédas, S. R. Marder, *J. Phys. Chem. B* **2010**, *114*, 14397.

[18] H. Mo, K. R. Radke, K. Ogawa, C. L. Heth, B. T. Erpelding, S. C. Rasmussen, *Phys. Chem. Chem. Phys.* **2010**, *12*, 14585.

[19] K. R. Radke, K. Ogawa, S. C. Rasmussen, *Org. Lett.* **2005**, *7*, 5253.

[20] L. E. Polander, S. P. Tiwari, L. Pandey, B. M. Seifried, Q. Zhang, S. Barlow, C. Risko, J.-L. Brédas, B. Kippelen, S. R. Marder, *Chem. Mater.* **2011**, *23*, 3408.

[21] D. Sahu, H. Padhy, D. Patra, J.-F. Yin, Y.-C. Hsu, J.-T. S. Lin, K.-L. Lu, K.-H. Wei, H.-C. Lin, *Tetrahedron* **2011**, *67*, 303.

[22] A. Yassin, T. Rousseau, P. Leriche, A. Cravino, J. Roncali, *Sol. Energy Mater. Sol. Cells* **2011**, *95*, 462.

[23] A. Berlin, G. Pagani, G. Zotti, G. Schiavon, *Macromol. Chem. Phys.* **1992**, *193*, 399.

[24] P. Zanirato, P. Spagnolo, G. Zanardi, *J. Chem. Soc., Perkin Trans. 1* **1983**, 2551.

[25] K. Ogawa, S. C. Rasmussen, *J. Org. Chem.* **2003**, *68*, 2921.

[26] K. Ogawa, K. R. Radke, S. D. Rothstein, S. C. Rasmussen, *J. Org. Chem.* **2001**, *66*, 9067.

[27] M. S. Driver, J. F. Hartwig, *J. Am. Chem. Soc.* **1996**, *118*, 7217.

[28] J. F. Hartwig, *Angew. Chem.* **1998**, *110*, 2154; *Angew. Chem. Int. Ed.* **1998**, *37*, 2046.

[29] J. P. Wolfe, S. Wagaw, S. L. Buchwald, *J. Am. Chem. Soc.* **1996**, *118*, 7215.

[30] G. Koeckelberghs, L. De Cremer, A. Persoons, T. Verbiest, *Macromolecules* **2007**, *40*, 4173.

[31] S. Gronowitz, *Acta Chem. Scand. B* **1961**, *15*, 1393.

[32] U. Dahlmann, R. Neidlein, *Helv. Chim. Acta* **1996**, *79*, 755.

[33] S. Gronowitz, A.-B. Hörnfeldt, *Thiophenes*, Elsevier, Oxford, **2004**.

[34] S. J. Evenson, S. C. Rasmussen, *Org. Lett.* **2010**, *12*, 4054.

[35] R. Fitzner, E. Reinold, A. Mishra, E. Mena-Osteritz, H. Ziehlke, C. Körner, K. Leo, M. Riede, M. Weil, O. Tsaryova, A. Weiß, C. Uhrich, M. Pfeiffer, P. Bäuerle, *Adv. Funct. Mater.* **2011**, *21*, 897.

[36] M. S. Wrackmeyer, M. Hummert, H. Hartmann, M. K. Riede, K. Leo, *Tetrahedron* **2010**, *66*, 8729.

[37] G. Koeckelberghs, L. De Cremer, W. Vanormelingen, W. Dehaen, T. Verbiest, A. Persoons, C. Samyn, *Tetrahedron* **2005**, *61*, 687.

[38] M. Schnürch, M. Spina, A. F. Khan, M. D. Mihovilovic, P. Stanetty, *Chem. Soc. Rev.* **2007**, *36*, 1046.

[39] S. A. Odom, K. Lancaster, L. Beverina, K. M. Lefler, N. J. Thompson, V. Coropceanu, J.-L. Brédas, S. R. Marder, S. Barlow, *Chem. Eur. J.* **2007**, *13*, 9637.

[40] A. Yassin, P. Leriche, J. Roncali, *Macromol. Rapid Commun.* **2010**, *31*, 1467.

[41] S. Gronowitz, A. Hallberg, T. Frejd, *Tetrahedron* **1979**, *35*, 2607.

[42] F. B. Iteke, L. Christiaens, M. Renson, *Tetrahedron* **1976**, *32*, 689.

[43] N.N., *Khim. Geterotsikl. Soedin.* **1978**, *4*, 435.

[44] G. Fuhrmann, G. Nelles, A. B. Zilai, A. Yasuda (Sony Corporation), WO2009/053108A1, **2009**.

[45] P. J. Beswick, C. C. F. Hamlett, V. Patel, M. L. Sierra, N. G. Ramsden (Glaxo Group Limited), WO02/092590A1, **2002**.

[46] H. Chen, H. Huang, Z. Tian, P. Shen, B. Zhao, S. Tan, *Eur. Polym. J.* **2010**, *46*, 673.

[47] H. Chen, H. Huang, X. Huang, J. N. Clifford, A. Forneli, E. Palomares, X. Zheng, L. Zheng, X. Wang, P. Shen, B. Zhao, S. Tan, *J. Phys. Chem. C* **2010**, *114*, 3280.

[48] E. Brier, Bachelor thesis, University Ulm (Ulm), **2011**.

[49] C. M. Cardona, W. Li, A. E. Kaifer, D. Stockdale, G. C. Bazan, *Adv. Mater.* **2011**, *23*, 2367.

[50] A. Mishra, P. Bäuerle, *Angew. Chem.* **2012**, *124*, 2060; *Angew. Chem. Int. Ed.* **2012**, *51*, 2020.

[51] Y. Sun, G. C. Welch, W. L. Leong, C. J. Takacs, G. C. Bazan, A. J. Heeger, *Nat. Mater.* **2012**, *11*, 44.

[52] P. Franchetti, L. Cappellacci, G. A. Sheikha, H. N. Jayaram, V. V. Gurudutt, T. Sint, B. P. Schneider, W. D. Jones, B. M. Goldstein, G. Perra, A. De Montis, A. G. Loi, P. La Colla, M. Grifantini, *J. Med. Chem.* **1997**, *40*, 1731.

[53] J. Hollinger, A. A. Jahnke, N. Coombs, D. S. Seferos, *J. Am. Chem. Soc.* **2010**, *132*, 8546.

[54] C. Steck, Bachelor thesis, Ulm Umiversity (Ulm), **2011**.

[55] H. Nakanishi, S. Inoue, T. Otsubo, *Mol. Cryst. Liq. Cryst.* **1997**, *296*, 335.

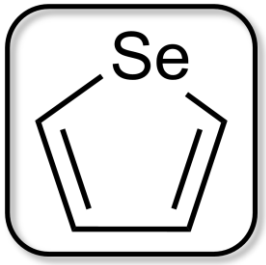

CHAPTER 5

BENZOTHIADIAZOLE-BASED ORGANIC SENSITIZERS

This project was accomplished in collaboration with the group of Prof. Michael Grätzel in Lausanne who fabricated and characterized the solar cells. They also carried out the quantumchemical calculations and photophysical investigations. A different font (Cambria) was used for the paragraphs that were written in collaboration with the Grätzel group and have been published in the following article: S. Haid, M. Marszałek, A. Mishra, M. Wielopolski, J. Teuscher, J.-E. Moser, R. Humphry-Baker, S. M. Zakeeruddin, M. Grätzel, P. Bäuerle, Adv. Funct. Mater. **2012**, 22, 1291.

5.1 Introduction

Dye-sensitized solar cells (DSSC) are one of the most promising environmental-friendly photovoltaic devices because of their low material costs and easy manufacturing process (for a detailed description of the functional principle see **Chapter 2**).[1-3] DSSCs based on ruthenium complexes have broad absorption spectra extending into the near-IR region, and for about 20 years they held the record in solar-to-electrical energy conversion efficiency with PCEs of up to 11.5% under AM 1.5 illumination.[3-5] The most efficient among these ruthenium sensitizers are the bipyridine complexes **N3**,[4-5] **N719**[5-7] and **CYC-B11**,[8] or terpyridine complexes such as the "**black dye**"[9-11] (structures see **Chapter 2**). However, ruthenium complexes also present certain disadvantages, e.g., use of expensive ruthenium, tedious purification processes and relatively low molar extinction coefficients in the visible region. In 2011, a zinc porphyrin dye established a new efficiency record of 12.3% (see **Chapter 2**).[12] In that work, a new cobalt(II)/cobalt(III) redox couple was used instead of the commonly used iodide/triiodide couple.

The PCEs of metal-free organic dyes are lower (≥ 10%) in comparison to the ruthenium-based sensitizers, but organic dyes present several advantages, such as lower material costs, higher extinction coefficients, and better tunable absorption and band gap by variation of the molecular structure. Metal-free organic dyes typically consist of a π-conjugated donor-acceptor (D-A) system with an anchoring group for efficient adsorption on TiO_2. A plethora of D-π-A-substituted organic dyes have been prepared and used as sensitizers in DSSCs.[13-16] The most efficient organic sensitizers in liquid electrolyte DSSCs achieved efficiencies of up to 10.3%, both in devices with the iodide/triiodide redox couple (dye **C229**)[17] and cobalt(II)/cobalt(III) redox couple (dye **C219**)[18] (see **Chapter 2**). Dye **C219** also showed a remarkable efficiency of 8.9% in a device with an ionic liquid electrolyte. The current record efficiency for a solid-state DSSC, obtained with dye **C220**, is 6.08%.[19]

One of the drawbacks of organic dyes is their relatively narrow absorption spectra, whose maxima usually remain in the shorter wavelength region. The optimal organic sensitizer should possess a broadly extended absorption spectrum ranging to the near-IR regime in order to attain good overlap

with the solar emission spectrum and to produce large photocurrents. In addition, the HOMO and LUMO energy levels of the dye need to match the iodide/triiodide redox potential and the conduction band edge level of the TiO_2 semiconductor electrode in order to assure efficient electron injection into the TiO_2 conduction band. For an unidirectional electron flow, the electron density distribution in the dye's HOMO and LUMO is also of crucial importance. One way of extending the absorption range in order to enhance the photocurrent response is to reduce the HOMO-LUMO energy gap of the sensitizer. For this purpose, various low band gap sensitizers for DSSCs have been prepared by implementing, e.g., the electron-deficient benzothiadiazole (BTDA) unit into the bridging framework of D-π-A molecules.[20-25]

Following the same approach, we designed four novel D-A sensitizers **16**-**19** (**Figure 5.1**). Dyes **16**-**18** consist of a triarylamine donor, a conjugated π-bridge and a BTDA-substituted cyanoacrylic acid as acceptor and anchoring group. As π-bridge, thieno[3,2-*b*]thiophene (dye **16**), 2,2'-bithiophene (dye **17**) and 2,2'-biselenophene (dye **18**) were used. Dye **19** contains the same π-bridge as dye **17** with an additional phenyl ring between the BTDA unit and the anchoring group. Dyes **16**-**19** were characterized with optical and electrochemical methods and used as sensitizers in liquid electrolyte DSSCs. For dyes **17** and **19**, the devices were optimized by variation of the electrolyte composition. Furthermore, these two dyes were intensively investigated with photophysical methods.

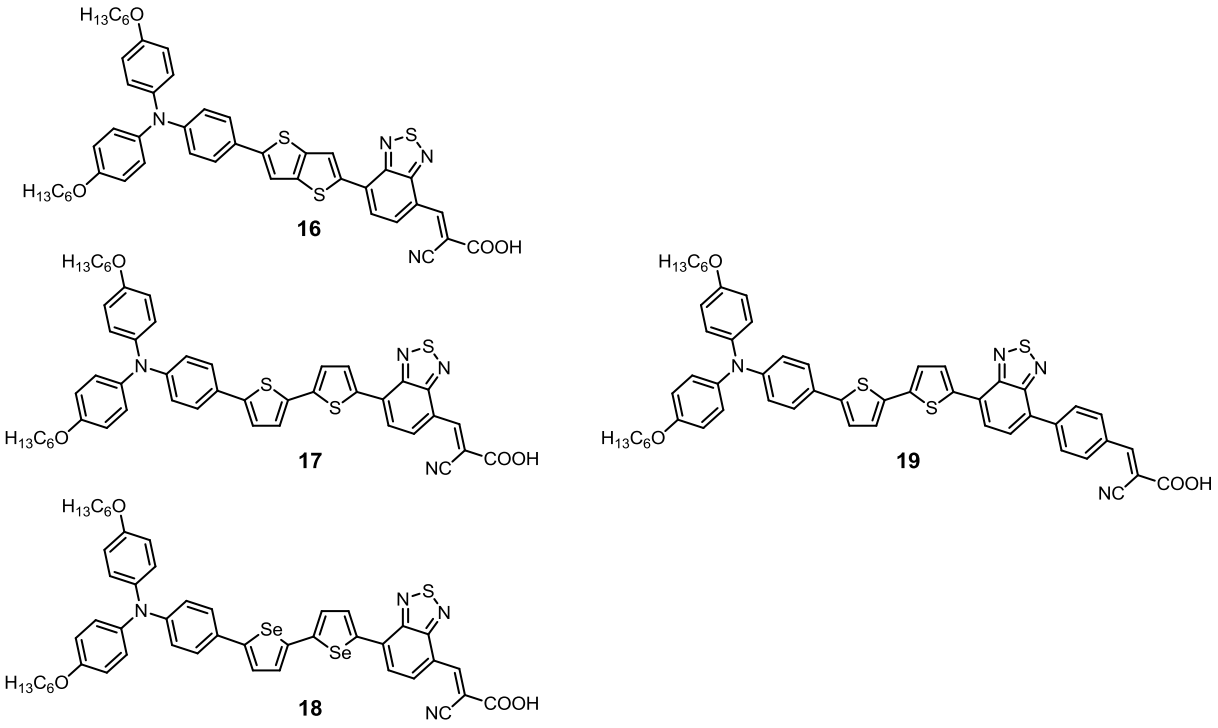

Figure 5.1: Investigated dyes **16**-**19**.

5.2 Synthesis of Dyes 16-19

The sensitizers **16**-**18** were synthesized on a convergent route by Stille cross-coupling of the stannylated building blocks **86a**-**c**, which comprised the donor and the π-bridge, and the brominated benzothiadiazole-carbaldehyde **84** (**Scheme 5.1** and **Scheme 5.2**). In the last step, the anchoring group was introduced by Knoevenagel condensation with cyanoacetic acid.

The first building block, benzothiadiazole **82,** was synthesized according to a literature procedure from benzo[*c*][1,2,5]thiadiazole by monobromination to 4-bromobenzo[c][1,2,5]thiadiazole[26] and subsequent bromomethylation with trioxane and aq. HBr.[27] In ref. [27] compound **82** was directly oxidized to aldehyde **84** in 74% yield with sodium periodate in refluxing DMF. However, this result could not be reproduced because product **84** could not be separated from an unknown by-product. Therefore, a small detour was taken. The bromomethylated compound **82** was hydrolyzed with potassium carbonate (3 eq.) in a dioxane/water mixture to obtain alcohol **83** in 64% yield. These reaction conditions were chosen according to a procedure for the synthesis of 5-hydroxymethyl-benzo[*c*][1,2,5]thiadiazole.[28] Finally, alcohol **83** was oxidized with manganese oxide[28] (4 eq.) in refluxing chloroform to obtain aldehyde **84** in 90% yield.

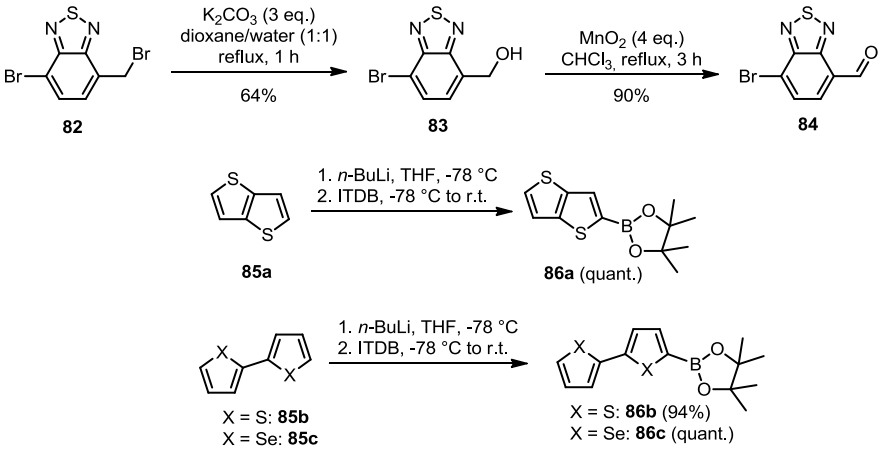

Scheme 5.1: Synthesis of building blocks **84** and **86a-c**.

The synthesis of the donor/π-bridge building block started from the respective π-bridging units thieno[3,2-*b*]thiophene **85a**,[29] 2,2'-bithiophene **85b**,[30] and 2,2'-biselenophene **85c**,[31] which were synthesized according to literature methods. They were lithiated with *n*-BuLi (1 eq.) in THF at -78 °C, and then quenched with ITDB (1 eq.) to obtain the pinacol boronic esters **86a**-**c** in quantitative or almost quantitative yields.

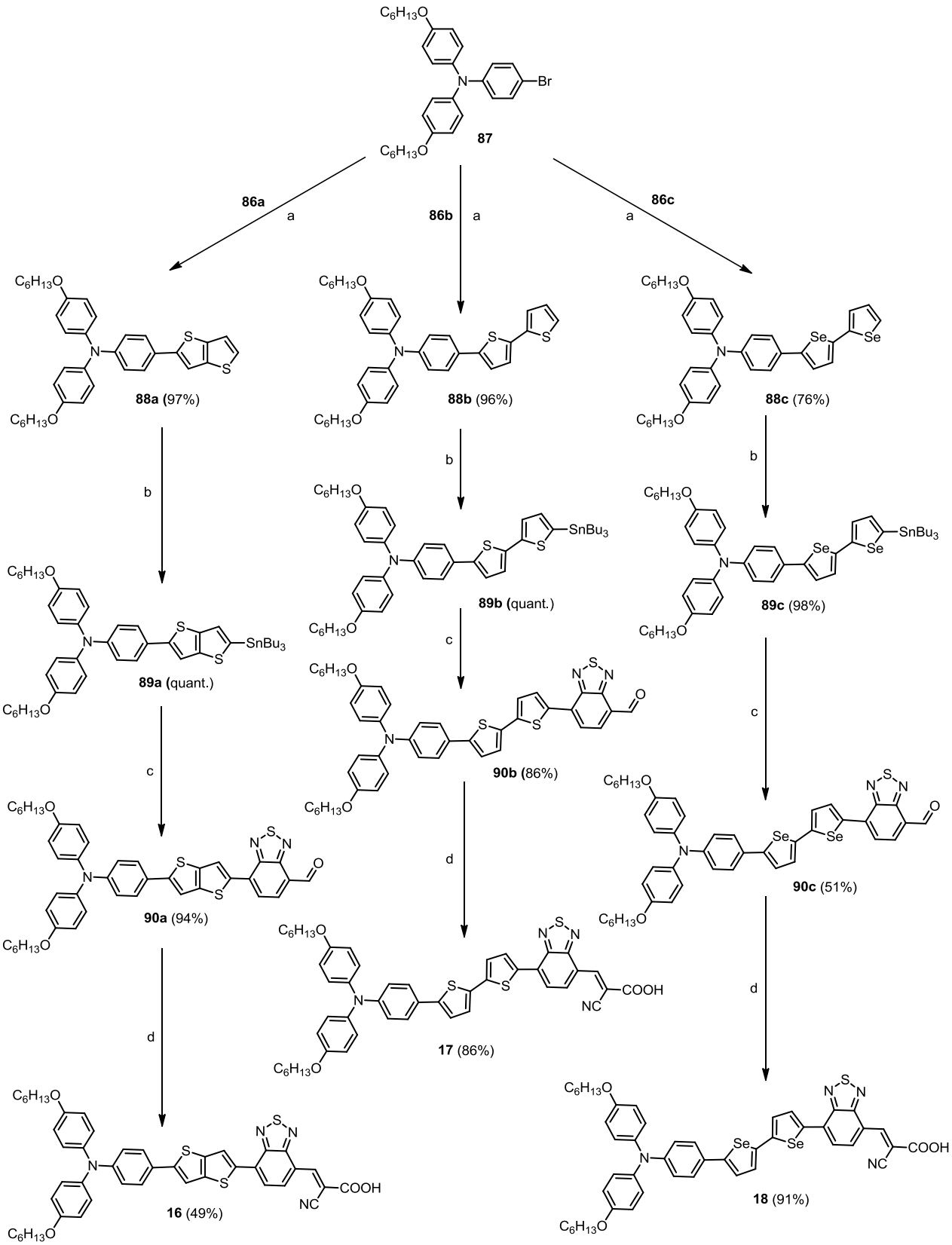

Scheme 5.2: Synthesis of dyes **16**-**18**: (a) $Pd_2(dba)_3{\cdot}CHCl_3$, $HP^tBu_3BF_4$, 2 M aq. K_3PO_4 (4 eq.), THF, r.t.; (b) (i) n-BuLi, THF, - 78 °C (ii) $SnBu_3Cl$; (c) **84**, $Pd(PPh_3)Cl_2$, THF, reflux, 4-22 h; (d) cyanoacetic acid, NH_4OAc or piperidine, CH_2Cl_2/CH_3CN, reflux.

These boronic esters were coupled with the brominated triphenylamine donor **87** in a Suzuki-Miyaura cross-coupling using $Pd_2(dba)_3{\cdot}CHCl_3/HP^tBu_3BF_4$ as catalytic system (**Scheme 5.2**). The coupling products were obtained in good (76% for biselenophene **88c**) to excellent yields (97% for thienothiophene **88a** and 96% for bithiophene **88b**). Lithiation of compounds **88a**-**c** with *n*-BuLi in THF at -78 °C and subsequent quenching with tributyltin chloride afforded stannyl compounds **89a**-**c** in quantitative yields. Stille-type cross-coupling of **89a**-**c** with benzothiadiazole derivative **84** using $Pd(PPh_3)_2Cl_2$ as catalyst gave aldehydes **90a** and **90b** in very good yields of 94% and 86%, respectively. For aldehyde **90c** only a moderate yield of 51% was obtained. This might be due to the lower stability of the stannyl compound, whose stannyl group was completely cleaved of after storage at r.t. for several weeks. Final Knoevenagel condensation of aldehyde **90a** with cyanoacetic acid in a DCM/acetonitrile mixture and in the presence of piperidine as catalyst yielded D-A-dye **16** in 49% yield. For the Knoevenagel condensation of aldehydes **90b** and **90c**, ammonium acetate was used instead of piperidine, and the yields were improved to 86% for dye **17** and 91% for dye **18**.

Sensitizer **19** was synthesized by coupling of stannylated triphenylaminobithiophene **89b** with brominated phenyl-BTDA-carbaldehyde **91** (**Scheme 5.3**). The latter had been synthesized in a rather low yield of 25% via a Suzuki coupling of 4,7-dibromobenzo[c][1,2,5]thiadiazole[26] and commercially available (4-formylphenyl)boronic acid according to a literature procedure.[32] The Stille coupling was carried out with $Pd(PPh_3)_2Cl_2$ (3 mol%) in THF at 75 °C for 4.5 h and the desired D-A-dye **92** was obtained in an excellent yield of 92% after column chromatography. In the last step, aldehyde **92** was reacted in a Knoevenagel condensation with cyanoacetic acid using ammonium acetate as catalyst. After column chromatography dye **19** was obtained in 38% yield. The lower yield is due to losses during the several chromatography steps that were necessary to purify the compound completely.

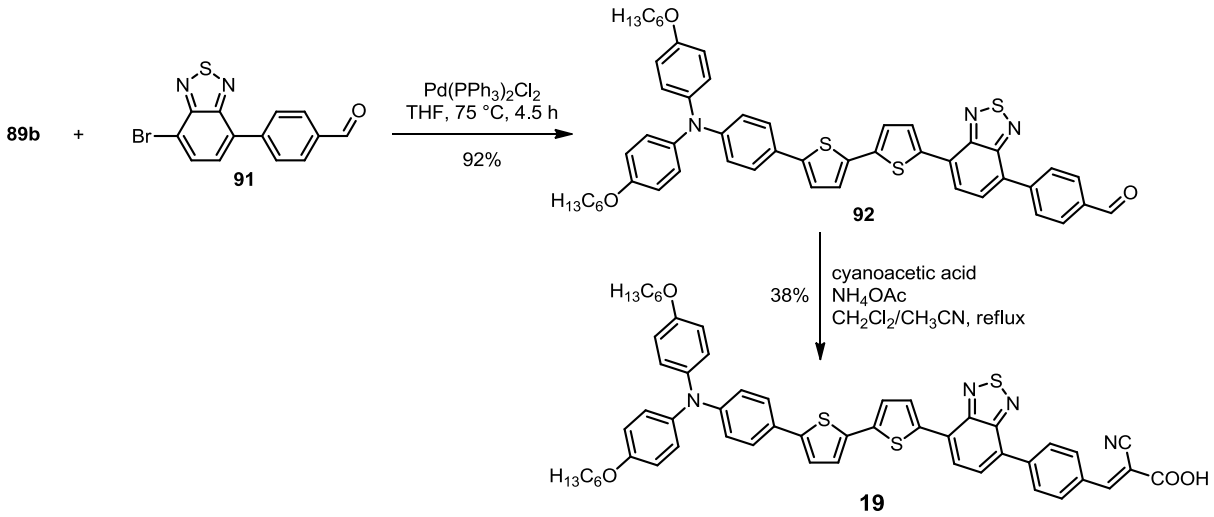

Scheme 5.3: Synthesis of dye **19**.

5.3 Optical and Electrochemical Properties of Dyes 16-19

The UV-Vis absorption spectra of dyes **16**-**18** are shown in **Figure 5.2a**, whereas the UV-Vis absorption and emission spectra of the bithiophene-based dyes **17** and **19** are compared in **Figure 5.2b**. All spectra were measured in dichloromethane. The data are summarized in **Table 5.1**.

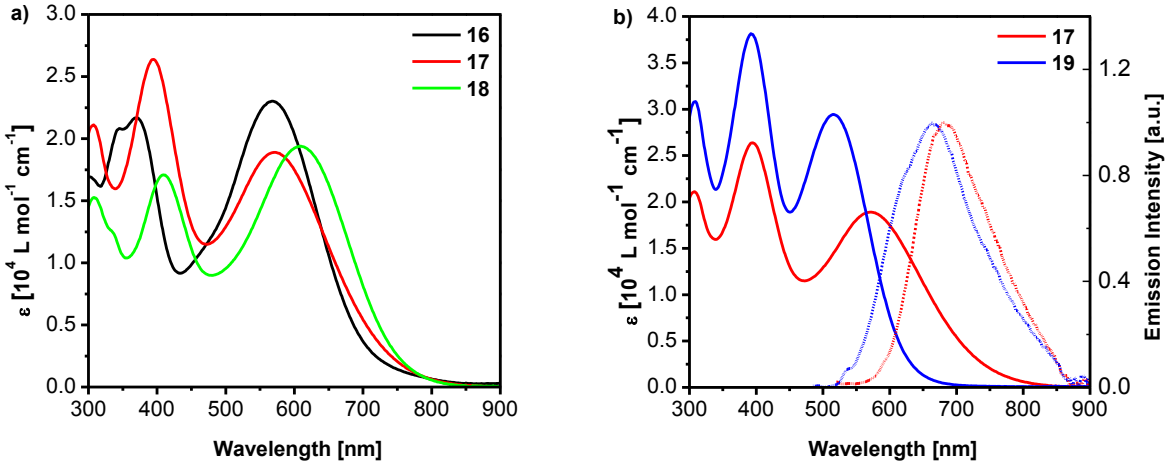

Figure 5.2: (a) UV-Vis absorption spectra of dyes **16**-**18** in dichloromethane. (b) UV-Vis absorption and emission spectra of dye **17** and **19** in dichloromethane.

All dyes exhibit three absorption bands over a range of 300 to 800 nm. The absorption band between 350 to 450 nm corresponds to the π-π* transitions of the conjugated system. The low energy bands between 570 nm and 610 nm were assigned to a charge transfer (CT) transition from the donor to the acceptor moiety. The CT transition shifts from 569 nm for thienothiophene dye **16** to 579 nm for bithiophene dye **17** and 609 nm for biselenophene dye **18**. Thus, the replacement of thiophene by selenophene leads to a significant red-shift of 30 nm. The insertion of BTDA as low band gap chromophore between the linker and anchoring group caused a red shift of 30-110 nm compared to corresponding dyes without this chromophore.[33-35] Furthermore, attachment of the BTDA unit directly to the acceptor resulted in a bathochromic shift of the spectral response compared to dyes comprising a central BTDA unit.[20]

The longest wavelength absorption of dye **19** (515 nm) is significantly blue-shifted compared to the CT-band of dye **17** (570 nm) although dye **19** contains an additional phenyl ring which should lead to a longer conjugated system and, consequently, to a red-shifted absorption. Simultaneously, the intensity and molar extinction coefficient for the CT transition of dye **19** (ε = 29,400 L mol^{-1} cm^{-1}) is increased by a factor of 1.6 compared to dye **17** (ε = 18,900 L mol^{-1} cm^{-1}). The emission maxima of dyes **17** and **19** can be found at 681 and 665 nm, respectively. Dye **19** shows a much larger Stokes shift (4,379 cm^{-1}) in comparison to **17** (2,860 cm^{-1}), which is an indication of significant structural reorganization of **19** upon photoexcitation.

Table 5.1: Optical and electrochemical data of dyes **16**-**19**.

compound	$\lambda_{max,abs}$ [nm]	ε_{max} [L mol^{-1} cm^{-1}]	$\lambda_{max,em}$ [nm]	E^0_{ox1} [V]	E^0_{ox2} [V]	E^0_{red} [V]	HOMO [eV][a]	LUMO [eV][a]	E_g^{CV} [eV][b]	E_g^{opt} [eV][c]
16	302	16,900	679	0.20	0.72	-1.56	-5.22	-3.63	1.59	1.76
	371	21,700								
	569	23,000								
17	308	21,000	681	0.20	0.61	-1.58	-5.22	-3.63	1.59	1.67
	395	26,400								
	570	18,900								
18	308	15,300	686	0.16	0.52	-1.51	-5.17	-3.71	1.46	1.65
	410	17,100								
	609	19,400								
19	308	30,800	665	0.11	0.47	-1.75	-5.14	-3.47	1.67	1.98
	392	38,000								
	515	29,400								

[a]Calculated vs. Fc^+/Fc = -5.1 eV.[36] [b] Calculated from the difference between the values of $E_{onset, red1}$ and $E_{onset, ox1}$. [c]Estimated using the onset of the UV-Vis spectra in dichloromethane.

The UV-Vis spectra of dyes **17** and **19** adsorbed on transparent TiO_2 films (**Figure 5.3**) exhibit a slight blue-shift of the CT band for dye **19** (506 nm) compared to the solution spectra, while the shift is more pronounced for dye **17** (540 nm). These results clearly hint to a reduction of the overall π-conjugation in **19** due to a possible torsion of the additional phenyl ring. This would explain the blue-shifted absorption of dye **19** compared to dye **17**.

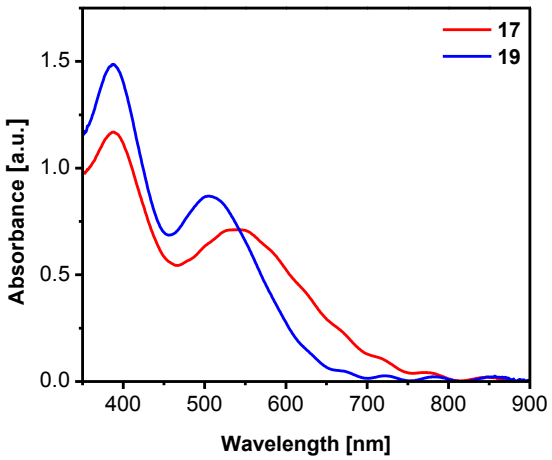

Figure 5.3: UV-Vis spectra of dyes **17** and **19** on a TiO_2 film (5 µm).

The redox properties of the four sensitizers **16**-**19** were measured by cyclic voltammetry in dichloromethane with 0.1 M tetrabutylammonium hexafluorophosphate ($TBAPF_6$) as supporting electrolyte and ferrocene (Fc) as internal standard (**Figure 5.4**). For all four dyes, two reversible oxidation waves were observed. The first oxidation potential corresponds to the oxidation of the triphenylamino moiety and is found between 0.11 and 0.20 V. The second oxidation potential was

assigned to the oxidation of the corresponding π-conjugated linker with decreasing values from 0.72 V for **16** over 0.61 V for **17** to 0.52 V for **18**. This indicates an increasing degree of conjugation going from thieno[3,2-*b*]thiophene to 2,2'-bithiophene and 2,2'-biselenophene.

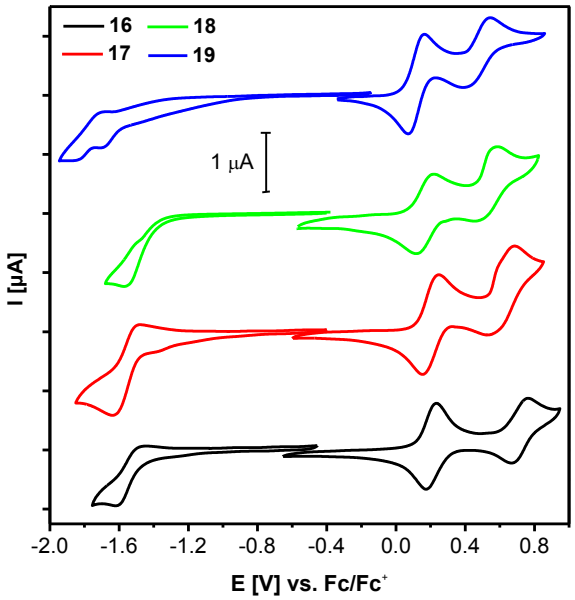

Figure 5.4: Cyclic voltammograms of dyes **16**-**19** in DCM/$TBAPF_6$ (0.1 M), c = 5 × 10^{-4} mol L^{-1}, 295 K, scan rate = 100 mV s^{-1}, vs. Fc^+/Fc.

Compared to dye **17** (E^0_{Ox1} = 0.20 V), the first oxidation potential of dye **19** (E^0_{Ox1} = 0.11 V) is shifted to more negative values. This is another hint for the weaker donor-acceptor interaction in dye **19** due to probable torsion of the phenyl ring. From the onset of the first oxidation potential, HOMO energy levels between -5.20 and -5.10 eV vs. vacuum were calculated for dyes **16**-**19**. In the reductive regime, they show one reduction wave at around -1.5 to -1.6 V. From the onset of this reduction wave, LUMO energy levels were calculated, the values being between -3.47 eV and -3.75 eV vs. vacuum. These LUMO levels lie above the conduction band edge of titanium dioxide (~4.0 eV vs. vacuum), which should ensure a sufficiently high driving force for electron injection from the dye into the conduction band of the semiconductor. Compared to the corresponding dyes without benzothiadiazole,[34-35, 37] sensitizers **16**-**18** showed a lower band gap (~1.6-1.7 eV) due to a lowering of the LUMO energy levels.

5.4 Quantumchemical Calculations for Dyes 17 and 19

In order to gain insight into the electronic structure, the electron density distribution of the frontier orbitals of both dyes was analyzed by density functional theory (DFT) using the B3LYP

hybrid functional with the 6-31G* basis set (see Experimental Section for details). Firstly, the ground state geometries of **17** and **19** were optimized using restricted Hartree-Fock conditions. The calculations show that the CT absorption bands of these dyes are based on HOMO→LUMO transitions. The calculated HOMO and LUMO energies were -4.96 and -3.36 eV, respectively, for **17** and -4.81 and -3.01 eV for **19**. Compared to HOMO and LUMO energies determined by cyclovoltammetry the calculated values are by 0.3-0.4 eV higher but the same trend is observed, i.e. the values for dye **19** are lowered in comparison to dye **17**. In the neutral form, both molecules do not exhibit significant differences in the electron density distribution of the orbitals (**Figure 5.5**).

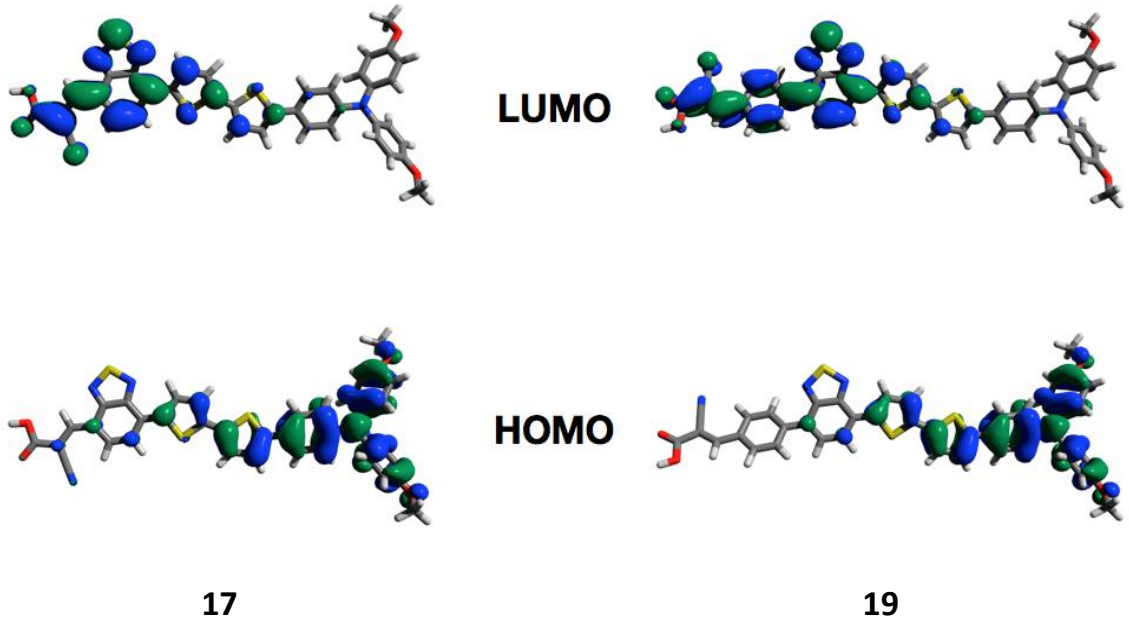

Figure 5.5: HOMO and LUMO electron density distributions for frontier orbitals of dyes **17** and **19** calculated with DFT methods (B3LYP/6-31G*).

The HOMO and LUMO orbitals of dye **17** are slightly more delocalized, giving rise to a better conjugation between the donor and acceptor moiety, which complies well with the outcome of the UV-Vis studies. The additional phenyl ring in dye **19** induces an out-of-plane torsion of 18° with respect to the BTDA moiety. The electron density distribution of the HOMO of both molecules is mainly located on the donor part (oligothiophene and triphenylamine), whereas the electron density of the LUMO is primarily located on the BTDA and cyanoacrylic acid acceptor units and to a small extent on the neighboring thiophene ring. Hence, both orbitals provide sufficient overlap between donor and acceptor to guarantee a fast charge transfer transition. Thus, excitation from the HOMO to the LUMO should lead to efficient photo-induced electron transfer from the electron donating triarylamine moiety to the TiO_2 film via the terminal cyanoacrylic acid. This is nicely corroborated by the almost identical charge separation rates for **17** and **19** as stated in the photophysical section (*vide infra*). Significant differences arise when

the cationic forms of **17** and **19** are considered, which were calculated using the unrestricted Hartree-Fock method. The optimized cationic structure of **17** becomes completely planar with dihedral angles of ~1° each (**Figure 5.6**). In contrast, the BTDA unit and the adjacent phenyl rings in the radical cation of dye **19** are twisted out-of-plane by ~48°. It should be noted that the phenyl ring is more twisted by 30° in the cationic form compared to the neutral state (dihedral angle = 18°).

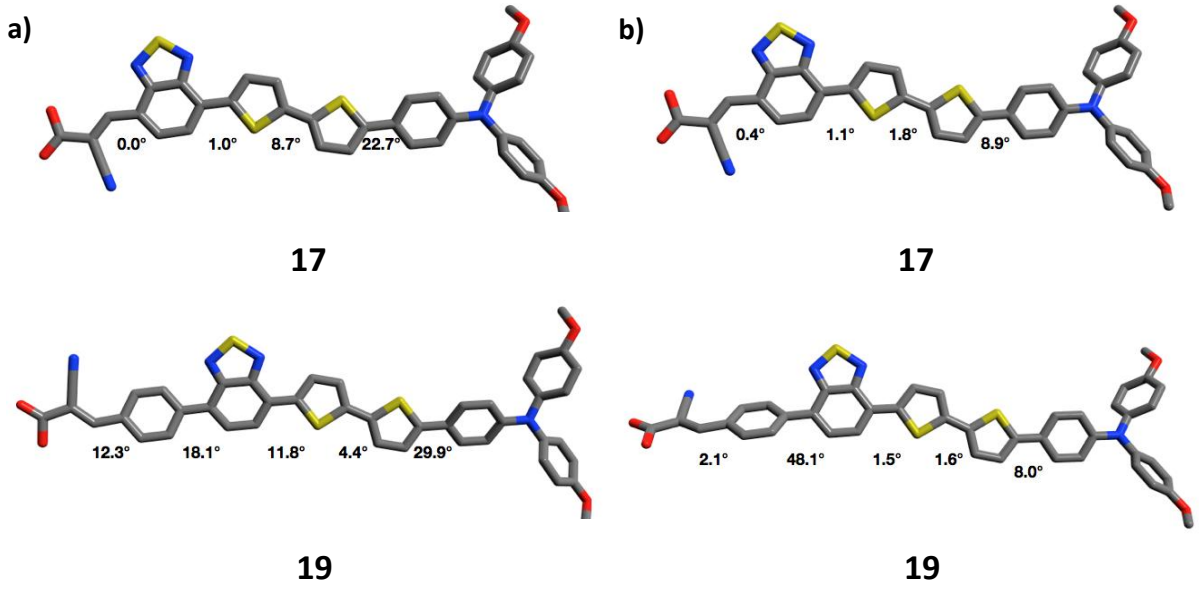

Figure 5.6: Geometry optimized structures of the (a) neutral and (b) cationic species of **17** and **19** with the corresponding dihedral angles between each plane.

This deviation from planarity as suggested by the large Stokes-shift of **19** compared to **17** has also an impact on the orbital energies. The energy of the singly-occupied molecular orbital (SOMO) of **19** (-6.80 eV) is lowered by 0.2 eV compared to **17** (-6.61 eV). This leads to the conclusion that releasing an electron from dye **19** results in a more stable radical cation than in the case of dye **17**. This finding is in good accordance with the difference in solar cell performance of devices with **17** vs. **19** as discussed in the photovoltaic section. As shown below, the charge recombination rates in **19** are remarkably slower due to a better stabilization of its cationic form. Furthermore, the insertion of the phenyl ring in **19** and the consecutive out-of-plane torsion of the adjacent plane upon oxidation lead to an interruption of the π-conjugation between donor and anchoring group. In contrast, the cationic form of **17** remains entirely planar and the π-conjugation is preserved as shown in **Figure 5.6**. This fact is clearly in favor of an *intra*molecular back-electron transfer process as the deactivation pathway of the charge separated state. In other words, the back-electron-transfer within the donor-acceptor moieties of **17** is energetically preferred over the charge recombination from TiO_2 or a regenerating electrolyte.

5.5 Photovoltaic Performance of Dyes 16-19 in DSSCs

Dyes **16**-**19** were used to fabricate dye-sensitized solar cells with the standard electrolyte E1 (**Table 5.3**). The *J*-*V* characteristics of these devices were measured under illumination with standard AM 1.5G simulated sunlight (100 mW cm^{-2}) and are displayed in **Figure 5.7a**. The data is summarized in **Table 5.2**.

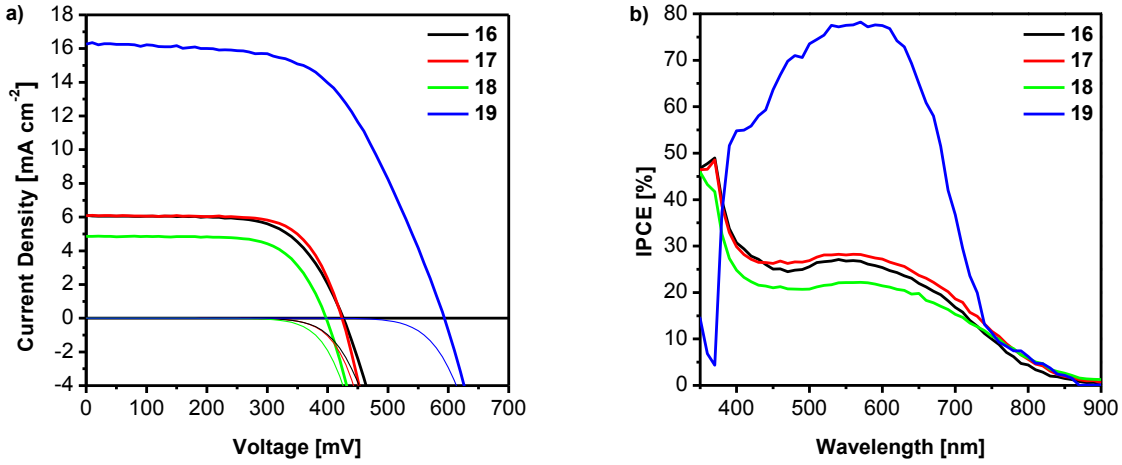

Figure 5.7: (a) Photocurrent density-voltage (*J*-*V*) characteristics of devices using sensitizers **16**-**19** under AM 1.5G illumination (100 mW cm^{-2}). Thin layer 5 µm TiO_2 film, electrolyte E1. Cells were tested using a metal mask with an aperture area of 0.159 cm^2. (b) Incident photon-to-current efficiency (IPCE) spectra of the same devices.

The cell sensitized with dye **19** provides a J_{sc} of 16.26 mA cm^{-2}, a V_{oc} of 0.593 V and a FF of 0.57, yielding an overall power conversion efficiency of 5.59%. The J_{SC} and V_{OC} values for dyes **16** and **17** are almost identical (J_{SC} ≈ 6.05 mA cm^{-2}, V_{OC} ≈ 425 mV) except for a small difference in the FF (**16**: FF = 0.65, **17**: FF = 0.70). This results in similar PCEs of 1.68% for **16** and 1.78% for **17**. The device sensitized with the selenophene derivative **18** yields a lower photocurrent (4.83 mA cm^{-2}) and open-circuit voltage (397 mV), which leads to a lower efficiency of 1.30%. The J_{SC} obtained with dye **19** is significantly higher than for the other dyes, and V_{OC} is increased by almost 140 mV. Hence, the overall performance obtained by sensitization with dye **19** is more than three times higher than for the other dyes in this series.

Figure 5.7b depicts the incident photon to conversion efficiency (IPCE) spectra of the devices with **16**-**19**, which exhibit a broad spectral coverage from 400 nm to 750 nm. The dramatically increased J_{SC} value for dye **19** can also clearly be seen in the IPCE spectra with a maximum of ~78% at 570 nm for the **19**-based device compared to 20-30% at ~550 nm for dyes **16**-**18**. For dyes **17** and **19**, the number of molecules desorbed from TiO_2 films of the same surface area, thickness and porosity was found to be 1.20 × 10^{17} and 1.07 × 10^{17}, respectively. Dye loading experiments showed only a small

difference in the concentration of the two dyes, indicating that the resulting absorptivity is not the reason for the lower J_{SC} of the device with dye **17**.

Table 5.2: Photovoltaic parameters of **16-19** adsorbed on 5 µm nanocrystalline TiO_2 films with electrolyte E1.

dye	J_{SC} [mA cm^{-2}]	V_{OC} [mV]	FF	PCE [%]
16	6.07	426	0.65	1.68
17	6.04	423	0.70	1.78
18	4.83	397	0.68	1.30
19	16.26	593	0.57	5.59

In order to optimize the conditions of the photovoltaic performance for dye **19**, a thicker TiO_2 layer with scattering nanoparticles (8 µm transparent + 5 µm scattering) was used and the LiI content in the electrolyte (coded as E1 to E4, **Table 5.3**) was varied. The photovoltaic parameters in dependence of the LiI content are summarized in **Table 5.4**.

Table 5.3: Composition of electrolytes used for optimization of the performance of the devices with dye **19**. The components were dissolved in a solvent mixture of acetonitrile and valeronitrile (85:15, v/v). DMII: 1,3-dimethylimidazolium iodide; GuNCS: guanidinium thiocyanate; TBP: *tert*-butylpyridine; LiI: lithium iodide.

code	DMII [M]	I_2 [M]	GuNCS [M]	TBP [M]	LiI [M]
E1	0	0.044	0	0.25	1
E2	1	0.03	0.1	0.5	0
E3	1	0.03	0.1	0.5	0.05
E4	1	0.03	0.1	0.5	0.1

Table 5.4: Photovoltaic parameters of dye **17** and **19** adsorbed on nanocrystalline TiO_2 films of different thicknesses. Electrolyte optimization by varying the LiI content and its influence on the photovoltaic parameters of the cells sensitized with dye **19**. Devices were made using single (5 µm) and double layered TiO_2 films (8 µm transparent + 5 µm scattering layer).

dye	electrolyte	LiI content [mM]	TiO_2 film thickness [µm]	J_{SC} [mA cm^{-2}]	V_{OC} [mV]	FF	PCE [%]
17	E1	1000	5	6.04	423	0.70	1.78
19	E1	1000	5	16.26	593	0.57	5.59
17	**E4**	**100**	**8+5**	**3.40**	**489**	**0.74**	**1.24**
19	**E4**	**100**	**8+5**	**18.47**	**640**	**0.69**	**8.21**
19	E2	0	8+5	14.26	688	0.73	7.19
19	E3	50	8+5	17.52	655	0.65	7.26
19	E1	1000	8+5	18.97	558	0.55	5.91

A very high J_{SC} value of 18.97 mA cm^{-2} for a LiI concentration of 1 M (E1) was achieved. Unfortunately, V_{OC} and FF decreased with increasing Li^+ concentration in the electrolyte and on the TiO_2 surface.[38] The system turned out to be very sensitive to the change of Li^+ concentration in the electrolyte and J_{SC} saturated even with small amounts of Li^+. At an optimal LiI concentration of 100 mM (electrolyte E4), an excellent PCE of 8.21% was achieved.

The significant difference in the photocurrents obtained for electrolytes containing different concentrations of Li^+ may be ascribed to an extended electron lifetime in the TiO_2 and suppressed recombination processes while using an electrolyte with higher concentration of Li^+. For the cells with lower content of Li^+, the electron lifetime was one order of magnitude shorter than for the one with 100 mM Li^+ (**Figure 5.8**).

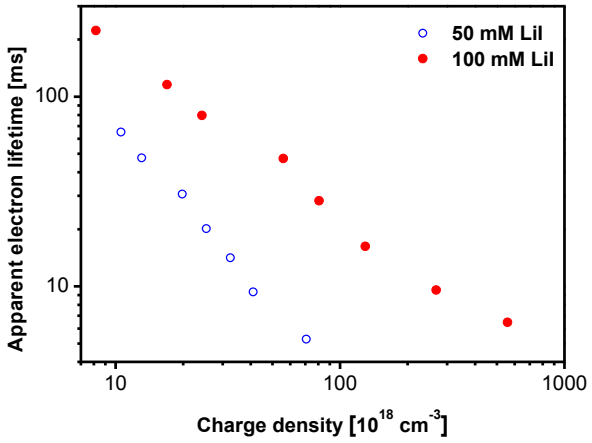

Figure 5.8: Influence of the concentration of Li^+ in the electrolyte on the apparent electron lifetime in TiO_2 for cells sensitized with dye **19**.

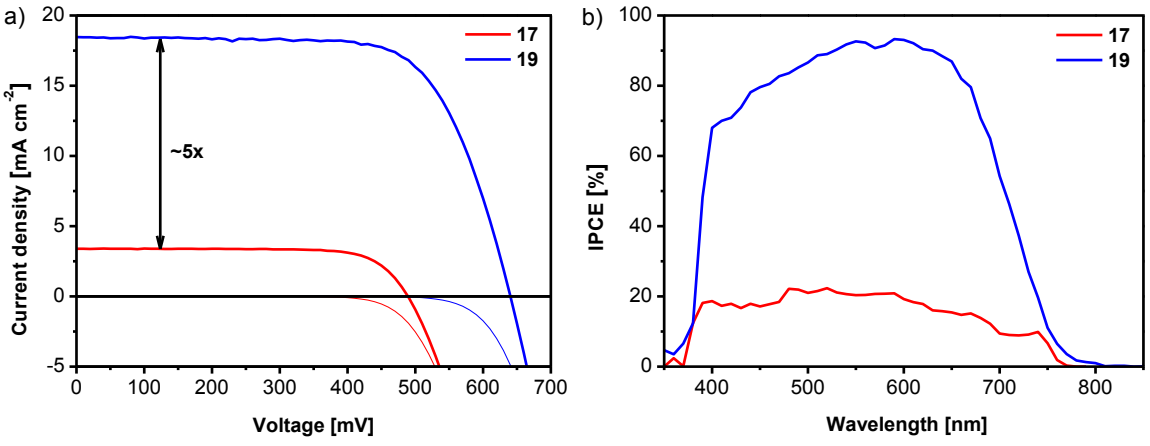

Figure 5.9: (a) *J-V* curves and (b) IPCE spectra for devices sensitized with dye **17** and **19** using a double-layered TiO_2 film (8+5 µm) and electrolyte E4.

The molecular structures of dye **17** and **19** differ only in the additional phenyl ring between the BTDA unit and the anchoring group in dye **19**. Nevertheless, this subtle modification has a significant impact on the photovoltaic performance. In direct comparison with the above

mentioned champion cell of **19**, using electrolyte E4, dye **17** exhibited a more than 5 times lower J_{SC} and the resulting PCE was over 6 times lower as shown in **Figure 5.9a** and **Table 5.4**. The difference in J_{SC} was further confirmed by the IPCE spectra. Both dyes showed a wide spectral coverage of the 380-750 nm region (**Figure 5.9b**), but the maximum IPCE at 600 nm for dye **17** was only 20% as compared to >90% for dye **19**.

5.6 Photophysical Investigation of Dyes 17 and 19

In order to explain the much better photovoltaic performance of dye **19** compared to dye **17**, transient photovoltage and photocurrent measurements were carried out, revealing that the apparent electron lifetime in the case of the device with dye **19** exhibits typical exponential behavior when plotted against charge density in the film. It seems that for dye **17** an asymptotic-like saturation limit exists for the amount of charges injected into TiO_2. Above this limit, the recombination processes are vastly enhanced, thus reducing the lifetime of injected electrons (**Figure 5.10**).

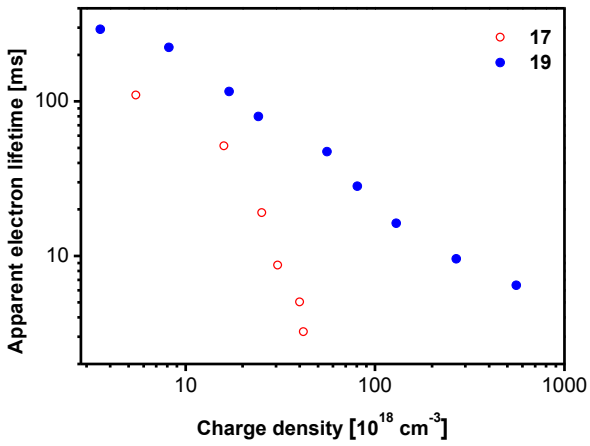

Figure 5.10: Apparent electron lifetimes of dye **17** and **19** measured with the transient photovoltage technique.

The time-correlated single photon counting (TCSPC) technique was used to study the excited state lifetimes of dyes **17** and **19** in solution and adsorbed on the TiO_2 surface (**Figure 5.11**). The lifetimes of the species in solution were in the nanosecond range, 5.6 ns for dye **17** and 7 ns for dye **19**. When the molecules were adsorbed on the TiO_2 layer, the lifetimes decreased significantly as a result of the injection of the electron into the conduction band of the semiconductor. Adsorbed on the TiO_2 substrate, dye **17** is characterized by an excited state lifetime (τ_{TiO2}) of 296 ps, whereas dye **19** is slightly longer-lived (τ_{TiO2} = 373 ps). The estimated electron injection efficiencies for both dyes were found to be fairly similar (dye **17:** 94.8%; dye **19:** 94.7%) (equation 5.1). The lack of a significant difference between electron injection efficiencies cannot explain the difference in device performance of **17** and **19** and may turn the

focus on the charge collection efficiency or enhanced recombination processes as main reasons for the dramatically different performance of the two dyes in DSSCs.

$$\eta_{inj} = 1 - \frac{\tau_{TiO_2}}{\tau_{solution}} \quad (5.1)$$

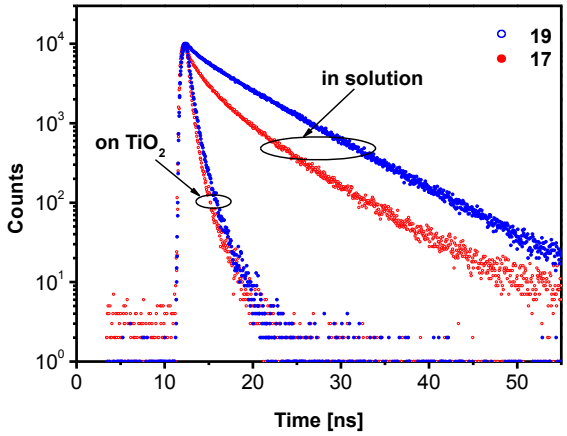

Figure 5.11: Histograms of dyes **17** and **19** dissolved in acetonitrile and adsorbed on the surface of a TiO_2 film. Faster exponential decays when adsorbed on TiO_2 are an indication of efficient electron injection into the semiconductor. There is no significant difference between the injection yields of the two dyes.

Nanosecond laser photolysis experiments focusing on the decay of the oxidized state of the dye performed on TiO_2 films covered with dye **17** and **19** in absence and presence of the redox electrolyte have confirmed 5 times faster recombination (half-reaction time $\tau_{½}$ = 12 µs) in the case of dye **17** (**Figure 5.12**). Spectra recorded in the presence of redox electrolyte exhibited a fast decay (9 μs) due to the efficient regeneration of the oxidized dye molecules by iodide. Nevertheless, in the absence of the redox couple, the dye radical cations can only be reduced by the dye-injected electrons from TiO_2 (recombination). In order to ensure quantitative electron collection at the back contact of the cell, this process must be rather slow and non-competing with the dye regeneration by I^-. This prerequisite is fulfilled in case of dye **19** and allows for the generation of high current densities in the device. In contrast, dye **17** recombines with electrons from TiO_2 in the absence of a redox couple at a time-scale comparable to that of the dye regeneration rate. This undesirable behavior may indicate a facilitated electron flow from the TiO_2 back to the dye radical cation. Furthermore, this is in agreement with the planar molecular geometry of the radical cation of dye **17** as compared to the twisted structure of the radical cation of dye **19** as discussed above. In addition to the TCSPC and nanosecond flash photolysis studies, further insight into the excited state deactivation processes was provided by transient absorption measurements. Dyes **17** and **19** were studied on TiO_2 films in the absence of a redox electrolyte in order to focus particularly on the interactions between the dyes and TiO_2. 530 nm laser excitation was used, which directs the light energy mainly to the CT absorption band of

both dyes. At this wavelength, both dyes exhibit similar extinction coefficients, which allows for a good comparison even at slight variations of film thickness on TiO_2.

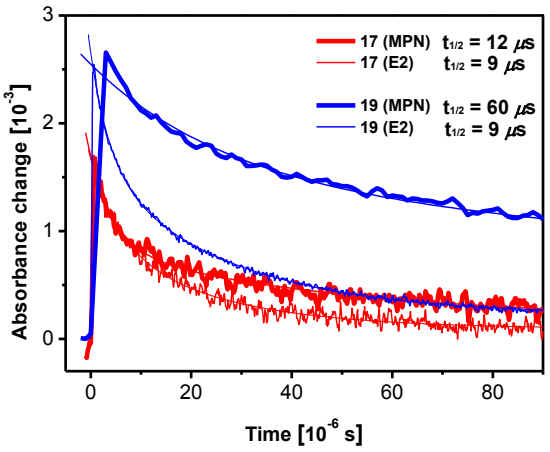

Figure 5.12: Transient absorption data following the decay of the oxidized state of dyes **17** and **19** adsorbed on a transparent TiO_2 nanocrystalline film in presence and absence of a redox couple.

Immediately after laser excitation, the instantaneous formation of the singlet-excited states of dyes **17** and **19** was observed. Those were characterized by a maximum at 501 nm and transient bleach between 535 and 598 nm. After only 0.6 ps singlet-excited features of both dyes transformed into new bands (**Figure 5.13**). This transduction of singlet-excited state energy was then identified by the shift of the minimum of the transient bleach from 555 to 584 nm and a broadening of the signal. The bleaching is attributed to the ground-state bleaching due to the radical cation formation of the triarylamine ($TA^{\bullet+}$), which is represented by the appearance of a new absorption beyond 680 nm (**Figure 5.13**).

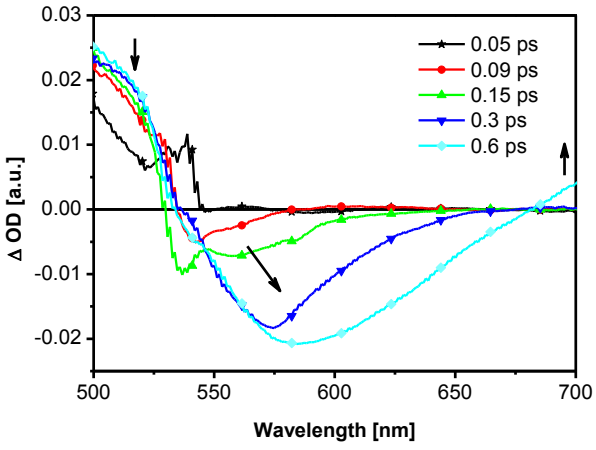

Figure 5.13: Differential absorption spectrum obtained upon femtosecond flash photolysis (λ_{exc} = 530 nm) of a film of **17** on 5 µm thick TiO_2 with several time delays between 0 and 0.6 ps at room temperature, illustrating the radical cation formation with the ground-state transient bleaching between 555 and 590 nm and the triarylamine cation (TA•+) beyond 680 nm.

For both dyes, these features appeared on a time-scale of less than 2 ps. Hence, after a rapid transfer of singlet-excited state energy, the formation of the charge separated state occurs with

equal rate constants for both dyes. Averaging first-order fits of the time-absorption profiles leads to singlet-excited state lifetimes of 0.95 ps for **17** and 0.79 ps for **19**. This supports comparable charge-separation dynamics for both dyes and complies well with the fact that the charge-injection efficiencies will be equal when a redox electrolyte is present.

The analysis of the decay dynamics revealed the key difference between both dyes (**Figure 5.14**). For dye **17**, the ground-state bleaching and the radical cation signature vanished after 300 ps, whereas for **19** they remained visible beyond this time scale. The results clearly revealed the faster recombination process in devices prepared with dye **17** compared to devices with dye **19**.

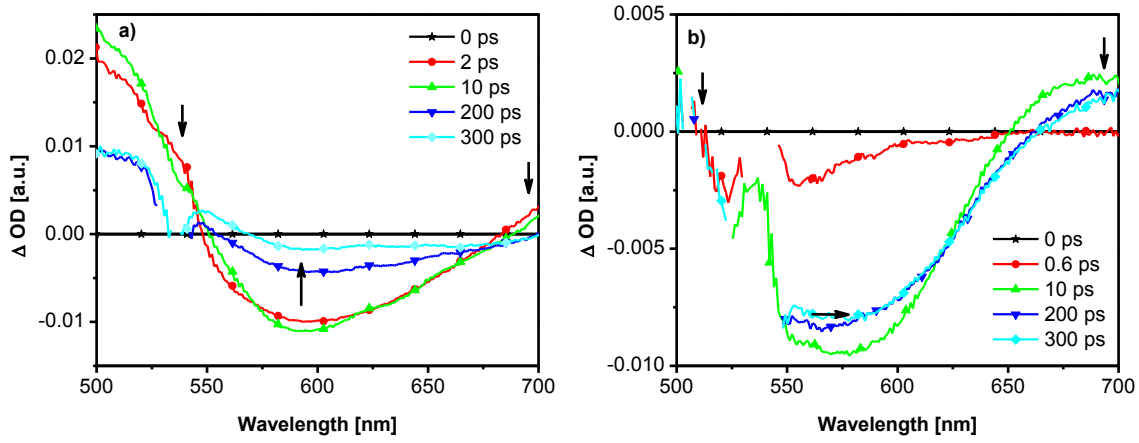

Figure 5.14: Differential absorption spectra obtained upon femtosecond flash photolysis (λ_{exc} = 530 nm) of films of **17** (a) and **19** (b) on 5 µm thick TiO_2 with several time delays between 0 and 300 ps at room temperature, illustrating the different decay dynamics of the radical cation signatures as stated in the text.

In particular, the radical cation features of dye **17** decayed with a lifetime of 18 ps. On the contrary, those of dye **19** were persistent on the time-scale of our experiment (1100 ps) and gave rise to a much higher lifetime of 526 ps (**Figure 5.15**). As a consequence, charge recombination in **17** occurred almost 30 times faster than in **19**, which is in accordance with the fact that the back-electron transfer in the radical cationic form of **17** is facilitated due to the preserved planarity of the π-conjugated system. In other words, dye **17** recombines with electrons from TiO_2 in the absence of a redox couple due to a facilitated electron flow from the TiO_2 back to the dye radical cation. In contrast, the back electron transfer in **19** is hindered by the out-of-plane twist of the additional phenyl ring upon oxidation. This leads to longer lifetimes of the charge-separated state and thus may explain the improved device performances. Importantly, in this context the charge recombination lifetimes do not match the lifetimes obtained by nanosecond laser photolysis because the laser intensities used for the transient absorption studies exceeded the laser power of the nanosecond experiment by two orders of magnitude. Hence, interfacial back electron flow was facilitated due to the high intensities and

the generation of many more electrons per laser pulse. This, on the other hand, led to study much faster charge recombination dynamics as compared with the nanosecond experiments.

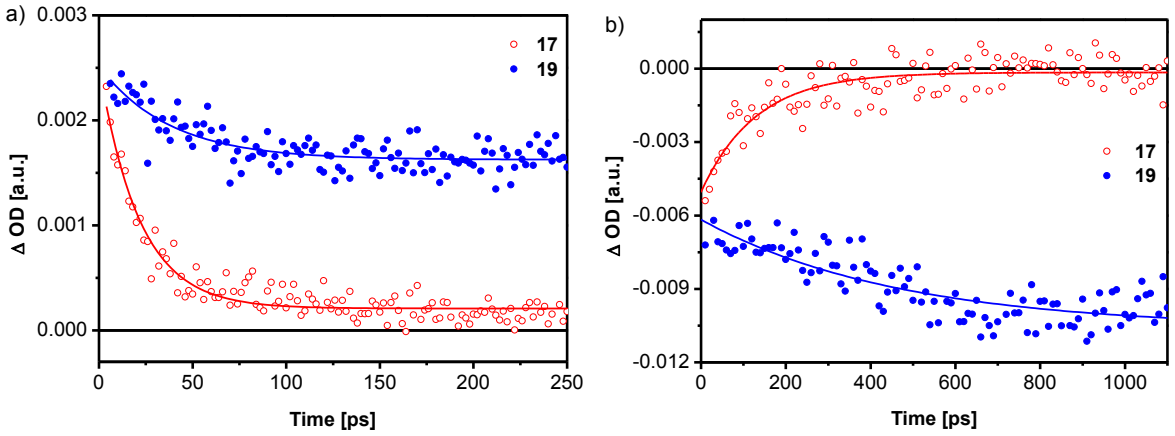

Figure 5.15: First-order-fits of the time-absorption profiles obtained from the femtosecond flash photolysis studies of **17** and **19** illustrating the different charge recombination dynamics of the radical cation signatures at 700 nm (a) and the ground-state bleaching at 580 nm (b).

Electrochemical impedance spectroscopy (EIS) measurements performed on complete cells in the dark revealed that the charge transfer resistance of the TiO_2/electrolyte interface in the cell sensitized with dye **17** was lower than that with dye **19** (**Figure 5.16a**). This may be the reason for faster recombination in the device with dye **17**, which is in accordance with the above-mentioned results.

$$\eta_{coll} = \frac{R_{ct}}{R_{ct} + R_t} \qquad (5.2)$$

Using equation 5.2, where R_{ct} stands for the charge transfer resistance and R_t is the transfer resistance, the charge collection efficiency (η_{coll}) for the best performing cell measured under 0.5 sun with dye **19** was found to be over 90% (**Figure 5.16b**).

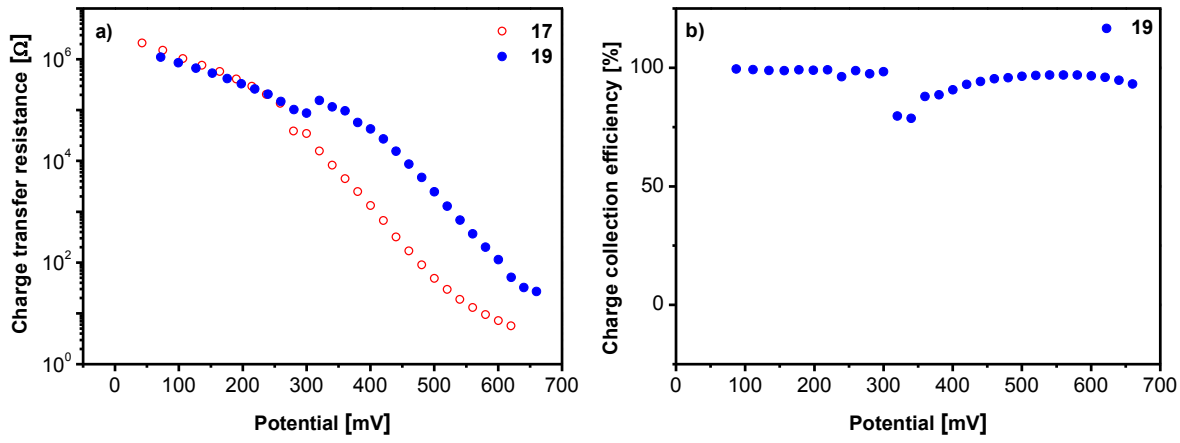

Figure 5.16: (a) Charge transfer resistance as a function of the corrected potential at the TiO_2/electrolyte interface measure by EIS in the dark on the complete cells. (b) Charge collection efficiency for a cell with dye **19** as a function of the corrected potential calculated from EIS measurement under 0.5 Sun.

The fitting of EIS measurements could not provide the values required to calculate the charge collection efficiency for the cell with dye **17** because a Gerischer-type impedance was observed, where the transport resistance R_t and recombination resistance cannot be resolved explicitly.[39] Nevertheless, the presence of Gerischer impedance confirms that the back electron transfer reaction is faster than the transport of charge carriers through the film, which explains the very low J_{SC} measured for the device with dye **17**.

5.7 Summary and Conclusion

A series of low band gap donor-π-acceptor (D-π-A) sensitizers **16**-**18** with different π-bridges and a benzothiadiazole unit adjacent to the anchoring group was synthesized. Thus, the absorption wavelengths were shifted to the NIR-region up to 800 nm and narrow HOMO-LUMO energy gaps of 1.6-1.7 eV were obtained. Although the IPCE spectra of these dyes in DSSCs were extended up to 850 nm, the photocurrent density was relatively low and poor PCEs of 1.3-1.8% were obtained. Furthermore, a fourth sensitizer **19** was synthesized by insertion of an additional phenyl unit between the BTDA moiety and the anchoring group in dye **17**. Sensitizer **19** exhibited a blue-shifted absorption spectrum and a smaller Stokes shift compared to **17**, which pointed towards a possible twist of the additional phenyl ring with respect to the π-conjugated donor and BTDA part. Under optimized conditions, dye **19** exhibited a more than six times higher PCE (8.21%) in DSSCs than dye **17** (1.24%). The reasons hereof were elucidated by theoretical calculations and photophysical investigations. DTF calculations revealed that upon formation of the radical cation of **19** the out-of-plane torsion of the adjacent BTDA and cyanoacrylic acid unit was enhanced leading to an interruption of the π-conjugation between donor and anchoring group. The formation of a stable radical cation and the interruption of the π-conjugation between the donor and acceptor inhibited the back electron transfer. In particular, the electron injection rate was barely affected, but the recombination reaction of **19** was slowed down over 5 times compared to **17**.

5.8 Experimental Section

Instruments and Measurements

NMR spectra were recorded on a Bruker AMX 500 (^{1}H NMR: 500 MHz, ^{13}C NMR: 125 MHz) or an Avance400 spectrometer (^{1}H NMR: 400 MHz, ^{13}C NMR: 100 MHz), normally at 25 °C. Chemical shift values (δ) are expressed in parts per million using residual solvent protons (^{1}H NMR, δ_H = 7.26 for $CDCl_3$ and δ_H = 2.50 for DMSO-d_6; ^{13}C NMR, δ_C = 77.0 for $CDCl_3$ and δ_C = 39.43 for DMSO-d_6) as

internal standard. The splitting patterns are designated as follows: s (singlet), d (doublet), t (triplet), q (quartet) and m (multiplet). The assignments are Ph-H (phenyl protons), CHO (aldehyde protons), TT-H (thienothiophene protons), Sel-H (selenophene protons), Th-H (thiophene protons), BTDA-H (benzothiadiazole protons), HexOPh-H (4-hexyloxyphenyl protons). Melting points were determined using a Büchi B-545 apparatus and were not corrected. Elemental analyses were performed on an Elementar VarioEL. Thin layer chromatography was carried out on aluminum plates, pre-coated with silica gel, Merck Si60 F_{254}. Preparative column chromatography was performed on glass columns packed with silica gel, Merck Silica 60, particle size 40 − 63 µm. EI mass spectra were recorded on a Varian Saturn 2000 GC-MS, CI mass spectra on a Finnigan MAT SSQ-7000 and MALDI-TOF mass spectra on a Bruker Daltonics Reflex III. High resolution MALDI-TOF mass spectra were recorded on a Bruker solariX mass spectrometer.

Optical and Cyclic Voltammetry Measurements

Optical measurements were carried out in 1 cm cuvettes with Merck Uvasol grade solvents, absorption spectra recorded on a Perkin Elmer Lambda 19 spectrometer. Transparent TiO_2 films (5 µm) screen printed onto a FTO substrate were immersed in 0.3 mM dye solutions in chlorobenzene for 4 h. UV-Vis spectra were measured with a CARY 5 UV-Vis-NIR spectrophotometer (Varian, Inc.). Cyclic voltammetry experiments were performed with a computer-controlled Autolab PGSTAT30 potentiostat in a three-electrode single-compartment cell with a platinum working electrode, a platinum wire counter electrode, and an Ag / AgCl reference electrode. All potentials were internally referenced to the ferrocene/ferrocenium couple.

Computational Details.

All molecular orbital calculations were carried out using the Gaussian 09 suite[40] of programs with the B3PW91[41-42] and B3LYP[43] hybrid functionals and the 6-31G*[44-45] basis set. First, the ground state geometries of **17** and **19** were optimized using the restricted Hartree-Fock method. To ensure that the resulting structures represented the global minimum on the potential energy surface we computed the geometries using the B3LYP functional and the semi-empirical AM1* level[46-47] as implemented in VAMP 10.0 software package29. The resulting deviation of the dihedral angles between the BTDA and phenyl ring was less than 1˚, which assured the global minimum. The long hexyloxy chains, which have no significant impact on the frontier orbitals of the chromophores, were replaced with methoxy-substituents in order to accelerate the convergence of optimizations.

Device Fabrication

Screen-printed double layers of TiO_2 particles were used as photoelectrodes in this study. For transparent films, a 5 µm thick layer of 20 nm-sized TiO_2 particles was printed on the fluorine doped

SnO_2 (FTO) conducting glass electrode. Double layered films consisted of a 8 μm thick transparent layer of 20 nm-sized TiO_2 covered with a 5 μm thick scattering layer of 400 nm sized TiO_2 particles. The porosity was evaluated as 67% for the 20 nm TiO_2 transparent layer and 42% for the scattering layer, determined from BET measurements. After sintering at 500 °C and cooling to 80 °C, the sintered TiO_2 electrodes were sensitized by dipping for 5 h in the respective dye solution (0.3 mM of the dye with 2 mM of chenodeoxycholic acid, CDCA, in chlorobenzene), and then assembled using a thermally platinized FTO/glass counter electrode. The working and counter electrodes were separated by a 25 μm thick hot melt ring (Surlyn, DuPont) and sealed by heating. The cell's internal space was filled with electrolyte using a vacuum pump. The composition of the electrolytes is given in **Table 5.3**. The electrolyte-injecting hole on the thermally platinized FTO glass counter electrode was finally sealed with a Surlyn sheet and a thin glass cover by heating. Cells were equipped with self-adhesive anti-reflective foil that acted as UV-cut-off filter.

Photovoltaic Characterization

A 450 W xenon light source (Oriel, USA) was used to characterize the solar cells. The spectral output of the lamp was matched in the region of 350–750 nm with the aid of a Schott K113 Tempax sunlight filter (Präzisions Glas & Optik GmbH, Germany) so as to reduce the mismatch between the simulated and true solar spectra to less than 2%. The current–voltage characteristics of the cell under these conditions were obtained by applying external potential bias to the cell and measuring the generated photocurrent with a Keithley model 2400 digital source meter (Keithley, USA). A similar data acquisition system was used to control the incident photon-to-current conversion efficiency (IPCE) measurement. Under computer control, light from a 300 W xenon lamp (ILC Technology, USA) was focused through a Gemini-180 double monochromator (Jobin Yvon Ltd., UK) onto the photovoltaic cell under test. The devices were masked to attain an illuminated active area of 0.159 cm^2.

Dye loading. Screen-printed transparent TiO_2 films (4 μm) on a non-conducting microscope slide were immersed in the solutions identical to the ones used for cell preparation (0.3 mM dye powder + 2 mM of CDCA in chlorobenzene) and kept in the dark for 4 h. The films were rinsed with chlorobenzene and placed in a solution of tetrabutylammonium hydroxide (TBAOH) in DMF (0.5 g/ 50 ml) for overnight desorption. The UV-Vis spectra were measured using a TBAOH/DMF solution as a blank on a CARY 5 UV-Vis-NIR spectrophotometer (Varian, Inc.).

Photophysical Measurements

Photocurrent and photovoltage transient measurements. Transient decays were measured under white light bias with superimposed red light perturbation pulses (both light sources were LEDs). The voltage dynamics were recorded using a Keithley 2400 source meter. Varying the intensity of white

light bias allowed the estimate of recombination rate constant (and thus apparent electron lifetime) at different open-circuit potentials by controlling the concentration of the free charges in TiO_2. Red perturbation pulses were adjusted to a very low level in order to maintain single-exponential voltage decay.

Time-correlated single photon counting. Steady-state excited state emission was measured with a FluoroLog-322 (Horiba) spectrometer equipped with a 450W Xe arc lamp. Time-correlated single photon counting experiments were conducted using the above mentioned setup with additional FluoroHub (Horiba) unit with TBX-04 photomultiplier as a detector. For measurement a NanoLED pulsed laser-diode emitting at 406 nm was used. In case of measurement of the dye adsorbed on the TiO_2 surface (transparent, 3 µm) the setup was switched to the front-face detection mode.

Electrochemical impedance spectroscopy. The electrochemical measurements were conducted on the complete devices in the dark at 20 °C. A sinusoidal potential perturbation of an amplitude of 10 mV was applied over a frequency range of 1 MHz – 0.1 Hz (Autolab PG30) for a potential bias varying between 100 and 660 mV with a 20 mV step. Obtained spectra were resolved using the transmission model line.

Laser studies. The nanosecond laser flash photolysis technique was applied to dye-sensitized, 8 µm thick, transparent TiO_2 mesoporous films deposited on normal flint glass. Pulsed excitation (λ = 505 nm, 7 ns pulse duration, 30 Hz repetition rate) was carried out by a Powerlite 7030 frequency-doubled Q-switched Nd:YAG laser (Continuum, Santa Clara, California, USA). The laser beam output was expanded by a planoconcave lens to irradiate a large cross-section of the sample, whose surface was kept at a 30° angle to the excitation beam. The laser fluence on the sample was kept at a low level (30 µJ cm^{-2} per pulse) to ensure that, on average, less than one electron was injected per nanocrystalline TiO_2 particle on pulsed irradiation. The probe light, produced by a continuous wave xenon arc lamp, was first passed through a monochromator tuned at 650 nm, various optical elements, the sample, and then through a second monochromator, before being detected by a fast photomultiplier tube (Hamamatsu, R9110). Data waves were recorded on a DSA 602A digital signal analyzer (Tektronix, Beaverton, Oregon, USA). Satisfactory signal-to-noise ratios were typically obtained by averaging over 1,500 laser shots.

Femtosecond Transient Absorption. Time-resolved transient absorption measurements by the pump-probe technique used a compact CPA-2001, 1 kHz, Ti:Sapphire-amplified femtosecond laser (Clark-MXR), with a pulse width of about 120 fs and a pulse energy of 1 mJ at a central wavelength of 775 nm. The output beam was split into two parts for pumping a double-stage noncollinear optical parametric amplifier (NOPA) and to produce a white light continuum in a sapphire plate or 387 nm UV light by second harmonic generation of the CPA output in a thin BBO crystal. The NOPAs was

pumped by 200 *μJ* pulses at a central wavelength of 775 nm and the excitation wavelength was tuned to 530 nm to generate pulses of approximately 10 *μJ*. The output pulses of the NOPAs were compressed in a SF10-glass prism pair compressor down to a duration of less than 50 fs (fwhm). Iris diaphragms were used to decrease the pulse energy down to a few microjoules for the pump beam and to less than 1 *μJ* for the probe beam. Transient spectra were measured using a white light continuum (WLC) for probing. The latter was generated from pulses (energy <10 *μJ)* focused into a 2 mm thick sapphire plate. The monofilament white beam was collimated using a 90° off-axis paraboloid mirror and steered to the sample using only reflective optics. A smooth monotonic spectral distribution between 480 and 720 nm was obtained by controlling the pump energy with an iris and a variable density filter. The polarization between the pump and probe beams was controlled using a coherent zero-order half waveplate, and experiments were carried out at the magic angle (54.7°) configuration. Pump and probe beams were directed parallel to each other toward a 60° off-axis paraboloid mirror that focused them into the sample. A broadband membrane-beam splitter was placed before the sample to split the probe beam into reference and signal arms. Both were collected by a lens system and directed into two Andor Shamrock 163 imaging spectrographs. The absorbance change was calculated using the ratio between data obtained with and without the pump pulses reaching the sample and corrected for fluctuations in the WLC intensity using the reference beam spectra.

Photoinduced Absorbance. The PIA spectra of the various cells were recorded over a wavelength range of approximately 500 to 1500 nm following an (on/off) photo-modulation using a 9 Hz square wave emanating from a blue LED. White probe light from a halogen lamp was used as illumination source.

Materials

THF (Merck) was dried under reflux over sodium/benzophenone (Merck). CH_2Cl_2, $CHCl_3$, *n*-hexane, ethyl acetate, acetonitrile, dioxane and methanol were purchased from Merck and distilled prior to use. All synthetic steps were carried out under an argon atmosphere (except Knoevenagel condensations). 2-Isopropoxy-4,4,5,5-tetramethyl-1,3,2-dioxaborolane was purchased from Aldrich and was dried over molecular sieve (4 Å) prior to use. Ammonium acetate and potassium carbonate were purchased from Merck, $Pd_2(dba)_3{\cdot}CHCl_3$, $Pd(PPh_3)_2Cl_2$, $HP^tBu_3BF_4$, n-BuLi (1.6 mol L^{-1} in hexane) from Acros and cyanoacetic acid from ABCR. The potassium phosphate solution was prepared by dissolving potassium phosphate (ABCR) in deionized water and was degassed prior to use.

4-Bromo-7-(bromomethyl)benzo[c][1,2,5]thiadiazole **82**,[27] thieno[3,2-*b*]thiophene **85a**,[29] 2,2'-bithiophene **85b**,[30] 2,2'-biselenophene **85c**,[31] 4-bromo-*N*,*N*-bis[4-(hexyloxy)phenyl]aniline **87**,[35] and 4-(7-bromobenzo[c][1,2,5]thiadiazol-4-yl)benzaldehyde **91**[32] were prepared according to literature procedures.

4-Bromo-7-(hydroxymethyl)benzo[c][1,2,5]thiadiazole (83).

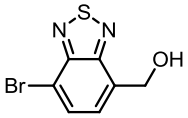

4-Bromo-7-(bromomethyl)benzo[c][1,2,5]thiadiazole **82** (2.67 g, 8.67 mmol) and potassium carbonate (3.60 g, 26.0 mmol) were suspended in a dioxane/water mixture (50 mL, 1:1 v/v) and the mixture was refluxed for 1 h. The solvents were removed in vacuum and the residue was partitioned between 2 M hydrochloric acid (60 mL) and dichloromethane (60 mL). The aqueous phase was extracted with DCM (2 × 50 mL) and the combined organic phases were dried over Na_2SO_4. Removal of the solvent afforded 2.13 g of crude product. It was purified by column chromatography (silica; *n*-hexane/EtOAc 4:1). Product **83** was obtained as an off-white powder (1.36 g, 5.57 mmol, 64%).

Mp.: 139 °C.

^{1}H NMR (400 MHz, $CDCl_3$): δ = 7.82 (d, ^3J = 7.2 Hz, 1H, BTDA-H-5), 7.47 (dt, ^3J = 7.2 Hz, ^4J = 1.0 Hz, 1H, BTDA-H-6), 5.13 (d, ^4J = 1.0 Hz, 2H, C*H*$_2$OH), 2.52 (s br, 1H, CH$_2$O*H*).

^{13}C NMR (100 MHz, $CDCl_3$): δ = 153.47, 153.08, 133.27, 132.01, 126.94, 113.21, 61.82.

MS (CI): *m/z* (%) = 247 ($M+H^+$, 94), 245 (100), 229 (87), 227 (83), 217 (18), 215 (18).

Elemental analysis: calc. (%) for $C_7H_5BrN_2OS$: C 34.30, H 2.06, N 11.43; found: C 34.55, H 2.22, N 11.30.

7-Bromobenzo[c][1,2,5]thiadiazole-4-carbaldehyde (84).

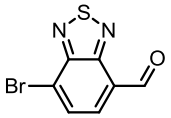

4-Bromo-7-(hydroxymethyl)benzo[c][1,2,5]thiadiazole **83** (1.00 g, 4.08 mmol) and manganese(IV) oxide (1.43 g, 16.4 mmol) were suspended in chloroform (40 mL) and the mixture was first stirred at r.t. for 16 h then refluxed for 3 h. The mixture was filtered, the filtrate was evaporated and the

residue was purified by column chromatography (silica; *n*-hexane/EtOAc 4:1). The pure aldehyde **84** (884 mg, 3.64 mmol, 89%) was obtained as a slightly yellowish solid.

Mp. 192 °C.

^{1}H NMR (400 MHz, $CDCl_3$): δ = 10.74 (s, 1H, CHO), 8.09 (d, ^3J = 7.6 Hz, 1H, BTDA-H-5), 8.04 (d, ^3J = 7.6 Hz, 1H, BTDA-H-6).

^{13}C NMR (100 MHz, $CDCl_3$): δ = 188.34, 153.99, 152.28, 132.16, 131.68, 126.79, 121.89.

MS (CI): *m/z* (%) = 245 ($M+H^+$, 100), 243 (99).

Elemental analysis: calc. (%) for $C_7H_3BrN_2OS$: C 34.59, H 1.24, N 11.52; found: C 34.40, H 1.26, N 11.39.

2-(2,2'-Bithien-5-yl)-4,4,5,5-tetramethyl-1,3,2-dioxaborolane (86b).

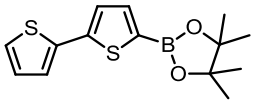

2,2'-Bithiophene **85b** (2.00 g, 12.0 mmol) was dissolved under argon in dry THF (30 mL). At -78 °C, *n*-BuLi (1.6 M in hexane, 7.52 mL, 12.0 mmol) was added dropwise within 20 min. The greenish solution was allowed to warm to r.t. within 75 min. 2-Isopropoxy-4,4,5,5-tetramethyl-1,3,2-dioxaborolane (ITDB) (2.50 mL, 12.3 mmol) was slowly added at -78 °C, the solution was allowed to warm to r.t. within 2 h and was stirred at r.t. for 6 h. The reaction mixture was poured into a sat. NH_4Cl solution (30 mL) and was extracted with diethyl ether (3 × 30 mL). The combined organic layers were washed with water, dried over Na_2SO_4, and the solvent was evaporated to provide boronic ester **86b** as a viscous oil (3.31 g, 11.3 mmol, 94%). The product was dried in high vacuum and directly used in the next step without further purification.

^{1}H NMR (400 MHz, $CDCl_3$): δ = 7.55 (d, ^3J = 3.6 Hz, 1H, Th-H), 7.28-7.24 (m, 3H, Th-H), 7.05-7.02 (m, 1H, Th-H), 1.38 (s, 12H, $-CH_3$).

^{13}C NMR (100 MHz, $CDCl_3$): δ = 144.01, 137.88, 137.26, 127.86, 124.93, 124.91, 124.33, 124.31, 84.14, 24.74.

MS (EI): *m/z* (%) = 292 (100, M^+).

2-(2,2'-Biselenophen-5-yl)-4,4,5,5-tetramethyl-1,3,2-dioxaborolane (86c).

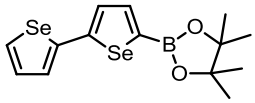

2,2'-Biselenophene **85c** (1.50 g, 5.77 mmol) was dissolved under argon in dry THF (20 mL). At -78 °C, *n*-BuLi (1.6 M in hexane, 3.70 mL, 5.92 mmol) was added dropwise within 10 min. The deeply red solution was stirred at -78 °C for 1 h. ITDB (1.24 mL, 6.06 mmol) was added slowly, the solution was allowed to warm to r.t. within 2 h and was stirred at r.t. overnight. The reaction mixture was poured into a sat. NH_4Cl solution (20 mL) and was extracted with diethyl ether (3 × 20 mL). The combined organic phases were dried over Na_2SO_4 and the solvent was evaporated to provide boronic ester **86c** as a viscous oil (2.40 g, quant.). The product was dried in high vacuum and directly used without further purification.

^{1}H NMR (400 MHz, $CDCl_3$): δ = 7.90 (dd with ^{77}Se-satellites, ^3J = 5.6 Hz, ^4J = 0.8 Hz, $^2J_{Se\text{-}H}$ = 47.6 Hz, 1H, Sel-H), 7.35-7.32 (m, 2H, Sel-H), 7.25-7.21 (m, 2H, Sel-H), 1.35 (s, 12H, -CH_3).

^{13}C NMR (100 MHz, $CDCl_3$): δ = 151.36, 144.68, 140.23, 130.37, 130.33, 128.14, 127.44, 84.11, 24.70.

MS (EI): *m/z* = 388 (100, M^+), 387 (51), 386 (97), 385 (48).

2-[*N*,*N*-Bis(4-hexyloxyphenyl)-4-aminophenyl]-thieno[3,2-*b*]thiophene (88a).

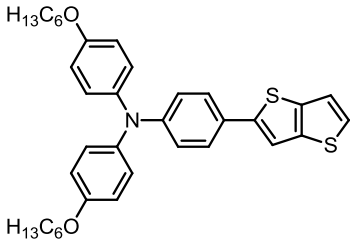

Triphenylamine **87** (454 mg, 0.867 mmol) and boronic ester **86a** (300 mg, 1.13 mmol) were dissolved under argon in THF (8 mL) and the solution was degassed. $Pd_2(dba)_3$ (7.9 mg, 8.6 µmol, 1 mol%) and $HP^tBu_3BF_4$ (5.0 mg, 17.3 µmol, 2 mol%) were added and the solution was degassed again. An aqueous solution of K_3PO_4 (2 M, 0.85 mL, 1.7 mmol) was added and the mixture was stirred at 55 °C overnight. The reaction mixture was poured into water and extracted with DCM. The combined organic phases were dried over Na_2SO_4 and the solvent was removed in vacuum. The crude product was purified by column chromatography (silica; *n*-hexane/DCM 3:1). Thienothiophene **88a** (491 mg, 0.842 mmol, 97%) was obtained as a yellow oil.

^{1}H NMR (400 MHz, DMSO-d_6): δ = 7.64 (d, ^5J = 1.2 Hz, 1H, TT-H), 7.58 (dd, ^3J = 5.2 Hz, ^5J = 1.2 Hz, 1H, TT-H), 7.47 (dd, ^3J = 8.4 Hz, ^5J = 1.6 Hz, 2H, Ph-H), 7.39 (dd, ^3J = 5.2 Hz, ^5J = 1.2 Hz, 1H, TT-H), 7.01 (dd,

^3J = 8.8 Hz, ^5J = 2.0 Hz, 4H, HexOPh-H), 6.89 (dd, ^3J = 8.8 Hz, ^5J = 2.0 Hz, 4H, HexOPh-H), 6.77 (d, ^3J = 8.4 Hz, 2H, Ph-H), 3.92 (t, ^3J = 6.2 Hz, 4H, -OCH_2-), 1.74-1.65 (m, 4H, -OCH$_2$CH_2-), 1.45-1.37 (m, 4H, -OCH$_2$CH$_2$CH_2-), 1.33-1.25 (m, 8H, -CH_2CH_2CH$_3$), 0.87 (t, ^3J = 7.2 Hz, 6H, -CH$_3$).

^{13}C NMR (100 MHz, DMSO-d$_6$): δ = 155.31, 148.11, 145.52, 139.68, 139.43, 136.76, 127.19, 126.72, 126.09, 125.57, 119.89, 119.09, 115.38, 114.19, 67.53, 30.89, 28.60, 25.10, 21.96, 13.78.

MS (MALDI-TOF): *m/z* [M$^+$] = 583.2 (calc. for $C_{36}H_{41}NO_2S_2$: 583.3).

Elemental analysis: calc. (%) for $C_{36}H_{41}NO_2S_2$: C 74.06, H 7.08, N 2.40; found: C 73.95, H 7.21, N 2.28.

5-[*N*,*N*-Bis(4-hexyloxyphenyl)-4-aminophenyl]-2,2'-bithiophene (88b).

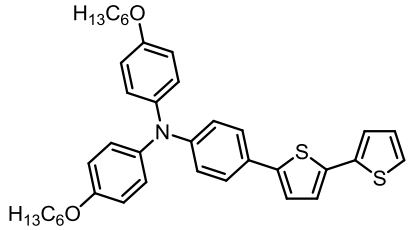

Triphenylamine **87** (834 mg, 1.59 mmol) and boronic ester **86b** (550 mg, 1.88 mmol) were dissolved under argon in dry THF (12 mL) and the solution was degassed. $Pd_2(dba)_3$ (29.8 mg, 32.5 µmol, 2 mol%) and HP^{t}Bu$_3$BF$_4$ (18.6 mg, 62.2 µmol, 4 mol%) were added and the solution was degassed again. An aqueous solution of K_3PO_4 (2 M, 3.2 mL, 6.4 mmol) was added and the mixture turned from dark red to green. It was stirred at r.t. overnight. The reaction mixture was poured into a saturated NH_4Cl solution (15 mL) and extracted with DCM (3 × 15 mL). The combined organic phases were dried over Na_2SO_4 and the solvent was removed in vacuum. The resulting brown oil was purified by column chromatography (silica; *n*-hexane/DCM 9:1 to 6:4). Bithiophene **88b** (930 mg, 1.53 mmol, 96%) was obtained as a greenish yellow solid.

Mp.: 61-64 °C.

^{1}H NMR (400 MHz, DMSO-d$_6$): δ = 7.47 (dd, ^3J = 5.2 Hz, ^4J = 0.8 Hz, 1H, Th-H), 7.44 (m, 2H, Ph-H), 7.27 (dd, ^3J = 3.6 Hz, ^4J = 1.2 Hz, 1H, Th-H), 7.26 (d, ^3J = 3.6 Hz, 1H, Th-H), 7.23 (d, ^3J = 3.6 Hz, 1H, Th-H), 7.07 (dd, ^3J = 5.2 Hz, ^4J = 3.6 Hz, 1H, Th-H), 7.01 (m, 4H, HexOPh-H), 6.89 (m, 4H, HexOPh-H), 6.75 (m, 2H, Ph-H), 3.92 (t, ^3J = 6.6 Hz, 4H, -OCH_2-), 1.72-1.65 (m, 4H, -OCH$_2$CH_2-), 1.44-1.36 (m, 4H, -OCH$_2$CH$_2$CH_2-), 1.32-1.27 (m, 8H, -CH_2CH_2CH$_3$), 0.87 (t, ^3J = 7.0 Hz, 6H, -CH$_3$).

^{13}C NMR (100 MHz, DMSO-d$_6$): δ = 155.41, 148.10, 142.50, 139.52, 136.56, 134.22, 128.30, 126.84, 126.04, 125.05, 124.98, 124.79, 123.60, 122.84, 119.12, 115.48, 67.63, 30.98, 28.69, 25.19, 22.05, 13.88.

MS (MALDI-TOF): *m/z* [M^+] = 609.6 (calc. for $C_{38}H_{43}NO_2S_2$: 609.3).

Elemental analysis: calc. (%) for $C_{38}H_{43}NO_2S_2$: C 74.84, H 7.11, N 2.30; found: C 74.70, H 7.09, N 2.27.

5-[*N*,*N*-Bis(4-hexyloxyphenyl)-4-aminophenyl]-2,2'-biselenophene (88c).

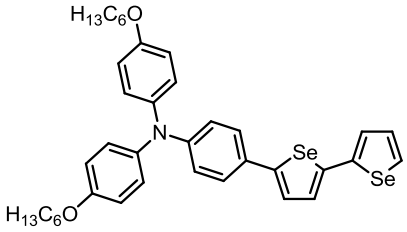

Triphenylamine **87** (592 mg, 1.13 mmol) and boronic ester **86c** (764 mg, 1.58 mmol) were dissolved under argon in THF (15 mL) and the solution was degassed. $Pd_2(dba)_3$ (21.5 mg, 23.5 µmol) and $HP^tBu_3BF_4$ (14.2 mg, 47.5 µmol) were added and the solution was degassed again. An aqueous solution of K_3PO_4 (2 M, 2.3 mL, 4.6 mmol) was added and the mixture was stirred at 50 °C for 6 h and at 80 °C for 6 h. The reaction mixture was poured into water (20 mL) and extracted with DCM (3 × 25 mL). The combined organic layers were dried over Na_2SO_4 and the solvent was removed in vacuum. The crude product was purified by column chromatography (silica; *n*-hexane/DCM 7:3). Biselenophene **88c** (605 mg, 1.20 mmol, 76%) was obtained as a brownish oil.

^{1}H NMR (400 MHz, $CDCl_3$): δ = 7.84 (dd with ^{77}Se-satellites, ^3J = 5.2 Hz, ^4J = 1.2 Hz, $^2J_{Se\text{-}H}$ = 24 Hz, 1H, SeI-H), 7.35-7.31 (m, 2H, Ph-H), 7.24-7.19 (m, 4H, SeI-H), 7.09-7.05 (m, 4H, HexOPh-H), 6.92-6.88 (m, 2H, Ph-H), 6.86-6.82 (m, 4H, HexOPh-H), 3.95 (t, ^3J = 6.4 Hz, 4H, -OCH_2-), 1.83-1.75 (m, 4H, -OCH$_2$CH_2-), 1.52-1.44 (m, 4H, -OCH$_2$CH$_2$CH_2-), 1.39-1.34 (m, 8H, -CH_2CH_2CH$_3$), 0.84 (t, ^3J = 7.0 Hz, 6H, -CH_3).

^{13}C NMR (100 MHz, $CDCl_3$): δ = 155.60, 149.74, 148.46, 144.99, 141.94, 140.23, 130.21, 129.10, 127.84, 127.72, 126.70, 126.52, 126.06, 124.07, 120.12, 115.24, 68.19, 31.58, 29.29, 25.73, 22.60, 14.05.

MS (MALDI-TOF): *m/z* [M^+] = 706.1 (calc. for $C_{38}H_{43}NO_2Se_2$: 705.2).

Elemental analysis: calc. (%) for $C_{38}H_{43}NO_2Se_2$: C 64.86, H 6.16, N 1.99; found: C 65.08, H 6.25, N 1.85.

2-[*N*,*N*-Bis(4-hexyloxyphenyl)-4-aminophenyl]-5-(tri-*n*-butylstannyl)-thieno[3,2-*b*]thiophene (89a).

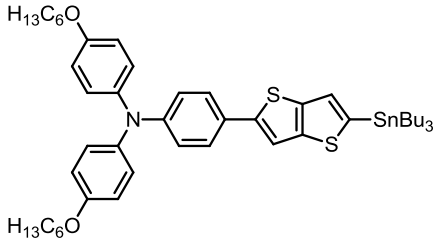

Thienothiophene **88a** (477 mg, 0.820 mmol) was dissolved in dry THF (5 mL) and the solution was cooled to -78 °C. A 1.6 M solution of *n*-BuLi in hexane (0.57 ml, 0.912 mmol) was added dropwise and the solution turned green. It was stirred for 1 h at -78 °C, then tributyltin chloride (345 mg, 1.02 mmol) was added. The reaction mixture was allowed to warm to r.t. within 3 h. Water (25 mL) was added and the mixture was extracted with DCM (2 × 25 mL). The combined organic layers were dried over Na_2SO_4 and the solvent was removed in vacuum. The crude stannyl compound **89a** (733 mg, quant.) was obtained as a brownish oil. It was used in the next step without further purification.

^{1}H NMR (400 MHz, $CDCl_3$): δ = 7.41 (d, ^3J = 8.8 Hz, 2H, Ph-H), 7.33 (s, 1H, TT-H), 7.22 (s, 1H, TT-H), 7.07 (d, ^3J = 9.2 Hz, 4H, HexOPh-H), 6.94-6.91 (m, 2H, Ph-H), 6.83 (d, ^3J = 9.2 Hz, 4H, HexOPh-H), 3.94 (t, ^3J = 6.6 Hz, 4H, -OCH_2-), 1.82-1.75 (m, 4H, -OCH$_2$CH_2-), 1.63-1.56 (m, 6H, -CH_2-), 1.51-1.43 (m, 4H, -CH_2-), 1.40-1.32 (m, 14H, -CH_2-), 1.17-1.12 (m, 6H, -CH_2-), 0.92 (t, ^3J = 7.2 Hz, 6H, -CH_3), 0.92 (t, ^3J = 7.2 Hz, 9H, -CH_3).

^{13}C NMR (100 MHz, $CDCl_3$): δ = 155.68, 148.59, 146.77, 140.34, 140.08, 137.49, 126.74, 126.68, 126.43, 120.31, 120.21, 119.54, 115.32, 113.67, 68.27, 31.60, 29.32, 27.84, 27.25, 25.75, 22.60, 14.02, 13.58, 10.96.

MS (MALDI-TOF): *m/z* [M^+] = 873.6 (calc. for $C_{48}H_{67}NO_2S_2Sn$: 873.4).

5-[*N*,*N*-Bis(4-hexyloxyphenyl)-4-aminophenyl]-5'-(tri-*n*-butylstannyl)-2,2'-bithiophene (89b).

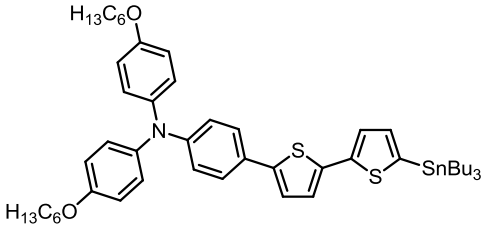

Bithiophene **88b** (601 mg, 0.99 mmol) was dissolved in dry THF (10 mL) and the solution was cooled to -78 °C. *n*-BuLi (1.6 M in hexane, 0.63 mL, 1.01 mmol) was added dropwise and the solution turned dark green. It was stirred for 1 h at this temperature, then tributyltin chloride (360 mg, 1.06 mmol)

was added. The reaction mixture was allowed to slowly warm to r.t. and was stirred at r.t. overnight. Water (30 mL) was added and the mixture was extracted with DCM (2 × 30 mL). The combined organic layers were washed with water, dried over Na_2SO_4 and the solvent was removed. The crude stannyl compound **89b** (943 mg, quant.) was obtained as a brownish oil. It was directly used in the next step without further purification.

^{1}H NMR (400 MHz, $CDCl_3$): δ = 7.39 (d, ^3J = 8.8 Hz, 2H, Ph-H), 7.28 (d, ^3J = 3.2 Hz, 1H, Th-H), 7.10 (d, ^3J = 4.0 Hz, 1H, Th-H), 7.08-7.04 (m, 6H, HexOPh-H + Th-H), 6.91 (d, ^3J = 8.8 Hz, 2H, Ph-H), 6.85-6.81 (m, 4H, HexOPh-H), 3.94 (t, ^3J = 6.4 Hz, 4H, -OCH_2-), 1.82-1.75 (m, 4H, -OCH$_2$CH_2-), 1.63-1.55 (m, 6H, -CH$_2$-), 1.51-1.45 (m, 4H, -CH$_2$-), 1.43-1.31 (m, 14H, -CH$_2$-), 1.15-1.10 (m, 6H, -CH$_2$-), 0.92 (t, ^3J = 7.2 Hz, 6H, -CH$_3$), 0.91 (t, ^3J = 7.2 Hz, 9H, -CH$_3$).

^{13}C NMR (100 MHz, $CDCl_3$): δ = 155.62, 148.30, 143.10, 143.08, 140.48, 136.30, 136.11, 135.60, 126.71, 126.60, 126.24, 126.18, 124.47, 124.30, 122.22, 120.46, 115.33, 68.31, 31.63, 29.36, 28.97, 27.27, 25.79, 22.63, 14.05, 13.67, 10.92.

MS (MALDI-TOF): *m/z* [M^+] = 899.5 (calc. for $C_{50}H_{69}NO_2S_2Sn$: 899.4).

5-[*N*,*N*-Bis(4-hexyloxyphenyl)-4-aminophenyl]-5'-(tri-*n*-butylstannyl)-2,2'-biselenophene (89c).

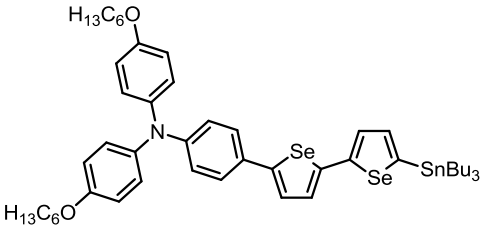

Biselenophene **88c** (596 mg, 0.847 mmol) was dissolved in dry THF (10 mL) and the solution was cooled to -78 °C. *n*-BuLi (1.6 M in hexane, 0.53 ml, 0.848 mmol) was added dropwise and the solution turned dark green. It was stirred for 45 min at this temperature, then tributyltin chloride (300 mg, 0.885 mmol) was added. The reaction mixture was allowed to slowly warm to room temperature within 3 h. It was poured into a sat. NH_4Cl solution (25 mL) and extracted with DCM (3 × 30 mL). The combined organic layers were dried over Na_2SO_4, the solvent was removed in vacuum, and the crude product was dried in high vacuum. Product **89c** was obtained as a brown oil (828 mg, 0.833 mmol, 98%) and was used in the next step without further purification.

^{1}H NMR (400 MHz, $CDCl_3$): δ = 7.35-7.31 (m, 2H, Ph-H), 7.21-7.18 (m, 3H, Sel-H), 7.06 (d, ^3J = 9.0 Hz, 4H, HexOPh-H), 6.90-6.86 (m, 2H, Ph-H), 6.83 (d, ^3J = 9.0 Hz, 4H, HexOPh-H), 3.93 (t, ^3J = 6.6 Hz, 4H, -OCH_2-), 1.81-1.74 (m, 4H, -OCH$_2$CH_2-), 1.63-1.54 (m, 6H, -CH$_2$-), 1.50-1.43 (m, 4H, -CH$_2$-), 1.40-1.30 (m, 14H, -CH$_2$-), 1.13-1.08 (m, 6H, -CH$_2$-), 0.94-0.88 (m, 15H, -CH$_3$).

^{13}C NMR (100 MHz, $CDCl_3$): δ = 155.64, 149.81, 149.36, 148.42, 143.91, 142.39, 140.38, 140.32, 138.70, 128.16, 127.80, 127.49, 126.74, 126.72, 126.68, 126.52, 124.21, 120.29, 120.18, 115.31, 68.28, 31.60, 29.33, 28.97, 27.27, 25.76, 22.61, 14.03, 13.65, 11.18.

MS (MALDI-TOF): *m/z* [M^+] = 994.6 (calc. for $C_{50}H_{69}NO_2Se_2Sn$: 995.3).

7-{2-[*N*,*N*-Bis(4-hexyloxyphenyl)-4-aminophenyl]-thieno[3,2-*b*]thien-5-yl}-benzo[c][1,2,5]thiadiazole-4-carbaldehyde (90a).

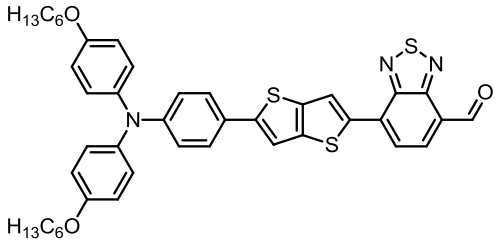

In a Schlenk tube, stannyl compound **89a** (690 mg, 0.63 mmol) and aldehyde **84** (125 mg, 0.51 mmol) were dissolved under argon in dry THF (7 mL) and the solution was degassed. $Pd(PPh_3)_2Cl_2$ (10.4 mg, 14.8 µmol, 3 mol%) was added, the solution was degassed again and stirred at 70 °C for 4 h. The solution became deeply purple. The reaction mixture was poured into water (20 mL) and was extracted with DCM (3 × 25 mL). The combined organic layers were dried over Na_2SO_4 and the solvent was removed. The crude product was purified by column chromatography (silica; DCM/*n*-hexane 1:1 to 100:0). Aldehyde **90a** (330 mg, 0.44 mmol, 86%) was obtained as a deeply purple solid.

Mp.: 92 °C.

^{1}H NMR (400 MHz, $CDCl_3$): δ = 10.67 (s, 1H, CHO), 8.56 (s, 1H, TT-H), 8.16 (d, ^3J = 7.6 Hz, BTDA-H), 7.88 (d, ^3J = 7.6 Hz, BTDA-H), 7.41 (d, ^3J = 8.8 Hz, 2H, Ph-H), 7.32 (s, 1H, TT-H), 7.08 (d, ^3J = 8.8 Hz, 4H, HexOPh-H), 6.92 (d, ^3J = 8.8 Hz, 2H, Ph-H), 6.85 (d, ^3J = 8.8 Hz, 4H, HexOPh-H), 3.95 (t, ^3J = 6.6 Hz, 4H, -OCH_2-), 1.82-1.75 (m, 4H, -OCH$_2$CH_2-), 1.51-1.45 (m, 4H, -CH_2-), 1.38-1.33 (m, 8H, -CH_2-), 0.92 (t, ^3J = 7.0 Hz, 6H, -CH_3).

^{13}C NMR (100 MHz, $CDCl_3$): δ = 188.26, 155.92, 153.83, 152.14, 150.01, 149.20, 142.98, 140.00, 138.87, 138.76, 133.47, 132.57, 126.99, 126.54, 125.55, 125.12, 123.57, 123.58, 119.71, 115.38, 113.47, 68.29, 31.60, 29.31, 25.75, 22.60, 14.03.

MS (MALDI-TOF): *m/z* [M^+] = 745.1 (calc. for $C_{43}H_{43}N_3O_3S_3$: 745.2).

Elemental analysis: calc. (%) for $C_{43}H_{43}N_3O_3S_3$: C 69.23, H 5.81, N 5.63; found: C 69.02, H 5.80, N 5.55.

7-{5-[*N*,*N*-Bis(4-hexyloxyphenyl)-4-aminophenyl]-2,2'-bithien-5'-yl}benzo[c]-[1,2,5]thiadiazole-4-carbaldehyde (90b).

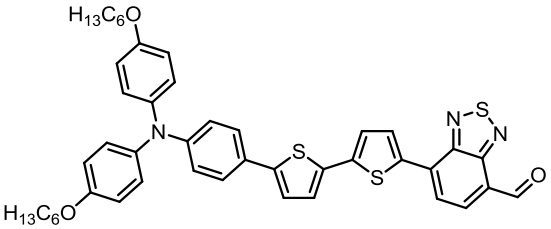

In a Schlenk tube, stannyl compound **89b** (805 mg, 0.716 mmol) and 7-bromobenzo[c]-[1,2,5]thiadiazole-4-carbaldehyde **84** (148 mg, 0.609 mmol) were dissolved under argon in dry THF (15 mL) and the solution was degassed. $Pd(PPh_3)_2Cl_2$ (13.0 mg, 18.5 µmol, 3 mol%) was added and the solution was degassed again. It was stirred at 70 °C for 15 h. The reaction mixture was poured into water (30 mL) and extracted with DCM (3 × 30 mL). The combined organic layers were dried over Na_2SO_4 and the solvent was removed. The crude product was purified by column chromatography (silica; DCM/*n*-hexane 3:7 to 100:0, product eluted with DCM/EtOAc 9:1). Aldehyde **90b** (406 mg, 0.616 mmol, 86%) was obtained as a purple solid.

^{1}H NMR (400 MHz, $CDCl_3$): δ = 10.68 (s, 1H, CHO), 8.23-8.18 (m, 2H, BTDA-H + Th-H), 7.93 (dd, ^3J = 7.6 Hz, ^5J = 1.6 Hz, 1H, BTDA-H), 7.39 (d, ^3J = 8.4 Hz, 2H, Ph-H), 7.26-7.25 (m, 2H, Th-H), 7.11 (d, ^3J = 3.6 Hz, 1H, Th-H), 7.07 (d, ^3J = 8.8 Hz, 4H, HexOPh-H), 6.91 (d, ^3J = 8.4 Hz, 2H, Ph-H), 6.86-6.82 (m, 4H, HexOPh-H), 3.94 (t, ^3J = 6.6 Hz, 4H, -OC*H*$_2$-), 1.82-1.74 (m, 4H, -OCH$_2$C*H*$_2$-), 1.51-1.43 (m, 4H, -OCH$_2$CH$_2$C*H*$_2$-), 1.37-1.32 (m, 8H, -C*H*$_2$C*H*$_2$CH$_3$), 0.92 (t, ^3J = 7.2 Hz, 6H, -CH$_3$).

^{13}C NMR (100 MHz, $CDCl_3$): δ = 188.42, 155.73, 153.72, 152.19, 148.71, 145.12, 142.26, 140.14, 136.35, 134.22, 132.79, 132.76, 131.20, 126.83, 126.27, 125.75, 125.32, 125.13, 124.26, 123.23, 122.42, 119.96, 115.29, 68.23, 31.59, 29.30, 25.75, 22.61, 14.05.

MS (MALDI-TOF): *m/z* [M^+] = 771.7 (calc. for $C_{45}H_{45}N_3O_3S_3$: 771.3).

Elemental analysis: calc. (%) for $C_{45}H_{45}N_3O_3S_3$: C 70.01, H 5.87, N 5.44; found: C 69.87, H 5.86, N 5.34.

7-{5-[*N*,*N*-Bis(4-hexyloxyphenyl)-4-aminophenyl]-2,2'-biselenophen-5'-yl}-benzo[c][1,2,5]thiadiazole-4-carbaldehyde (90c).

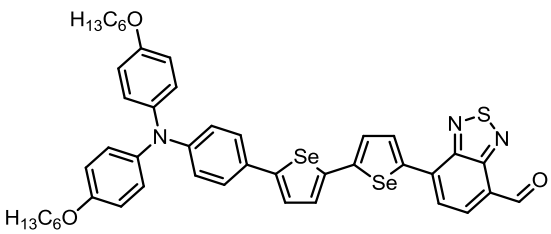

In a Schlenk tube, stannyl compound **89c** (577 mg, 0.581 mmol) and aldehyde **84** (120 mg, 0.494 mmol) were dissolved under argon in dry THF (10 mL) and the solution was degassed. $Pd(PPh_3)_2Cl_2$ (23.4 mg, 33.3 µmol, 7 mol%) was added and the solution was degassed again. It was stirred at 75 °C for 22 h. The reaction mixture was poured into water (15 mL) and extracted with DCM (3 × 25 mL). The combined organic layers were dried over Na_2SO_4 and the solvent was removed. The crude product was purified by column chromatography (silica; *n*-hexane/DCM 7:3 to 0:100). The pure aldehyde **90c** (216 mg, 0.230 mmol, 51%) was obtained as a purple solid.

^{1}H NMR (400 MHz, $CDCl_3$): δ = 10.67 (s, 1H, CHO), 8.19 (d, ^3J = 7.8 Hz, 1H, BTDA-H), 8.18 (d, ^3J = 4.0 Hz, 1H, Sel-H), 7.96 (d, ^3J = 7.8 Hz, 1H, BTDA-H), 7.37-7.31 (m, 4H, Sel-H + Ph-H), 7.26-7.22 (m, 1H, Sel-H), 7.07 (d, ^3J = 8.8 Hz, 4H, HexOPh-H), 6.98 (d, ^3J = 8.0 Hz, 2H, Ph-H), 6.84 (d, ^3J = 8.8 Hz, 4H, HexOPh-H), 3.94 (t, ^3J = 6.6 Hz, 4H, -OCH_2-), 1.82-1.74 (m, 4H, -OCH$_2$CH_2-), 1.50-1.43 (m, 4H, -CH$_2$-), 1.37-1.32 (m, 8H, -CH$_2$-), 0.91 (t, ^3J = 7.0 Hz, 6H, -CH$_3$).

^{13}C NMR (100 MHz, $CDCl_3$): δ = 188.34, 155.76, 153.49, 152.33, 151.50, 151.39, 148.82, 141.21, 140.36, 140.05, 134.60, 132.81, 131.79, 128.82, 127.36, 126.87, 126.79, 126.62, 124.90, 124.36, 122.31, 119.83, 115.28, 68.22, 31.59, 29.29, 25.74, 22.61, 14.50.

MS (MALDI-TOF): *m/z* [M^+] = 867.7 (calc. for $C_{45}H_{45}N_3O_3SSe_2$: 867.2).

Elemental analysis: calc. (%) for $C_{45}H_{45}N_3O_3SSe_2$: C 62.42, H 5.24, N 4.85; found: C 62.22, H 5.23, N 4.79.

(*E*)-2-Cyano-3-(7-{2-[*N*,*N*-bis(4-hexyloxyphenyl)-4-aminophenyl]-thieno[3,2-*b*]-thien-5-yl}benzo[c][1,2,5]thiadiazole-4-yl)acrylic acid (16).

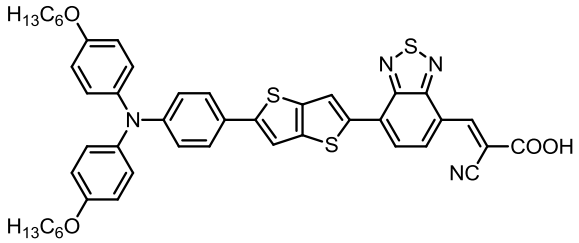

Aldehyde **90a** (150 mg, 0.202 mmol) and cyanoacetic acid (22.3 mg, 0.262 mmol) were dissolved in acetonitrile (15 mL) and some drops of piperidine were added. The mixture was refluxed for 48 h. After 26 h another portion (21 mg, 0.247 mg) of cyanoacetic acid was added. After 48 h the reaction mixture was diluted with DCM and brine was added. The organic phase was separated and the aqueous phase was extracted with DCM. The combined organic layers were dried over Na_2SO_4 and the solvent was removed in vacuum. The residue was purified by column chromatography (silica; DCM/MeOH 9:1). Dye **16** (80.0 mg, 49%) was obtained as a deeply purple solid.

^{1}H NMR (400 MHz, DMSO-d_6): δ = 8.71 (s, 1H, C=CH), 8.46 (s, 1H, TT-H), 8.43 (d, ^3J = 8.0 Hz, BTDA-H), 8.08 (d, ^3J = 8.0 Hz, BTDA-H), 7.67 (s, 1H, TT-H), 7.47 (d, ^3J = 8.8 Hz, 2H, Ph-H), 7.02 (d, ^3J = 8.8 Hz, 4H, HexOPh-H), 6.91 (d, ^3J = 8.8 Hz, 4H, HexOPh-H), 6.76 (d, ^3J = 8.8 Hz, 2H, Ph-H), 3.93 (t, ^3J = 6.4 Hz, 4H, -OCH_2-), 1.74-1.67 (m, 4H, -OCH$_2$CH_2-), 1.45-1.37 (m, 4H, -CH$_2$-), 1.33-1.28 (m, 8H, -CH$_2$-), 0.88 (t, ^3J = 7.0 Hz, 6H, -CH$_3$).

^{13}C NMR: Solubility not sufficient.

HRMS (MALDI-TOF): *m/z* [M$^+$] = 812.25182 (calc. for $C_{46}H_{44}N_4O_4S_3$: 812.25182).

(*E*)-2-Cyano-3-(7-{5-[*N*,*N*-bis(4-hexyloxyphenyl)-4-aminophenyl]-2,2'-bithien-5'-yl}benzo[c][1,2,5]thiadiazole-4-yl)acrylic acid (17).

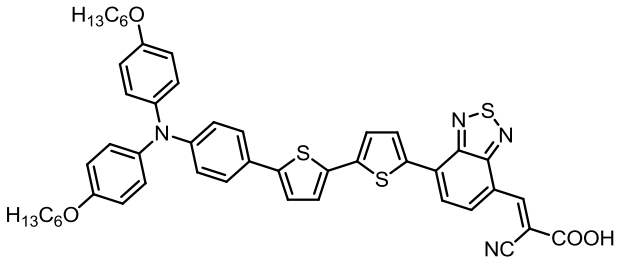

Aldehyde **90b** (165 mg, 0.214 mmol), cyanoacetic acid (363 mg, 4.27 mmol) and ammonium acetate (14.7 mg, 0.191 mmol) were dissolved in a DCM/MeCN mixture (30 mL, 2:1 v/v), and the deeply purple solution was refluxed for 7 h. The almost black reaction mixture was poured into water (30 mL) and extracted with DCM. The combined organic layers were dried over Na_2SO_4. After removal of DCM a dark solid precipitated, which was collected and washed thoroughly with ethanol. The product contained some aldehyde; therefore, it was further purified by column chromatography (silica; aldehyde eluted with DCM, product with DCM/MeOH 9:1 to 1:1). Dye **17** (155 mg, 3.68 mmol, 86%) was obtained as a deeply purple solid.

^{1}H NMR (400 MHz, DMSO-d_6): δ = 8.84 (s, 1H, C=CH), 8.57 (d, ^3J = 7.6 Hz, 1H, BTDA-H), 8.20 (d, ^3J = 7.6 Hz, 1H, BTDA-H), 8.12 (d, ^3J = 3.2 Hz, 1H, Th-H), 7.39 (d, ^3J = 8.0 Hz, 2H, Ph-H), 7.35-7.32 (m, 2H, Th-H), 7.24 (d, ^3J = 2.8 Hz, 1H, Th-H), 7.00 (d, ^3J = 8.4 Hz, 4H, HexOPh-H), 6.88 (d, ^3J = 8.4 Hz, 4H, HexOPh-H), 6.71 (d, ^3J = 8.0 Hz, 2H, Ph-H), 3.91 (t, ^3J = 6.0 Hz, 4H, -OCH_2-), 1.72-1.65 (m, 4H, -OCH$_2$CH_2-), 1.44-1.35 (m, 4H, -OCH$_2$CH$_2$CH_2-), 1.33-1.24 (m, 8H, -CH_2CH_2CH$_3$), 0.87 (t, ^3J = 7.2 Hz, 6H, -CH$_3$).

^{13}C NMR: Solubility not sufficient.

HRMS (MALDI-TOF): *m/z* [M$^+$] = 838.26747 (calc. for $C_{48}H_{46}N_4O_4S_3$: 838.26757).

(*E*)-2-Cyano-3-(7-{5-[*N*,*N*-bis(4-hexyloxyphenyl)-4-aminophenyl]-2,2'-biselenophen-5'-yl}benzo[c][1,2,5]thiadiazole-4-yl)acrylic acid (18).

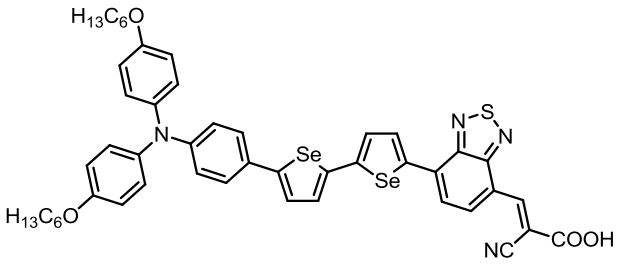

Aldehyde **90c** (116 mg, 0.134 mmol), cyanoacetic acid (227 mg, 2.67 mmol) and NH_4OAc (10.0 mg, 0.130 mmol) were dissolved in a DCM/MeCN mixture (18 mL, 2:1 v/v) and the deeply purple solution was refluxed for 7 h. The reaction mixture was poured into water (25 mL) and extracted with DCM. The combined organic phases were dried over Na_2SO_4 and the solvent was evaporated. The crude product was purified by column chromatography (silica; aldehyde eluted with DCM, product with DCM/MeOH 9:1 to 1:1). The deeply purple solid was washed thoroughly with ethanol and dried in high vacuum. Dye **18** (114 mg, 2.44 mmol, 91%) was obtained as a deeply purple solid.

^{1}H NMR (400 MHz, DMSO-d_6): δ = 8.64 (s, 1H, C=CH), 8.41 (d, ^3J = 7.2 Hz, 1H, BTDA-H), 8.22 (m, 2H, BTDA-H + Sel-H), 7.45-7.38 (m, 5H, Sel-H + Ph-H), 6.99 (d, ^3J = 8.8 Hz, 4H, HexOPh-H), 6.89 (d, ^3J = 8.8 Hz, 4H, HexOPh-H), 6.72 (d, ^3J = 8.4 Hz, 2H, Ph-H), 3.92 (t, ^3J = 6.0 Hz, 4H, -OCH_2-), 1.73-1.66 (m, 4H, -OCH$_2$CH_2-), 1.45-1.36 (m, 4H, -OCH$_2$CH$_2$CH_2-), 1.34-1.25 (m, 8H, -CH_2CH_2CH$_3$), 0.88 (m, 6H, -CH$_3$).

^{13}C NMR: Solubility not sufficient.

HRMS (MALDI-TOF): *m/z* [M^+] = 934.15657 (calc. $C_{48}H_{46}N_4O_4SSe_2$: 934.15746).

4-{7-[5'-(4-{Bis[4-(hexyloxy)phenyl]amino}phenyl)-2,2'-bithien-5-yl]benzo[c][1,2,5]thiadiazol-4-yl}benzaldehyde (92).

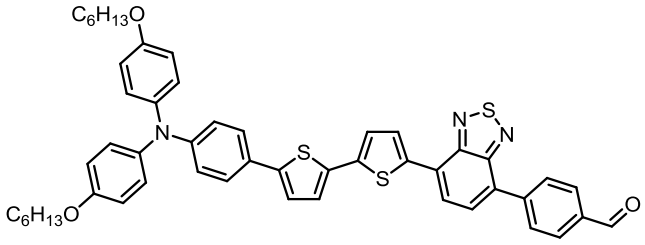

In a Schlenk tube, 4-(7-bromobenzo[c][1,2,5]thiadiazol-4-yl)benzaldehyde **91** (94.0 mg, 0.29 mmol) and stannylated bithiophene **89b** were dissolved under argon in dry THF (10 mL) and the solution was degassed. $Pd(PPh_3)_2Cl_2$ (6.60 mg, 9.40 µmol, 3 mol%) was added and the solution was degassed again. Afterwards, it was stirred at 75 °C for 4.5 h. The deeply red reaction mixture was poured into

water (20 mL) and extracted three times with DCM. The combined organic layers were washed with water (20 mL), dried over Na_2SO_4 and the solvent was removed. The crude product was purified by column chromatography (flash silica; DCM/*n*-hexane 1:1 to 100:0, product eluted with pure DCM). Product **92** (229 mg, 0.27 mmol, 92%) was obtained as a red solid.

^{1}H NMR (400 MHz, $CDCl_3$): δ = 10.10 (s, 1H, CHO), 8.15 (d, ^3J = 8.4 Hz, 2H, Ph-H), 8.09 (d, ^3J = 4.0 Hz, 1H, Th-H), 8.03 (d, ^3J = 8.4 Hz, 2H, Ph-H), 7.91 (d, ^3J = 7.5 Hz, 1H, BTDA-H), 7.79 (d, ^3J = 7.5 Hz, 1H, BTDA-H), 7.40 (d, ^3J = 8.7 Hz, 2H, HexOPh-H), 7.25 (d, ^3J = 3.8 Hz, 1H, Th-H), 7.23 (d, ^3J = 3.8 Hz, 1H, Th-H), 7.12-7.06 (m, 5H, Th-H + HexOPh-H), 6.91 (d, ^3J = 7.9 Hz, 2H, HexOPh-H), 6.84 (d, ^3J = 8.8 Hz, 4H, HexOPh-H), 3.94 (t, ^3J = 6.6 Hz, 4H, -OCH_2-), 1.82-1.75 (m, 4H, -OCH$_2$CH_2-), 1.51-1.43 (m, 4H, -OCH$_2$CH$_2$CH_2-), 1.38-1.33 (m, 8H, -CH_2CH_2CH$_3$), 0.92 (t, ^3J = 7.0 Hz, 6H, -CH$_3$).

^{13}C NMR (100 MHz, $CDCl_3$): δ = 191.73, 155.72, 153.65, 152.53, 148.59, 144.36, 143.09, 140.27, 139.77, 137.15, 135.72, 134.75, 130.72, 129.90, 129.66, 128.99, 128.85, 127.33, 126.78, 126.24, 125.64, 125.12, 124.74, 124.01, 122.35, 120.13, 115.33, 68.28, 31.60, 29.32, 25.75, 22.60, 14.02.

MS (MALDI-TOF): *m/z* [M$^+$] = 847.7 (calc. for $C_{51}H_{49}N_3O_3S_3$: 847.3).

Elemental analysis: calc. (%) for $C_{51}H_{49}N_3O_3S_3$: C 72.22, H 5.82, N 4.95; found C 72.36, H 5.84, N 4.96.

(E)-3-(4-{7-[5'-(4-{Bis[4-(hexyloxy)phenyl]amino}phenyl)-2,2'-bithien-5-yl]benzo[c][1,2,5]thiadiazol-4-yl}phenyl)-2-cyanoacrylic acid (19).

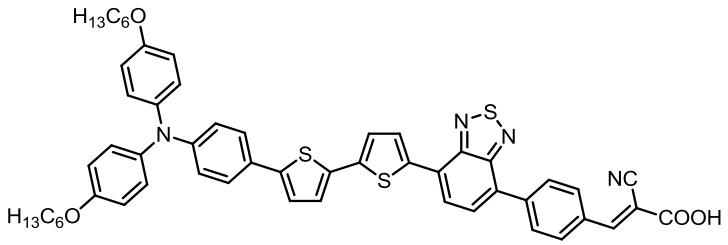

Aldehyde **92** (150 mg, 0.18 mmol), cyanoacetic acid (302 mg, 3.55 mmol) and ammonium acetate (13.2 mg, 0.17 mmol) were dissolved in a DCM/MeCN mixture (20 mL, 2:1 v/v) and the deeply red solution was refluxed for 45 h. DCM was evaporated and a dark solid precipitated. It was filtered, washed with ethanol and dried. It was further purified by column chromatography (silica; aldehyde eluted with DCM, product with DCM/MeOH 9:1). The product still contained some cyanoacetic acid; therefore, it was washed thoroughly with ethanol and dried in high vacuum to obtain 62 mg (0.07 mmol, 38%) of dye **19** as deeply purple solid.

^{1}H NMR (400 MHz, DMSO-d_6): δ = 8.36 (s, 1H, C=CH), 8.24 (d, ^3J = 8.2 Hz, 2H, Ph-H), 8.18-8.13 (m, 4H, Ph-H + Th-H + BTDA-H), 8.03 (d, ^3J = 7.6 Hz, 1H, BTDA-H), 7.46 (d, ^3J = 8.4 Hz, 2H, HexOPh-H), 7.42 (d,

^{3}J = 3.7 Hz, 1H, Th-H), 7.38 (d, ^{3}J = 3.5 Hz, 1H, Th-H), 7.31 (d, ^{3}J = 3.5 Hz, 1H, Th-H), 7.02 (d, ^{3}J = 8.6 Hz, 4H, HexOPh-H), 6.90 (d, ^{3}J = 8.6 Hz, 4H, HexOPh-H), 6.75 (d, ^{3}J = 8.4 Hz, 2H, HexOPh-H), 3.93 (t, ^{3}J = 6.3 Hz, 4H, -OCH_2-), 1.73-1.66 (m, 4H, -OCH$_2$CH_2-), 1.45-1.37 (m, 4H, -OCH$_2$CH$_2$CH_2-), 1.35-1.26 (m, 8H, -CH_2CH_2CH$_3$), 0.88 (t, ^{3}J = 6.5 Hz, 6H, -CH$_3$).

^{13}C NMR: Solubility not sufficient.

HRMS (MALDI-TOF): *m/z* [M^+] = 914.29877 (calc. for $C_{54}H_{50}N_4O_4S_3$: 914.29887).

5.9 References

[1] B. O'Regan, M. Grätzel, *Nature* **1991**, *353*, 737.

[2] M. Grätzel, *Nature* **2001**, *414*, 338.

[3] A. Hagfeldt, G. Boschloo, L. Sun, L. Kloo, H. Pettersson, *Chem. Rev.* **2010**, *110*, 6595.

[4] M. K. Nazeeruddin, A. Kay, I. Rodicio, R. Humphry-Baker, E. Müller, P. Liska, N. Vlachopoulos, M. Grätzel, *J. Am. Chem. Soc.* **1993**, *115*, 6382.

[5] M. Grätzel, *J. Photochem. Photobiol. A* **2004**, *164*, 3.

[6] M. K. Nazeeruddin, R. Splivallo, P. Liska, P. Comte, M. Grätzel, *Chem. Commun.* **2003**, 1456.

[7] M. K. Nazeeruddin, F. De Angelis, S. Fantacci, A. Selloni, G. Viscardi, P. Liska, S. Ito, B. Takeru, M. Grätzel, *J. Am. Chem. Soc.* **2005**, *127*, 16835.

[8] C.-Y. Chen, M. Wang, J.-Y. Li, N. Pootrakulchote, L. Alibabaei, C.-h. Ngoc-le, J.-D. Decoppet, J.-H. Tsai, C. Grätzel, C.-G. Wu, S. M. Zakeeruddin, M. Grätzel, *ACS Nano* **2009**, *3*, 3103.

[9] M. K. Nazeeruddin, P. Pechy, T. Renouard, S. M. Zakeeruddin, R. Humphry-Baker, P. Comte, P. Liska, L. Cevey, E. Costa, V. Shklover, L. Spiccia, G. B. Deacon, C. A. Bignozzi, M. Grätzel, *J. Am. Chem. Soc.* **2001**, *123*, 1613.

[10] Y. Chiba, A. Islam, Y. Watanabe, R. Komiya, N. Koide, L. Han, *Jpn. J. Appl. Phys.* **2006**, *45*, L638.

[11] M. K. Nazeeruddin, P. Péchy, M. Grätzel, *Chem. Commun.* **1997**, 1705.

[12] A. Yella, H.-W. Lee, H. N. Tsao, C. Yi, A. K. Chandiran, M. K. Nazeeruddin, E. W.-G. Diau, C.-Y. Yeh, S. M. Zakeeruddin, M. Grätzel, *Science* **2011**, *334*, 629.

[13] M. Wang, M. Xu, D. Shi, R. Li, F. Gao, G. Zhang, Z. Yi, R. Humphry-Baker, P. Wang, S. M. Zakeeruddin, M. Grätzel, *Adv. Mater.* **2008**, *20*, 4460.

[14] H. Imahori, T. Umeyama, S. Ito, *Acc. Chem. Res.* **2009**, *42*, 1809.

[15] A. Mishra, M. K. R. Fischer, P. Bäuerle, *Angew. Chem.* **2009**, *121*, 2510; *Angew. Chem. Int. Ed.* **2009**, *48*, 2474.

[16] Y.-S. Yen, H.-H. Chou, Y.-C. Chen, C.-Y. Hsu, J. T. Lin, *J. Mater. Chem.* **2012**, *22*, 8734.

[17] Y. Bai, J. Zhang, D. Zhou, Y. Wang, M. Zhang, P. Wang, *J. Am. Chem. Soc.* **2011**, *133*, 11442.

[18] W. Zeng, Y. Cao, Y. Bai, Y. Wang, Y. Shi, M. Zhang, F. Wang, C. Pan, P. Wang, *Chem. Mater.* **2010**, *22*, 1915.

[19] N. Cai, S.-J. Moon, L. Cevey-Ha, T. Moehl, R. Humphry-Baker, P. Wang, S. M. Zakeeruddin, M. Grätzel, *Nano Lett.* **2011**, *11*, 1452.

[20] M. Velusamy, K. R. JustinThomas, J. T. Lin, Y. C. Hsu, K. C. Ho, *Org. Lett.* **2005**, *7*, 1899.

[21] J.-J. Kim, H. Choi, J.-W. Lee, M.-S. Kang, K. Song, S. O. Kang, J. Ko, *J. Mater. Chem.* **2008**, *18*, 5223.

[22] J. A. Mikroyannidis, P. Suresh, M. S. Roy, G. D. Sharma, *J. Power Sources* **2010**, *195*, 3002.

[23] Z.-M. Tang, T. Lei, K.-J. Jiang, Y.-L. Song, J. Pei, *Chem. Asian J.* **2010**, *5*, 1911.

[24] S. Kim, H. Lim, K. Kim, C. Kim, T. Kang, M. Ko, N. Park, *IEEE J. Sel. Top. Quant. Electron.* **2010**, *16*, 1627.

[25] W. Zhu, Y. Wu, S. Wang, W. Li, X. Li, J. Chen, Z.-s. Wang, H. Tian, *Adv. Funct. Mater.* **2011**, *21*, 756.

[26] K. Pilgram, M. Zupan, R. Skiles, *J. Heterocycl. Chem.* **1970**, *7*, 629.

[27] J. U. Ju, S. O. Jung, Q. H. Zhao, Y. H. Kim, J. T. Je, S. K. Kwon, *Bull. Kor. Chem. Soc.* **2008**, *29*, 335.

[28] W. A. Carroll, R. J. Altenbach, H. Bai, J. D. Brioni, M. E. Brune, S. A. Buckner, C. Cassidy, Y. Chen, M. J. Coghlan, A. V. Daza, I. Drizin, T. A. Fey, M. Fitzgerald, M. Gopalakrishnan, R. J. Gregg, R. F. Henry, M. W. Holladay, L. L. King, M. E. Kort, P. R. Kym, I. Milicic, R. Tang, S. C. Turner, K. L. Whiteaker, L. Yi, H. Zhang, J. P. Sullivan, *J. Med. Chem.* **2004**, *47*, 3163.

[29] L. S. Fuller, B. Iddon, K. A. Smith, *J. Chem. Soc., Perkin Trans. 1* **1997**, 3465.

[30] A. Srinivasan, V. M. Reddy, S. J. Narayanan, B. Sridevi, S. K. Pushpan, M. Ravikumar, T. K. Chandrashekar, *Angew. Chem. Int. Ed.* **1997**, *36*, 2598.

[31] H. Nakanishi, S. Inoue, T. Otsubo, *Mol. Cryst. Liq. Cryst.* **1997**, *296*, 335.

[32] A. S. D. Sandanayaka, Y. Taguri, Y. Araki, T. Ishi-i, S. Mataka, O. Ito, *J. Phys. Chem. B* **2005**, *109*, 22502.

[33] M. Xu, R. Li, N. Pootrakulchote, D. Shi, J. Guo, Z. Yi, S. M. Zakeeruddin, M. Grätzel, P. Wang, *J. Phys. Chem. C* **2008**, *112*, 19770.

[34] R. Li, X. Lv, D. Shi, D. Zhou, Y. Cheng, G. Zhang, P. Wang, *J. Phys. Chem. C* **2009**, *113*, 7469.

[35] J.-H. Yum, D. P. Hagberg, S.-J. Moon, K. M. Karlsson, T. Marinado, L. Sun, A. Hagfeldt, M. K. Nazeeruddin, M. Grätzel, *Angew. Chem.* **2009**, *121*, 1604; *Angew. Chem. Int. Ed.* **2009**, *48*, 1576.

[36] C. M. Cardona, W. Li, A. E. Kaifer, D. Stockdale, G. C. Bazan, *Adv. Mater.* **2011**, *23*, 2367.

[37] H. Qin, S. Wenger, M. Xu, F. Gao, X. Jing, P. Wang, S. M. Zakeeruddin, M. Grätzel, *J. Am. Chem. Soc.* **2008**, *130*, 9202.

[38] N. Kopidakis, K. D. Benkstein, J. van de Lagemaat, A. J. Frank, *J. Phys. Chem. B* **2003**, *107*, 11307.

[39] J. Bisquert, *J. Phys. Chem. B* **2001**, *106*, 325.

[40] M. J. Frisch, G. W. Trucks, H. B. Schlegel, G. E. Scuseria, M. A. Robb, J. R. Cheeseman, G. Scalmani, V. Barone, B. Mennucci, G. A. Petersson, H. Nakatsuji, M. Caricato, X. Li, H. P. Hratchian, A. F. Izmaylov, J. Bloino, G. Zheng, J. L. Sonnenberg, M. Hada, M. Ehara, K. Toyota, R. Fukuda, J. Hasegawa, M. Ishida, T. Nakajima, Y. Honda, O. Kitao, H. Nakai, T. Vreven, J. J. A. Montgomery, J. E. Peralta, F. Ogliaro, M. Bearpark, J. J. Heyd, E. Brothers, K. N. Kudin, V. N. Staroverov, R. Kobayashi, J. Normand, K. Raghavachari, A. Rendell, J. C. Burant, S. S. Iyengar, J. Tomasi, M. Cossi, N. Rega, J. M. Millam, M. Klene, J. E. Knox, J. B. Cross, V. Bakken, C. Adamo, J. Jaramillo, R. Gomperts, R. E. Stratmann, O. Yazyev, A. J. Austin, R. Cammi, C. Pomelli, J. W. Ochterski, R. L. Martin, K. Morokuma, V. G. Zakrzewski, G. A. Voth, P. Salvador, J. J. Dannenberg, S. Dapprich, A. D. Daniels, O. Farkas, J. B. Foresman, J. V. Ortiz, J. Cioslowski, D. J. Fox, Gaussian, Inc., Wallingford, CT, **2009**.

[41] A. D. Becke, *J. Chem. Phys.* **1993**, *98*, 5648.

[42] K. Burke, J. P. Perdew, Y. Wang, in *Electronic Density Functional Theory: Recent Progress and New Directions* (Eds.: J. F. Dobson, G. Vignale, M. P. Das), Plenum Press, New York, **1998**.

[43] P. J. Stephens, F. J. Devlin, C. F. Chabalowski, M. J. Frisch, *J. Phys. Chem.* **1994**, *98*, 11623.

[44] R. Ditchfield, W. J. Hehre, J. A. Pople, *J. Chem. Phys.* **1971**, *54*, 724.

[45] V. A. Rassolov, J. A. Pople, M. A. Ratner, T. L. Windus, *J. Chem. Phys.* **1998**, *109*, 1223.

[46] P. Winget, A. Horn, C. Selçuki, B. Martin, T. Clark, *J. Mol. Model.* **2003**, *9*, 408.

[47] H. Kayi, T. Clark, *J. Mol. Model.* **2007**, *13*, 965.

Summary

In this thesis, functionalized selenophene oligomers and co-oligomers were synthesized and their optoelectronic properties were investigated. Furthermore, these compounds were implemented in different types of organic solar cells, in particular vacuum-processed planar heterojunction (PHJ) solar cells, vacuum-processed and solution-processed bulk-heterojunction (BHJ) solar cells, and dye-sensitized solar cells (DSSC).

While thiophene is one of the most frequently used building blocks for oligomeric donor materials in organic solar cells, selenophene has only scarcely been used in this respect. Investigations on polyselenophenes and selenophene-containing copolymers had revealed several advantageous properties, e.g., bathochromically shifted absorption spectra and lower band gaps compared to corresponding thiophene materials.

In order to investigate the influence of the stepwise replacement of thiophene by selenophene, dicyanovinyl (DCV)-substituted selenophene-thiophene pentamers **1**-**3** were synthesized (**Figure S.1**), and their thermal, optical and electrochemical properties and photovoltaic performance were studied and compared to the *all*-thiophene analog **DCV5T-Bu**. Increasing selenophene content resulted in higher melting points, bathochromically shifted absorption spectra, lower band gaps, and higher molar extinction coefficients, while the electrochemical properties stayed relatively unaffected. It was found that the replacement of the thiophenes adjacent to the DCV groups sufficed to achieve a considerable red-shift of almost 20 nm. When implemented as donor materials in bulk-heterojunction (BHJ) solar cells, pentamers **1**-**3** attained power conversion efficiencies (PCE) of 2.5-3.1% compared to 3.5% for **DCV5T**. The PCE decreased with increasing number of selenophenes, probably due to a lower degree of phase separation in the blend layer, resulting in recombination losses and lower charger carrier extraction efficiencies.

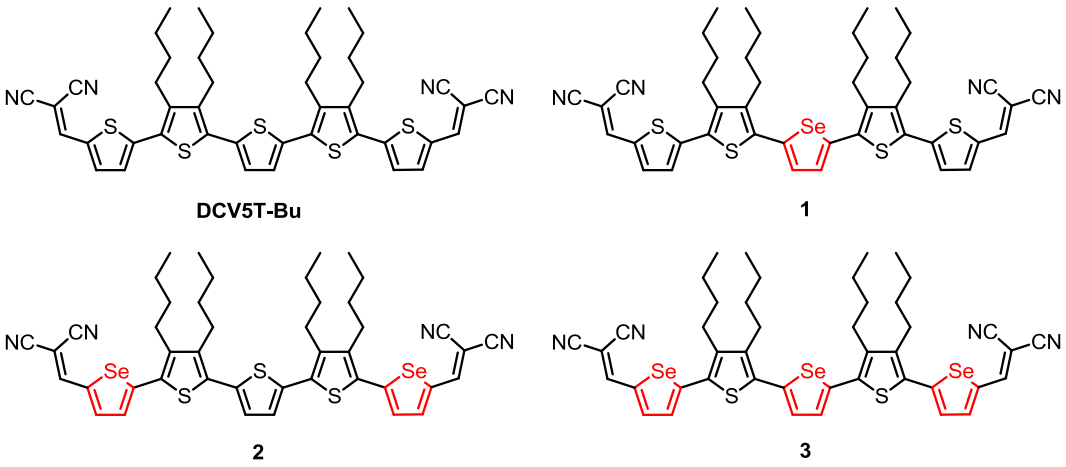

Figure S.1: DCV-substituted selenophene-thiophene pentamers.

In the non-alkylated terminally DCV-substituted oligoselenophenes **5**-**7** (**Figure S.2**) thiophene was completely replaced by selenophene. Compared to the corresponding oligothiophenes **DCVnT**, the thermal, optical, and electrochemical properties of **5**-**7** exhibited similar chain length dependence. Furthermore, red-shifted absorption bands and lowering of the band gap were observed for **5**-**7** in comparison to **DCVnT**. The replacement of sulfur by selenium resulted in a lowering of the lowest unoccupied molecular orbital (LUMO) energy level while the highest occupied molecular orbital (HOMO) level stayed relatively unaffected. The single crystal structure of quaterselenophene **6** showed a large resemblance to that of quaterthiophene **DCV4T**. A crystal structure analysis corroborated the important role that the DCV groups play for molecular ordering, whereas the introduction of selenium resulted in increased intermolecular distances. Oligoselenophenes **6** and **7** were implemented as donor materials in vacuum-processed PHJ and BHJ solar cells with C_{60} as acceptor. In PHJ devices, the PCEs of the oligoselenophenes exceeded those of their thiophene analogs, the best efficiency being 3.4% for **7**. In BHJ devices, the selenophene and thiophene tetramers attained similar PCEs, but the PCE of the selenophene pentamer **7** was lower than that of its thiophene analog **DCV5T**. Apparently, the morphology of oligoselenophene-C_{60} blends is less favorable than that of oligothiophene-C_{60} blends, supposedly due to larger donor-acceptor domains in the former.

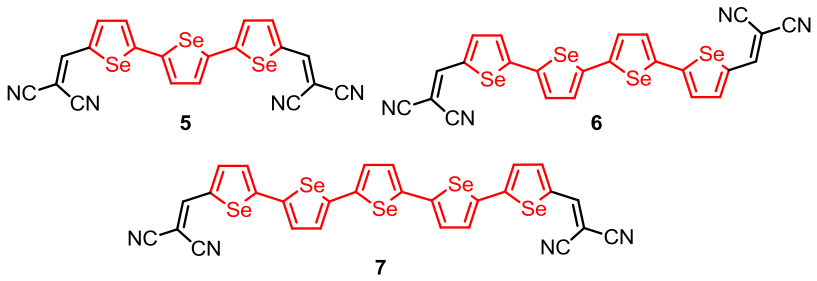

Figure S.2: DCV-substituted oligoselenophenes.

The absorption maxima of the aforementioned oligomers were still not in the desired region, i.e., beyond 600 nm. In order to further red-shift the absorption spectra, we combined a stronger donor moiety with the well-established DCV acceptor groups. As donor moieties, dithienopyrrole and diselenophenopyrrole were chosen, leading to target compounds **9**-**14** (**Figure S.3**). Diselenopheno-pyrrole is still a rather unexplored building block in the literature; therefore, several new methods for the synthesis of this building block and its derivatives had to be established. Especially the synthesis of *N*-propyl diselenophenopyrrole proved to be more difficult than expected. The stannylation of this building block was not successful due to an unexpected ring-opening reaction during lithiation. The absorption range of co-oligomers **9**-**14** depended on the selenophene content, i.e., the absorption spectra were bathochromically shifted with increasing number of selenophene units. Co-oligomers **9**-

14 were implemented as donor materials in vacuum-processed BHJ solar cells, but the results cannot be disclosed here in order to maintain confidentiality.

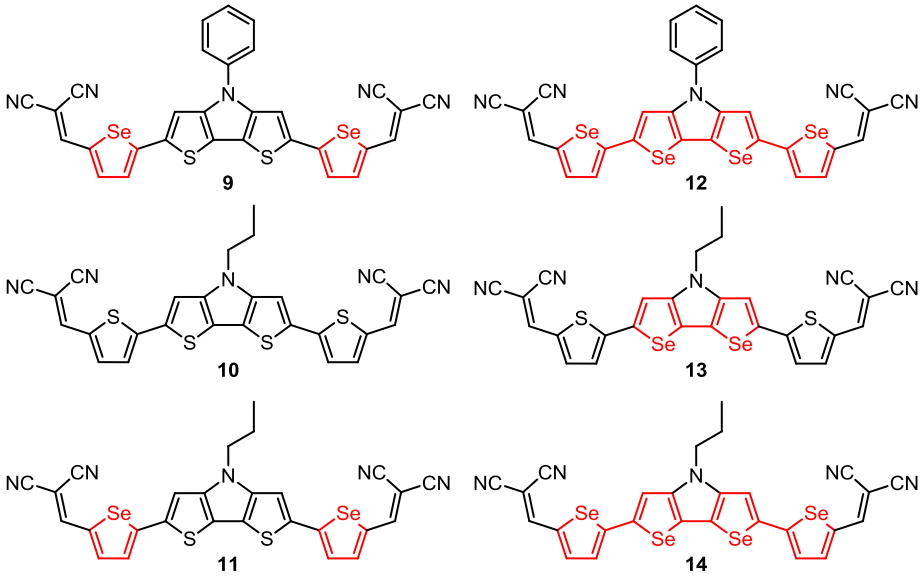

Figure S.3: DCV-substituted co-oligomers with a dichalcogenophenopyrrole core.

Due to these high efficiencies in vacuum-processed devices, derivative (**15**, **Figure S.4**) for solution-processed solar cells was synthesized which contained the same conjugated backbone as **14** but longer alkyl chains to improve solubility. It showed promising optoelectronic properties, but its performance in solution-processed BHJ solar cells was relatively poor with a maximum PCE of 0.64%. Presumably, the solubility of co-oligomer **15** was still not sufficient which resulted in very rough blend films and large leakage currents.

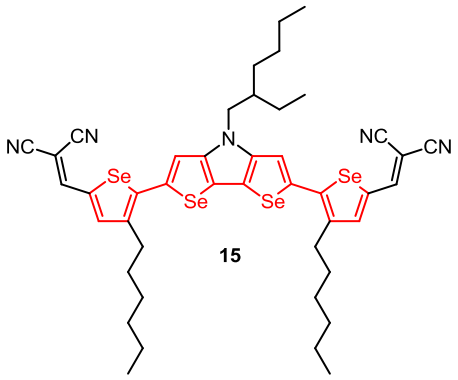

Figure S.4: Solution-processable DSP-based donor compound.

In another project, a series of low band gap donor-π-acceptor (D-π-A) sensitizers **16**-**18** with different π-bridges and a benzothiadiazole (BTDA) unit adjacent to the anchoring group was synthesized (**Figure S.5**). The thin film absorption range of these dyes extended into the NIR-region up to 800 nm with narrow HOMO-LUMO energy gaps of 1.6-1.7 eV. Although the indicent photon to electron conversion efficiency (IPCE) spectra of these dyes in DSSCs were extended up to 850 nm, the

photocurrent density was relatively low and poor PCEs of 1.3-1.8% were obtained. Additionaly, a fourth sensitizer **19** was synthesized by insertion of a phenyl unit between the BTDA moiety and the anchoring group in dye **17**. Sensitizer **19** exhibited a blue-shifted absorption spectrum and a smaller Stokes shift compared to **17**, hinting at a possible twist of the additional phenyl ring with respect to the π-conjugated donor and BTDA part. Under optimized conditions, dye **19** showed a more than six times higher PCE (8.21%) in DSSCs than dye **17** (1.24%). The reasons hereof were elucidated by theoretical calculations and photophysical investigations at the Grätzel laboratory in Lausanne. Density functional theory (DFT) calculations revealed that upon formation of the radical cation of **19** the out-of-plane torsion of the adjacent BTDA and cyanoacrylic acid unit was enhanced leading to an interruption of the π-conjugation between donor and anchoring group. The formation of a stable radical cation and the interruption of the π-conjugation between the donor and acceptor inhibited the back electron transfer. In particular, the electron injection rate was barely affected, but the recombination reaction of **19** was slowed down over 5 times compared to **17**.

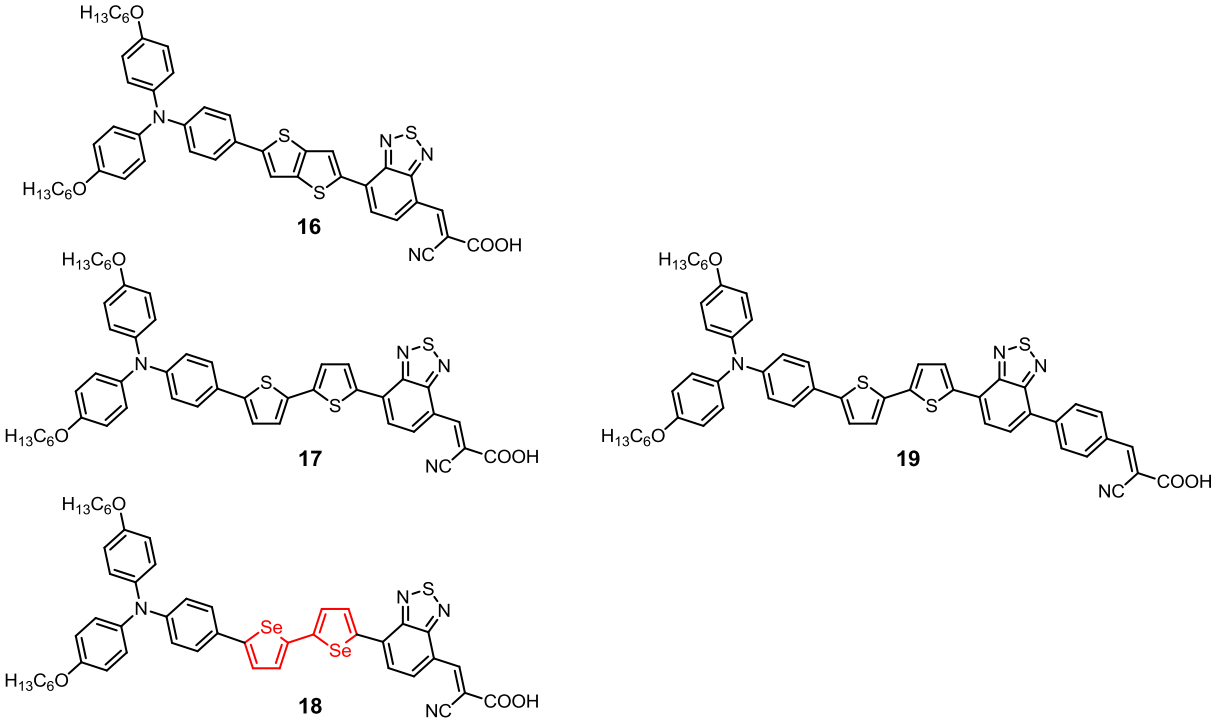

Figure S.5: Benzothiadiazole-based sensitizers for dye-sensitized solar cells (DSSC).

Zusammenfassung

Die vorliegende Arbeit beschäftigt sich mit der Synthese und Untersuchung der optoelektronischen Eigenschaften funktionalisierter Selenophen-Oligomere und Co-Oligomere. Außerdem wurden diese Verbindungen in organischen Solarzellen unterschiedlicher Bauart eingesetzt; im Speziellen sind dies vakuumprozessierte Zellen mit planarem Heteroübergang (PHJ), vakuum- und lösungsprozessierte Bulk-Heteroübergangszellen (BHJ) und farbstoffsensibilisierte Solarzellen (DSSC).

Während Thiophen zu den am häufigsten verwendeten Bausteinen in oligomeren Donormaterialien für organische Solarzellen gehört, wurde Selenophen bisher nur äußerst selten hierfür verwendet. Untersuchungen an Polyselenophenen und selenophenhaltigen Copolymeren zeigten jedoch einige vorteilhafte Eigenschaften im Vergleich zu entsprechenden Thiophenmaterialien wie z.B. rotverschobene Absorptionsspektren und schmalere Bandlücken.

Um den Einfluss der schrittweisen Substitution von Thiophen durch Selenophen zu untersuchen, wurden die Dicyanovinyl(DCV)-substituierten Selenophen-Thiophen-Pentamere **1**-**3** synthetisiert (**Abbildung 1**). Ihre thermischen, optischen und elektrochemischen Eigenschaften wurden untersucht und mit denen des Oligothiophens **DCV5T-Bu** verglichen. Ein zunehmender Selenophengehalt führte dabei zu höheren Schmelzpunkten, rotverschobenen Absorptionsspektren, kleineren Bandlücken und höheren molaren Extinktionskoeffizienten, während die elektrochemischen Eigenschaften relativ unverändert blieben. Es stellte sich heraus, dass bereits der Ersatz der Selenophen-Einheiten, die den DCV-Gruppen benachbart sind, genügte um eine Rotverschiebung von beinahe 20 nm zu erreichen.

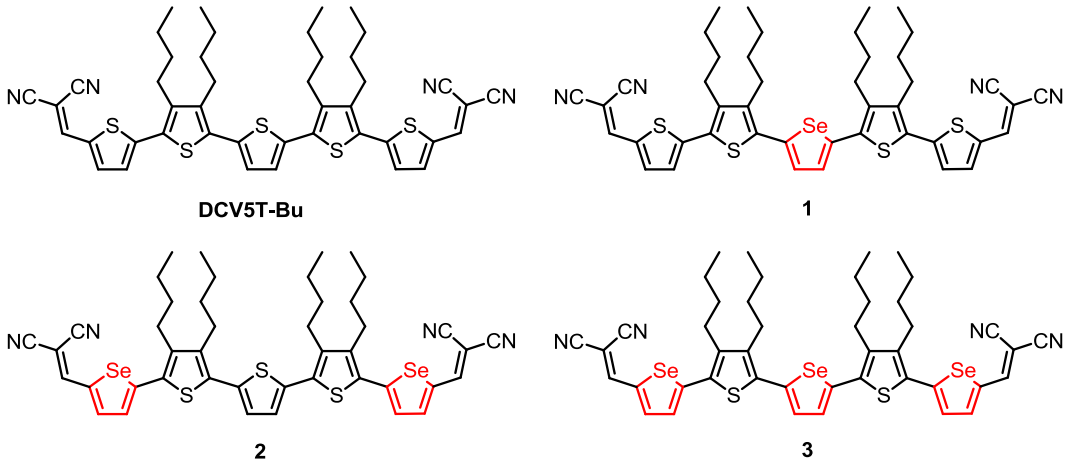

Abbildung 1: DCV-substituierte Selenophen-Thiophen-Pentamere.

Als Donormaterialien in BHJ-Solarzellen erreichten die Pentamere **1**-**3** Energieumwandlungs-effizienzen (PCE) von 2.5-3.1% verglichen mit 3.5% für **DCV5T-Bu**. Die Effizienz nahm mit zunehmendem Selenophengehalt ab, wahrscheinlich aufgrund einer weniger ausgeprägten

Phasenseparation in der Blendschicht. Dies führte zu Rekombinationsverlusten und weniger effizienter Ladungsträgerextraktion.

In den nichtalkylierten endständig DCV-substituierten Oligoselenophenen **5**-**7** (**Abbildung 2**) wurde Thiophen schließlich komplett durch Selenophen ersetzt. Verglichen mit den entsprechenden Oligothiophenen **DCVnT** wiesen die thermischen, optischen und elektrochemischen Eigenschaften der Oligomere **5**-**7** eine ähnliche Abhängigkeit von der Kettenlänge auf. Desweiteren wurden rotverschobene Absorptionsbanden und kleinere Bandlücken im Vergleich zu **DCVnT** beobachtet. Der Ersatz von Schwefel durch Selen bewirkte eine Absenkung des niedrigsten unbesetzten Molekülorbitals (LUMO), während das höchste besetzte Molekülorbital (HOMO) nur geringfügig beeinflusst wurde. Die Kristallstruktur des Quaterselenophens **6** wies große Ähnlichkeit mit der des Quaterthiophens **DCV4T** auf. Eine Analyse der Kristallstruktur verdeutlichte die wichtige Rolle der DCV-Gruppen für die Anordnung der Moleküle im Kristall, während die Einführung von Selen zu erhöhten intermolekularen Abständen führte. Die Oligoselenophene **6** und **7** wurden als Donormaterialien in Kombination mit C_{60} als Akzeptor in vakuumprozessierten PHJ- und BHJ-Solarzellen eingesetzt. In den PHJ-Zellen erzielten sie höhere Effizienzen als ihre Thiophen-Analoga, wobei die beste PCE von 3.4% mit Oligomer **7** erreicht wurde. In BHJ-Zellen erreichten die Selenophen- und Thiophen-Tetramere vergleichbare Effizienzen, die PCE für das Selenophen-Pentamer **7** lag jedoch unter der des entsprechenden Thiophen-Analogons **DCV5T**. Die Morphologie der Oligoselenophen-C_{60}-Blendschichten scheint weniger vorteilhaft zu sein als die der Oligothiophen-C_{60}-Blends, möglicherweise aufgrund größerer Donor-Akzeptor-Domänen in ersteren.

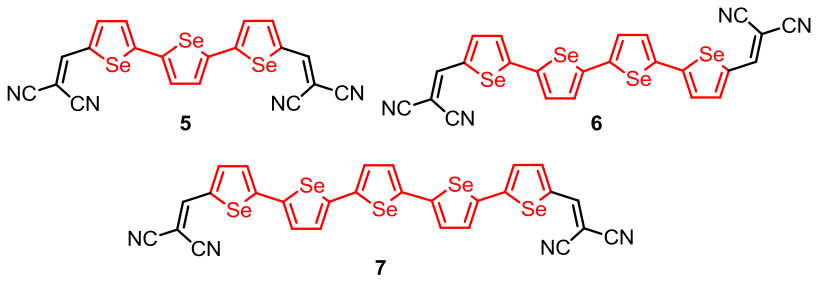

Abbildung 2: DCV-substituierte Oligoselenophene.

Die Absorptionsmaxima der bisher erwähnten Oligomere lagen immer noch nicht im gewünschten Bereich, d. h. jenseits von 600 nm. Um diese weiter ins Rote zu verschieben, kombinierten wir die starken Donorbausteine Dithienopyrrol und Diselenophenopyrrol mit den bewährten DCV-Gruppen, was zu den Zielverbindungen **9**-**14** führte (**Abbildung 3**). In der Literatur wurde Diselenophenopyrrol bisher kaum untersucht. Daher mussten einige neue Synthesewege für diesen Baustein und seine Derivate entwickelt werden. Insbesondere die Synthese von *N*-Propyldiselenophenopyrrol stellte sich als schwieriger als erwartet heraus. Die Stannylierung dieses Bausteins gelang nicht, da hierbei eine

unerwartete Ringöffnungsreaktion auftrat. Der Absorptionsbereich der Co-Oligomere **9**-**14** hing stark vom Selenophengehalt ab, d. h. die Absorptionsspektren verschoben sich mit steigender Anzahl an Selenopheneinheiten ins Rote. Die Co-Oligomere **9**-**14** wurden als Donormaterialien in vakuumprozessierten BHJ-Solarzellen eingesetzt, die erzielten Ergebnisse können hier jedoch aus Geheimhaltungsgründen nicht offengelegt werden.

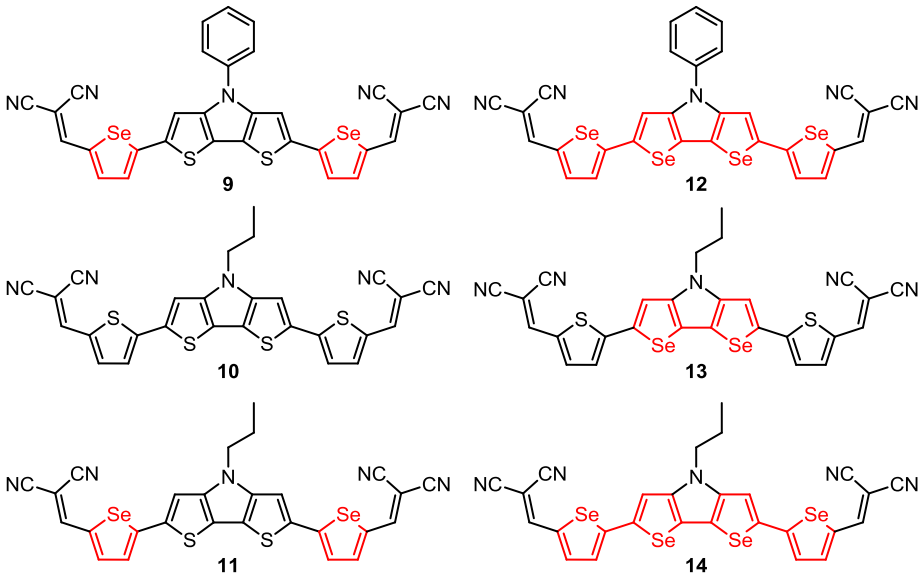

Abbildung 3: DCV-substituierte Co-Oligomere mit einem Dichalkogenophenopyrrol-Kern.

Aufgrund dieser hohen Effizienzen in vakuumprozessierten Solarzellen wurde das Derivat **15** (**Abbildung 4**) für lösungsprozessierte Zellen entwickelt. Dieses besitzt das gleiche konjugierte Rückgrat wie **14** aber längere Alkylketten zur Verbesserung der Löslichkeit. Die Verbindung zeigte vielversprechende optoelektronische Eigenschaften, aber mit einer maximalen PCE von 0.64% nur eine relativ schlechte Leistung in lösungsprozessierten BHJ-Solarzellen. Vermutlich war die Löslichkeit des Co-Oligomers **15** immer noch nicht ausreichend, was zu sehr rauen Blendfilmen und entsprechend hohen Leckströmen führte.

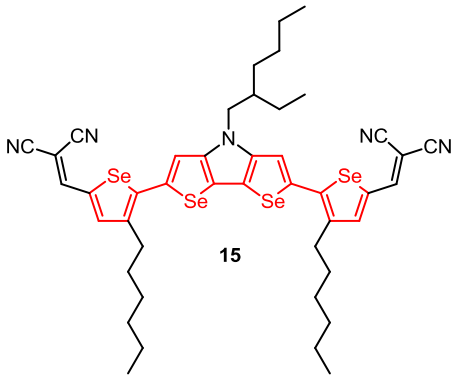

Abbildung 4: Lösungsprozessierbare DSP-basierte Donorverbindung.

Für ein weiteres Projekt wurden die Donor-π-Akzeptor-Farbstoffe **16**-**18** synthetisiert. Diese enthielten unterschiedliche π-Brücken und eine Benzothiadiazol(BTDA)-Einheit benachbart zur Ankergruppe (**Abbildung 5**). In dünnen Filmen reichte der Absorptionsbereich dieser Farbstoffe bis in den nahen Infrarotbereich mit schmalen HOMO-LUMO-Energielücken von 1.6-1.7 eV. Obwohl sich ihre IPCE-Spektren bis 850 nm erstreckten, waren die Photostromdichten relativ niedrig und entsprechend geringe PCEs von 1.3-1.8% wurden erzielt.

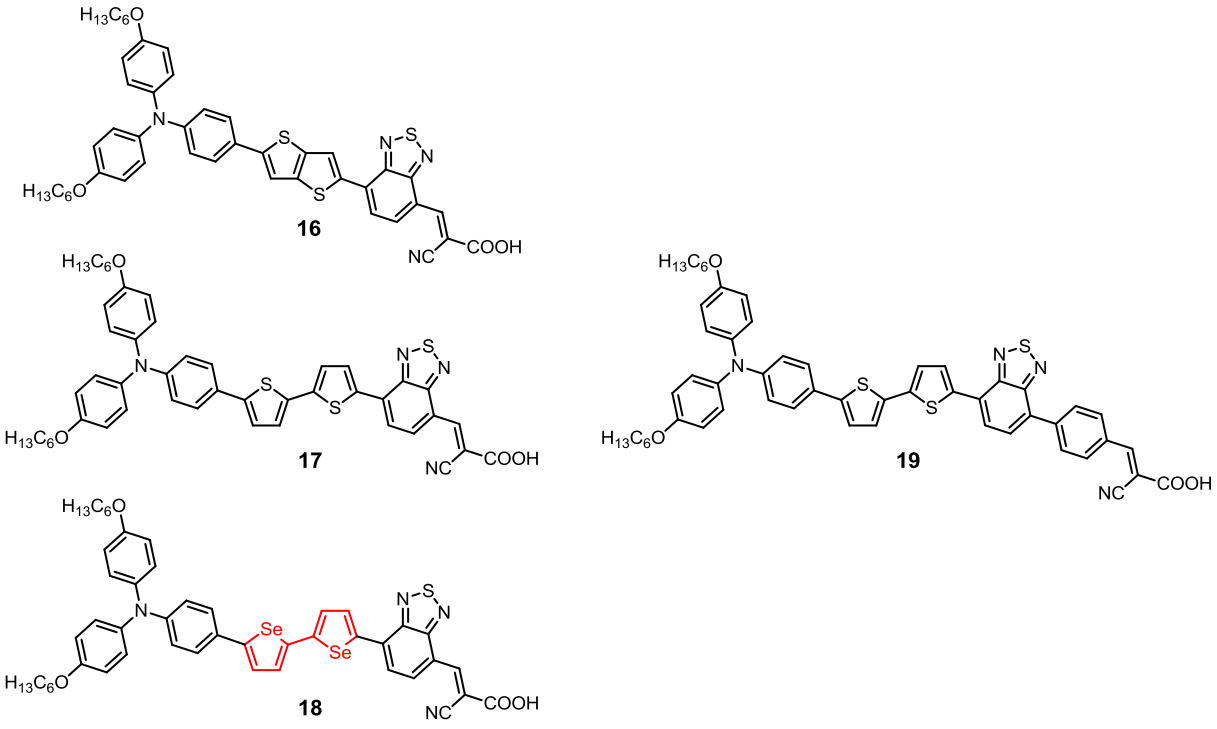

Abbildung 5: Benzothiadiazol-basierte Farbstoffe für farbstoffsensibilisierte Solarzellen (DSSCs).

Zusätzlich wurde noch ein vierter Farbstoff **19** synthetisiert, der sich von **17** durch einen zusätzlichen Phenylring zwischen BTDA-Einheit und Ankergruppe unterschied. Im Vergleich zu **17** wies Farbstoff **19** ein blauverschobenes Absorptionsspektrum und eine kleinere Stokes-Verschiebung auf, was auf eine mögliche Verdrillung des Phenylrings in Bezug auf die π-Brücke und BTDA-Einheit hindeutet. Unter optimierten Bedingungen erzielte Farbstoff **19** eine mehr als sechsmal so hohe PCE (8.21%) wie Farbstoff **17** (1.24%). Die Gründe hierfür wurden von der Grätzel-Gruppe in Lausanne mittels theoretischer Berechnungen und photophysikalischer Messungen untersucht. Berechnungen auf Grundlage der Dichtefunktionaltheorie zeigten, dass bei der Bildung des Radikalkations von **19** die Verdrillung zwischen BTDA und der Cyanoacrylsäuregruppe zunimmt, was zu einer Unterbrechung der π-Konjugation zwischen Donor- und Akzeptorgruppe führt. Die Bildung eines stabilen Radikalkations und diese Unterbrechung der π-Konjugation behinderten den Elektronenrücktransfer. Die Elektroneninjektionsrate wurde hiervon kaum beeinflusst aber die Rekombinationsreaktion war im Falle von Farbstoff **19** mehr als fünfmal langsamer als für Farbstoff **17**.

Curriculum Vitae

EDUCATION

11/08-10/12	PhD studies with Prof. Peter Bäuerle, Institute of Organic Chemistry II and Novel Materials, Ulm University *„Functionalized Selenophene Oligomers and Co-oligomers and Their Application in Organic Solar Cells“*
10/03-09/08	Studies in Chemistry, Ulm University Degree: Diplom-Chemiker (Grade 1.1) Diploma thesis: *„Synthese und Reaktivität symmetrischer und unsymmetrischer Platin(II)-Oligothienyl-Komplexe“* (Synthesis and reactivity of symmetrical and unsymmetrical platinum(II) oligothienyl complexes)
09/93-07/02	Wieland-Gymnasium, Biberach/Riß Degree: Abitur (Grade 1.0)

CIVIL SERVICE

08/02-05/03	Fachklinik Hohenrodt, Oggelsbeuren

INTERNSHIPS

04/11	Research internship with Prof. Andrew B. Holmes, Bio21 Institute, Melbourne, Australia (4 weeks)
02/07-04/07	Internship in organic chemistry at Boehringer Ingelheim, Biberach

PRIZES AND SCHOLARSHIPS

05/09	Dr. Barbara-Mez-Starck prize for excellent diploma
05/06	Prize for excellent „Vordiplom“ awarded by the Department of Chemistry, Ulm University
10/03-09/05	„Jubiläums-Stipendium für Studienanfänger“ by the German Chemical Industry Fund (Fonds der Chemischen Industrie)
07/02	Hilde-Frey prize awarded by the city of Biberach an der Riß

Publications and Presentations

PUBLICATIONS

S. Haid, A. Mishra, M. Weil, C. Uhrich, M. Pfeiffer, P. Bäuerle, *Adv. Funct. Mater.* **2012**, *22*, 4322.
"Synthesis and Structure-Property Correlations of Dicyanovinyl-substituted Oligoselenophenes and their Application in Organic Solar Cells."

S. Haid, M. Marszałek, A. Mishra, M. Wielopolski, J. Teuscher, J.-E. Moser, R. Humphry-Baker, S. M. Zakeeruddin, M. Grätzel, P. Bäuerle, *Adv. Funct. Mater.* **2012**, *22*, 1291.
"Significant Improvement of Dye-Sensitized Solar Cell Performance by Small Structural Modification in π-Conjugated Donor-Acceptor Dyes."

S. Haid, A. Mishra, C. Uhrich, M. Pfeiffer, P. Bäuerle, *Chem. Mater.* **2011**, *23*, 4435.
"Dicyanovinylene-Substituted Selenophene-Thiophene Co-oligomers for Small-Molecule Organic Solar Cells."

H. Seyler, S. Haid, T.-H. Kwon, D. Jones, P. Bäuerle, A. Holmes, W. Wong, *Austr. J. Chem.* **2012**, accepted; DOI: 10.1071/CH12406
„Continuous Flow Synthesis of Organic Electronic Materials - Case Studies in Methodology Translation and Scale-up".

PRESENTATIONS

Fπ9 (International Symposium on Functional π-Electron Systems), Atlanta, 23/05-28/05/2010
Poster presentation
S. Haid, M. Marszałek, A. Mishra, S. M. Zakeeruddin, M. Grätzel, P. Bäuerle, *"Synthesis of Low-band-gap Organic Chromophores - Performance in Dye-sensitized Solar Cells"*.

ISNA 13 (International Symposium on Novel Aromatic Compounds), Luxembourg, 19/07-25/07/2009
Poster presentation
S. Haid, F. Zhang, P. Bäuerle, "*A Novel Cross-Coupling Reaction Based On Unsymmetrical Platinum(II)-Oligothienyl Complexes"*.